NTNU
Norwegian University of
Science and Technology

Non-Stationary Buffeting Response of Slender Suspension Bridges

Åsmund Romstad Løvik

Civil and Environmental Engineering
Submission date: June 2018
Supervisor: Ole Andre Øiseth, KT
Co-supervisor: Aksel Fenerci, KT

Norwegian University of Science and Technology
Department of Structural Engineering

MASTEROPPGAVE 2018

for

Åsmund Romstad Løvik

Vindindusert dynamisk respons av hengebruer usatt for skrå ikke stasjonær vind

Wind induced dynamic response of suspension bridges subjected to skew nonstationary wind.

I forbindelse med prosjektet ferjefri e30 vurderes ei hengebru som skal krysse Sulafjorden. Brua vil få et hovedspenn på over 3000 meter og vil bli verdens lengste hengebru. Terrenget rundt brua vil forme vindfeltet og det er svært sannsynlig at vindfeltet treffer konstruksjonen på skrå og at det er ikke stasjonært. Denne oppgaven dreier seg om å sette seg inn i og anvende teorien for ikke stasjonær og skrå vind for å vurdere hvor viktig det er å ha med disse effektene i modelleringen.

Oppgaven bør inneholde følgende temaer:

- Grunnleggende teori for stasjonær vindindusert dynamisk respons
- Grunnleggende teori av stasjonær vindindusert dynamisk respons der vinden er skrå
- Teori for ikke stasjonære responsmodeller
- Anvendelser på et valgt case studie

Besvarelsen organiseres i henhold til gjeldende retningslinjer.

Veileder(e): Ole Andre Øiseth, Aksel Fenerci, Tor Martin Lystad

NTNU, 14.01.2018

Ole Andre Øiseth
faglærer

PREFACE

This master's thesis is written under the Department of Structural Engineering at the Norwegian University of Science and Technology (NTNU) during the spring semester of 2018 and completes my master's degree in Civil Engineering with an emphasis on Wind Engineering. My supervisors have been Associate Professor Ole Andre Øiseth and Postdoctoral Fellow Aksel Fenerci.

This particular thesis focuses only on non–stationary wind buffeting theory when the wind field itself is defined to act perpendicular to the bridge span. The effects of skew winds are therefore not investigated because such was found to be too extensive for the purpose of this thesis. The same reason lies behind the choice of not investigating the effects of vortex shedding, or complex terrain that may obscure the wind field.

Finally, many of the drawings presented in this thesis are created with great inspiration from the relevant drawings in [10] and [11] which according to Strømmen is prepared by Anne Gaarden.

ACKNOWLEDGEMENTS

During the work of this thesis in particular, I would like to thank Associate Professor Ole Andre Øiseth for his positive attitude and great hospitality when providing me with this thesis on a relatively short notice. I would especially like to thank Postdoctoral Fellow Aksel Fenerci for his positive attitude, flexibility and open–mindedness during our long–lasting phone calls regarding the very work with this thesis. His help was crucial when it came to obtain fundamental knowledge about the phenomenology of non-stationary winds.

There are many people to whom I would like to express my deep gratitude when it comes to supporting me throughout the process of combining the Civil Engineering studies at NTNU with my semi-professional cycling career in during the years 2013 – 2017. This regards first and foremost my better half and my family who have always been there for me no matter the circumstance. I would also like to thank the different cycling teams for whom I have been riding in this period, as well as NTNU itself for both being flexible and understandable when it comes to letting me fulfil my personal dreams.

Åsmund Romstad Løvik　　Jar, 13.06.2018

ABSTRACT

This thesis presents a generalized framework for predicting dynamic structural response of slender, horizontal and line–like structures. This general framework is subsequently adopted and streamlined to the Hardanger Bridge which crosses the Hardanger Fjord in Hordaland, Norway. During this process, several central arising issues regarding the non–stationary theory is put onto the agenda.

The thesis itself is formulated in the following way. First, the general multi–mode, frequency domain stationary buffeting theory is established in chapter 1, in which many concepts that are also vital in the formulation of the non-stationary theory are explained**.** Chapter 2 presents a detailed description of the proposed solutions to the issues that arises when the stationary frequency domain framework presented in chapter 1 is adapted to model non–stationary winds. This process consists of three main steps in which the first one is to define the mean wind speed as being a deterministic, time varying trend. Second, the remaining turbulence component of the non–stationary wind field is modelled as being an *evolutionary stochastic process*. The trends of this evolutionary process are similarly defined to be deterministic, time varying functions and are estimated in an appropriate manner. Finally, a good amount of attention is given to how the frequency spectrum of the stochastic turbulence components can be estimated as accurately and as wisely as possible. This involves the introduction of a simple and intuitive spectral data denoising algorithm that together with a weighted least square fit toolbox available in MATLAB R2018a that can operate on a user–specified equation, is able to much more accurately determine the "true" frequency distribution of a scattered spectral data set. Chapter 3 presents the adaptation and streamlining of the established general non–stationary buffeting theory framework to the Hardanger Bridge in particular. In order to obtain knowledge about transient effects in the dynamic structural response, a simplified SDOF system representing the fundamental mode of the Hardanger Bridge is applied from which structural response is calculated via time domain Monte Carlo simulations. A comparison between the frequency domain response and simulated time domain response of this simplified SDOF system provides the necessary information about when transient effects of the dynamic response of the Hardanger Bridge will prevail. The validity of this comparison is based on presented specific findings that suggest that horizontal motion at the bridge midspan is completely dominated by the fundamental mode alone.

The results of the case study of the Hardanger Bridge is given in chapter 4 from which discussions and conclusions are given in chapters 5 and 6, respectively. The major findings of this thesis are first that there exist many valid ways to draw the line between what one defines as being deterministic and stochastic, however, the probability distribution of maximum structural response seems to depend somewhat less on the location of this deterministic–stochastic separation point. Second, the SDOF system is able to show that transient effects will start to become a significant feature of the airflow–structure interaction picture if the highest included frequency in the deterministic mean wind speed is above roughly 1/50th of the fundamental frequency of the Hardanger Bridge. Above this limit, the validity of the frequency domain method is violated, and structural response seems to be overestimated.

SAMMENDRAG

Denne masteroppgaven presenterer et generelt teorigrunnlag for beregning av dynamisk respons på slanke, horisontale og strek–liknende konstruksjoner. Dette generelle teorigrunnlaget vil så bli tilpasset og strømlinjeformet til Hardangerbrua som krysser Hardangerfjorden i Hordaland i Norge. I denne tilpasningsprosessen vil flere sentrale problemstillinger som oppstår i forbindelse med et ikke stasjonært vindfelt og en følgende ikke–stasjonær responsberegning, bli satt på dagsorden.

Selve oppgaven er disponert på følgende måte. Det generelle teorigrunnlaget for fler–modale konstruksjonsmodeller utsatt for stasjonær vindturbulens beregnet i frekvensplanet er først etablert i kapittel 1, hvor en rekke konsepter som også er vitale i forbindelse med ikke stasjonære betraktninger vil bli forklart. Kapittel 2 presenterer deretter en detaljert beskrivelse av hvordan løsningene til problemstillingene som oppstår når det stasjonære frekvensplan–teorigrunnlaget i kapittel 1 tilpasses til å modellere ikke–stasjonære vindfelt. Denne tilpasningsprosessen består av hovedsakelig tre steg hvor det første er å definere den gjennomsnittlige vindhastigheten til å være en deterministisk varierende trend. Steg to er å modellere den gjenværende turbulenskomponenten som en *evolusjonær, stokastisk prosess*. Trendene til denne evolusjonære, stokastiske prosessen vil i likhet med den gjennomsnittlige vindhastigheten bli definert til å være en deterministisk varierende funksjon og vil bli estimert på en passende måte. Til slutt vil en god del oppmerksomhet bli viet til hvordan frekvensspektrumet til de stokastiske turbulenskomponentene kan bli estimert på en så klok og nøyaktig måte som mulig. På bakgrunn av dette er det utviklet en enkel og intuitiv algoritme for avstøyning av råspektraldata som, sammen med en vektet minste kvadraters metode innebygd i MATLAB R2018a som kan tilpasses en brukerspesifisert likning, er i stand til å mye mer nøyaktig anslå den ekte og «bortgjemte» frekvensfordelingen det spredte råsprektraldatasettet representerer. Kapittel 3 presenterer en spesialtilpasning og strømlinjeforming av det nå etablerte ikke–stasjonære generelle frekvensplan–teorigrunnlaget til Hardangerbroen i særskilthet. For å kunne tilegne kunnskap om faseovergangseffekter i den dynamiske responsen på brokonstruksjonen er det etablert et forenklet énfrihetsgradsystem som representerer fundamantalegensvingeformen til Hardangerbroen, hvor de statistiske karakteristika til dets dynamiske respons blir estimert fra Monte Carlo simuleringer i tidsplanet. En sammenlikning av den tidsavhengige variansen av responsen til dette forenklede énfrihetsgradsystem beregnet i frekvensplanet og estimert via simuleringer i tidsplanet vil gi den nødvendige informasjonen for å fastslå når faseovergangseffekter i den dynamiske responsen på Hardangerbroen vil råde. Gyldigheten til dette sammenlikningsgrunnlaget er basert på spesifikke funn som fastslår at den horisontale bevegelsen på midspennet til Hardangerbroen er fullstendig dominert av fundamentalegensvingeformen alene.

Resultatene av eksempelstudiet av Hardangerbroen er gitt i kapittel 4 hvorfra kommentarer og tilhørende konklusjoner er gitt i henholdsvis kapittel 5 og 6. Hovedfunnene i denne oppgaven er først at det finnes mange gyldige steder for hvor man skal sette grensen mellom hva man definerer til å være deterministiske trender og hva man velger å definere som stokastiske prosesser. Imidlertid viser det seg at sannsynlighetsfordelingen til den største responsen konstruksjonen vil utvise ikke synes å være sterkt preget av nettopp hvor denne deterministisk–stokastiske seperasjonsgrensen settes. For det andre viser det forenklede énfrihetsgradsystemet at faseovergangseffekter vil utgjøre en signifikant del av last–respons samvirket hvis den høyeste inkluderte frekvensen i den tidsavhengige deterministiske gjennomsnittlige vindhastigheten er større enn omtrent 1/50 av fundamentalegensvingefrekvensen til Hardangerbroen. Inkluderes frekvensbidrag over denne grensen vil gyldigheten av en responsberegning i frekvensplanet bli krenket og den dynamiske responsen til systemet synes i så tilfelle å bli overestimert.

TABLE OF CONTENTS

LIST OF TABLES

LIST OF FIGURES

1 STATIONARY BUFFETING THEORY

1.1 DESCRIPTION AND FORMULATION OF A STOCHASTIC WIND FIELD

1.1.1 Characteristics of structural wind loading

According to Strømmen (2006, p. 1–3), the interaction between the airflow and the structure can take place in primarily two fundamentally different ways. The first one, which may occur for mostly low mean wind speeds is called *vortex shedding*. Vortex shedding takes place when friction and sharp edges on the surface of the structure causes the oncoming airflow to separate and being shed into the wake of the structure, alternating from side to side at a certain frequency. These “shedded vortices” causes net pressure differences over the surface of the structure and thus oscillating structural forces.

As the mean wind velocity increases, *buffeting* will eventually become the predominant type of flow/structure interaction. Buffeting is simply characterized by the fact that the turbulence in the oncoming airflow produces fluctuating forces on the structure in a direct manner rather than in the case of vortex shedding, where it is the shedded, alternating vortices in the wake of the structure that produces the vortex shedding loads, and not the oncoming airflow itself. If the mean wind speed increases even more, *motion induced load effects*, or *self–excited forces*, will be present. This phenomenon arises when the oscillations of the structure becomes large enough to interact with the turbulence in the oncoming airflow such that further forces are generated.

In this thesis, whose purpose is to examine the effect of non–stationary buffeting winds, the effect of vortex shedding is not investigated.

1.1.2 Stochastic processes

As in the case of most physical processes, the wind field is a *stochastic process*. According to Strømmen (2006, p. 4), a physical process is labelled stochastic “if its numerical outcome at any time or position in space is random and can only be predicted with a certain probability”. Every stochastic process has certain characteristics and can therefore be described mathematically by certain parameters. In this context, the term “random” indicates that a recording of a certain process is only “one particular set of realizations of the process” (Strømmen 2006, p. 4).

Strømmen (2006, p. 5) further emphasizes that the wind field as a stochastic process can be treated at two levels of randomness, namely *time domain statistics* (short term), and *ensemble statistics* (long term). Time domain statistics involves the probability distribution of the *turbulent part* (see chapter 1.1.5) of the wind field itself, while ensemble statistics has to do with the probability distribution of parameters such as the average value, maximum value and variance of a recording with arbitrary length, T, both being important concepts in the buffeting theory.

1.1.3 Stationary processes

A *stationary process* is a process whose statistical parameters does not change with time. To determine the characteristic parameters of a stochastic wind field recording, first and foremost its mean wind speed and variance, an averaging process over a time window of sufficient length must be carried out. Obviously, sudden short time variations in the wind speed recording such as gusts will render a relatively large variation in the numerical values of the aforementioned parameters if they are calculated over a correspondingly short time period, however, stationarity will generally not hold if the averaging period is disproportionally long because weather changes with time. As suggested by Strømmen (2006, p. 54), the time period used for determining the mean value and variation of a presumed stationary wind speed recording is therefore usually set to $T = 10$ minutes.

In thesis, *stationarity* is not treated as being a binary term in any way, because there is no definite boundary that separates stationary recordings from non–stationary ones. The reason for this is that the characteristics of the wind field must be put into context because it is the very response of the structure onto which it causes dynamic loading that is of particular interest. Therefore, one cannot take for granted that if a given wind field with good reason really can be treated as being stationary when action on structure A, it can also be treated as being stationary when action on structure B. Structure A and B might have widely different eigenfrequencies, hence the relationship between input and output will also be different. Clearly, this concept can be illustrated when letting structurs A and B be a long–span, slender suspension bridge, and a 10 m telephone line, respectively, in which them both are subjected to wind induced loads from the same wind field. Nevertheless, chapter 2 presents the theoretical framework for calculating buffeting response when the wind loading is considered as being strictly stationary.

1.1.4 Homogeneous processes

Analogous to a stationary process, the input parameters of a *homogenous process* do not change in space. In the case of a bridge, such may sound reasonable since the size of the weather system creating the local wind field is usually very large compared to the structure itself. However, since the turbulent part of the wind field is created due to friction with the ground, local terrain or nearby obstacles may obstruct the wind field such that one can no longer assume constant wind field parameters across the span of a long horizontal structure such as a suspension bridge. However, different non–homogeneous effects are not included in this thesis and every wind field parameter is therefore set to be constant across the bridge span.

1.1.5 Coordinate system and key definitions

Strømmen (2006, p. 8) adopts the following definition of the coordinate system used for a stationary wind field. The mean wind velocity, V, is defined as the average value of the wind speed in the direction of the respective average wind direction over a period of $T = 10$ minutes. Then, one can introduce an airflow specific Cartesian coordinate system in which the x_f–axis (sub index "f" for air flow) is parallel to the mean wind direction. Such an orientation is of great convenience because the mean wind speed in the y_f–, and z_f–directions thus will be zero, and any wind in these directions is then exclusively turbulence. In theory, V will vary in all three special coordinates and time, which renders the general expression for the wind speed components,

$$\begin{aligned} U &= V(x_f, y_f, z_f, t) + u(x_f, y_f, z_f, t) \\ v &= v(x_f, y_f, z_f, t) \\ w &= w(x_f, y_f, z_f, t) \end{aligned} \tag{1.1}$$

Normal practice is to define the mean wind direction to be horizontal and perpendicular to the bridge girder. Assuming stationarity and homogeneousness implies V to be independent of t and y_f, respectively. The effect of the vertical mean wind profile described by Strømmen (2010, p. 53–54.) together with the upward facing arc of the bridge girder is also neglected, thus excluding z_f from the variable portfolio in equation 1.1. According to the defined orientation of the wind field coordinate system, x_f is constant along the bridge span, thus making equation 1.1 take the following form,

$$\begin{aligned} U &= V + u(y_f, t) \\ \mathrm{v} &= v(y_f, t) \\ \mathrm{w} &= w(y_f, t) \end{aligned} \tag{1.2}$$

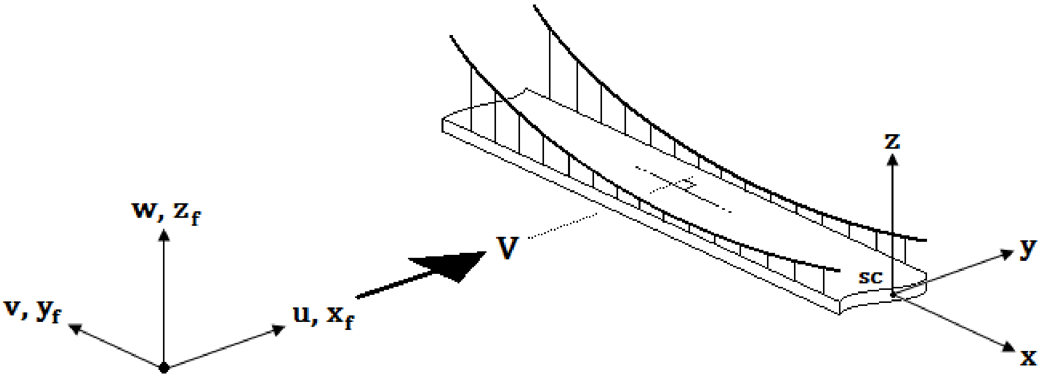

Figure 1.1: Wind field specific–, and structural coordinate system.

1.1.5.1 Variance

The variance of a stochastic, zero–mean variable x is given by,

$$Var(x) = \sigma_x^2 = E\left[(x(t))^2\right] = \frac{1}{T}\int_0^T (x(t))^2 dt \tag{1.3}$$

The mean value of the U–component is obviously not zero, but because being constant, it gives no contribution to the total variance. Therefore, U must intuitively have the same variance as u. The variances of the wind components U, v and w in equation 1.1 is given by the integral expression in equation 1.3 where $x(t)$ is simply replaced by $u(y_f, t)$, $v(y_f, t)$ and $w(y_f, t)$, respectively. As before, wind field homogeneousness sets the variance as being constant along the bridge span.

1.1.5.2 Turbulence integral length scales

The turbulence integral length scales of a wind field are indirect measures of its average local shape. Together with the mean value and variance it is an important tool for describing the stochastic characteristics of a wind field. According to Strømmen (2006, p. 65) its general definition, having assumed stationarity is given by,

$${}^{s}L_n = \frac{1}{\sigma_n^2}\int_0^\infty \left[\frac{1}{T}\int_0^T n(s,t) \cdot m(s+\Delta s, t)\, dt\right] d\Delta s, \quad \begin{cases} n, m = u, v, w \\ s = x_f, y_f, z_f \end{cases} \tag{1.4}$$

The integral expression inside the brackets in equation 1.4 is the cross covariance between the processes n and m with a spatial separation, Δs. Increasing Δs from zero to infinity will according to Strømmen (2006, p. 65) generally give a corresponding decrease in the cross–covariance function from σ_n^2 to zero with a shape–wise similarity to an exponential function with a negative argument.

There are generally 3 choices for both n, m, and s, rendering $3^2 = 27$ possible different length scales. However, flow components u, v and w can be considered mutually independent (Strømmen 2006, p. 64) hence, $n = m$ is the only interesting consideration. Also, as shall be seen in chapter 1.1.6.2, the only length scales required to obtain statistical information about the turbulence components u and w, are ${}^{y}L_u$ and ${}^{y}L_w$.

Equation 1.4 suggests that in order to calculate the relevant turbulence integral length scales one must have anemometers installed at a number of points along the s–axis such that integration with respect to Δs can be performed with sufficient accuracy. However, this is highly inconvenient for practical purposes because anemometers can usually only be installed at a single point along the flow axis. Nevertheless, length scales ${}^{y}L_u$ and ${}^{y}L_w$ can be calculated from single point wind recordings by instead introducing a similar parameter, namely the *integral time scale*. Using this, Strømmen (2006, p. 61) defines the length scales ${}^{y}L_u$ and ${}^{y}L_w$ as the respective integral time scale multiplied with the mean wind speed, namely,

$$ {}^{y}L_n = V \cdot T_n = V \cdot \frac{1}{\sigma_n^2} \int_0^\infty \left[\frac{1}{T} \int_0^T n(t) \cdot n(t + \Delta t)\, dt \right] d\Delta\tau\,, \quad n = u, w \qquad (1.5) $$

1.1.6 Transformation to frequency domain

1.1.6.1 Motivation

The solution to a dynamic response problem is usually associated with the time history of the response, namely the solution function of the governing differential equations. Frankly, the very time history of the response is not the primary interest for a problem like the one at hand, because, “if a physical event may mathematically be described by certain laws of nature, a stochastic input will provide a stochastic output” (Strømmen, 2006, p. 4). Hence, the output is only one of infinitely many possible realizations of the stochastic process it represents. To get around this problem, a more convenient solution strategy is introduced, such that the variance of the structural response may be obtained directly, in contrast to being estimated from a large number of individual time domain solution functions (so–called *Monte Carlo simulations*).

The fundamental principle of the aforementioned solution strategy is surprisingly simple and intuitive and consists of several steps in which the first one is expressing the fluctuating parts of the wind field recording (equation 1.2) as a finite set of orthogonal harmonic components using a Fourier decomposition. From then on, the contribution to the total variance of the dynamic response from each harmonic component will be established in the form of “intermediary” functions which depend on the aerodynamical and dynamic properties of the bridge. The key steps in this procedure will be explained in the following.

1.1.6.2 Power spectral density

The *power spectral density* (PSD) of a signal, sometimes denoted by the *auto spectral density*, is its distribution of variance over the frequency axis. The mathematical procedure of obtaining the Fourier components of any signal $x(t)$ is given by equation 1.6:

$$\begin{Bmatrix} a_k \\ b_k \end{Bmatrix} = \frac{2}{T}\int_0^T x(t)\begin{Bmatrix} \cos(\omega_k t) \\ \sin(\omega_k t) \end{Bmatrix} dt \qquad \text{where} \qquad \begin{cases} k = 1,2,3,\dots \\ \omega_k = \Delta\omega \cdot k = \dfrac{2\pi}{T} \cdot k \end{cases} \tag{1.6}$$

Such that,

$$x(t) = \sum_{k=1}^{\infty} a_k \cos(\omega_k t) + b_k \sin(\omega_k t) \tag{1.7}$$

This general definition in a real format with a signal not necessarily having any symmetries with respect to $T = 0$, demands two nonzero constants a_k and b_k for each harmonic component. However, what we seek is the amplitude, c_k, of each component which can easily be obtained from equation 1.8.

$$c_k = \sqrt{a_k^2 + b_k^2} \tag{1.8}$$

$$\varphi_k = arctan\left(\frac{b_k}{a_k}\right) \tag{1.9}$$

The phase lag, φ_k, is of no particular interest for the purpose of obtaining the power spectral density because it only describes the stochastic properties of the wind field presented in chapter 1.1.2. Nevertheless, with the introduction of equations 1.8 and 1.9, eq. 1.7 can be expressed as,

$$x(t) = \sum_{k=1}^{\infty} X_k(\omega_k t) = \sum_{k=1}^{\infty} c_k \cos(\omega_k t + \varphi_k) \tag{1.10}$$

The calculation of the variance of harmonic component X_k is trivial, namely,

$$\begin{aligned} Var\big(X_k(\omega_k t)\big) &= E\big[c_k^2 \cdot cos^2(\omega_k t + \varphi_k)\big] \\ &= c_k^2 \cdot \frac{1}{\pi}\int_0^{\pi} cos^2(t)dt \\ &= \frac{c_k^2}{2} \end{aligned} \tag{1.11}$$

At this moment, one may introduce the very definition of the auto spectral density, namely,

$$S_x(\omega_k) \equiv \frac{Var\big(X_k(\omega_k t)\big)}{\Delta\omega} = \frac{c_k^2}{2 \cdot \Delta\omega} \tag{1.12}$$

where $\Delta\omega$ obeys the definition in equation 1.6. With this definition, every component will have period T, and they will be mutually orthogonal, that is, the covariance between them all is exactly equal to zero. This very fact gives birth to the most central property of the PSD function and indeed its mathematical convenience, namely that the variance of the sum of all components is equal to the sum of the variances of the components themselves,

$$\sigma_x^2 \quad \approx \quad var\left[\sum_{k=1}^{\infty} X_k\right] \quad = \quad \sum_{k=1}^{\infty} \sigma_{X_k}^2 \quad = \quad \sum_{k=1}^{\infty} S_x(\omega_k) \cdot \Delta\omega \tag{1.13}$$

For a stationary recording of infinite length, T, $\Delta\omega$ will correspondingly approach zero and thus giving the continuously defined counterparts of equations 1.12 and 1.13, namely,

$$S_x(\omega) \quad = \quad \lim_{\Delta\omega \to 0} \frac{Var\big(X(\omega, t)\big)}{\Delta\omega} \quad = \quad \lim_{\Delta\omega \to 0} \frac{c_k^2}{2 \cdot \Delta\omega} \tag{1.14}$$

$$\sigma_x^2 \quad = \quad \int_0^{\infty} S_x(\omega) d\omega \tag{1.15}$$

The recent presentation and definition of the power spectral density of an arbitrary stochastic signal has been performed in the real number domain, which is nothing but intuitive for the sake of calculating the Fourier components of the given signal. Unfortunately, this real–valued formulation is rather inconvenient when it comes to establishing a formulation of the dynamic response in the frequency domain. If, however, the power spectral density is formulated using the mathematical tool of complex numbers, the formulation of the dynamic response calculations becomes much easier to establish. Strømmen (2006, p. 36 – 38) presents the deductive reasoning leading up to the complex expression for the power spectral density which as from now is defined in the following way:

$$x(t) \; = \sum_{\pm\omega_1}^{\pm\omega_\infty} a_k e^{i\omega_k t}, \qquad a_k \; = \int_0^T x(t)\, e^{-i\omega_k t} dt\,, \qquad \begin{cases} k = 1,2,3,\ldots \\ \omega_k = \dfrac{2\pi k}{T} \end{cases} \tag{1.16}$$

$$S_x(\omega_k) = \frac{1}{\pi T} a_k \cdot a_k^* \tag{1.17}$$

Taking the limit of equation 1.17 as T approaches infinity gives the definition of the power spectral density of a stochastic, stationary signal on the format which will be used in the dynamic response calculation, namely,

$$S_x(\omega) \quad = \quad \lim_{T \to \infty} \frac{1}{\pi T} \cdot a(\omega)\, a^*(\omega) \tag{1.18}$$

where the superscript, *, denotes the complex conjugate.

When the PSD of a signal is calculated scatter will always occur, no matter the signal length. The convergence–like behaviour that one usually expects to see in many estimation procedures of physical quantities are absent in the case of the PSD. This has to do with the properties of the Fourier transform. Hence as will be demonstrated in chapter 1.3, a mathematical function that serves as a best–fit approximation, is needed. According to Strømmen (2006, p. 62 – 63) many such functions has been suggested, however, the expressions suggested by Kaimal (1972) and von Kármán (1948) is often seen in literature. Kaimal's definition is given by,

$$\frac{\omega \cdot S_n(\omega)}{\sigma_n^2} \quad = \quad \frac{A_n \cdot \hat{\omega}_n}{\left[1 + 1.5 \cdot A_n \cdot \hat{\omega}_n\right]^{5/3}} \quad \text{where} \quad \begin{cases} n = u, v, w \\ \hat{\omega}_n = \omega \cdot \dfrac{{}^{y}L_n}{U} \end{cases} \tag{1.19}$$

${}^{y}L_n$ is the integral length scale of turbulence component n in structural coordinate direction y. von Kármán’s spectrum formulae are similar but exhibits a somewhat sharper transition between the magnitude of low and high frequency content as well as being specialized to fit the behaviour of turbulence components parallel and perpendicular to the mean wind speed direction. They are given by,

$$\frac{\omega \cdot S_u(\omega)}{\sigma_u^2} = \frac{4 \cdot \widehat{\omega}_u}{[1 + 70.8 \cdot \widehat{\omega}_u^2]^{5/6}} \tag{1.20}$$

$$\frac{\omega \cdot S_n(\omega)}{\sigma_n^2} = \frac{4 \cdot \widehat{\omega}_n \cdot [1 + 755.2 \cdot \widehat{\omega}_n^2]}{[1 + 283.2 \cdot \widehat{\omega}_n^2]^{11/6}} \quad \text{where} \quad n = v, w \tag{1.21}$$

1.1.6.3 Cross spectral density and normalized Co–spectrum

The *cross spectral density* between two stochastic processes gives the distribution of covariance between their respective Fourier components over the omega axis. When formulated for the specific use in this very context, a complex valued method used to define the power spectral density might just as well be adopted. Consider two stochastic processes $x(t)$ and $y(t)$ with their respective Fourier component expansions,

$$\left\{\begin{matrix} x(t) \\ y(t) \end{matrix}\right\} = \sum_{k=\pm 1}^{\pm\infty} \left\{\begin{matrix} X_k(\omega_k, t) \\ Y_k(\omega_k, t) \end{matrix}\right\} = \frac{1}{T} \sum_{k=\pm 1}^{\pm\infty} \left\{\begin{matrix} a_{X_k}(\omega) \\ a_{Y_k}(\omega) \end{matrix}\right\} e^{i\omega_k t} \tag{1.22}$$

where,

$$\left\{\begin{matrix} a_{X_k}(\omega) \\ a_{Y_k}(\omega) \end{matrix}\right\} = \int_0^T \left\{\begin{matrix} x(t) \\ y(t) \end{matrix}\right\} e^{-i\omega_k t} dt \tag{1.23}$$

Analogous to equation 1.18, the cross spectral density of the two processes $x(t)$ and $y(t)$ is given by,

$$S_{xy}(\omega) = \lim_{T\to\infty} \frac{1}{\pi T} \cdot a_X(\omega) a_Y^*(\omega) \tag{1.24}$$

Due to Fourier component orthogonality, the summation properties in equation 1.13 applies to the total covariance between $x(t)$ and $y(t)$ in an analogue manner, namely,

$$\begin{aligned} Cov_{\substack{xy \\ yx}} &\approx Cov\left(\sum_{\omega_k = \pm\omega_1}^{\pm\infty} \begin{smallmatrix} X_k \\ Y_k \end{smallmatrix}(\omega_k) \ , \sum_{\omega_k = \pm\omega_1}^{\pm\infty} \begin{smallmatrix} Y_k \\ X_k \end{smallmatrix}(\omega_k) \right) \\ &= \sum_{\omega_k = \pm\omega_1}^{\pm\infty} Cov\left(\begin{smallmatrix} X_k \\ Y_k \end{smallmatrix}(\omega_k), \begin{smallmatrix} Y_k \\ X_k \end{smallmatrix}(\omega_k) \right) \end{aligned} \tag{1.25}$$

$$= \sum_{\omega_k = \pm\omega_1}^{\pm\infty} \underset{yx}{Sxy}(\pm\omega_k)\,\Delta\omega$$

In the specific case of a suspension bridge onto which a stochastic wind field is creating structural loads across its span, what is sought is an expression for the cross spectral density of two stochastic wind speed recordings along the span, separated with a given distance, Δs. Wind field homogeneousness implies that two such recordings $x(t)$ and $y(t)$ at separate locations are simply two unique realizations of the same process (Strømmen, 2006, p. 43). The cross spectral density between them is then rewritten to the more convenient formulation,

$$S_{xy}(\omega) \quad = \quad S_{xx}(\omega, \Delta s) \tag{1.26}$$

As can be seen from equation 1.24, $S_{xy}(\omega)$ itself will generally be complex since $a_X(\omega)$ is not the complex conjugate of $a_Y(\omega)$. According to Strømmen (2006, p. 40), the real part of $S_{xy}(\omega)$ is an even function of ω labelled the *Co–spectral density*, $Co_{xy}(\omega)$, or in this case, $Co_x(\omega, \Delta s)$. Normal practice is to normalize the Co–spectrum with respect to the auto spectral density of the single point process $x(t)$, namely,

$$\hat{C}o_x(\omega, \Delta s) \; = \; \frac{Co_x(\omega, \Delta s)}{S_x(\omega)} \tag{1.27}$$

thus giving the following expression for the cross spectral density of two spatially separated recordings along the bridge span,

$$Re[S_{xx}(\omega, \Delta s)] \quad = \quad S_x(\omega) \cdot \hat{C}o_x(\omega, \Delta s) \tag{1.28}$$

Strømmen (2010, p. 67) states that the following approximation for the normalized Co–spectrum may be used,

$$\hat{C}o_x(\omega, \Delta s) \quad = \quad exp\left(-c_{ns} \cdot \frac{\omega \Delta s}{U}\right) \quad \text{where} \quad \begin{cases} n = u, v, w \\ s = \; x_f, x_f, z_f \end{cases} \tag{1.29}$$

As per now, only the real part of $S_{xx}(\omega, \Delta s)$ has been established. Obviously, the covariance between two real valued variables cannot be complex, however, the reason for this complex formulation is simply as stated by Strømmen (2010, p. 67) that during the crucial step of the dynamic response calculations in the frequency domain called *spatial averaging*, all imaginary parts cancel out. Hence, only the real value of the cross spectrum needs to be included in the first place and is given by equations 1.28 and 1.29.

1.2 ESTABLISHMENT OF BUFFETING LOADS

1.2.1 Introduction

Again, it must be emphasized that this thesis investigates the nature and effects of wind buffeting exclusively with this being the only existing load effect on the structure, even though such an assumption is not always suitable.

For all practical purposes wind loading is a nonlinear process. A requirement for making the transformation to the frequency domain mathematically convenient, is linearizing the wind loading with respect to the flow components, u and w. Such an approximation may sound inaccurate and somewhat nonshalant, but in the following it will be demonstrated that such is feasible.

All the calculations, assumptions and simplifications done in chapters 1.2.2–1.2.4 are in direct correspondence with the ones done by Strømmen (2010, p. 91–99).

1.2.2 Displacement components, mean and fluctuating part

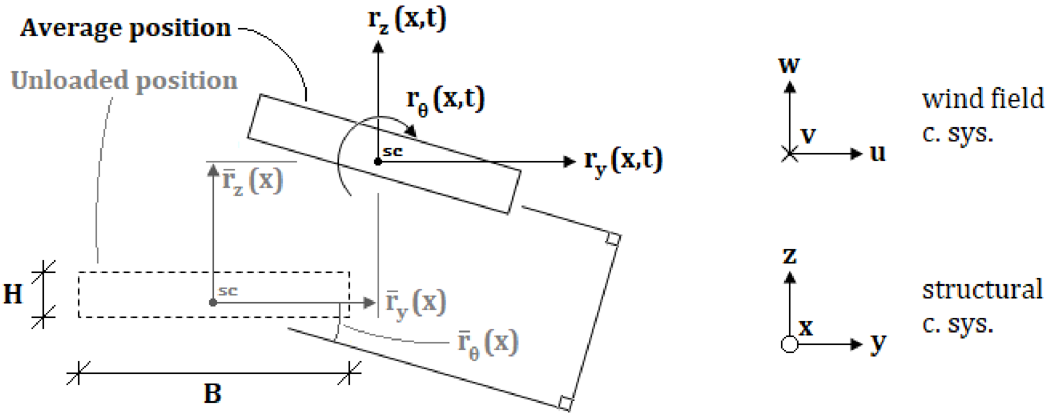

Figure 1.2: Mean value of displacement components

As illustrated in figure 1.2, the displacements of the bridge girder can, similarly to the wind field flow components, be split into a constant (average) part and a zero–mean fluctuating part,

$$\boldsymbol{r}_{tot}(x,t) \quad = \quad \bar{\boldsymbol{r}}(x) + \boldsymbol{r}(x,t) \quad = \quad \begin{Bmatrix} \bar{r}_y(x) \\ \bar{r}_z(x) \\ \bar{r}_\theta(x) \end{Bmatrix} + \begin{Bmatrix} r_y(x,t) \\ r_z(x,t) \\ r_\theta(x,t) \end{Bmatrix} \tag{1.30}$$

The idea behind dividing all time dependent variables into a mean, time invariant part and a zero–mean fluctuating part is simply because variance and covariance properties can be calculated from the fluctuating variables directly. Obviously, a static input gives a static output, and because the governing equations of our dynamic system are linear, the fluctuating output can be calculated on the basis of the fluctuating input due to the *principle of superposition* which applies to all linear systems.

1.2.3 Calculation of buffeting loads

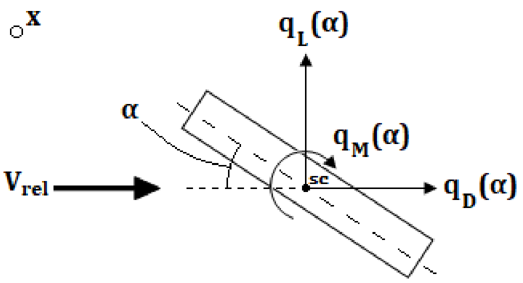

Figure 1.3: Cross–sectional force resultants

Initially, the simple schematic situation illustrated in figure 1.3 is considered. When the oncoming air molecules meets the bridge girder, they will undergo a change in both speed and direction, thus creating net pressure differences across the surface of the bridge girder according to Bernoulli's principle of energy conservation. For simplicity, the drag–, lift–, and pitch moment resultants can each be expressed as a constant multiple of the stagnation pressure,

$$\boldsymbol{q}(x,t) \quad = \quad \begin{Bmatrix} q_D(x,t) \\ q_L(x,t) \\ q_M(x,t) \end{Bmatrix} \quad = \quad \frac{1}{2}\rho V_{rel}^2 \begin{Bmatrix} D \cdot C_D(\alpha) \\ B \cdot C_L(\alpha) \\ B^2 \cdot C_M(\alpha) \end{Bmatrix} \tag{1.31}$$

Where C_D, C_L and C_M are called load coefficients, and are dimensionless numbers obtained from practical or numerical experiments. D, B and B^2 is simply included to maintain correct dimensions. As one might expect, the load resultants will change with the angle of incidence, α. For simplicity, this behaviour is implemented into the load coefficients, so that only they change with the angle of incidence, α.

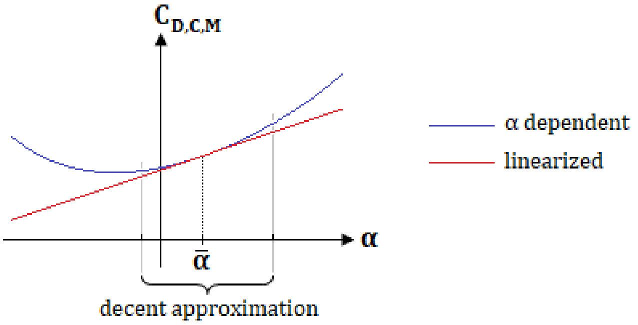

Figure 1.4: Non–linear load coefficients

The relationship between the angle of incidence and the load coefficients themselves is not necessarily linear, as illustrated in figure 1.4. To meet the requirement of load linearity, they are linearized as a first order Taylor series expansion about $\alpha = \bar{\alpha}$,

$$\begin{Bmatrix} C_D(\alpha) \\ C_L(\alpha) \\ C_M(\alpha) \end{Bmatrix} \approx \begin{Bmatrix} C_D(\bar{\alpha}) \\ C_L(\bar{\alpha}) \\ C_M(\bar{\alpha}) \end{Bmatrix} + \alpha_f \cdot \frac{\partial}{\partial \alpha} \begin{Bmatrix} C_D(\bar{\alpha}) \\ C_L(\bar{\alpha}) \\ C_M(\bar{\alpha}) \end{Bmatrix} = \begin{Bmatrix} \bar{C}_D \\ \bar{C}_L \\ \bar{C}_M \end{Bmatrix} + \alpha_f \cdot \begin{Bmatrix} C_D' \\ C_L' \\ C_M' \end{Bmatrix} \tag{1.32a}$$

where α_f is the fluctuating part of the angle of incidence,

$$\alpha_f = \alpha - \bar{\alpha} = \beta + r_\theta \tag{1.32b}$$

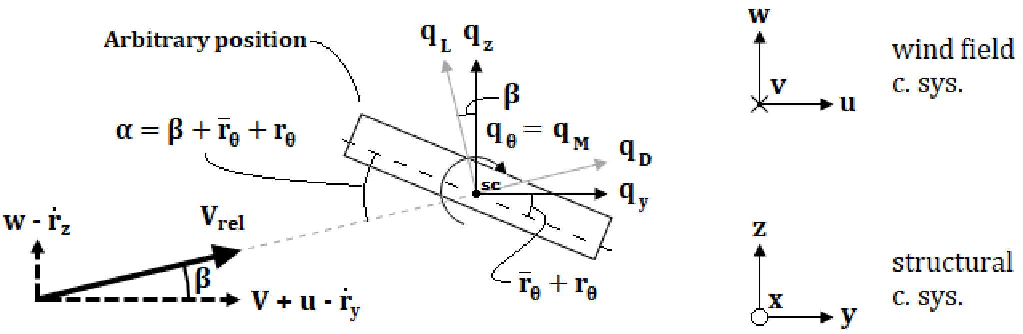

Figure 1.5: Wind load actions in local and global coordinate system.

Figure 1.5 considers the same loading actions illustrated in figure 1.3 but now from a global perspective. Intuitively, V_{rel} is equal to the closing speed between the airflow and the bridge girder, and because the velocity components of structural motion in some cases might reach the same order of magnitude as the wind turbulence components, they must equally be included in the expression of V_{rel}. This very fact gives raise to what in chapter 1.1.1 was labelled as motion induced load effects or self–excited forces. In accordance with figure 1.5, Pythagoras gives,

$$V_{rel}^2 = (V + u - \dot{r}_y)^2 + (w - \dot{r}_z)^2 \tag{1.33}$$

As one can see from figure 1.5 the direction of V_{rel} also varies with time as a function of the instant values of the fluctuating wind components and structural velocities. Therefore, so will the drag–, lift–, and pitch moment. For them to be projected onto the coordinate system in which the structural displacements are defined, the following coordinate transform must be applied,

$$\boldsymbol{q}_{tot}(x,t) = \begin{Bmatrix} q_{y,tot}(x,t) \\ q_{z,tot}(x,t) \\ q_{\theta,tot}(x,t) \end{Bmatrix} = \begin{bmatrix} \cos\beta & -\sin\beta & 0 \\ \sin\beta & \cos\beta & 0 \\ 0 & 0 & 1 \end{bmatrix} \begin{Bmatrix} q_D(x,t) \\ q_L(x,t) \\ q_M(x,t) \end{Bmatrix} \tag{1.34a}$$

where,

$$\beta = \arctan\left(\frac{w - \dot{r}_z}{V + u - \dot{r}_y}\right) \tag{1.34b}$$

The combination of equations 1.31 – 1.34 will render the general expression for the total buffeting load in the structural coordinate system. However, a few more linearizations must be used in order for

$\boldsymbol{q}_{tot}$ to be linearly dependent on the wind turbulence components and structural velocities. What gives raise to such a linearization is the fact that V is relatively large in comparison with namely the turbulence components and structural velocities. First, consider the fully expanded version of equation 1.33. Knowing that when u, w, $\dot{r}_y$, $\dot{r}_z$ and r_θ are small compared to V, then u^2, w^2 and $u \cdot v$ etc., will be even smaller compared to V^2 thus rendering,

$$V_{rel}^2 \quad = \quad (V + u - \dot{r}_y)^2 \;+\; (w - \dot{r}_z)^2 \quad \approx \quad V^2 + 2Vu - 2V\dot{r}_y \tag{1.35}$$

As for β in equation 1.34b, the denominator is likewise approximated as being constant such that the fraction becomes linear. w and $\dot{r}_z$ are still small compared to V such that,

$$\cos\beta \;\approx\; 1 \tag{1.36a}$$

$$\sin\beta \approx \tan\beta \;\approx\; \arctan\beta \;\approx\; \beta \;\approx\; \frac{w - \dot{r}_z}{V} \tag{1.36b}$$

At this point, all formulas that are to be combined, are successfully linearized. However, when the linear formulas are combined, multiplication between linear terms will create nonlinear terms. These terms can be omitted similarly as in equation 1.35. The final linearized version of equation 1.34a then becomes,

$$\boldsymbol{q}_{tot}(x,t) \quad = \quad \begin{Bmatrix} \bar{q}_y(x) \\ \bar{q}_z(x) \\ \bar{q}_\theta(x) \end{Bmatrix} + \begin{Bmatrix} q_y(x,t) \\ q_z(x,t) \\ q_\theta(x,t) \end{Bmatrix} \quad = \quad \bar{\boldsymbol{q}} + \boldsymbol{B}_q \boldsymbol{v} + \boldsymbol{C}_{ae}\dot{\boldsymbol{r}} + \boldsymbol{K}_{ae}\boldsymbol{r} \tag{1.37a}$$

where,

$$\boldsymbol{v}(x,t) \quad = \quad \begin{Bmatrix} u \\ w \end{Bmatrix} \tag{1.37b}$$

$$\bar{\boldsymbol{q}} \quad = \quad \begin{Bmatrix} \bar{q}_y \\ \bar{q}_z \\ \bar{q}_\theta \end{Bmatrix} \quad = \quad \frac{\rho V^2 B}{2} \cdot \hat{\boldsymbol{b}}_q \quad = \quad \frac{\rho V^2 B}{2} \cdot \begin{Bmatrix} (D/B)\bar{C}_D \\ \bar{C}_L \\ B\bar{C}_M \end{Bmatrix} \tag{1.37c}$$

$$\boldsymbol{B}_q \quad = \quad \frac{\rho V B}{2} \cdot \hat{\boldsymbol{B}}_q \quad = \quad \frac{\rho V B}{2} \cdot \begin{bmatrix} 2(D/B)\bar{C}_D & (D/B)C_D' - \bar{C}_L \\ 2\bar{C}_L & C_L' + (D/B)\bar{C}_D \\ 2B\bar{C}_M & BC_M' \end{bmatrix} \tag{1.37d}$$

$$\boldsymbol{C}_{ae} \quad = \quad -\frac{\rho V B}{2} \cdot \begin{bmatrix} \hat{\boldsymbol{B}}_q & \underbrace{\mathbf{0}}_{(3x1)} \end{bmatrix} \tag{1.37e}$$

$$\boldsymbol{K}_{ae} \quad = \quad \frac{\rho V^2 B}{2} \cdot \begin{bmatrix} & (D/B)C_D' \\ \underbrace{\mathbf{0}}_{(3x2)} & C_L' \\ & BC_M' \end{bmatrix} \tag{1.37f}$$

Equations 1.37a and 1.37c shows that the buffeting loads indeed can be divided into a mean, time–invariant (static) part, and a zero–mean, fluctuating part. The static part is calculated from the system stiffness directly and treated independently of the fluctuating forces.

The idea behind formulating the motion dependent contributions as $\boldsymbol{K}_{ae}\boldsymbol{r}$ and $\boldsymbol{C}_{ae}\dot{\boldsymbol{r}}$, is simply because they consequently can be merged with the system stiffness–, and damping matrix, respectively, thus effectively changing the total stiffness and damping properties of the system. Hence, $\boldsymbol{C}_{ae}$ and $\boldsymbol{K}_{ae}$ are called the aerodynamic damping–, and stiffness matrix. One can see that the name *motion induced load effects* may seem more appropriate to describe the phenomenon than simply just *motion induced loads*, because $\boldsymbol{C}_{ae}$ and $\boldsymbol{K}_{ae}$ will not be mathematically treated as explicit loading contributions in the dynamic response calculations in chapter 1.3.

1.2.4 Improvements to buffeting load model

1.2.4.1 Motivation

The theory and calculations presented in chapter 1.2.3 is only a mathematical description of the aerodynamic forces acting on a generalized cross section with an arbitrary orientation, at an arbitrary time. Thus, apart from being linear, the formulation of the cross–sectional loads is not particularly specialized for a transformation into the frequency domain even though it was formulated and prepared for this future transformation. For this reason, it is according to Strømmen (2006, p. 96), “favourable to introduce two major improvements”.

1.2.4.2 Flow induced dynamic loads

The first improvement is as suggested by Strømmen (2006, p. 96), to let the flow induced dynamic loads, $\boldsymbol{B}_q\boldsymbol{v}$, be frequency dependent. Illustratively, Strømmens approach is to multiply the respective entries in $\hat{\boldsymbol{B}}_q$, with “so–called cross–sectional admittance functions”, namely,

$$\hat{B}_{q,ij}(\omega) \quad = \quad \hat{B}_{q,ij} \cdot A_{ij}(\omega) \qquad \text{where} \qquad \begin{cases} i = 1,2,3 \; or \; y,z,\theta \\ j = 1,2 \; or \; u,w \end{cases} \tag{1.38}$$

However, for the purpose of this thesis, a similar procedure is adopted, but the admittance functions are multiplied with the load coefficients directly,

$$C_n(\omega) \quad = \quad C_{n_0} \cdot \frac{1}{\left(1+a_n\frac{\omega B}{V}\right)^{b_n}} \qquad \text{where} \qquad C_n \quad = \quad \{\bar{C}_D, \bar{C}_L, \bar{C}_\theta, C_D', C_L', C_\theta' \tag{1.39}$$

The values of C_{n_0}, a_n and b_n can be found in Appendix C and are of course specific to the cross section of the bridge girder in question, in this case, the Hardanger Bridge. As can be seen from equation 1.39, $C_n(\omega)$ decreases from C_{n_0} to zero as ω increases from zero to infinity. The motivation behind such a behaviour is according to Strømmen (2006, p. 97) to “filter off load contributions at high frequencies”.

1.2.4.3 Aerodynamic stiffness and –damping matrices – Aerodynamic derivatives

The second improvement involves establishing a new set of entries in $\boldsymbol{C}_{ae}$ and $\boldsymbol{K}_{ae}$ which are more suitable in the formulated frequency domain framework. Unlike the flow induced dynamic loads, motion induced load effects turns out to be a modal phenomenon, and the shape of the functions which make up the entries in $\boldsymbol{C}_{ae}$ and $\boldsymbol{K}_{ae}$, the so–called *aerodynamic derivatives*, are best estimated through scaled wind tunnel tests where the modes they are associated with are under investigation. According to Strømmen (2010, p. 98), the aerodynamic derivates must be extracted as functions of $\hat{V}_i = V/(B\omega_i)$ because of "similarity requirements between model scale and full–scale conditions". The formulation of $\boldsymbol{C}_{ae}$ and $\boldsymbol{K}_{ae}$ is according to Strømmen (2010, p. 99),

$$\boldsymbol{C}_{ae} = \frac{\rho B^2}{2} \cdot \omega_i(V) \cdot \hat{\boldsymbol{C}}_{ae} \qquad \text{and} \qquad \boldsymbol{K}_{ae} = \frac{\rho B^2}{2} \cdot (\omega_i(V))^2 \cdot \hat{\boldsymbol{K}}_{ae} \tag{1.40a}$$

where,

$$\hat{\boldsymbol{C}}_{ae} = \begin{bmatrix} P_1^* & P_5^* & BP_2^* \\ H_5^* & H_1^* & BH_2^* \\ BA_5^* & BA_1^* & B^2A_2^* \end{bmatrix} \qquad \text{and} \qquad \hat{\boldsymbol{K}}_{ae} = \begin{bmatrix} P_4^* & P_6^* & BP_3^* \\ H_6^* & H_4^* & BH_3^* \\ BA_6^* & BA_4^* & B^2A_3^* \end{bmatrix} \tag{1.40b}$$

More specifically, it is the dimensionless functions P_k^*, H_k^* and A_k^* in equation 1.40b that is called the aerodynamic derivatives. Obviously, because they are extracted from wind tunnel tests, they also depend on the cross section in question and is specific to each considered case. For the purpose of this thesis and the considered Hardanger bridge, they are defined on the following form,

$$AD_i = p_1\hat{V}_i^3 + p_2\hat{V}_i^2 + p_3\hat{V}_i + p_4 \quad , \qquad \begin{cases} AD = P^*, H^*, A^* \\ i = 1,2,\dots,6 \end{cases} \tag{1.41a}$$

Where $p_1 - p_4$ are constants and can be found in Appendix B.

$$\hat{V}_i = \frac{V}{B \cdot \omega_i(V)} \tag{1.41b}$$

Because the magnitude of the motion induced load effects increases with V, the eigenfrequencies of the system will consequently change with V because the effective system stiffness changes. Therefore, iterations are required in order for the effective system stiffness and the eigenfrequencies to be in agreement with each other. However, as stated by Strømmen (2010, p. 100), "under normal circumstances, the effect of $\boldsymbol{K}_{ae}$ will only be of significant importance in the velocity region at or immediately below an instability limit (…) and the effects of the changes of ω_i with increasing V to the determination of the aerodynamic derivatives are most often only of minor importance". For the purpose of this thesis, the detection of any instability limits will not be given any attention, and the effect of an effective system stiffness that depends on V is consequently neglected.

1.3 DYNAMIC RESPONSE CALCULATIONS

1.3.1 Continuous system

1.3.1.1 Motivation

The system in question is formulated in a continuous format. The motivation behind this very choice can best be illustrated by suggesting the opposite. Namely, if a discrete format is chosen, a mesh of six degree–of–freedom beam elements would be given the role to approximate the structural system. The minimum number of beam elements is determined based on two major design limitations:

1. The ability to represent a certain number of eigenmodes with a sufficient level of accuracy.
2. The ability to represent the loading process across the bridge span with a sufficient level of accuracy, taking into account the nature of its expected shape–wise distribution.

As explained by Strømmen (2006, p. 73), the number of elements needed to adequately describe the dynamic response is considerably smaller than the number of elements needed to accurately represent the loading process. Hence, for the purpose of a frequency domain buffeting response calculation, using a discrete system formulation represents both computational inefficiency and mathematical inconvenience.

With this being said, an initial discrete formulation for the sake of calculating the eigenmodes might be highly efficient because of the relatively quick convergence rate that is usually associated with beam elements. The shape of the eigenmodes can be determined via finite Fourier series obtained by considering the discrete vectors of the relevant lengthwise degrees of freedom.

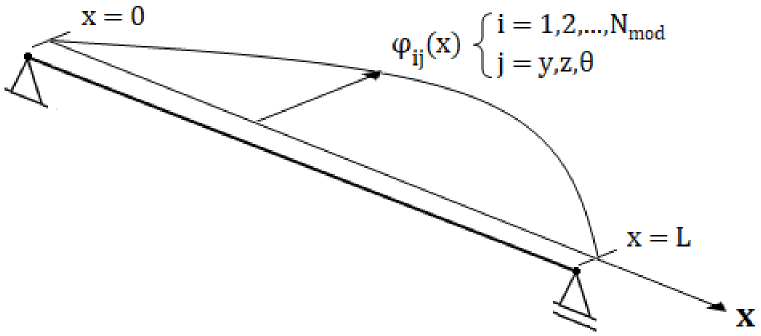

Figure 1.6: Continuous mode shape components

1.3.1.2 Formulation

As mentioned in chapter 1.3.1.1, the mode shapes of a continuously formulated system take the form of continuous functions rather than relative displacement vectors,

$$\boldsymbol{r}(x,t) = \begin{Bmatrix} r_y(x,t) \\ r_z(x,t) \\ r_\theta(x,t) \end{Bmatrix} \approx \sum_{i=1}^{N_{mod}} \begin{Bmatrix} \varphi_{iy}(x) \\ \varphi_{iz}(x) \\ \varphi_{i\theta}(x) \end{Bmatrix} \eta_i(t) = \boldsymbol{\phi}(x)\boldsymbol{\eta}(t) \tag{1.42a}$$

where,

$$\boldsymbol{\phi}(x) \;=\; \left[\boldsymbol{\varphi}_1(x) \;\; \boldsymbol{\varphi}_2(x) \cdots \boldsymbol{\varphi}_{N_{mod}}(x)\right] \tag{1.42b}$$

$$\boldsymbol{\eta}(t) \;=\; \left[\eta_1(t) \;\; \eta_2(t) \cdots \eta_{N_{mod}}(t)\right]^T \tag{1.42c}$$

As with any linear system, mode orthogonality and thereby mode superposition applies. Clearly, equation 1.42a depend absolutely on these features. An important question is how many eigenmodes one must include in order to represent the behaviour of the dynamic system in a satisfactory manner. For a short bridge with high stiffness, this number may be limited to only a few, however, in the case of a long and slender suspension bridge, several more will have to be included.

When a sufficiently numerous eigen–value solution is obtained, the dynamic equilibrium equations may be expressed in modal coordinates,

$$\widetilde{\boldsymbol{M}}_0\ddot{\boldsymbol{\eta}}(t) \;+\; \widetilde{\boldsymbol{C}}_0\dot{\boldsymbol{\eta}}(t) \;+\; \widetilde{\boldsymbol{K}}_0\boldsymbol{\eta}(t) \;=\; \widetilde{\boldsymbol{Q}}(t) \tag{1.43a)}$$

where,

$$\widetilde{\boldsymbol{M}}_0 \;=\; diag\left[\widetilde{M}_i\right] \tag{1.43b}$$

$$\widetilde{\boldsymbol{C}}_0 \;=\; diag\left[2\zeta_i\widetilde{M}_i\omega_i\right] \tag{1.43c}$$

$$\widetilde{\boldsymbol{K}}_0 \;=\; diag\left[\widetilde{M}_i\omega_i^2\right] \tag{1.43d}$$

$$\widetilde{\boldsymbol{Q}}(t) \;=\; \int_0^{L_{exp}} \boldsymbol{\phi}^T(x)\boldsymbol{q}_{tot}(x,t)dx \tag{1.43e}$$

where $\boldsymbol{q}_{tot}(x,t)$ in equation 1.57e corresponds to the fluctuating part of $\boldsymbol{q}_{tot}(x,t)$ in equation 1.51a. The subindices "0" in the characteristic matrices of the system simply denotes that the eigen–value solution from which they have been obtained is performed such that motion induced effects has zero contribution to their content.

The motion dependent terms in $\boldsymbol{q}_{tot}(x,t)$ (equation 1.37a) might now, according to the purpose of their specific formulation, be merged with $\widetilde{\boldsymbol{K}}_0$ and $\widetilde{\boldsymbol{C}}_0$ to form the mean wind speed dependent effective system stiffness and damping matrices. The governing equations of motion now takes the following and final form,

$$\widetilde{\boldsymbol{M}}_0\ddot{\boldsymbol{\eta}}(t) \;+\; \left[\widetilde{\boldsymbol{C}}_0 - \widetilde{\boldsymbol{C}}_{ae}\right]\dot{\boldsymbol{\eta}}(t) \;+\; \left[\widetilde{\boldsymbol{K}}_0 - \widetilde{\boldsymbol{K}}_{ae}\right]\boldsymbol{\eta}(t) \;=\; \widetilde{\boldsymbol{Q}}_v(t) \tag{1.44a}$$

where,

$$\widetilde{\boldsymbol{K}}_{ae} \;=\; \int_0^{L_{exp}} \boldsymbol{\phi}^T(x)\boldsymbol{K}_{ae}\boldsymbol{\phi}(x)dx \tag{1.44b}$$

$$\widetilde{\boldsymbol{C}}_{ae} = \int_{0}^{L_{exp}} \boldsymbol{\phi}^T(x)\boldsymbol{C}_{ae}\boldsymbol{\phi}(x)dx \tag{1.44c}$$

$$\widetilde{\boldsymbol{Q}}_v(t) = \int_{0}^{L_{exp}} \boldsymbol{\phi}^T(x)\boldsymbol{B}_q\boldsymbol{v}(x,t)dx \tag{1.44d}$$

1.3.2 Part 1: Cross spectral density of structural response components

The supreme goal of the dynamic response calculations is to obtain an expression for the variance of the structural displacement components, r_y, r_z, r_θ at the desired position $x = x_r$, usually at the midspan. As a convenient part of the solution strategy shown in the following, one might just as well define the covariance between all displacement components. This is done by introducing a so–called covariance matrix,

$$\boldsymbol{Cov}_{rr}(x_r) = \begin{bmatrix} \sigma_{r_y}^2 & Cov_{r_y r_z} & Cov_{r_y r_\theta} \\ Cov_{r_z r_y} & \sigma_{r_z}^2 & Cov_{r_z r_\theta} \\ Cov_{r_\theta r_y} & Cov_{r_\theta r_z} & \sigma_{r_\theta}^2 \end{bmatrix} \tag{1.45}$$

Fourier component orthogonality renders,

$$\boldsymbol{Cov}_{rr}(x_r) = \int_{0}^{\infty} \boldsymbol{S}_{rr}(x_r,\omega)d\omega = \int_{0}^{\infty} \left[S_{r_i r_j}\right] d\omega\,, \quad (i,j) = y,z,\theta \tag{1.46}$$

Because the governing equations of motion is linear, it is possible to establish a linear relation between the cross spectral density matrix, $\boldsymbol{S}_{rr}(x_r,\omega)$, and the cross spectral density of the modal loads. This starts with considering Fourier series expansions of the structural displacement components and the modal coordinates according to equation 1.16,

$$\boldsymbol{r}(x,t) = \sum_{\omega=0}^{\infty} \boldsymbol{a}_r(x,\omega)e^{i\omega t}, \qquad \boldsymbol{a}_r(x,\omega) = \begin{Bmatrix} a_{r_y}(x,\omega) \\ a_{r_z}(x,\omega) \\ a_{r_\theta}(x,\omega) \end{Bmatrix} \tag{1.47a}$$

$$\boldsymbol{\eta}(t) = \sum_{\omega=0}^{\infty} \boldsymbol{a}_\eta(\omega)e^{i\omega t}\,, \qquad \boldsymbol{a}_\eta(\omega) = \left\lfloor a_{\eta_1}(\omega) \cdots a_{\eta_{N_{mod}}}(\omega)\right\rfloor^T \tag{1.47b}$$

For the purpose of this procedure, the only appropriate thing will be to take these Fourier expansions over the same, infinite time period T, hence the sums will consequently be performed over the same values of ω. Hence, when equations 1.47a and 1.47b are inserted into equation 1.42a, the following must be true for every value of ω,

$$\boldsymbol{a}_r(x,\omega) = \boldsymbol{\phi}(x)\,\boldsymbol{a}_\eta(\omega) \tag{1.48}$$

Equation 1.24 gives the definition of the covariance between the structural displacement components which indeed are the entries of $\boldsymbol{S}_{rr}(x_r,\omega)$. On a matrix format, it is formulated as,

$$\begin{aligned}
\boldsymbol{S}_{rr}(x_r,\omega) &= \lim_{T\to\infty}\frac{1}{\pi T}\Big(\boldsymbol{\phi}(x)\,\boldsymbol{a}_{\eta}(\omega)\Big)^{*}\Big(\boldsymbol{\phi}(x)\,\boldsymbol{a}_{\eta}(\omega)\Big)^{T} \\
&= \lim_{T\to\infty}\frac{1}{\pi T}\Big(\boldsymbol{\phi}^{*}(x)\boldsymbol{a}_{\eta}^{*}(\omega)\Big)\Big(\boldsymbol{a}_{\eta}^{T}(\omega)\boldsymbol{\phi}^{T}(x)\Big) \\
&= \boldsymbol{\phi}(x)\left(\lim_{T\to\infty}\frac{1}{\pi T}\,\boldsymbol{a}_{\eta}^{*}(\omega)\,\boldsymbol{a}_{\eta}^{T}(\omega)\right)\boldsymbol{\phi}^{T}(x) \\
&= \boldsymbol{\phi}(x)\,\boldsymbol{S}_{\eta\eta}(\omega)\,\boldsymbol{\phi}^{T}(x)
\end{aligned} \tag{1.49}$$

Of course, $\boldsymbol{\phi}^{*}(x)=\boldsymbol{\phi}(x)$ because its entries are real.

Now, the same procedure will be adopted to $\boldsymbol{S}_{\eta\eta}(\omega)$ and the governing equations of motion as defined in equation 1.44a. Differentiating $\boldsymbol{\eta}(t)$ in equation 1.47b with respect to time is trivial because $\boldsymbol{a}_{\eta}(\omega)$ is time–invariant, hence the expressions for $\dot{\boldsymbol{\eta}}(t)$ and $\ddot{\boldsymbol{\eta}}(t)$ are simply constant multiples of $\boldsymbol{\eta}(t)$. The Fourier components of equation 1.44a then take the following form,

$$\boldsymbol{a}_{\eta}(\omega) \;=\; \widehat{\boldsymbol{H}}_{\eta}(\omega)\,\boldsymbol{a}_{\hat{Q}_v}(\omega) \tag{1.50a}$$

where,

$$\widehat{\boldsymbol{H}}_{\eta}(\omega) \;=\; \left[\boldsymbol{I}-\boldsymbol{\kappa}_{ae}-diag\left[\left(\frac{\omega}{\omega_i}\right)^{2}\right]+2i\cdot diag\left[\frac{\omega}{\omega_i}\right]\cdot(\boldsymbol{\zeta}-\boldsymbol{\zeta}_{ae})\right]^{-1} \tag{1.50b}$$

$$\boldsymbol{a}_{\hat{Q}_v}(\omega) \;=\; \widetilde{\boldsymbol{K}}_0^{-1}\boldsymbol{a}_{\tilde{Q}_v}(\omega) \tag{1.50c}$$

$$\boldsymbol{\kappa}_{ae} \;=\; \widetilde{\boldsymbol{K}}_0^{-1}\widetilde{\boldsymbol{K}}_{ae} \tag{1.50d}$$

$$\boldsymbol{\zeta}_{ae} \;=\; \frac{1}{2}\cdot diag[\omega_i]\cdot\widetilde{\boldsymbol{K}}_0^{-1}\widetilde{\boldsymbol{C}}_{ae} \tag{1.50e}$$

$$\boldsymbol{\zeta} \;=\; diag[\zeta_i] \tag{1.50f}$$

Analogous to equation 1.48 and 1.49 the relationship between $\boldsymbol{S}_{\eta\eta}(\omega)$ and $\boldsymbol{S}_{\hat{Q}_v}(\omega)$ emerges,

$$\boldsymbol{S}_{\eta\eta}(\omega) \;=\; \widehat{\boldsymbol{H}}_{\eta}^{*}(\omega)\,\boldsymbol{S}_{\hat{Q}_v}(\omega)\,\widehat{\boldsymbol{H}}_{\eta}^{T}(\omega) \tag{1.51}$$

Equation 1.46 and 1.50 finishes the calculation of the relationship between the cross spectral density matrix of the structural loads and the covariance matrix of the structural displacement components,

$$\boldsymbol{Cov}_{rr}(x_r) \quad = \quad \boldsymbol{\phi}(x_r)\left[\int_0^{\infty} \widehat{\boldsymbol{H}}_{\eta}^{*}(\omega)\, \boldsymbol{S}_{\hat{Q}_v}(\omega)\, \widehat{\boldsymbol{H}}_{\eta}^{T}(\omega) d\omega\right]\boldsymbol{\phi}^{T}(x_r) \tag{1.52}$$

1.3.3 Part 2: Formulation of cross spectral density of modal loads

Next up lies the establishment of the cross spectral density matrix for the structural loads, $\boldsymbol{S}_{\hat{Q}_v}(\omega)$, present in equation 1.52. Analogous to equation 1.48, the Fourier coefficients of $\boldsymbol{S}_{\hat{Q}_v}(\omega)$ will then be given by,

$$\boldsymbol{a}_{\hat{Q}_v}(x,\omega) \quad = \quad \widetilde{\boldsymbol{K}}_0^{-1}\int_0^{\infty} \boldsymbol{\phi}^{T}(x)\boldsymbol{B}_q\boldsymbol{a}_v(x,\omega)d\omega\ , \qquad \boldsymbol{a}_v(x,\omega) \quad = \quad \begin{Bmatrix} a_u(x,\omega) \\ a_w(x,\omega) \end{Bmatrix} \tag{1.53}$$

As per definition,

$$\boldsymbol{S}_{\hat{Q}_v}(\omega) \quad = \quad \lim_{T\to\infty}\frac{1}{\pi T}\,\widetilde{\boldsymbol{K}}_0^{-1}\left[\int_0^{L_{exp}} \boldsymbol{\phi}^{T}\boldsymbol{B}_q\boldsymbol{a}_v^{*}dx\right]\left[\int_0^{L_{exp}} \boldsymbol{a}_v^{T}\boldsymbol{B}_q^{T}\boldsymbol{\phi}dx\right]\widetilde{\boldsymbol{K}}_0^{-T} \tag{1.54}$$

To advance, a neat and clever reformulation of equating 1.54 is applied. This goes as follows. Since the matrix integrands inside the brackets in equation 1.54 is to be evaluated over the same integration domain, and then multiplied together, they may instead be multiplied together first and then integrated over the area defined by a square with sides L_{exp}, namely,

$$\boldsymbol{S}_{\hat{Q}_v}(\omega) \ = \widetilde{\boldsymbol{K}}_0^{-1}\left[\int_0^{L_{exp}}\int_0^{L_{exp}} \boldsymbol{\phi}^{T}(x_1)\boldsymbol{B}_q\left(\lim_{T\to\infty}\frac{1}{\pi T}\,\boldsymbol{a}_v^{*}(x_1,\omega)\boldsymbol{a}_v^{T}(x_2,\omega)\right)\boldsymbol{B}_q^{T}\boldsymbol{\phi}(x_2)dx_1dx_2\right]\widetilde{\boldsymbol{K}}_0^{-T} \tag{1.55}$$

The convenience of expressing equation 1.54 as equation 1.55 is obvious because the cross spectral density matrix of the wind field turbulence components, $\boldsymbol{S}_v(\Delta x,\omega)$, consequently may be introduced,

$$\boldsymbol{S}_{\hat{Q}_v}(\omega) \ = \widetilde{\boldsymbol{K}}_0^{-1}\left[\int_0^{L_{exp}}\int_0^{L_{exp}} \boldsymbol{\phi}^{T}(x_1)\boldsymbol{B}_q\,\boldsymbol{S}_v(\Delta x,\omega)\boldsymbol{B}_q^{T}\boldsymbol{\phi}(x_2)dx_1dx_2\right]\widetilde{\boldsymbol{K}}_0^{-T}\ , \quad \Delta x \quad = \quad |x_1 - x_2| \tag{1.56}$$

According to Strømmen (2006, p. 132), the spectral density between the components u and w can be assumed to be zero. Thus, $\boldsymbol{S}_v(\Delta x,\omega)$ takes the following form:

$$\boldsymbol{S}_v(\Delta x,\omega) \quad = \quad diag[S_{uu}(\Delta x,\omega)\ ,\ S_{ww}(\Delta x,\omega)] \tag{1.57a}$$

where $S_{nn}(\Delta x,\omega)$ can be defined from equation 1.28,

$$Re[S_{nn}(\Delta x,\omega)] \quad = \quad S_u(\omega)\cdot\hat{C}o_{nn}(\Delta x,\omega)\,, \qquad n = u,w \tag{1.57b}$$

Normal practice is to normalize $\boldsymbol{B}_q$ can be normalized as in equation 1.37d, and $\boldsymbol{S}_v(\Delta x,\omega)$ as,

$$\boldsymbol{S}_v(\Delta x,\omega) \;=\; V^2\cdot \boldsymbol{I}_v^2\,\widehat{\boldsymbol{S}}_v(\Delta x,\omega)\ , \qquad \boldsymbol{I}_v^2 \;=\; diag\left[\left(\frac{\sigma_u}{V}\right)^2,\left(\frac{\sigma_w}{V}\right)^2\right] \tag{1.58}$$

For the purpose of this thesis, L_{exp} is set equal to L and then the dimensionless longitudinal coordinate $\hat{x}_i = x_i/L$ may be introduced.

Because $\widetilde{\boldsymbol{K}}_0^{-1}$is a diagonal matrix, the matrix multiplication $\widetilde{\boldsymbol{K}}_0^{-1}\boldsymbol{A}\widetilde{\boldsymbol{K}}_0^{-T}$is equal to dividing every row of $\boldsymbol{A}$ by the corresponding value $\widetilde{K}_{0,i}$ and as well as every column by $\widetilde{K}_{0,j}$, or equivalently every entry of $\boldsymbol{A}$ by $\widetilde{K}_{0,i}\cdot\widetilde{K}_{0,j} = \widetilde{M}_i\omega_i^2\cdot\widetilde{M}_j\omega_j^2$ ($\boldsymbol{A}$ is here simply used as an arbitrary notation for the contents within the brackets in equation 1.56). Thus, the entry wise contents of $\boldsymbol{S}_{\hat{Q}_v}(\omega)$ may more conveniently be expressed by,

$$S_{\hat{Q}_{v,i}\hat{Q}_{v,j}}(\omega) = \left(\frac{\rho V^2 BL}{2}\right)^2\cdot\frac{1}{\widetilde{M}_i\omega_i^2\cdot\widetilde{M}_j\omega_j^2}\cdot J_{ij}^2 \tag{1.59a}$$

where,

$$J_{ij}^2 \;=\; \int_0^1\int_0^1 \boldsymbol{\varphi}_i^T(\hat{x}_1)\widehat{\boldsymbol{B}}_q\left[\boldsymbol{I}_v^2\,\widehat{\boldsymbol{S}}_v(\Delta\hat{x},\omega)\right]\widehat{\boldsymbol{B}}_q^T\boldsymbol{\varphi}_j(\hat{x}_2)d\hat{x}_1d\hat{x}_2 \tag{1.59b}$$

and where J_{ij}^2 is called the *joint acceptance function*.

1.4 MEAN RESPONSE

The static mean response is obtained by inserting equation 1.37e into equation 1.43e to form the static modal load vector, $\bar{\boldsymbol{Q}}$. The mean response vector, $\bar{\boldsymbol{r}}$, is obtained by dividing the mean load vector by the total system stiffness and subsequently multiplying with the modeshape matrix, namely,

$$\bar{\boldsymbol{r}}(x) \;=\; \boldsymbol{\Phi}(x)\cdot[\boldsymbol{I}-\boldsymbol{\kappa}_{ae}]^{-1}\cdot\boldsymbol{K}_0^{-1}\cdot\frac{\rho V^2BL}{2}\cdot\int_0^1\boldsymbol{\Phi}^T(\hat{x})d\hat{x} \tag{1.60}$$

1.5 DISTRIBUTION OF MAXIMUMS

From a design perspective, what level of maximum response one might expect during a time period of a given length is highly interesting. Equation 1.52 only gives the *variance* of the structural response, but since the response will be stochastic, its *maximum* value will follow a certain probability distribution. Strømmen (2010, ch. 2.3 – 2.4) estimates this distribution together with its expected value and variance and a brief summary of the steps involved are presented in the following. First, an expression for the average frequency for which a certain threshold of structural response, a, is crossed, is established. If a stochastic structural response function $n(t)$ is considered, it is given by,

$$f_n(a) \quad = \quad \frac{1}{2\pi} \cdot \frac{\sigma_{\dot{n}}}{\sigma_n} \cdot exp\left[-\frac{1}{2}\left(\frac{a}{\sigma_n}\right)^2\right] \quad = \quad f_n(0) \cdot exp\left[-\frac{1}{2}\left(\frac{a}{\sigma_n}\right)^2\right] \tag{1.61}$$

where $f_n(a)$ is the average up–crossing frequency for level a, and σ_n and $\sigma_{\dot{n}}$ is the standard deviations of structural response and velocity of component n, respectively. $f_n(0)$ is the so–called *zero up–crossing frequency* and is equal to $\sigma_{\dot{n}}/(2\pi\sigma_n)$. $f_n(a)$ is intuitively equal to $f_n(0)$ when $a = 0$. $\sigma_{\dot{n}}$ can be determined together with σ_n simply by exploiting that $S_{\dot{n}}(\omega) = \omega^2 \cdot S_n(\omega)$ applies for the derivative of $n(t)$ (Strømmen, p. 43). The term ω^2 can thus simply be added as a factor of the integrand inside the brackets in equation 1.52 when obtaining $S_{\dot{n}}(\omega)$. Also, a requirement for the validity of equation 1.61 is that $n(t)$ and $\dot{n}(t)$ follow a Gaussian distribution, and that the process $n(t)$ is relatively narrow banded such that for each zero–up crossing event, there exist a corresponding peak event.

The connection to the distribution of maximums starts with introducing,

$$\kappa \quad = \quad f_n(a) \cdot T \tag{1.62}$$

where κ is equal to the number of times threshold a is crossed during the time period, T. If a is set equal to n_{max}, κ should on average be equal to unity, signalizing a single occurrence within T. Further, κ is assumed to have a CDF equal to $exp(-\kappa)$ and the PDF of n_{max} can thus be calculated from differentiating the CDF numerically with respect to n_{max}. The mean value and variance of n_{max} can also be calculated numerically using the PDF. Strømmen does however provide approximate analytic expressions for the mean and variance of n_{max} and they are given by,

$$\bar{n}_{max} \quad = \quad \sigma_n \cdot \left[\sqrt{2 \cdot \ln(f_n(0) \cdot T)} + \frac{0.5772}{\sqrt{2 \cdot \ln(f_n(0) \cdot T)}}\right] \tag{1.63}$$

$$\sigma_{n_{max}}^2 \quad = \quad \sigma_n^2 \cdot \frac{\pi^2}{12 \cdot \ln(f_n(0) \cdot T)} \tag{1.64}$$

A requirement for the validity of equations 1.63 and 1.64 is that $n(t)$ is “fairly broad banded” (Strømmen, p. 29), thus one must interpret whether one can have simultaneous validity of equations 1.61, 1.63 and 1.64. Also, since only the turbulence components are considered in this derivation, the value of the mean response must be added in order to obtain the measure of distribution the maximum of total structural response.

2 NON–STATIONARY BUFFETING THEORY

2.1 INTRODUCTION TO ARISING ISSUES OF NON–STATIONARITY

Generally, every statistical property of the wind field will be time dependent since weather eventually changes with time. However, if these changes progress slowly enough, the wind field may consequently be considered as being stationary over a relatively short time window. A problem arises however when the assumption of stationarity is challenged when one might have reason to believe that one or more of either the mean wind speed, variance and time scales changes from one level to another within the course of a recording period as schematically illustrated in figure 2.1.

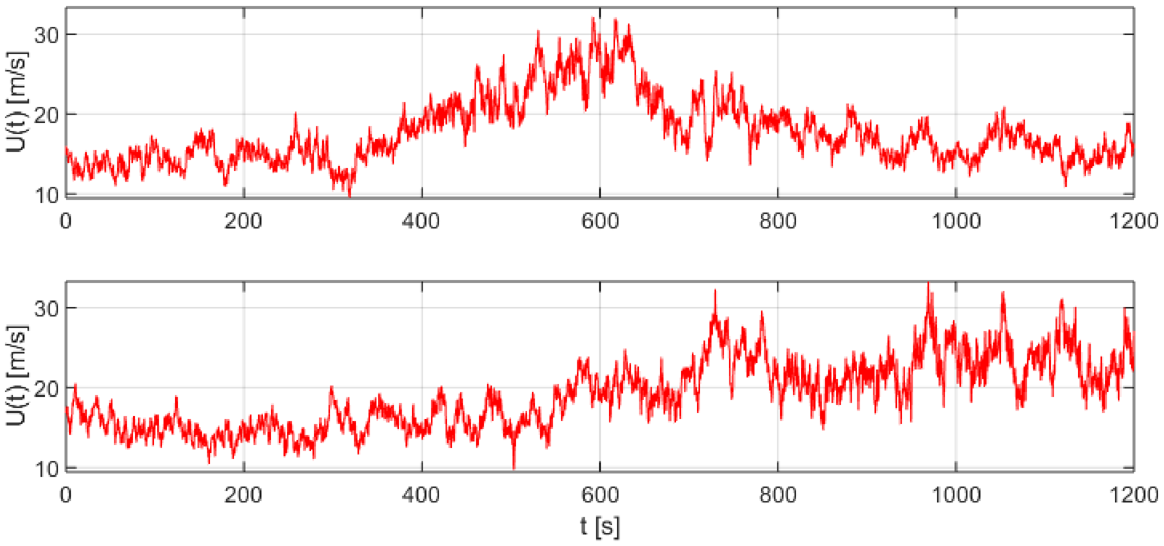

Figure 2.1: Presumed non–stationary arbitrary wind speed recordings

When stationarity is assumed, the convenience of the frequency domain methodology presented in chapter 1 is obvious because a single presumed stationary wind speed recording does not per definition represent anything unique in a stochastic sense. What is important is its statistical characteristics, namely its PSD function, which indeed is common for the infinitely large family of realizations it represents.

Adopting an equal approach when considering a non–stationary wind speed recording would initially be a mere attempt to somehow foresee what storm is next to hit our structure in question. Also, embedded into the wording of the term “non–stationary” is really the fact that no non–stationary signal is identical because they all generally exhibit their own specific non–stationary characteristics. Hence, in order for the convenience of the frequency domain methodology to be utilized, one must define a separation between what can be considered as unique to the non–stationary recording in question and what can be considered as being stochastic. Consequently, the fundamental building–block of the non–stationary buffeting theory is letting the mean wind speed be time–dependent, and the corresponding (remaining) turbulence components to be described by an *evolutionary stochastic process*. The key challenge in this non–stationary adaptation of the well–established stationary frequency domain buffeting theory framework is to determine exactly what can be considered as trends and randomness respectively, and also how to define and implement the presumed trends in a wise and appropriate manner.

2.2 TIME DEPENDENT VERTICAL MEAN WIND SPEED

The initial step when taking on the task of establishing the per now well mentioned non–stationary frequency domain buffeting theory is introducing a minor adaptation to the stationary–specific formulation of the wind field coordinate system. Its orientation as presented in chapter 1.1.5 is defined directly from the mean wind speed direction such that any perpendicular wind speed component will have zero mean value. For the purpose of treating non–stationary features a time–dependent vertical mean wind speed, $\overline{W}(t)$, is introduced. Such is physically reasonable even for a bridge structure over flat terrain where the *average* vertical mean wind speed will be close to zero because of air flow compatibility, nevertheless, some variations over a shorter time interval will surely be present.

As a consequence, the same definition of the orientation the wind field coordinate system is now theoretically invalid since it is now time dependent. However, the vertical mean wind speed, $\overline{W}$, has a magnitude must less than the horizontal mean wind speed, V, such that what from now on will be denoted as V is simply the true and mathematically correct mean wind speed V projected onto a horizontal line, perpendicular to the bridge girder. Because two flow components now have a time–varying mean subcomponent, the time–varying means of U and W is from now on denoted by $\overline{U}$ and $\overline{W}$, respectively. Equation 1.2 takes thus the following form,

$$\begin{aligned} U &= \overline{U}(t) + u(x,t) \\ v &= v(x,t) \\ W &= \overline{W}(t) + w(x,t) \end{aligned} \tag{2.1}$$

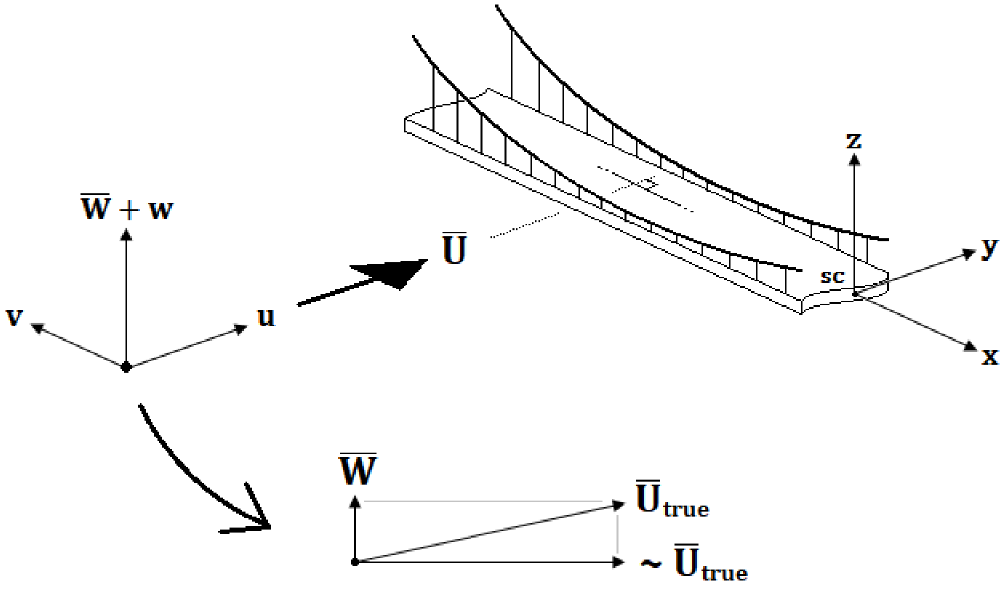

Figure 2.2: Non–stationary flow–coordinate system formulation

With the addition of $\overline{W}$ as an extra component to the vertical flow axis, the calculations leading up to the fully expanded version of equation 1.31 must be performed once again with $\overline{W}$ included. A brief summary of the calculations leading up to the now updated versions of equation 1.37 can be found in Appendix A. The only implication the inclusion of $\overline{W}$ has on equation 1.37 that another term is added to the expression of the mean wind loading $\bar{\boldsymbol{q}}$ in equation 1.37c, which now takes the following form,

$$\bar{\boldsymbol{q}} = \begin{Bmatrix} \bar{q}_y \\ \bar{q}_z \\ \bar{q}_\theta \end{Bmatrix} = \frac{1}{2}\rho B \cdot \left[\bar{U}^2 \cdot \begin{Bmatrix} (D/B)\bar{C}_D \\ \bar{C}_L \\ B\bar{C}_M \end{Bmatrix} + \bar{U}\bar{W} \cdot \begin{Bmatrix} (D/B)C_D' - \bar{C}_L \\ (D/B) + C_L' \\ BC_M' \end{Bmatrix} \right] \tag{2.2}$$

With reference to the calculations in Appendix A.1, it should be mentioned that excluding the terms $2\bar{W}w$ and $-2\bar{W}\dot{r}_z$ from equation A.3 is not because of a linearity violation, but rather for simplicity and an attempt to omit contributions that is of least importance but will give a disproportionally large complexity contribution to the buffeting theory as a whole. Excluding such contributions leaves us only with an added contributor to the mean structural loads but this does not represent any mathematical inconvenience as shall be shown in chapter 2.3. In fact, it is rather of practical convenience since components U and W now can be treated equally as also will be shown in the following.

2.3 EXTRACTION OF THE MEAN WIND SPEED

In literature, several different methods for extracting an appropriate mean wind speed is encountered. Extracting trends from signals and processing signals in general is nothing unique to wind engineering but rather a large field of study in itself. Hence, some of the methods used in literature to extract trends from non–stationary wind speed recordings are not designed with this specific purpose in mind or especially to fit in with the other steps making up our non–stationary frequency domain buffeting response framework, even though they are highly capable of performing this task exclusively. Namely, one must have in mind that the supreme goal of this thesis is to establish a theoretical framework which has the ability to predict the response of a structure onto which a storm induces dynamic loads. Hence, the method of choice for extracting the mean wind speed must indeed produce a result that is mathematically convenient when utilized in the subsequent steps of our model. Extracting the mean wind speed is simply a single, yet very important step on the way towards an appropriate solution of the dynamic problem in question.

A particular method that fits the above description well is the so–called *discrete wavelet transform* (DWT). Wang *et al.* (2016); Ma, Xu and Wang (2016); Tao, Wang and Wu (2016); Wang and Kareem (2005) uses the DWT as a part of modelling non–stationary winds. The fact that one must select from a variety of wavelets to be used in the DWT, and that modelling the wind field itself is not the exclusive goal in this thesis makes the DWT somewhat over–complicated in the context of this thesis despite having highly appreciated capabilities in for instance image processing and sound or radio signal denoising.

With the desired property to conveniently fit in with the rest of the mathematical framework defining our non–stationary frequency domain buffeting response model, three unique methods are in the following taken into consideration. The three methods are presented in chapters 2.3.1 – 2.3.3. With all three methods of course being adaptive with respect to how precisely the resulting deterministic trend should resemble the non–stationary wind speed recording itself, a wise level of such adaptation is key. Obviously, an absolute requirement when defining the mean wind speed is that the resulting time–varying mean modal loads (equation 2.2) produces a strictly quasi–static mean response, otherwise violating the key principle of the buffeting model, namely separating deterministic trends and stochastic processes.

However, assuring a quasi–static mean response is alone not sufficient because the square of the mean wind speed is also present as a factor in the expression for the variance of the modal loads in equation 1.59. Another key property of the stationary frequency domain buffeting response framework is that because input is presumed stationary, the homogeneous solution of the governing differential equations will be damped out. On the contrary, if the frequency–wise distribution of variance in the input changes with time, as will generally be the case with a non–stationary wind field, one cannot assume the now continuously changing homogeneous solution to be damped out. What will effectively happen is that the dynamic system will go through a "transition phase" when settling from one level of response to the next resulting from the time–varying characteristics of the input. Such behaviour is labelled *transient effects* and cannot be described by the frequency domain framework that is presented in this thesis as the output at any particular moment in time is defined directly from the input at the same moment in time.

Nevertheless, the inertia and dynamic properties of the structure at hand can be taken into consideration together with an appropriate level of adaptation in the mean wind speed extraction method such that the structure in question will remain in a close to *quasi–stationary state of equilibrium* such that transient effect from winds speed recordings with not too violent non–stationary features is not disproportionally large. Such a treatment will be covered in chapter 3.7 by time domain simulations.

In the following, the workings of the three extraction methods are presented and illustratively applied to a generated arbitrary non–stationary wind speed recording displayed in figure 2.3.

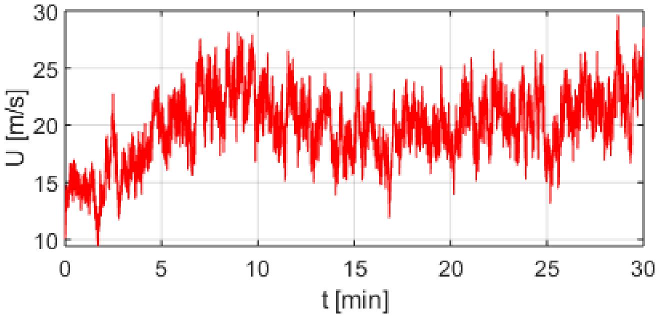

Figure 2.3: Arbitrary non–stationary wind speed recording

The signal in equation 2.3 is generated from a von Kármán spectrum with V = 20 m/s, I_u = 0.16 and ${}^{y}L_u$ = 162 m to which a linear function and a Gaussian probability density function is added as to represent some non–stationary trends. The magnitude of the turbulence is also scaled with a factor proportional to the sum of these two added trends to resemble the fact that the variance usually increases with the mean wind speed.

2.3.1 Weighted moving average method – WMAM

The simplest and least technical method possible for extracting the mean wind speed is by the means of a moving average. Hu, Xu and Huang (2013) uses this method to extract a mean wind speed that is later used in dynamic response calculations on the Stonecutters Bridge in Hong Kong. It is simply given by,

$$\bar{U}(t) \;=\; \frac{1}{2T_A} \cdot \int_{-T_A}^{T_A} U(t+\tau)\, d\tau \qquad (3.3)$$

Obviously, the average is centralized such that no time–lag effects will be present.

Because $\bar{U}(t)$ is a factor in the expression for the time–varying variance of the structural loads, a weighted average version of equation 2.3 is instead used with the purpose being of obtaining a smoother curve for $\bar{U}(t)$ when T_A is relatively short. The chosen weighting function is simply a parabola which is equal to zero at $|\tau| = T_A$ and unity at $\tau = 0$. When using a discrete format to calculate $\bar{U}(t)$ from a discrete time–series, equation 2.3 takes the form of equation 2.4, having also normalized the weighting factors so that their sum is unity,

$$\bar{U}(t) = \sum_{i=-N}^{i=N} U(t + i\Delta t) \cdot w_i \tag{2.4}$$

Ma, Xu, Wang (2016) uses a similar procedure when calculating time–varying variance of a non–stationary turbulence component with the use of the WMAM, however with a Gaussian PDF curve as weights because of their different particular purpose and context.

Figure 2.4 illustrates the behaviour of the WMAM by setting T_A to $T_A = \{1,2,5\}$ min. The Fourier spectrum of the resulting turbulence component is also presented so it is visible what the WMAM is able to eliminate from $U(t)$ frequency–wise. Finally, in order for equation 3.4 to be defined on the entire length of the recording, the recording itself is only a subset of a longer duration "parent recording" from which data can be collected when performing different types of time averaging processes on the extremities of the subset recording.

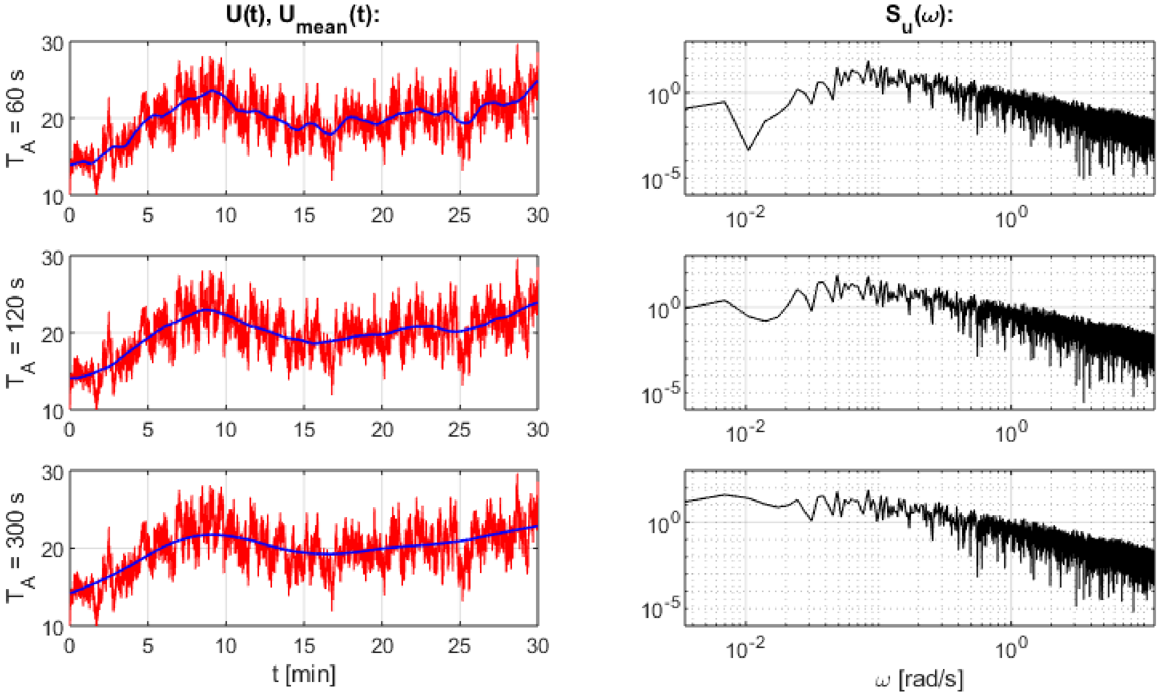

Figure 2.4: WMAM for extracting mean wind speed

The scatter visible in the corresponding spectrum data in figure 2.4 forces us to interpret what stochastic processes the respective resulting turbulence components represents. Because of the scatter itself, a smooth curve is an absolute requirement when performing response calculations due to sharp and prominent peaks of the modal frequency response matrix (equation 1.50b) forming around the eigenfrequencies. If adopting the Kaimal or von Kármán formulae to the spectrum data via a least square fit over the entire frequency axis, unfavourable results might arise in the lower portion of the frequency axis. As can be seen from the spectrum data in figure 2.4, the shape of the lowest most portion of the frequency axis seem to depend on T_A. Therefore, this effect must be taken into consideration when adopting a Kaimal or von Kárman curve fit to the spectrum data, together with the domain of definition of such a curve. The advantage with the WMAM is however, as will be shown in chapters 2.4.3.1 and 2.4.4.1, that also a weighted moving average is used when determining the time–varying variance of the turbulence component of the recording. This is convenient when adapting T_A to the given the situation at hand.

2.3.2 Empirical mode decomposition – EMD

Similar to the DWT, the *empirical mode decomposition* (EMD) which was first proposed by Huang *et al.* (1998) is excellent at extracting a trend from a nonstationary signal, however it was established as an attempt to provide time–varying spectral content from non–stationary signals with a higher level of accuracy than what was possible at the time via the well–known Fourier transform. The proposed method called the *Hilbert–Huang Transform* (HHT) performs *Hilbert spectral analysis* (HSA) on the individual *intrinsic mode functions* (IMFs) obtained directly from the EMD.

The mathematics behind the EMD is also fairly simple and it is similar to the Fourier transform because it decomposes a signal into oscillatory functions – IMFs. What is new is however that the IMFs are not harmonic functions but rather curves with time–varying frequency and amplitude. Consequently, a far less number of components is needed to resemble a signal using the EMD than the Fourier transform, which surely is of great convenience given the context within it was designed to operate but for the purpose of this thesis, this very fact might be the Achilles' heel of the EMD since the available domain of adaptation is quite limited.

Thankfully, MATLAB R2018a features for the first time the built–in function *emd* which extracts IMFs from an arbitrary signal given a certain tolerance level. If the generated non–stationary wind speed recording in figure 2.3 again is considered, the 10 IMFs that the MATLAB function *emd* in this case produces and the residual function are shown in figure 2.5.

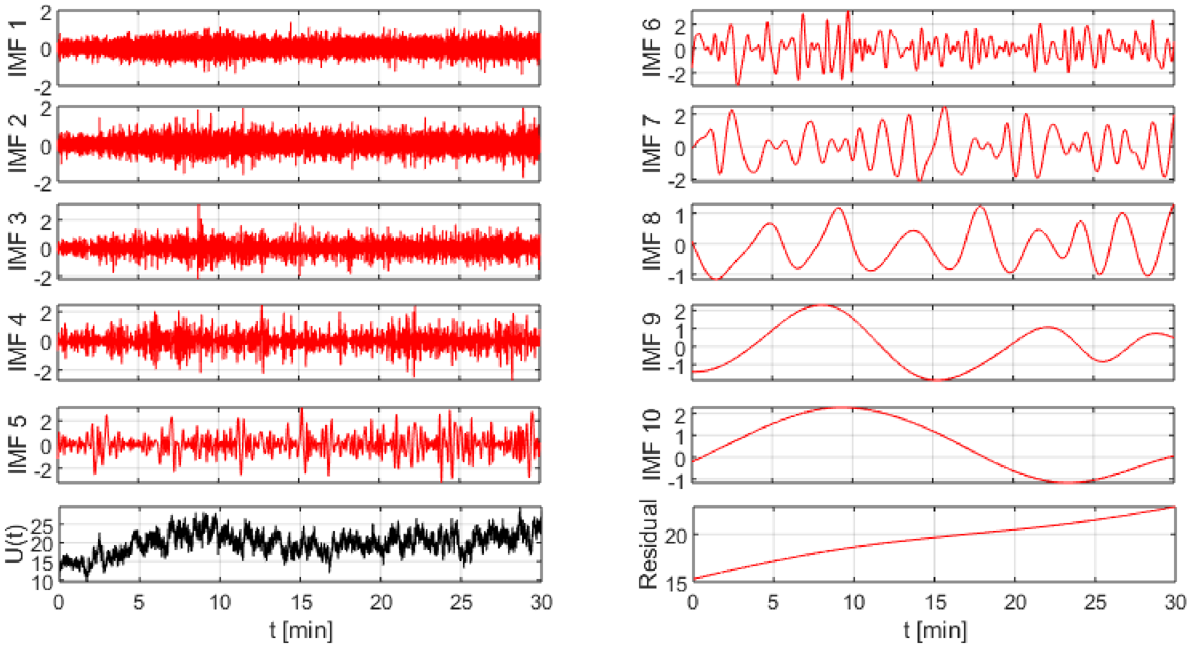

Figure 2.5: Intrinsic mode functions (IMFs) of $U(t)$

From IMF no. 10 and down the oscillations quickly become too rapid to be suitable as components of the mean wind speed. In case of the Hardanger bridge which has a fundamental period of 19.6 seconds, 91.7 corresponding cycles of this mode will take place within the 30–minute duration of the recording now in question. This mode does also have a damping ratio of 0.005 and without any further calculations, a mere qualified guess is therefore that the absolute lowest IMF that can be included in the extraction of the mean wind speed in the case of the Hardanger bridge, is IMF no. 8. Figure 2.6 shows the extracted mean as a sum of the last 3 IMFs, last 2 IMFs and the last IMF plus the residual together with the respective corresponding spectrum for the remaining turbulence components.

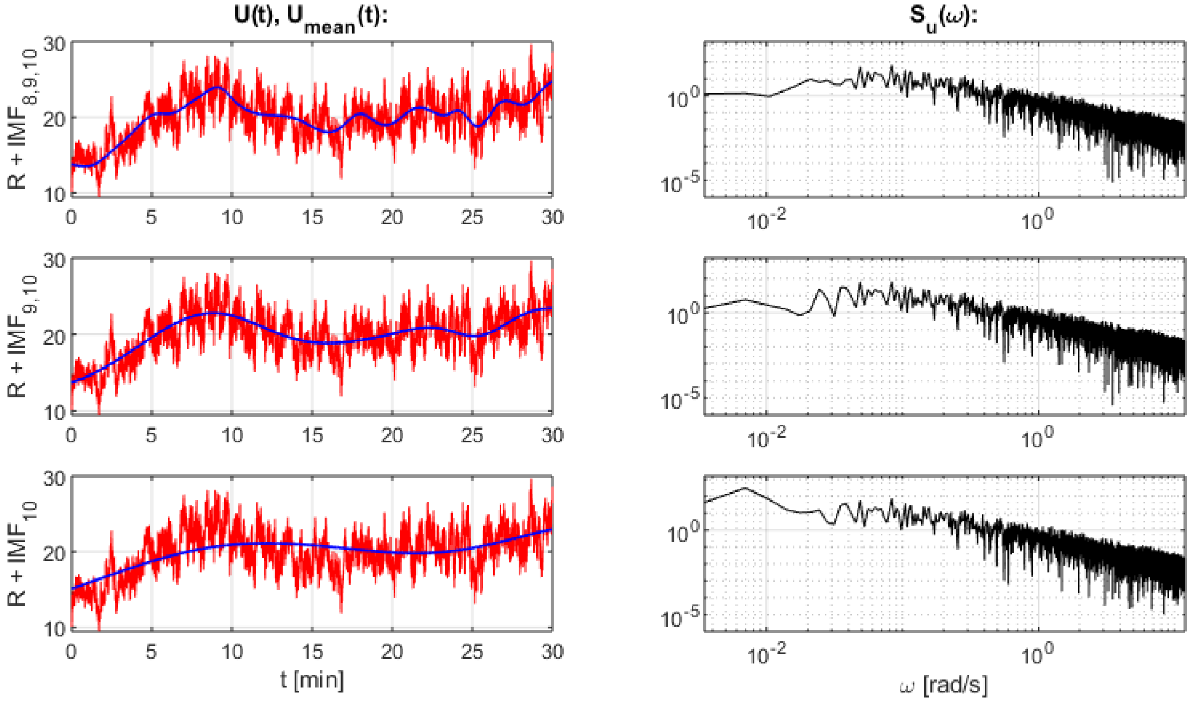

Figure 2.6: EMD for extracting mean wind speed

The results of the EMD looks much like the results from the WMAM with the somewhat arbitrarily chosen values of T_A. However with the WMAM, T_A can be chosen from a practically infinitely fine mesh giving it much greater flexibility when it comes to adaptation. Also, much like the WMAM, the EMD seems to lack consistency when it comes to the behaviour of the lowest–most portion of the spectrum data. Nevertheless, such behaviour does not necessarily represent a big problem in practice since the T_A–dependent behaviour of this portion only affects a very limited number of frequency components, thus potentially having only a small impact compared to the otherwise consistent shape of the spectrum data.

2.3.3 Incomplete Fourier expansion – IFE

This proposed method is really as simple as its given name suggests, namely to perform a Fourier series expansion of the wind speed recording only including components up to a certain frequency. Determining this very frequency limit is obviously the method of adaptation in itself, and it will depend on the dynamic properties of the structure at hand and will be covered in chapters 3 and 4.

Apart from its simplicity, this method has one major advantage compared to the previous two which is that the mean wind speed and the spectrum is defined via the same mathematical tool, namely the Fourier transform. As with the WMAM and EMD three levels of adaptation is considered, now expressed as a certain fraction of the fundamental frequency of the Hardanger bridge, ω_1 = 0.32 rad/s.

An important thing to have in mind when adopting the IFE is that all Fourier components of course are periodic on the interval onto which they are obtained. Thus, when using an IFE one should preferably perform it on the parent recording from which our withdrawn subset recording originates. This is especially important with an IFE using few components because the corresponding “commissioning phase" of the extracted curve will be of substantial length if the magnitude of the parent signal starts and ends at different levels (ref. the *sawtooth curve*).

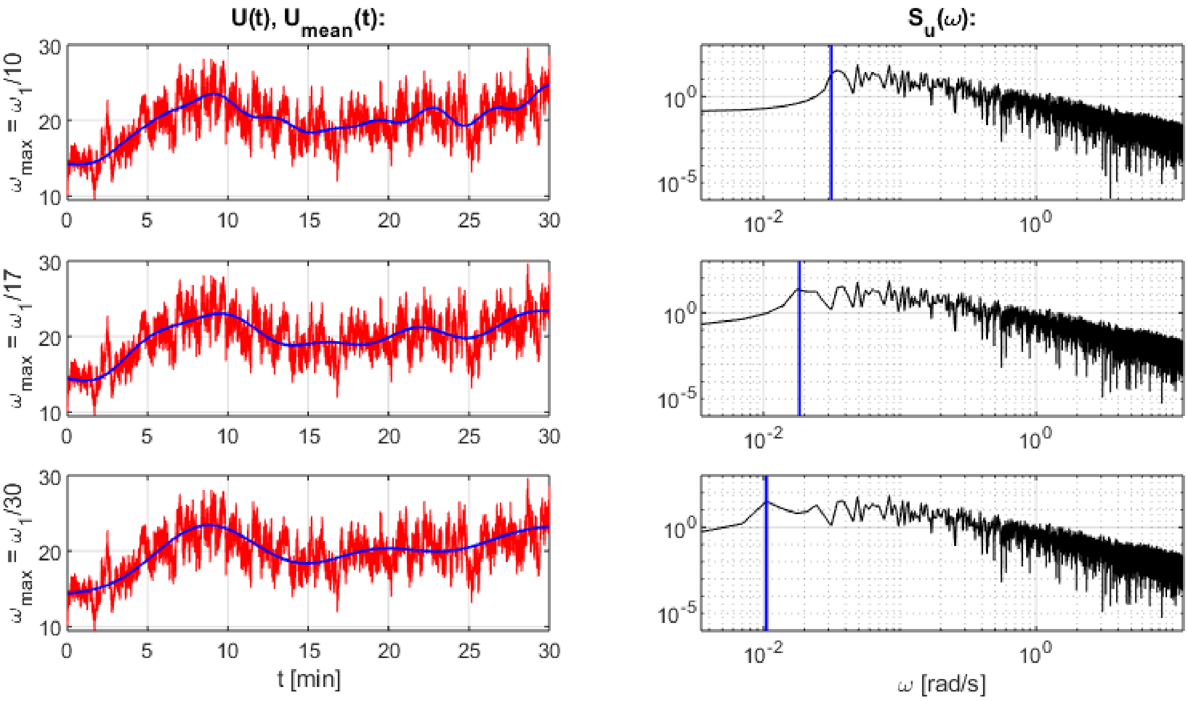

Figure 2.7: IFE for extraction of mean wind speed. The vertical blue line represents ω_{max}.

By first glance, all three presented methods seem to produce appropriate curves that resemble some sort of trend from the non–stationary data, given a user–specified level of precision. The interesting aspect is therefore even though their respective shapes look relatively similar, the turbulence component spectrum they produce display relatively different characteristics. When looking at the spectrums provided by the IFE in particular, the obvious difference from the WMAM and EMD is that there is a sharp and definite change in characteristics in the spectral content below and above the highest included frequency in the IFE, ω_{max}. Specifically, the spectral magnitude below ω_{max} seems to be well–behaved and scatter–free and these properties seem also to be independent of ω_{max} itself. This comes as no big surprise since the Fourier transform is used both to extract the mean and to produce the resulting spectrum of the remaining turbulence component, effectively subtracting frequency content from U and adding it to $\bar{U}$. Hence, the spectral region below ω_{max} contains nothing but "left–overs" from an extraction process where the frequency settings used to obtain the spectrum is not equal to the settings used to extract the mean wind speed due to the subset–, and parent recording having different lengths. (ref. equation 1.6). Consequently, this portion of the spectrum does not have zero magnitude but it can simply by neglected because of its magnitude being relatively low compared to the region just above ω_{max}, and because of its very narrow domain of definition along the frequency axis.

The advantage of using the IFE is namely because the numerical integration procedure required to solve a time dependent version of equation 1.52 can be performed by fitting a Kaimal or von Kármán curve (equations 1.19 – 1.21) to the portion of the spectrum above ω_{max} and let integration start from here. Such is also neat and tidy because an intuitive mathematical separation between what can be regarded as deterministic (time varying mean) and stochastic (turbulence) is clearly defined.

Finally, it should be mentioned that because the signal in figure 2.3 that was used as a tool to illustrate the three methods of extracting the mean wind speed is generated from a stationary spectrum to which arbitrary non–stationary trends are added, the resulting spectral data in figures 2.4, 2.6 and 2.7

is therefore quite well–behaved. However, the purpose of chapters 2.3.1 – 2.3.3 was to illustrate the workings and central features of the three methods and their method of formulation, and no real–life recording is needed for this categoric information to be provided. Nevertheless, spectral data from real–life recordings will generally be more scattered and somewhat less well–behaved when it comes to fitting an appropriate trend function onto it, but the behaviour of the WMAM, EMD and IFE will then be categorically similar to what was shown in chapters 2.3.1 – 2.3.3.

2.3.4 Selecting mean wind speed extraction method

Generally, there is no clear rule that determines which one of the three methods to adopt in the dynamic response calculations. All three methods are mutually indistinguishable when it comes to the resulting spectral content of the turbulence component for higher frequencies because only a low frequency trend is extracted. However, the fact that the IFE is designed from a problem specific perspective and that it as a direct consequence is able to define a clear separation between the deterministic trend and the stochastic left–overs, is appreciative. Such also makes interpretation much easier when it comes to fitting a Kaimal or von Kármán spectral curve to the spectral data as is the topic of chapter 2.4.5. Clearly, the WMAM and EMD does not provide any information the IFE cannot provide but rather quite the opposite. The IFE will therefore be the only included method for extracting the mean wind speed in the non–stationary response calculations.

2.4 FORMULATION OF THE NON–STATIONARY STOCHASTIC PROCESSES

2.4.1 Introduction

With now having established several flexible and intuitive methods for extracting the mean wind speed, what remains is proposing a proper procedure for incorporating the remaining, presumed non–stationary turbulence components into our frequency domain response calculation framework. When dealing with a non–stationary signal, the intuitiveness of the information about its frequency–wise variance distribution provided by the Fourier spectrum is challenged since it assumes that the signal is composed of a sum of harmonic components whose amplitude and frequency is time–invariant. Obviously, any signal, stationary or not, can be expressed as a sum of harmonic components via the Fourier transform, however with a severely non–stationary signal, the corresponding Fourier spectrum will probably give spurious results if being interpreted in the context of stationarity. Nevertheless, the Fourier spectrum of a mildly non–stationary signal may be interpreted as being the *average* distribution of the variance over the frequency axis.

Again, the intuitive and compact way the Fourier spectrum describes a stationary stochastic signal is of great convenience in our frequency domain buffeting response model. To establish a similar procedure for mathematically describing a non–stationary signal is however a more challenging task. Priestley (1965) first introduced the idea of an *evolutionary spectrum* by generalizing the definition of the stationary spectrum where instead of letting pure sine and cosine functions represent the orthogonal basis of the signal, these are instead *modulated* by time dependent functions, $A(\omega, t)$, such that the non–stationary signal can be formulated as follows,

$$x(t) \quad = \quad \int_{-\infty}^{\infty} A(\omega, t) e^{i\omega t} dZ(\omega)\,, \qquad E[|dZ(\omega)|^2] \;=\; \mu(\omega) d\omega \tag{2.5}$$

The *evolutionary power spectral density*, EPSD, of the process $x(t)$ will then be given by,

$$S_x(\omega,t) \quad = \quad |A(\omega,t)|^2 \cdot \mu(\omega) \tag{2.6}$$

where $\mu(\omega)$ (here: "$S_x(\omega)$") represents a time–invariant spectrum which is to be modulated with $A(\omega,t)$ to form the EPSD of $x(t)$.

Priestley's method is mathematically effective in the sense that the only modification required to formulate an evolutionary spectrum is to introduce time varying modulation functions to the harmonic components which would else form the orthogonal basis of a stationary signal. The drawback is however that these modulation functions can never be determined *a priori* from the non–stationary signal itself, and for the method to be implemented in practice, they must be chosen *a posteriori* (Huang *et al*, 1998). Huang *et al.* later got around this problem by introducing the recently mentioned Empirical Mode Decomposition which together with Hilbert spectral analysis makes up the Hilbert–Huang Transform which enables a close to orthogonal set of components with time–varying amplitude and "instantaneous" frequency (IMFs) to be obtained directly — a priori, via a sifting process (see figure 2.5).

At this point however, an important boarder must be drawn between what is considered convenient for the exclusive purpose of establishing mathematical expressions for the non–stationary stochastic wind field recording itself, and what method is most suitable and convenient if ones supreme objective is to calculate the dynamic response of a structure onto which the non–stationary wind induces dynamic loads. Of course, there is no reason to question the capabilities of the HHT when it comes to describing time–varying variance distribution of non–stationary winds for this purpose only, however, the HHT does not conveniently integrate into the "non–stationary modified" frequency domain buffeting response framework that will be used in this thesis. Also, an important concept is what level of precision is really required when describing non–stationary features of the wind field. The structure itself has certain desired frequencies of oscillation — eigenfrequencies, each one having an associated damping ratio which together gives raise to the fact that a certain amount of "build–up time" must pass before for the output reaches a new level of variance as a result of a rather sudden change in input. Consequently, how rapidly one should interpret and thereby model the fluctuations of the non–stationary features of the wind field, must be in correspondence with the dynamic properties of the structure in question.

Due to the argumentation above, Priestley's (1965) idea of an evolutionary spectrum is adopted in which the presumed non–stationarity features of the turbulence components will be treated at three "levels of approximation", namely being modelled as,

1. Stationary (unmodulated)
2. Uniformly modulated.
3. Non–uniformly modulated.

Common for all these three methods is that a time–invariant (approximated as stationary) or "average" spectrum must be calculated. This spectrum is then "modulated" according to equation 2.6, and on the format suggested by the above methods 1 – 3. These methods of modulation are presented in chapter 2.4.2 – 2.4.4, respectively. The procedure of estimating the time invariant spectrum is presented in chapter 2.4.5.

Finally, a comment on the usage of equation 2.6 must be given. This again regards the desire to formulate the EPSD of the wind field with the purpose being of only providing wise and most useful information when it comes to calculating structural dynamic response. When multiplying the harmonic, orthogonal components of a presumed stationary signal with a chosen set of modulation functions, they will generally no longer be mutually orthogonal, hence violating equation 1.13 and subsequently equation 1.15, which are indeed fundamental building–blocks of the frequency domain response method. However, the fundamental principle of the *evolutionary* buffeting response calculation method proposed in this thesis is that for every unique time instant, $t = t_i$, structural response can be considered a stochastic process that obeys a PSD function which is derived directly from the PSD function that is defined to represent the stochastic characteristics of the wind field at $t = t_i$. Such is done for all values of t such that the EPSD function (here: a discrete matrix) of structural response is calculated from a wisely defined EPSD function of the wind field in direct correspondence with equations 1.52 and 1.59. Consequently, the modulation function $A(\omega, t)$ no longer needs to be interpreted as a function that is supposed to modulate the individual harmonic components of a signal, but a function whose square value, $|A(\omega, t)|^2$, is supposed to modulate a calculated "average" spectrum in both frequency and time, thereby avoiding the orthogonality problem in the first place.

2.4.2 Stationary turbulence components

Xu and Chen (2004) uses this approach to treat presumed non–stationary wind speed recordings. Their findings suggest that "most of non–stationary wind data can be decomposed into a time–varying mean wind speed plus a well–behaved fluctuating wind speed admitted as a stationary random process with a Gaussian distribution." Xu and Chen use the EMD to extract the mean wind speed while the IFE– and WMAM method will be used in this thesis due to the reasons mentioned in chapter 2.3.3. Because of the much finer mesh of adaptation the IFE and WMAM is able to provide it is assumed for the purpose of this thesis that the family of non–stationary wind speed recordings that obeys the aforementioned findings of Xu and Chen also will do so if the IFE or WMAM is instead applied.

In the case of presumed stationary turbulence components, the calculated average spectrum mentioned in chapter 2.4.1 is obviously given no modifications because it alone is given the role to fully represent the stochastic characteristics of the wind speed recording in question.

2.4.3 Uniformly modulated turbulence components

A *uniformly modulated process* is a process that admits the representation of equation 2.5 and 2.6 but whose modulation function, $A(\omega, t)$, does not depend on ω (Priestley, 1965). The uniform modulation function $A(t)$ is hence common for all harmonic components and if a uniformly modulated process is modulated by the inverse of its presumed modulation function, $A(t)$, the outcome will per definition be a stationary process. The notation $A(t)$ is simply a generalized one but may for convenience be equated to the time varying standard deviation of the process itself, such that the stationary process that is being modulated by $A(t) = \sigma_n(t)$ is a zero–mean, unit variance stationary process (Ma, Xu and Wang, 2016). The estimation of the square of the time dependent standard deviation, $\sigma_n(t)$, the time varying variance, is presented in chapter 2.4.3.1. The mathematical formulation used by Ma, Xu and Wang is given by equation 2.7 where the uniformly modulated process $n(t)$ is considered,

$$n(t) \quad = \quad \sigma_n(t) \cdot g_n(t) \tag{2.7}$$

where $\sigma_n(t)$ is the time varying standard deviation of $n(t)$, and $g_n(t)$ is a stationary stochastic process described by the PSD of $g_n(t) = n(t)/\sigma_n(t)$, namely $n(t)$ modulated to having constant, unit variance from the point of view of the method used to define $\sigma_n(t)$ itself. Analogue to equation 1.48, the Fourier transform of $n(t)$ is equal to a time varying multiple of the Fourier transform of $g_n(t)$, which renders,

$$S_n(\omega, t) \quad = \quad \sigma_n^2(t) \cdot S_{g_n}(\omega) \tag{2.8}$$

2.4.3.1 Time varying variance

In contrast to the extraction of the mean wind speed, there is really only one convenient way to define the time–varying variance which is using a floating average method, identical to the procedure used to define the mean wind speed in chapter 2.3.1. Ma, Xu and Wang (2016) uses a weighted average in which a Gaussian distribution function with a “bandwidth parameter” (standard deviation) that corresponds to a 95 % confidence interval over a 60 second averaging period represents the weighting function. Their argument behind this choice is that recorded wind speed data separated by more than one minute “are assumed to be uncorrelated”, and a weighted average should hence be performed over the corresponding time interval. A level of 95 % significance is somewhat arbitrary but it is supposed to represent the aforementioned correlation properties at a time separation $|\tau| = T_A = 60$ s. The standard deviation, σ, in the expression of the Gaussian PDF can be found by setting the value of the CDF at $\tau = T_A$ to 0.975. Quantile values for the Gaussian CDF thus gives $\tau = 1.96 \cdot \sigma$. The resulting shape of the weighting function itself is displayed in figure 2.8.

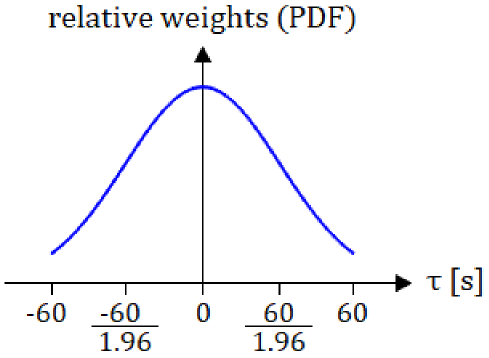

Figure 2.8: Relative shape of weighting function used by Ma, Xu and Wang (2016)

However, the objective of Ma, Xu and Wang is to describe the wind field and the wind field only, in which the weighting function is then chosen accordingly. Because of the concept of “build–up time” of structural response mentioned in chapter 2.4.1, but also for simplicity, a parabola with identical properties as presented in chapter 2.3.1 is instead adopted as the weighting function. Consequently, the method for estimating the time–varying variance of the stochastic, zero–mean process $n(t)$ is analogue to the WMAM for extracting the mean wind speed and is defined by,

$$\sigma_n^2(t) \;=\; \int_{-T_A}^{T_A} [u(t+\tau)]^2 \cdot w(\tau) d\tau \cdot \left[\int_{-T_A}^{T_A} w(\tau) d\tau \right]^{-1} \tag{2.9}$$

where $w(\tau)$ is the chosen parabolic weighting function. Adopting a discrete format and normalizing the now discrete weighting vector to having unit sum gives,

$$\begin{aligned} \sigma_n^2(t) &= \sum_{i=-N}^{i=N} [u(t+i\Delta t)]^2 \cdot w_i \\ w_i &= \left[1 - \left(\frac{i}{N}\right)^2\right] \cdot \left[\sum_{i=-N}^{N} \left[1 - \left(\frac{i}{N}\right)^2\right] \right]^{-1} \end{aligned} \tag{2.10}$$

The main purpose of using a weighted average at all is simply to obtain a smoother curve for the time–varying variance which is later supposed to be included as a function in the expression for the time–varying variance of structural response. The workings of the WHAM for estimating the time–varying variance is illustrated in figure 2.9 with an arbitrary generated non–stationary wind speed recording $n(t)$.

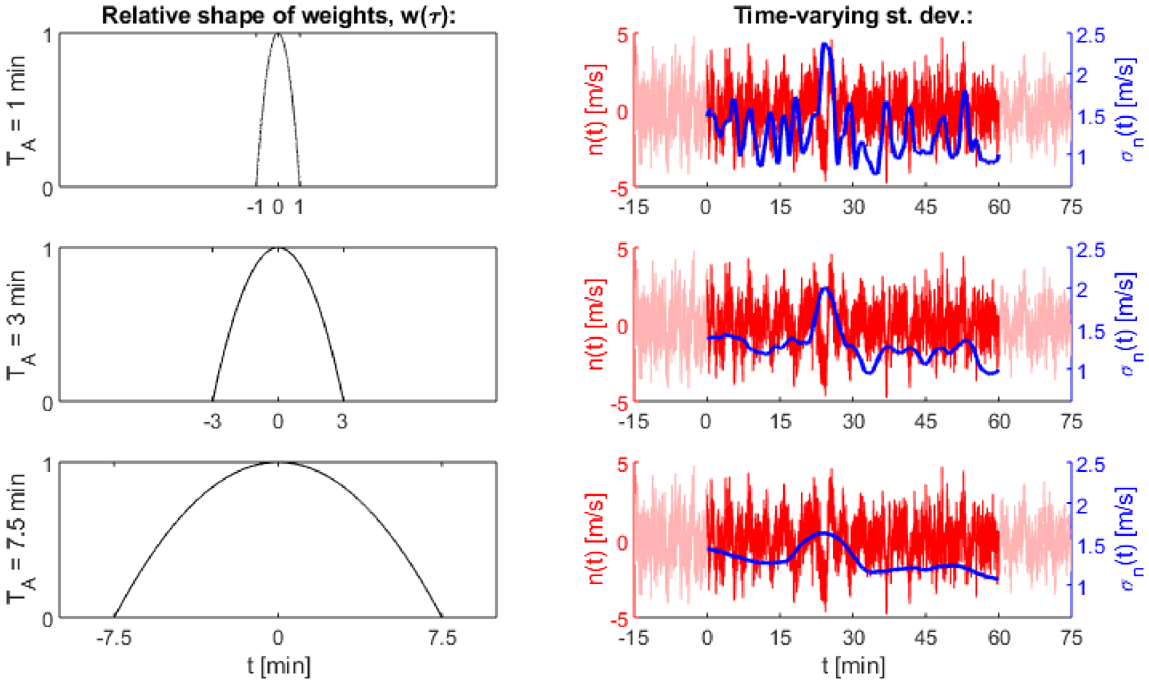

Figure 2.9: Estimation of time–varying variance (here: standard deviation).

2.4.4 Non–uniformly modulated turbulence components

Contrary to the uniformly modulated stationary process, each Fourier component of a *non–uniformly modulated* process is generally modulated with its own unique modulation function $A(\omega, t)$, hence being a process that admits the formulation suggested by Priestley (1965) in its most general form.

As mentioned in chapter 2.4.1, each individual modulation function $A(\omega, t)$ can never be calculated a priori in contrast to the Fourier components themselves, because no such method exists. Instead, an indirect estimation procedure is adopted in which Kaimal's and von Kármán's spectrum formulae in equations 1.19 – 1.21 is given the role to estimate the behaviour of the EPSD of the wind speed data by letting its parameters be time dependent. This principle of indirect estimation is utilized by Hu, Xu and Huang (2013) where time dependent versions of the mean wind speed, variance and integral length scale is inserted into the von Kármán spectrum formula to form a time dependent, evolutionary von Kármán spectrum. In this thesis a similar, but somewhat generalized method is used in which generalized versions of Kaimal and von Kármán spectrums with time dependent parameters takes the job of estimating the EPSD of the turbulence components.

The non–uniformly modulated EPSD is formulated on the format of equation 2.6, but now with a slight modification. With base and reference to the uniformly modulated process $n(t)$ defined in equations 2.7 and 2.8, $g_n(t)$ is now presumed to be *evolutionary*, and is thereby modelled as non–uniformly modulated but still with having unit variance, namely,

$$
\begin{aligned}
S_n(\omega,t) &= \sigma_n^2 \cdot S_{g_n}(\omega,t) \\
&= \sigma_n^2 \cdot \left|A_{g_n}(\omega,t)\right|^2 \cdot S_{g_n}(\omega) \qquad (2.11)
\end{aligned}
$$

The key element is to find a clever way to separate $S_{g_n}(\omega,t)$ into the factors $\left|A_{g_n}(\omega,t)\right|^2$ and $\mu(\omega)$ (here: $S_{g_n}(\omega)$). Tao, Wang and Wu (2016) presents such a separation technique which is illustrated in the following by considering a presumed evolutionary, zero mean, stochastic process, $n(t)$, to which the spectrum formula proposed by Kaimal (equation 1.19) is fitted (Kaimal: $n = \{u,w\}$). A general and explicit expression for a stationary, pre–fitted Kaimal specrum is given by,

$$
S_n(\omega) = \sigma_n^2 \cdot S_{g_n}(\omega) = \sigma_n^2 \cdot \frac{A_n \cdot {}^{x}L_n \cdot \bar{U}^{-1}}{\left[1 + B_n \cdot {}^{x}L_n \cdot \bar{U}^{-1} \cdot \omega\right]^{5/3}} \qquad (2.12)
$$

As will be argued in chapter 2.4.4.1, the turbulence integral length scales, ${}^{x}L_n$ will be approximated by equation 1.5. Inserting equation 1.5 into equation 2.12 cancels out the mean wind speed, $\bar{U}$, leaving only the integral time scales, T_n. When also adopting an evolutionary format, equation 2.12 takes the following form,

$$
S_n(\omega,t) = \sigma_n^2(t) \cdot \frac{A_n \cdot T_n(t)}{[1 + B_n \cdot T_n(t) \cdot \omega]^{5/3}} = \sigma_n^2(t) \cdot S_{g_n}(\omega,t) \qquad (2.13)
$$

The idea behind the separation technique of Tao, Wang and Wu is to let the time dependent variables (here: T_n) of $S_{g_n}(\omega,t)$ fluctuate around their respective average values. $S_{g_n}(\omega,t)$ as defined in equation 2.13 may then be rewritten to,

$$
S_{g_n}(\omega,t) = \frac{A_n^* \cdot \dfrac{T_n(t)}{E[T_n(t)]}}{\left[1 + B_n^* \cdot \dfrac{T_n(t)}{E[T_n(t)]} \cdot \omega\right]^{5/3}} \qquad (2.14)
$$

where,

$$
A_n^* = A_n \cdot E[T_n(t)] \qquad (2.15a)
$$

$$
B_n^* = B_n \cdot E[T_n(t)] \qquad (2.15b)
$$

Because $E\big[T_n(t)/E[T_n(t)]\big] \equiv E[T_n(t)]/E[T_n(t)] = 1$, equation 2.14 can be expanded by the factor $[1 + B_n^* \cdot \omega]^{5/3}$ and subsequently rearranged to,

$$
S_n(\omega,t) = \sigma_n^2(t) \cdot \frac{T_n(t)}{E[T_n(t)]} \cdot \frac{[1 + B_n^* \cdot \omega]^{5/3}}{\left[1 + B_n^* \cdot \dfrac{T_n(t)}{E[T_n(t)]} \cdot \omega\right]^{5/3}} \cdot \frac{A_n^*}{[1 + B_n^* \cdot \omega]^{5/3}} \qquad (2.16a)
$$

where,

$$\left|A_{g_n}(\omega,t)\right|^2 \quad = \quad \frac{T_n}{\overline{T}_n}\cdot\frac{[1+B_n^*\cdot\omega]^{5/3}}{\left[1+B_n^*\cdot\frac{T_n}{\overline{T}_n}\cdot\omega\right]^{5/3}} \tag{2.16b}$$

$$S_{g_n}(\omega) \quad = \quad \frac{A_n^*}{[1+B_n^*\cdot\omega]^{5/3}} \tag{2.16c}$$

Clearly, equation 2.16a is mathematically identical to equation 2.13 which was the starting point when separating $S_n(\omega,t)$ into $\sigma_n^2(t)$, $\left|A_{g_n}(\omega,t)\right|^2$ and $S_{g_n}(\omega)$. Thus, equation 2.16b would undoubtedly be correct if equation 2.13 was what we had real and definite knowledge about in advance. However, in practice it is of course the other way around because the objective is to modulate a function we can estimate and apply a curve fit to, namely $S_{g_n}(\omega)$, with the modulation function $\left|A_{g_n}(\omega,t)\right|^2$. One must therefore question the validity of the proposed expression of $\left|A_{g_n}(\omega,t)\right|^2$ as defined in equation 2.16b.

One could interpret the role of $\left|A_{g_n}(\omega,t)\right|^2$ to be to make $S_n(\omega,t)$ fluctuate around the average value of $S_{g_n}(\omega)$ for each setting for $\omega = \omega_i$. After all, $S_{g_n}(\omega)$ is a fitted curve to the very Fourier transform of the now presumed non–stationary, unit variance normalized recording in question and if this is assumed to have slowly evolving characteristics, $S_{g_n}(\omega)$ could be interpreted as to represent the *average* characteristics of the process over the considered time interval. Consequently, the expected value (average) of $\left|A_{g_n}(\omega,t)\right|^2$ for any given setting for ω should be equal to unity. The background for this alternative interpretation of the role of $\left|A_{g_n}(\omega,t)\right|^2$ is the fact that the expected value of the product of a set of time–dependent variables, $X_j(t)$, is not equal to the product of the expected values of the respective stochastic processes,

$$E\left[\prod_{j=1}^{N} X_j(t),\right] \quad \neq \quad \prod_{j=1}^{n} E\left[X_j(t),\right] \tag{2.17}$$

Because equation 2.16b is defined on the format of the right–hand side of equation 2.17 it will consequently have the following mathematical property, namely,

$$E\left[S_{g_n}(\omega_i,t)\right] \quad \neq \quad E\left[S_{g_n}(\omega)\right] \tag{2.18}$$

Thus, one might define $\left|A_{g_n}(\omega,t)\right|^2$ on the basis of mathematical expectation, namely on the format of the left–hand side of equation 2.17. Such is done by simply dividing the product of the time–varying parameters in equation 2.16b by its unique expected value for each setting for $\omega = \omega_i$, making $E\left[\left|A_{g_n}(\omega_i,t)\right|^2\right] \equiv 1$. The modified version of equation 2.16b will then take the following form,

$$\left|A_{g_n}(\omega_i,t)\right|^2 \quad = \quad \frac{T_n \cdot \left[1 + B_n^* \cdot \dfrac{T_n}{\overline{T}_n} \cdot \omega_i\right]^{-5/3}}{E\left[T_n \cdot \left[1 + B_n^* \cdot \dfrac{T_n}{\overline{T}_n} \cdot \omega_i\right]^{-5/3}\right]} \tag{2.19}$$

The two distinct methods of defining the non–uniform modulation function $\left|A_{g_n}(\omega,t)\right|^2$ given by equation 2.16 and 2.19 are labelled by Tao, Wang and Wu (2016) as the “XC–model“ and the “WK–model”, respectively. XC is short for Xu and Chen and WK is short for Wang and Kareem. Xu and Chen (2000) defines $\left|A_{g_n}(\omega,t)\right|^2$ equal to equation 2.16, namely by letting the time–varying variables involved fluctuate with respect to their own respective averages. Wang and Kareem (2004) does not have an expression for the EPSD but Tao, Wang and Wu labels the format of equation 2.19 the WK–model because Wang and Kareem generally defines variables that depends on several time dependent parameters with respect to the expected value of the entire variable itself. Even though the WK method sounds more correct because it is defined from the concept of mathematical expectation, it is by no means guaranteed to provide the more correct results when incorporated into the rest of the frequency domain buffeting response model. Therefore, both models are included and compared in chapter 3.

Due to its simple mathematical formula, the Kaimal spectrum was utilized as a tool to illustrate the implementation of the non–uniformly modulated model for the wind speed data. However, the von Kármán spectrums might or might not be a better approximation to an arbitrary wind speed recording and should also be included into a non–uniformly modulated model. Analogue to equation 2.13, the generalized, pre–fitted von Kármán spectrum formulae are given by,

$$S_u(\omega,t) \quad = \quad \sigma_u^2(t) \cdot \frac{A_u \cdot T_u(t)}{[1 + B_u \cdot [T_u(t) \cdot \omega]^2]^{5/6}} \tag{2.20a}$$

$$S_w(\omega,t) \quad = \quad \sigma_w^2(t) \cdot \frac{A_w \cdot T_w(t) \cdot [1 + B_w \cdot [T_w(t) \cdot \omega]^2]}{[1 + C_w \cdot [T_w(t) \cdot \omega]^2]^{11/6}} \tag{2.20b}$$

If the same procedures that was used to obtain equations 2.16 and 2.19 is applied to equation 2.20, their XC and WK colleagues are obtained. Of course, the format of equation 2.6 still applies and the difference lies in the expression for the modulation function $\left|A_{g_n}(\omega,t)\right|^2$. The four expressions for $\left|A_{g_n}(\omega,t)\right|^2$ now originating from the von Kármán spectrum is presented in the following.

Component u, XC model:

$$\left|A_{g_u}(\omega,t)\right|^2 \quad = \quad \frac{T_u}{\overline{T}_u} \cdot \frac{[1 + B_u^* \cdot \omega^2]^{5/6}}{\left[1 + B_u^* \cdot \left(\dfrac{T_u}{\overline{T}_u} \cdot \omega\right)^2\right]^{5/6}} \tag{2.21a}$$

$$S_{g_u}(\omega) \quad = \quad \frac{A_u^*}{[1 + B_u^* \cdot \omega^2]^{5/6}} \tag{2.21b}$$

Component w, XC model:

$$\left|A_{g_w}(\omega,t)\right|^2 = \frac{T_w}{\overline{T}_w}\cdot\frac{\left[1+B_w^*\cdot\left(\frac{T_w}{\overline{T}_w}\cdot\omega\right)^2\right]}{[1+B_w^*\cdot\omega^2]}\cdot\frac{[1+C_w^*\cdot\omega^2]^{11/6}}{\left[1+C_w^*\cdot\left(\frac{T_w}{\overline{T}_w}\cdot\omega\right)^2\right]^{11/6}} \tag{2.22a}$$

$$S_{g_w}(\omega) = \frac{A_w^*\cdot[1+B_w^*\cdot\omega^2]}{[1+C_w^*\cdot\omega^2]^{11/6}} \tag{2.22b}$$

Component u, WK model:

$$\left|A_{g_u}(\omega_i,t)\right|^2 = \frac{T_u\cdot\left[1+B_u^*\cdot\left(\frac{T_u}{\overline{T}_u}\cdot\omega_i\right)^2\right]^{-5/6}}{E\left[T_u\cdot\left[1+B_u^*\cdot\left(\frac{T_u}{\overline{T}_u}\cdot\omega_i\right)^2\right]^{-5/6}\right]} \tag{2.23}$$

Component w, WK model:

$$\left|A_{g_w}(\omega_i,t)\right|^2 = \frac{T_w\cdot\left[1+B_w^*\cdot\left(\frac{T_w}{\overline{T}_w}\cdot\omega_i\right)^2\right]\cdot\left[1+C_w^*\cdot\left(\frac{T_w}{\overline{T}_w}\cdot\omega_i\right)^2\right]^{-11/6}}{E\left[T_w\cdot\left[1+B_n^*\cdot\left(\frac{T_w}{\overline{T}_w}\cdot\omega_i\right)^2\right]\cdot\left[1+C_w^*\cdot\left(\frac{T_w}{\overline{T}_w}\cdot\omega_i\right)^2\right]^{-11/6}\right]} \tag{2.24}$$

The corresponding expressions for the time–invariant spectrum, $S_{g_n}(\omega)$, in equations 2.23 and 2.24 is given by equations 2.21b and 2.22b, respectively.

2.4.4.1 Integral time scale

The biggest challenge with the non–uniformly modulated EPSD is how to define the integral length scales, ${}^{x}L_n$. Hu, Xu and Huang (2013) does this by first using a method proposed by Priestley (1965) where the EPSD itself can be estimated directly from the discrete convolution of $n(t)$ and two subsequent window functions. Then, for a selected set of time instants, $\{t_i\}$, the respective von Kármán spectral formulae (equations 1.20 and 1.21) then is fitted to the estimated PSD data of n at $t = t_i$ (for instance via a *least square fit* (from now on: "LSF") algorithm) by varying ${}^{x}L_n$ itself, thus giving time–varying data for ${}^{x}L_n$. As illustrated by Hu, Xu and Huang, integral length scales may not only be estimated from direct measurements of wind speed data contrary to what its definition in equations 1.4 and 1.5 suggests. Nevertheless, a slightly modified version of the approximation of equation 1.5 is adopted for usage in this thesis, and hence the *integral time scale*, T_n, is the only parameters that is given attention in the following.

When adopting a time dependent format to equation 1.5 some adjustments must be made. First and foremost, integration of the auto covariance coefficient must be performed over the same time interval and by using the same weighting function used to derive the time varying variance. This is due to compatibility such that the auto covariance coefficient itself is unity at zero time lag. Of course, the auto covariance of a process with zero time lag is identical to the variance of the process. The time dependent auto covariance coefficient is now a two variable function and is given by,

$$\rho_n(t,\Delta t) \quad = \quad \frac{1}{\sigma_n^2(t)} \cdot \int_{-T_A}^{T_A} n(t+\tau) \cdot n(t+\tau+\Delta t) \cdot \widehat{w}(\tau) d\tau \qquad (2.25)$$

where τ is the integration variable, Δt is the auto covariance time lag, and $\widehat{w}(\tau)$ is the weighting function which is normalized to have unit are on the interval of integration. The principle of the auto covariance coefficient is illustrated in figure 2.10.

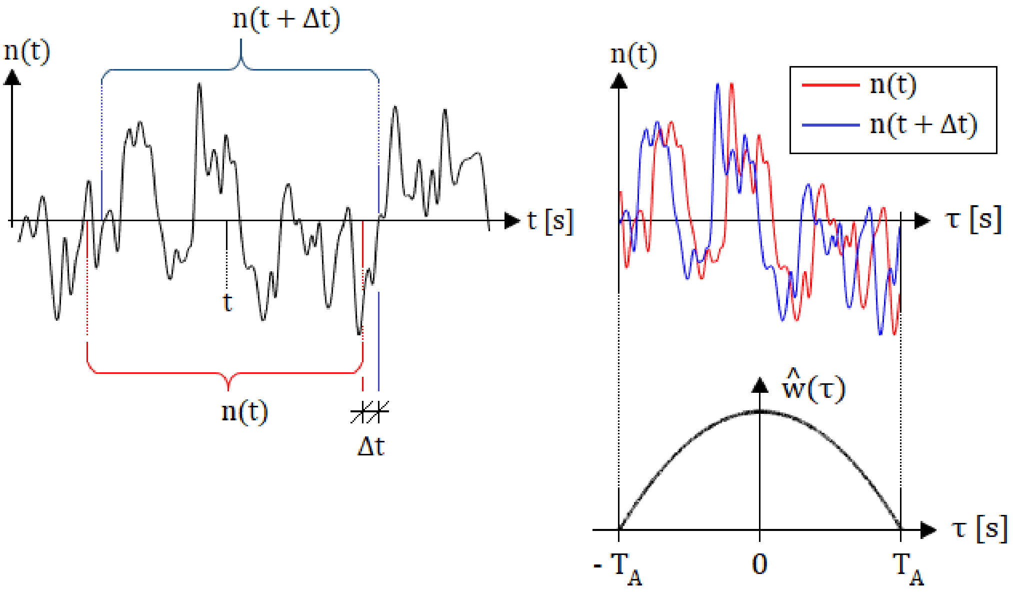

Figure 2.10: Calculation of time–varying auto covariance function

According to Strømmen (2010, p. 61), the auto covariance coefficient $\rho_n(\Delta t)$ will taper off from unity to zero as the time lag Δt goes from zero to infinity, much like an exponential function with a negative argument, as illustrated in figure 2.11. It is a direct result of this specific behaviour that the integral time scale can be calculated by integrating the auto covariance coefficient from zero to infinity and hence explaining the formulation of T_n as in equation 1.5.

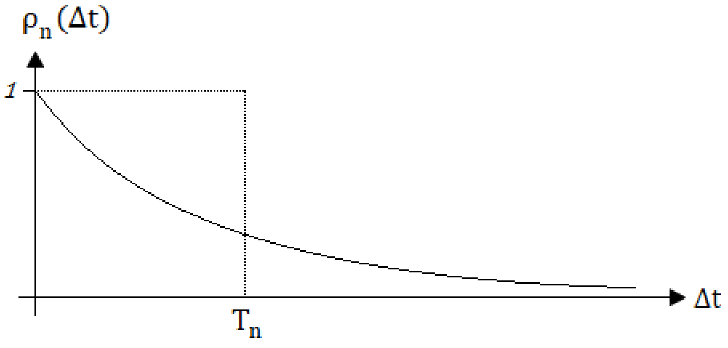

Figure 2.11: The auto covariance coefficient and the integral time scale

The shape–wise behaviour of the auto covariance function illustrated in figure 2.11 is probably a decent assumption when the radius of the integration domain, T_A, approaches infinity. However, such a procedure is not only irrelevant, but also inaccessible when it comes to obtaining time varying information about the integral time scale, T_n. The averaging period, T_A, is restricted by the method used to calculate the time varying variance, and another method of estimating T_n than what is suggested by equation 1.5 is therefore required. Fortunately, what provides an extra level of freedom is the fact that the numerical value of T_n itself is of zero interest because T_n always appears as normalized with respect to its average value in the expression for $\left|A_{g_n}(\omega, t)\right|^2$. Consequently, the only interesting feature is how T_n varies with time with respect to itself. To illustrate how one may calculate T_n from the time dependent auto covariance function, a generated and presumed non–stationary signal with zero mean value is considered, from which the auto covariance function $\rho_n(t, \Delta t)$ (equation 2.25) is calculated at four equally spaced instants in time, with Δt running from zero to Δt = 300 s., and with T_A = 300 s.

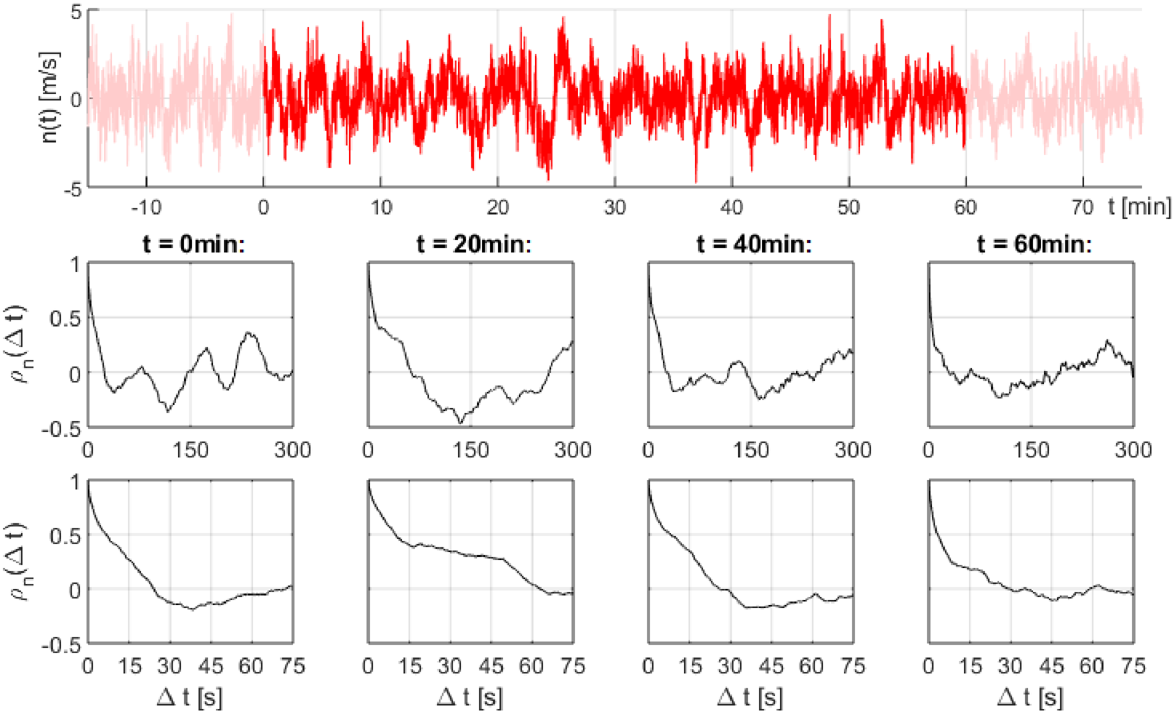

Figure 2.12: Δt – history for $\rho_n(t, \Delta t)$

The middle row of subplots in figure 2.12 clearly illustrates that after having passed the first value of Δt where $\rho_n(\Delta t)$ = 0, the shape of the curve cannot be used for determining T_n because of its unpredictable fluctuations. However, what is interesting is the shape of the curve up until this point, as is illustrated in the bottom row of subplot. These curves are the same as the ones above, only examined on another domain.

From the shape of these curves, the time scales, T_n, can be defined in two different ways. First, simply by determining the time lag, $\Delta t = \Delta T_{THR}$, that is required to make $\rho_n(\Delta t)$ drop below a certain threshold, ρ_{THR}, for the first time. Introducing ρ_{THR} = 0 is an obvious choice, but as the auto covariance curves in figure 2.12 illustrates, the irregular shape of the curve may start to form before $\rho_n(\Delta t)$ has reached zero. As with the time varying variance and the mean wind speed, the desired result is a relatively smooth curve with the absence of rapid, violent and unpredictable oscillations. Consequently, ρ_{THR} can be chosen such that there is assumed to be a small probability for the irregularities in the auto covariance curves to occur before $\rho_n(\Delta t)$ for the first time reaches ρ_{THR}. If however ρ_{THR} is set too close to unity, a sampling frequency of for instance 0.1 s might be highly significant compared to the time lag needed to make $\rho_n(\Delta t)$ reach ρ_{THR}, resulting in clearly visible "increment–like" behaviour of $T_n(t)$. Taking these to effects into account, ρ_{THR} = 0.25 might be a decent choice.

If the auto covariance curve is well–behaved for $\Delta t \leq \Delta T_{THR}$, the rate at which it decreases from zero will be inversely proportional to ΔT_{THR}. A rapidly decreasing auto covariance function and a corresponding short value of ΔT_{THR} implies that the local "eddy size" of the wind field is being equally small, and vice versa. This concept is in direct correspondence with Strømmen's (2010, p. 61) physical interpretation of the integral length (time) scales.

The second way T_n can be defined is the area between the auto covariance curve and the horizontal line ρ_n = ρ_{THR}. A possible advantage with this integral formulation is that if an irregularity forms above ρ_{THR} and before ΔT_{THR}, such would make a larger difference in the value of ΔT_{THR} than in the corresponding area between the auto covariance curve and ρ_n = ρ_{THR} (figure 2.13). Hence, the integral method might give more consistent results if ρ_{THR} is not chosen such that the part of the auto covariance curve for $\Delta t \leq \Delta T_{THR}$ will be as good as free of irregularities. The two respective methods are illustrated in figure 2.13.

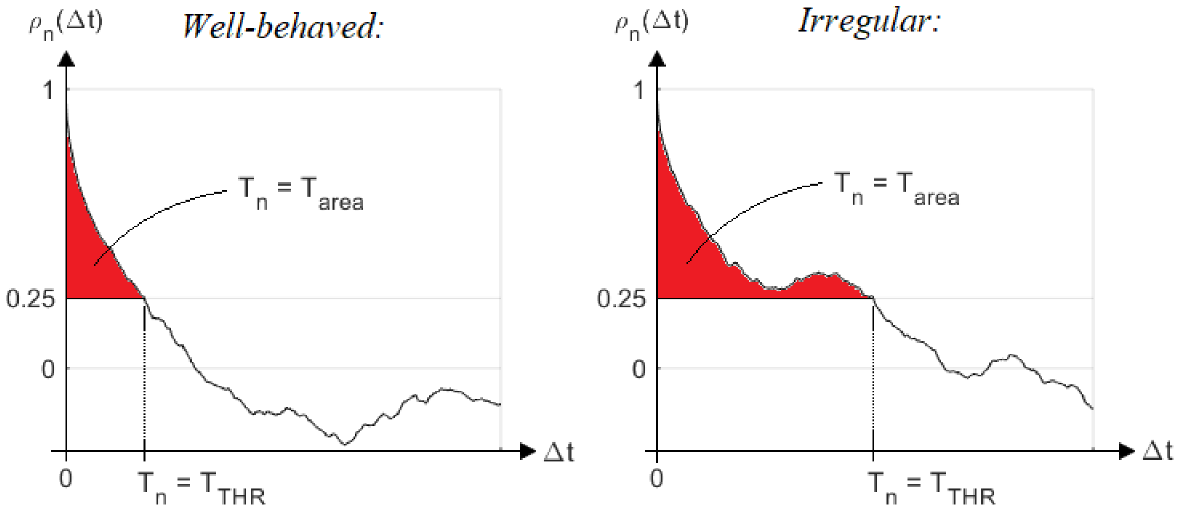

Figure 2.13: Principle of time scale methods (ρ_{THR} = 0.25)

To illustrate the resulting curves for the time varying time scales when considering both of the two aforementioned methods, they are simply applied to the generated signal in the top of figure 2.12. The resulting time varying time scales are shown and compared in figure 2.14 with T_A = 300 s., ρ_{THR} = 0.25, and parabolic weights.

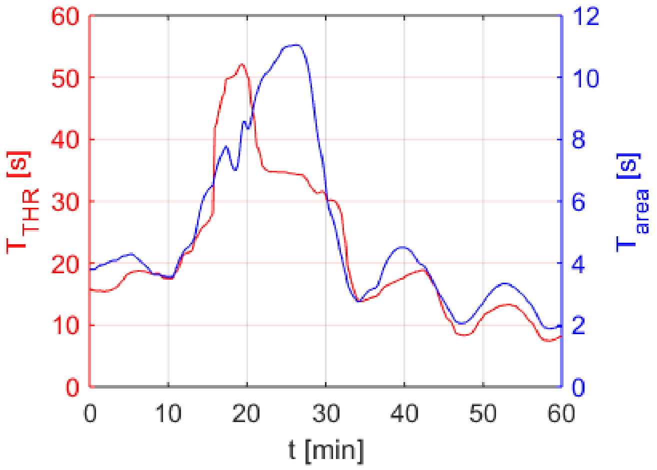

Figure 2.14: Threshold–, and integral method.

2.4.5 Determination of the time–invariant spectrum, $S_{g_n}(\omega)$

As suggested in chapter 2.4.4, time dependent versions of the spectral formulae proposed by Kaimal and von Kármán are given the role to estimate the EPSD of $g_n(t)$, $S_{g_n}(\omega,t)$. In contrast to its definition in equations 1.20 – 1.21, also the von Kármán spectrum is set to be free of any pre–determined constants, such that only the framework of its mathematical formulation is exploited for the purpose of producing a presumably better fit to the spectral dataset of an arbitrary wind speed recording.

However, how to select the respective constants, $\{A_n^*,B_n^*,C_n^*\}$, is by no means an easy task because our objective is to somehow interpret what physical process the scattered spectral data is a realization of and what physical process it thereby represents. No mathematical formula can provide us with a true answer to this question since no such thing exists, only interpretation can give indications towards the fact that a proposed solution is a decent one. Theoretically, one could try to fit a Kaimal or von Kármán curve by changing $\{A_n^*,B_n^*,C_n^*\}$ manually until the resulting curve fits the spectral dataset in a satisfactory manner, however such is usually difficult because the relation between the value of $\{A_n^*,B_n^*,C_n^*\}$ and the shape of the resulting curve in the log–log domain is rather abstract, apart from the fact that manual fitting is also highly ineffective. Consequently, a method that provides a good candidate for what can be regarded as the very physical process the spectral dataset represents, is needed. A method of such character is the LSF method where the parameters of a candidate curve is selected such that the sum of square deviations between the spectral data set and the candidate curve itself is minimized. Many LSF algorithms exists and MATLAB R2018a provides a very user–friendly one with the toolbox "*cftool*" where an iterative LSF process can be performed on a data set with a user specified equation of arbitrary format.

A fundamental problem that arises when using a LSF method is that one cannot interpret the solution of being anything else than the version of the adopted curve format that minimizes the sum of the squares. Hence the solution curve from the LSF method and the desired curve that represents the physical process in question, are not necessarily equated. The reason for this is that most spectral data is quite scattered as well as being spread over several orders of magnitude in both X and Y. To compensate for this undesired effect, proposed remedies are presented and discussed in the following, in which the first one is an algorithm that denoises spectral data.

2.4.5.1 Spectral data denoising algorithm – enhancement of LSF quality

To illustrate what a "correctly fitted" spectrum curve may look like, an arbitrary stationary signal $n(t)$ ($n = u, w$) with length T = 2 hours is generated from the arbitrarily chosen, dimensionless Kaimal spectrum, $S_n(\widehat{\omega})$ = $240[1 + 60\widehat{\omega}]^{-1.67}$. The highest included frequency is set to be ω_{max} = 15 rad/s, and the Fourier spectrum is calculated from a subset of this recording in order to generate scatter. The generated signal is shown in figure 2.15.

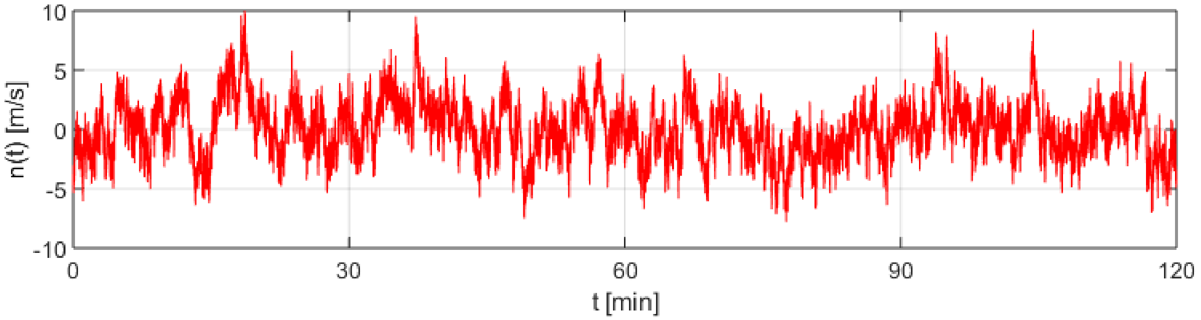

Figure 2.15: Generated, stationary Kaimal signal.

Figure 2.16 shows calculated spectral data from three subset recordings of duration T = 70 min. A uniformly weighted LSF from the MATLAB toolbox "cftool" is for comparison applied to these spectral data sets by using the Kaimal formula.

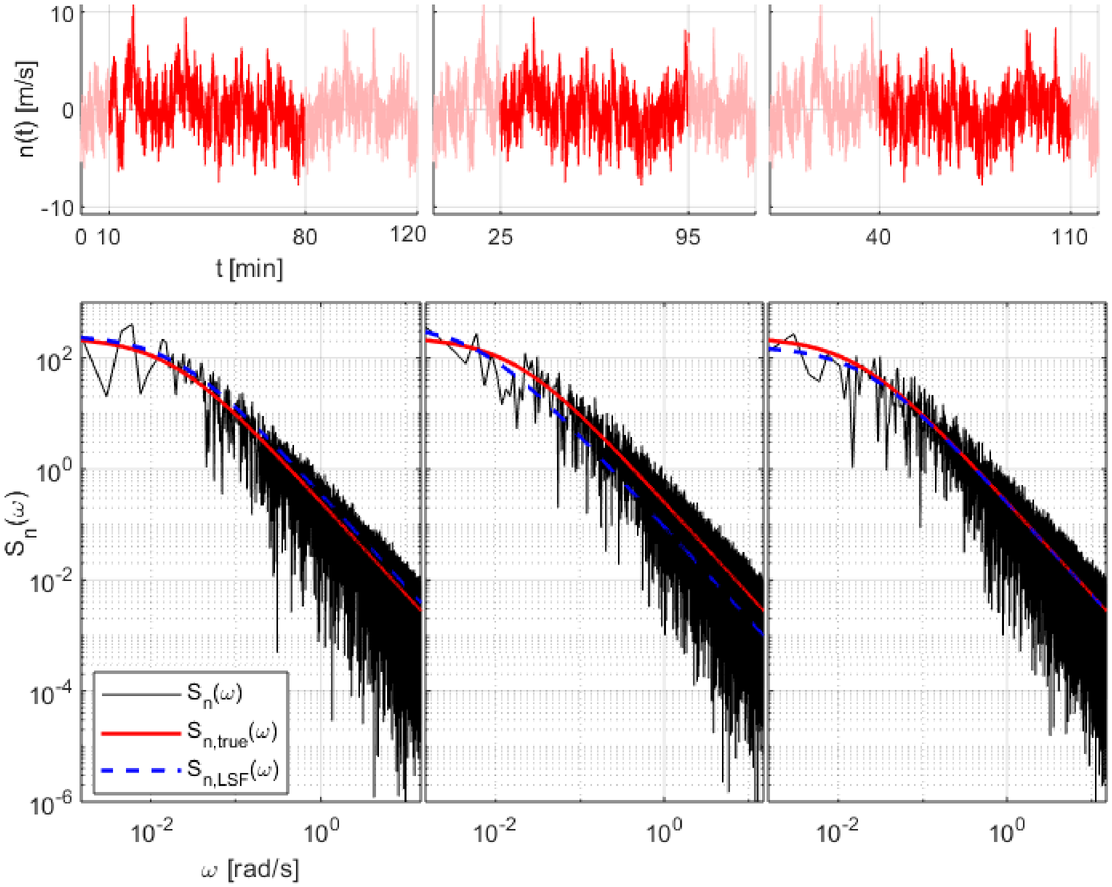

Figure 2.16: Comparisons of spectral data, "true" spectrums and LSF spectrums.

Figure 2.16 clearly illustrates the fact that the LSF simply minimizes the sum of the square deviations and nothing more, and that the LSF curve and the theoretically "correct" curve hence by no means are equated. Clearly, the data points at the lowest most portion of the spectrum does also have the largest magnitude and scatter in this region will consequently have a disproportionally large influence on the outcome of the LSF. This effect explains the variations int the outcome of the LSF in the considered cases illustrated in figure 2.16.

The impact of these undesired deviations from the theoretically "true" spectrum curves can be illustrated via considering the square root of the ratio between the true spectrum curve and the proposed LSF spectrum. The square root of this ratio as given by equation 1.12, is per definition proportional to the amplitude of the harmonic component with frequency, ω. Hence, if this very ratio for instance equals 1.10 at $\omega = \omega_k$, such can be interpreted as overestimating the magnitude of the amplitude of the harmonic component of the wind speed recording at $\omega = \omega_k$ with 10 %. Further, if ω_k lies in the frequency–region of one of the eigenmodes of the structure in question, the standard deviation of the magnitude of the oscillations from this very mode will also be overestimated by 10 %.

In reality, being able to estimate the magnitude of wind induced structural oscillations within, say 10 %, can in many ways be considered as decent from a design perspective considering all the uncertainties in the theory, and that a safety margin of much more than 10 % is usually accounted for in structural design. However, if we had not known the theoretically correct spectrum of the spectral data in advance, which one never does with real life data, there would be difficult to argue in favour of discarding especially the LSF curves to the left and to the right in figure 2.16, but if such is obvious, as clearly is the case in the middle spectrum plot of figure 2.16, one must find a way to come up with a better solution apart from a rather inaccurate manual fit.

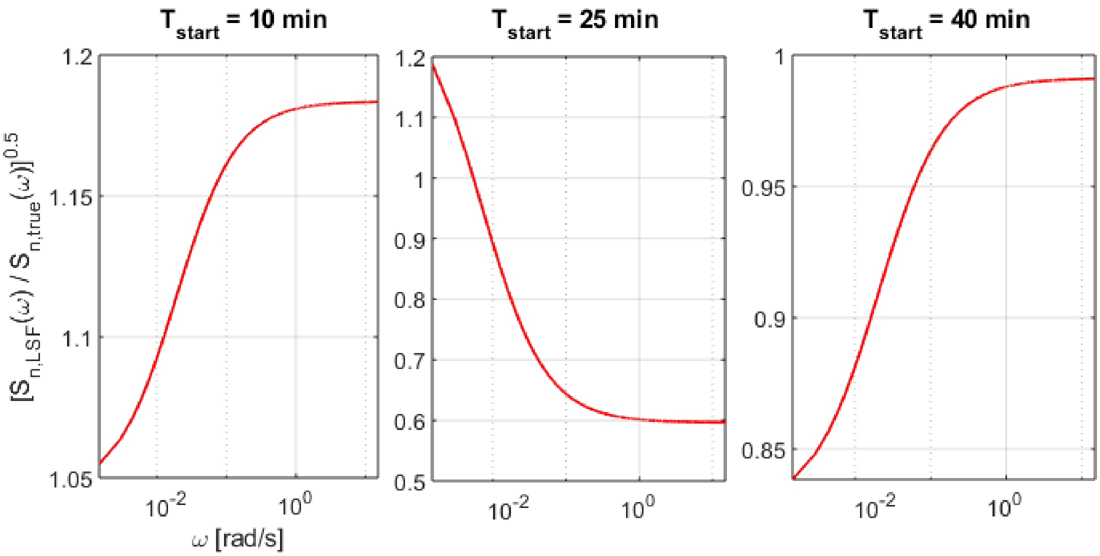

Figure 2.17: Magnitude ratio of the standard deviation (amplitude) of harmonic components.

In order to narrow down the possible outcome of the LSF method, two major improvements are proposed, in which the first one is a spectral data denoising method whose principle is based on the assumption that the scatter of the spectral data "fluctuates" around its local average in the non–logarithmic value domain. To estimate this local average a uniformly weighted moving average method is applied in which nearby spectral data at $\omega = \omega_i$ is averaged. Such a method may initially seem intuitive and straight–forward but this is not the case since one major challenge is faced. Namely, since the largest magnitude spectral data points represents a very small portion of the total number of spectral data points, they are very influential when it comes to the outcome of the LSF procedure, or generally when it comes to interpreting the ideal shape of the spectral curve that best represents the stochastic process. Hence, the bandwidth of the aforementioned averaging process should be formulated as a function dependent on ω, consequently accounting for the degree of influence of each spectral data point. For simplicity, the following function is proposed as to represent the bandwidth function, $BW(\omega)$:

$$BW(\omega) \quad = \quad \left\lfloor n_1 + (n_2 - n_1) \cdot \left[\frac{log(\hat{\omega}) - log(\hat{\omega}_{n_{1+1}})}{log(\hat{\omega}_{n_{2-1}}) - log(\hat{\omega}_{n_1})} \right]^m \right\rfloor, \qquad \hat{\omega} \geq \hat{\omega}_{n_{1+1}} \tag{2.26}$$

where $\hat{\omega}$ is a dimensionless frequency normalized by its own dimension, $\hat{\omega} = \omega/\omega_0$, $\omega_0 = 1$ rad/s. $BW(\omega)$ is an exponential function defined on the logarithmic domain which takes the values $\{n_1, n_2\}$ at $\omega = \{\omega_{n_1+1}, \omega_{n_2-1}\}$ where n_1 and n_2 are index bandwidths, that is, the number of indices left and right of ω_i in the ω settings vector that defines the subset $\{\omega_{i-BW(\omega_i)}\colon \omega_{i+BW(\omega_i)}\}$ from which the uniform average at $\omega = \omega_i$ is calculated. m is chosen simply by adapting the shape of $BW(\omega)$ such that the magnitude of the scatter of the averaged spectrum is more or less uniformly distributed over the frequency axis. Figure 2.18 shows a plot of $BW(\omega)$ with the illustrative values $\{n_1, n_2\} = \{5, 150\}$ and $m = \{1.25, 1.5, 2, 3\}$, together with the right most spectrum in figure 2.16.

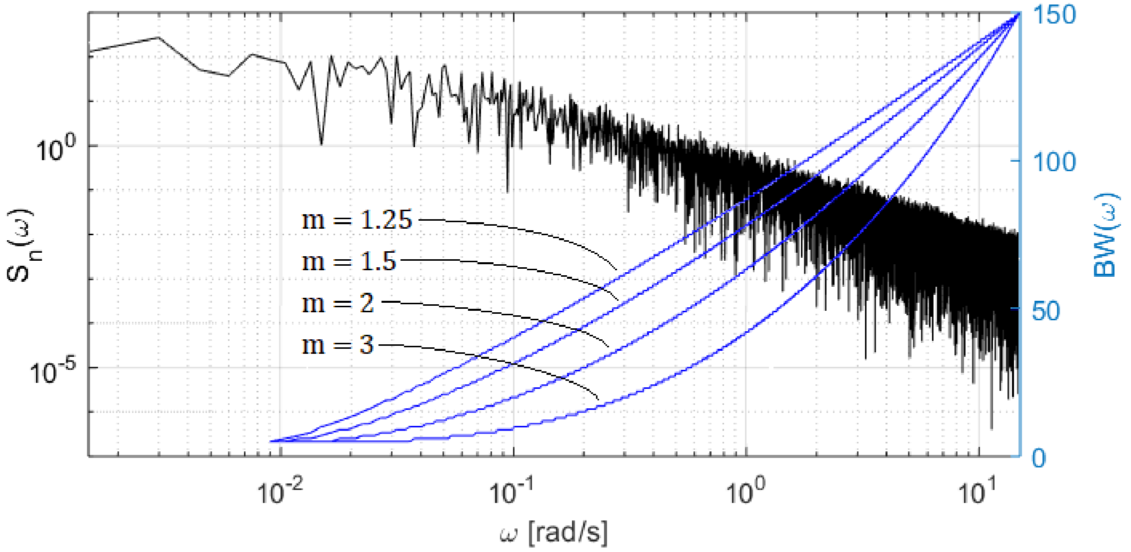

Figure 2.18: Bandwidth function

Equation 2.26 can obviously not be defined for indices less than $n_1 + 1$ because the lowest index in the corresponding averaging subset cannot be less than 1. Therefore, the rule given by equation 2.27 is adopted for this region.

$$\begin{array}{rrcl}
i = 1 & S_{n,avg}(\omega_1) & = & avg[S_n(\omega_1\colon \omega_2)] \\
2 & S_{n,avg}(\omega_2) & = & avg[S_n(\omega_1\colon \omega_3)] \\
3 & S_{n,avg}(\omega_3) & = & avg[S_n(\omega_1\colon \omega_5)] \\
\vdots & & \vdots & \\
i = n_1 & S_{n,avg}(\omega_{n_1}) & = & avg\left[S_n\left(\omega_1\colon \omega_{2n_1-1}\right)\right]
\end{array} \tag{2.27}$$

The second improvement when it comes to utilizing the LSF as a convenient curve fitting tool is introducing weighting factors to the now denoised (averaged) spectral dataset. The question is however, how the weighting factors should be chosen. Revisiting the fact that scatter in the high magnitude region of the spectral data set constitute a disproportionally large contribution to the sum of squares, one might compensate for such behaviour by introducing a weighting function which is inversely proportional to the square of the denoised spectral value,

$$W(\omega_i) \quad = \quad \left[S_{n,avg}(\omega_i)\right]^{-2} \tag{2.28}$$

The reason why the square of the denoised spectrum is used in equation 2.38 is because the LSF fits a curve by minimizing namely the sum of the *square* deviations between the proposed curve and the dataset. If a method that minimized the *absolute value* of the de sum of deviations, the exponent in equation 2.28 would be set accordingly.

With the introduction of the two aforementioned improvements to the LSF framework, they are now adopted and applied to the stationary generated recording in figure 2.15. The same comparisons between the theoretically true spectrum curve and the now enhanced LSF curves are displayed in figure 2.19.

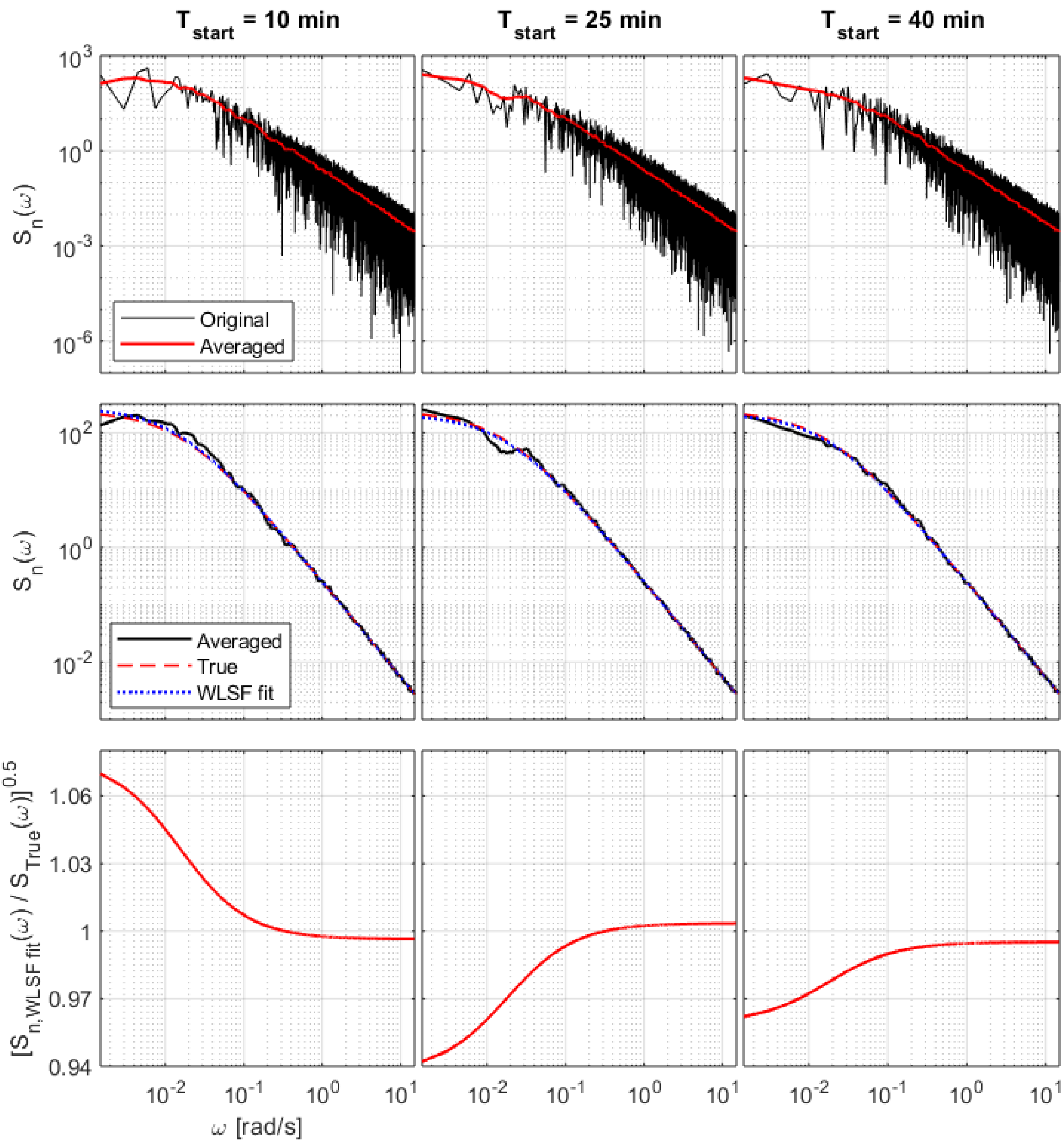

Figure 2.19: Enhanced WLSF procedure

Comparing the bottom row of subplots of figure 2.19 to the respective subplots in figure 2.17 indicates that when instead letting the LSF algorithm use the averaged spectral data as input together with the inclusion of the weighting function of equation 2.28, its ability to reveal what stochastic process the spectral data originates from, is enhanced. Of course, the fact that the spectral dataset originates from the very same function used as the candidate function in the LSF procedure might by slightly advantageous for the performance of the enhanced WLSF, however the main purpose of the method is clearly illustrated when it much more able to reveal the shape of an unknown virtual function which is hidden away by stochastic scatter.

The resulting coefficients of the Kaimal spectrum from the ordinary LSF method and the enhanced WLSF method is given in table 2.1. m, n_1 and n_2 are coefficients of the bandwidth function in equation 2.26. m was set equal to 2 since that seemed to produce a relatively uniform distribution of scatter in the averaged spectrum curve. Because of the different distribution of the scatter in the first few data points of the spectral data set, n_1 was selected such that this region took the form of a as smooth as possible averaged curve, nevertheless, such an adaptation is only of minor effect. Similarly, the formulation of the commissioning phase of the average process given by equation 2.27 may also be defined elsewise, however, equation 2.27 was defined simply for the sake of convenience and simplicity.

	Ordinary LSF:		Enhanced WLSF:				
Subset recording:	**A_n^*:**	**B_n^*:**	**A_n^*:**	**B_n^*:**	**m:**	**n_1:**	**n_2:**
T_{start} = 10 min	262.0	51.68	278.4	65.86	2	5	100
T_{start} = 25 min	415.4	154.7	210.7	55.27	2	5	100
T_{start} = 40 min	164.2	48.30	220.8	57.41	2	8	100

Table 2.1: Kaimal curve fit coefficients

Throughout this demonstration, the exponent in the Kaimal spectrum was set to -1.67. Tao, Wang and Wu (2016, p. 13) states that according to *Kolmogrov theory*, stationary turbulence can be described by the general formula,

$$S_n(\omega) \quad = \quad \frac{A \cdot \widehat{\omega}^{\gamma-1}}{[1 + B \cdot \widehat{\omega}^{\alpha}]^{\beta}} \tag{2.29}$$

where γ, α and β should follow the rule $\gamma - \alpha\beta = -2/3$. Given this rule, the derivative of $\log[S_n(\omega)]$ with respect to $\log[\widehat{\omega}]$ will approach the limit value $-5/3$ when $\widehat{\omega}$ approaches infinity. This very relation is the very property that derives the exponents in the Kaimal and von Kármán spectrum formulas. However, no rule gives information about at when the limit slope of $-5/3$ is indeed “reached” for any given wind field. Consequently, assigning the exponent in the spectrum formula another value prior to the WLSF procedure does not violate the fitted curves ability to fit to the spectral data at the high end of the frequency axis. The effect this has is only changing the general shape of the fitted curve so it becomes less restricted when it comes to fitting the less well–behaved spectral data from real–life wind speed recordings.

When the now presented WLSF procedure will be used in chapter 4 to fit an appropriate spectrum curve to real–life wind data, the exponent, β, is not set to be restricted by $\gamma - \alpha\beta = -2/3$ but set at other values nearby to optimize the shape of the fitted curve. However, introducing β as another degree of freedom in the WLSF procedure is generally not recommended because such might give spurious results. After all, what is the primary goal is finding a curve that by interpretation and common sense seems to represent the spectral data appropriately. One must also take into account the location of the eigenfrequencies of the structure in question because it is highly important to fit the spectral data as accurately as possible in these very regions due to modal dynamic amplification.

2.5 DISTRIBUTION OF MAXIMUMS

Chapter 1.4 showed the derivation of approximated expressions for the expected value and variance of the maximum value of the stochastic part of the structural response. As a result of the special case of stationarity, approximated analytic expressions for the expected maximum and variance of maximum structural response within a time window, T, are derived. These expressions, which are given by equations 1.63 and 1.64 are obtain partially via solving the time–invariant up–crossing function given by equation 1.61, with respect to the up–crossing level itself. Chen (2015) adopts a time–varying version of the up–crossing function where the variance and mean response is time–dependent. Also, the up–crossing level is defined as being the sum of the time varying mean response and the stochastic response, which is contrary to the stationary version where the mean response is added subsequently. The CDF of n_{max} is assumed to follow a Gumbel Type 1 distribution at high levels of extreme (Chen, 2015) because of its exponential tail that "tapers off" exponentially when n_{max} approaches infinity. The CDF of n_{max} where structural response component, $n(t)$, is considered, is given by,

$$CDF(n_{max}) \quad = \quad exp[-\kappa(n_{max})] \tag{2.30a}$$

where,

$$\kappa(n_{max}) \quad = \quad \frac{1}{2\pi}\int_0^T \frac{\sigma_{\dot{n}}(t)}{\sigma_n(t)} \cdot exp\left[-\frac{(n_{max}-\bar{N}(t))^2}{2\sigma_n^2(t)}\right] dt \tag{2.30b}$$

And where $\bar{N}(t)$ is the time–varying mean value of $n(t)$.

The integration procedure in equation 2.30b is intuitive because it considers $n(t)$ to be a relatively narrow banded evolutionary stochastic process where the expected number of occurrences of n_{max} within the infinitesimal time window, dt, is assumed to equate to the up–crossing frequency at level n_{max} at this point in time, multiplied with dt. $\kappa(n_{max})$ is then, analogue to its stationary counterpart, equal to the time–varying, expected number of occurrences of n_{max} within dt, summated over T.

Obviously, solving equation 2.30 with respect to n_{max} is for all practical purposes impossible, and no closed form expression of the expected value and variance of n_{max} consequently exists. Nevertheless, such is in many ways obsolete because every relevant piece of information can be obtained from the CDF itself, especially quantile values which come in handy when estimating return periods for n_{max}. When implementing equations 2.30a and b, a discrete mesh of values for n_{max} must anyway be used and the PDF can be obtained numerically by numerical differentiation of the CDF using for instance the "center–rule" of numerical differentiation, namely,

$$\begin{aligned} PDF(n_{max}) \quad &= \quad \frac{d}{dn_{max}} CDF(n_{max}) \\ &\approx \quad \frac{CDF\left(n_{max,i+1}\right) - CDF\left(n_{max,i-1}\right)}{2\Delta n_{max}} \end{aligned} \tag{2.31}$$

3 CASE STUDY – THE HARDANGER BRIDGE

3.1 INTRODUCTION

To investigate the effects of non–stationary winds, the theory presented in chapter 1 and 2 is applied to the Hardanger Bridge in Hordaland, Norway. In order to solve the very equations that that makes up the mathematical model of structural response, several MATLAB routines has been established whose supreme purpose is to provide the necessary computing power to solve these mathematical formulas when being applied and highly streamlined to the Hardanger Bridge, and the Hardanger Bridge only. Consequently, these scripts must be used with great caution since their range of intended applications is extremely narrow. The scripts themselves are given in Appendix B.

Again, because every bridge is unique, the specific form some of the steps of the mathematical framework presented in chapters 1 and 2 will take, will generally vary accordingly. Such variations may originate from for instance symmetry– and dynamic properties of the bridge structure in question. For such reasons, this chapter is devoted to present a set of arising concepts when applying the general buffeting theory framework to the Hardanger bridge specifically. A time domain Monte Carlo simulation algorithm that is highly specialized to the Hardanger bridge will also be presented, which will serve as a very handy aid when it comes to validating the non–stationary frequency domain buffeting response.

3.2 PHYSICAL CHARACTERISTICS AND DYNAMIC PROPERTIES

Figure 3.1: The Hardanger Bridge viewed from the North ([17])

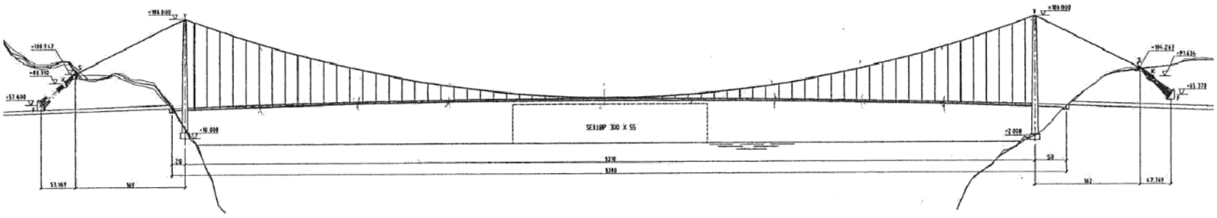

Figure 3.2: Sketch of the Hardanger Bridge

For the case study in this thesis, 18 eigenmodes are included in the dynamic model of the Hardanger bridge. Table 3.1 shows the eigenfrequency, the damping ratio and the respective displacement component for each mode. None of the included modes are coupled modes. Figure 3.3 shows the corresponding shape of the eigenmodes listen in table 3.1.

Eigenmode:	**Type:**	**ω_n [rad/s]:**	**ζ_n:**
1	Horizontal	0.32	.0050
2	Horizontal	0.64	.0052
3	Vertical	0.71	.0050
4	Vertical	0.90	.0051
5	Horizontal	1.11	.0062
6	Vertical	1.27	.0058
7	Vertical	1.36	.0060
8	Horizontal	1.56	.0079
9	Horizontal	1.66	.0084
10	Vertical	1.76	.0077
11	Horizontal	1.95	.0100
12	Vertical	2.14	.0100
13	Torsional	2.25	.0050
14	Torsional	3.49	.0052
15	Torsional	5.28	.0063
16	Torsional	7.00	.0083
17	Torsional	8.76	.0112
18	Torsional	10.50	.0150

Table 3.1: Eigenmode characteristics

The eigenmodes are in this case calculated using the FEM their length wise shape is subsequently obtained by calculating the Fourier components to the resulting discrete vector of DOFs constituting the respective mode shape components.

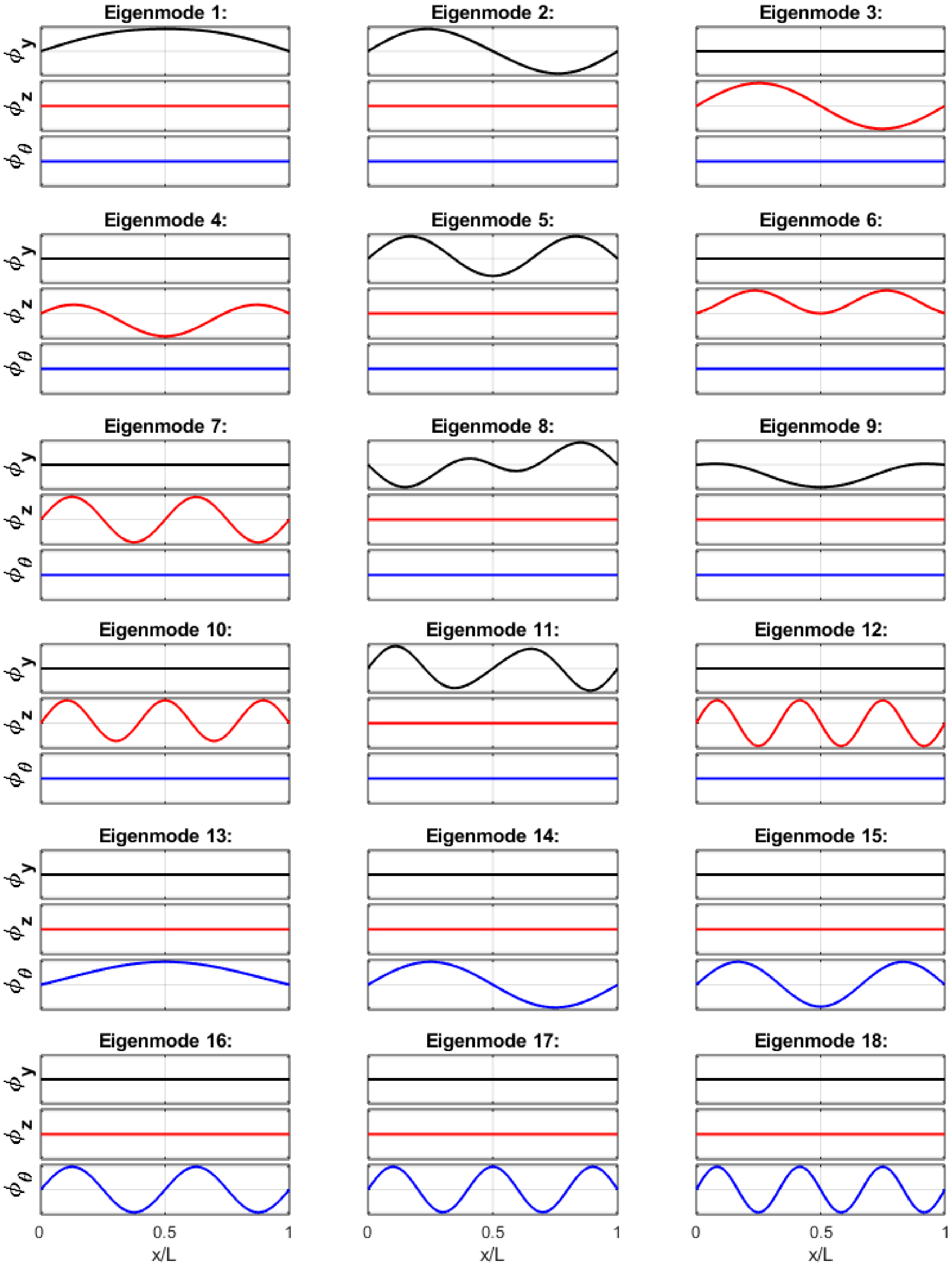

Figure 3.3: Relative span wise shape of included eigenmodes.

3.3 CALCULATION OF THE JOINT ACCEPTANCE FUNCTION

A consequence of expressing the eigenmodes as a sum of harmonic components is that the expression for the joint acceptance function as given by equation 1.59b can be evaluated analytically. Firstly, equation 1.59 may be rewritten to a format more suited to a non–stationary formulation, namely by not separating the PSD of the wind field into turbulence intensity and a normalized PSD,

$$S_{\hat{Q}_{v,i}\hat{Q}_{v,j}}(\omega,t) \;=\; \left(\frac{\rho BL\cdot\bar{U}(t)}{2}\right)^2\cdot\frac{1}{\widetilde{M}_i\omega_i^2\cdot\widetilde{M}_j\omega_j^2}\cdot J_{ij}^2 \tag{3.1a}$$

where,

$$J_{ij}^2 \;=\; \int_0^1\int_0^1 \boldsymbol{\varphi}_i^T(\hat{x}_1)\widehat{\boldsymbol{B}}_q\,\boldsymbol{S}_v(\omega,t,\Delta\hat{x})\widehat{\boldsymbol{B}}_q^T\boldsymbol{\varphi}_j(\hat{x}_2)d\hat{x}_1d\hat{x}_2 \tag{3.1b}$$

Since $\bar{C}_L$, C_D' and $\bar{C}_M$ are all approximated as being zero for the Hardanger Bridge, $\widehat{\boldsymbol{B}}_q$ in equation 1.37d takes the following entry–wise form,

$$\widehat{\boldsymbol{B}}_q \;=\; \begin{bmatrix} B_{q,11} & 0 \\ 0 & B_{q,22} \\ 0 & B_{q,32}\end{bmatrix}, \qquad \begin{cases} B_{q,11} \;=\; 1.4a_r \\ B_{q,22} \;=\; C_L' + 0.7a_r \\ B_{q,32} \;=\; BC_M' \end{cases} \tag{3.2}$$

Hence, the fully expanded and problem specific version of the joint acceptance function will be as follows,

$$\begin{aligned} J_{ij}^2(\omega,t) \;=\; \int_0^1\int_0^1 [\quad & B_{q,11}^2\cdot S_u(\omega,t)\cdot\varphi_{iy}(\hat{x}_1)\cdot\varphi_{jy}(\hat{x}_2)\cdot\hat{C}o_u(\omega,t,\Delta\hat{x}) \\ + \quad & B_{q,22}^2\cdot S_w(\omega,t)\cdot\varphi_{iz}(\hat{x}_1)\cdot\varphi_{jz}(\hat{x}_2)\cdot\hat{C}o_w(\omega,t,\Delta\hat{x}) \\ + \quad & B_{q,22}\cdot B_{q,32}\cdot S_w(\omega,t)\cdot\varphi_{iz}(\hat{x}_1)\cdot\varphi_{j\theta}(\hat{x}_2)\cdot\hat{C}o_w(\omega,t,\Delta\hat{x}) \\ + \quad & B_{q,22}\cdot B_{q,32}\cdot S_w(\omega,t)\cdot\varphi_{i\theta}(\hat{x}_1)\cdot\varphi_{jz}(\hat{x}_2)\cdot\hat{C}o_w(\omega,t,\Delta\hat{x}) \\ + \quad & B_{q,33}^2\cdot S_w(\omega,t)\cdot\varphi_{i\theta}(\hat{x}_1)\cdot\varphi_{j\theta}(\hat{x}_2)\cdot\hat{C}o_w(\omega,t,\Delta\hat{x})\;]\;d\hat{x}_1d\hat{x}_2 \end{aligned} \tag{3.3}$$

Because the mode shape components, φ_{nm}, are linear sums of harmonic components, J_{ij}^2 will be a sum of constant multiples of functions on the form,

$$F(\omega,t) \;=\; \int_0^1\int_0^1 sin(p\hat{x}_1)\cdot sin(q\hat{x}_2)\cdot e^{C|\hat{x}_1-\hat{x}_2|}d\hat{x}_1d\hat{x}_2\;, \qquad \begin{cases} p = P\pi \\ q = Q\pi \\ C = -\dfrac{c_{nx}\omega L}{U(t)} \end{cases} \tag{3.4}$$

where P, and Q are non–zero, positive integers representing the number of "half waves" the respective harmonic subcomponent display along the bridge span. The very derivation of the analytical solution to equation 3.4 can be found in Appendix A.2 and the result is that $F(\omega,t)=0$ for all P and Q having opposite parity, and in the case of P and Q having equal parity, $F(\omega,t)$ is given by,

$$F(\omega,t) \;=\; \frac{2q}{q^2+C^2}\left[\frac{cos(p-q)-1}{2(p-q)}+\frac{cos(p+q)-1}{2(p+q)}-\frac{p(1-e^C\cos p)}{p^2+C^2}\right] \quad , \quad p \neq q \qquad (3.5a)$$

$$F(\omega,t) \;=\; \frac{2}{p^2+C^2}\left[\frac{p^2(1-e^C\cos p)}{p^2+C^2}-\frac{C}{2}\right] \quad , \quad p = q \qquad (3.5b)$$

3.3.1 Increasing performance of MATLAB routine

As indicated in chapter 4.1, the objective is not to produce some sort of universal MATLAB algorithm that can calculate the response of any bridge, but rather quite the opposite. In the case of the joint acceptance matrix, $\boldsymbol{J}^2$, which is the very hub of the multi–mode, frequency domain buffeting response method, this is not due to the need for human interpretation as is the case when modelling the wind field, but rather because of a strong desire to minimize the computational expense associated with establishing $\boldsymbol{J}^2$ itself.

Of course, an ineffective algorithm will restrict the usability of the MATLAB routine when it comes to running it several times, which indeed must be done not only to ensure that it works correctly and according to its purpose, but also for investigational and learning purposes because such a MATLAB script is a very powerful tool when it comes to obtaining knowledge about the phenomenology of wind induced dynamic oscillations. Also, in situations where a relatively fine mesh is needed for both time and frequency, establishing $\boldsymbol{J}^2$ for all these combinations of T and ω might take 30 minutes or more if no effort is given to optimize the algorithm that establishes $\boldsymbol{J}^2$. Thankfully, such an optimization procedure is a relatively simple task in the case of the Hardanger Bridge because of three specific properties it displays:

1. *Single component eigenmodes.*

   Because all 18 included eigenmodes contains only one non–zero displacement component (see figure 3.3), there exists only one possible combination of displacement components m and n such that the product of two arbitrary components φ_{in} and φ_{jm} will be non–zero. Because only five out of the possible nine combinations are present in the expression for J_{ij}^2 in equation 3.3, roughly 5/9 of the entries of $\boldsymbol{J}^2$ will be non–zero, and where these entries themselves thus are constructed from only one of the five terms in equation 3.3.

2. *Structural symmetry with respect to the bridge midspan.*

   Because the Hardanger bridge is symmetric with respect to its midspan (or at least, this is the way it is indeed modelled), so must be the case of the eigenmodes. Hence, they must all fall into either of two categories, namely being oddly symmetric or evenly symmetric with respect to the bridge midspan. If this is the case for the eigenmodes themselves so must also be the case for the harmonic Fourier components constituting them, i.e. their wavenumbers (P, Q, equation 3.4) must all have the same parity, even or odd. This property can be observed directly in the input text file "A.txt" in Appendix B and is a general feature of all structures with this exact symmetry property.

The impact this symmetry property has on the procedure of establishing $\boldsymbol{J}^2$ is that all of the integral expressions on the format of equation 3.4 that makes up an arbitrary entry J_{ij}^2 will be zero and thereby giving the arbitrary entry J_{ij}^2 value zero *if* mode i and j consists of Fourier components with opposite parity. This specific feature, explained by equations A.6 through A.8, can simply be considered as a neat biproduct of the procedure of evaluating equation 3.4 analytically, because if two separate integral expressions of equation 3.4 instead had been adopted, one below the line $\hat{x}_1 = \hat{x}_2$, and another one above (see figure A.2), the same result would probably reveal itself without using the proof presented in equation A.6 which is indeed created from suspiciousness by looking at several surface plots of the integrand of equation 3.4. Nevertheless, the binary outcome of this eigenmode "parity test" results in that roughly one half of the portion of entries J_{ij}^2 that until now is presumed to be nonzero due to multiplication between two non–zero mode components will integrate to zero because over the areal domain defined by $\hat{x}_1$ and $\hat{x}_2$, due to opposite mode parity.

Taking advantage of this and the aforementioned property of the Hardanger Bridge is surprisingly easy, because a list of all combinations of modes i and j that does not integrate to zero due to mode parity can be made prior to the loop iterations for time and frequency together with the corresponding term in equation 3.3 that is indeed non–zero. This method represents almost zero administrative computational expence because $\boldsymbol{J}^2$ is established only from the very information required to obtain it, namely information that anyway has to be collected from the matrix "A.txt" and matrices that systematize and organizes the term–wise contents of equation 3.3.

3. *Narrow banded mode shape Fourier components.*

What can also be observed from the mode shape matrix "A.txt" is that the magnitude of some of the Fourier components that makes up the respective mode shape components is negligibly small compared to the most prominent ones. If one introduces a significance level, ε, such that Fourier components with a magnitude smaller than ε is set to zero, the effectiveness of the establishment of $\boldsymbol{J}^2$ is improved even further. The only reason why this measure is implemented is because a relatively large number of components can be eliminated without sacrificing any significant accuracy from an engineering perspective, especially considering the other uncertainties of the linear, frequency domain buffeting response theory.

Implementing these three properties into the algorithm that establishes $\boldsymbol{J}^2$ gives a relatively sparse matrix $\boldsymbol{J}^2$as illustrated in figure 3.4.

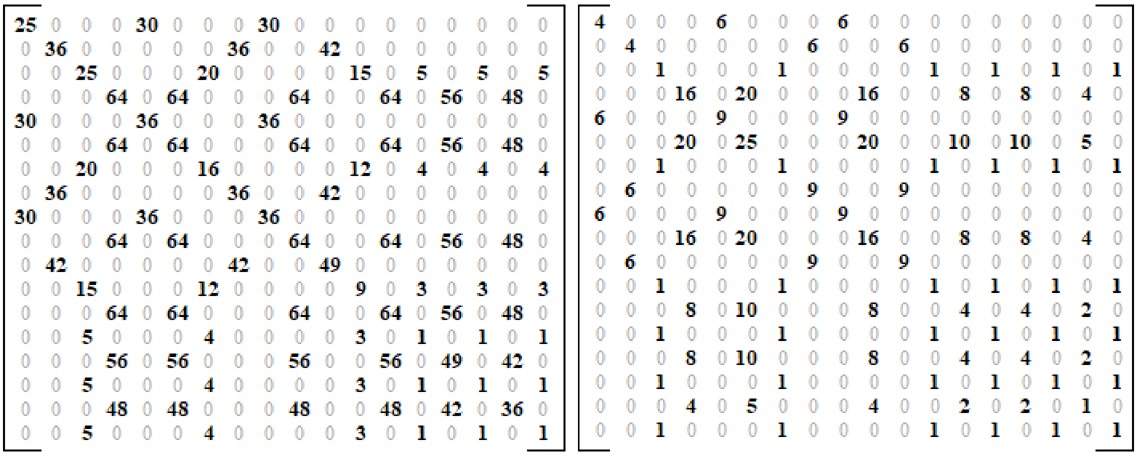

$$\begin{bmatrix}
25 & 0 & 0 & 0 & 30 & 0 & 0 & 0 & 30 & 0 & 0 & 0 & 0 & 0 & 0 & 0 & 0 & 0 \\
0 & 36 & 0 & 0 & 0 & 0 & 0 & 36 & 0 & 0 & 42 & 0 & 0 & 0 & 0 & 0 & 0 & 0 \\
0 & 0 & 25 & 0 & 0 & 0 & 20 & 0 & 0 & 0 & 0 & 15 & 0 & 5 & 0 & 5 & 0 & 5 \\
0 & 0 & 0 & 64 & 0 & 64 & 0 & 0 & 0 & 64 & 0 & 0 & 64 & 0 & 56 & 0 & 48 & 0 \\
30 & 0 & 0 & 0 & 36 & 0 & 0 & 0 & 36 & 0 & 0 & 0 & 0 & 0 & 0 & 0 & 0 & 0 \\
0 & 0 & 0 & 64 & 0 & 64 & 0 & 0 & 0 & 64 & 0 & 0 & 64 & 0 & 56 & 0 & 48 & 0 \\
0 & 0 & 20 & 0 & 0 & 0 & 16 & 0 & 0 & 0 & 0 & 12 & 0 & 4 & 0 & 4 & 0 & 4 \\
0 & 36 & 0 & 0 & 0 & 0 & 0 & 36 & 0 & 0 & 42 & 0 & 0 & 0 & 0 & 0 & 0 & 0 \\
30 & 0 & 0 & 0 & 36 & 0 & 0 & 0 & 36 & 0 & 0 & 0 & 0 & 0 & 0 & 0 & 0 & 0 \\
0 & 0 & 0 & 64 & 0 & 64 & 0 & 0 & 0 & 64 & 0 & 0 & 64 & 0 & 56 & 0 & 48 & 0 \\
0 & 42 & 0 & 0 & 0 & 0 & 0 & 42 & 0 & 0 & 49 & 0 & 0 & 0 & 0 & 0 & 0 & 0 \\
0 & 0 & 15 & 0 & 0 & 0 & 12 & 0 & 0 & 0 & 0 & 9 & 0 & 3 & 0 & 3 & 0 & 3 \\
0 & 0 & 0 & 64 & 0 & 64 & 0 & 0 & 0 & 64 & 0 & 0 & 64 & 0 & 56 & 0 & 48 & 0 \\
0 & 0 & 5 & 0 & 0 & 0 & 4 & 0 & 0 & 0 & 0 & 3 & 0 & 1 & 0 & 1 & 0 & 1 \\
0 & 0 & 0 & 56 & 0 & 56 & 0 & 0 & 0 & 56 & 0 & 0 & 56 & 0 & 49 & 0 & 42 & 0 \\
0 & 0 & 5 & 0 & 0 & 0 & 4 & 0 & 0 & 0 & 0 & 3 & 0 & 1 & 0 & 1 & 0 & 1 \\
0 & 0 & 0 & 48 & 0 & 48 & 0 & 0 & 0 & 48 & 0 & 0 & 48 & 0 & 42 & 0 & 36 & 0 \\
0 & 0 & 5 & 0 & 0 & 0 & 4 & 0 & 0 & 0 & 0 & 3 & 0 & 1 & 0 & 1 & 0 & 1
\end{bmatrix}
\begin{bmatrix}
4 & 0 & 0 & 0 & 6 & 0 & 0 & 0 & 6 & 0 & 0 & 0 & 0 & 0 & 0 & 0 & 0 & 0 \\
0 & 4 & 0 & 0 & 0 & 0 & 0 & 6 & 0 & 0 & 6 & 0 & 0 & 0 & 0 & 0 & 0 & 0 \\
0 & 0 & 1 & 0 & 0 & 0 & 1 & 0 & 0 & 0 & 0 & 1 & 0 & 1 & 0 & 1 & 0 & 1 \\
0 & 0 & 0 & 16 & 0 & 20 & 0 & 0 & 0 & 16 & 0 & 0 & 8 & 0 & 8 & 0 & 4 & 0 \\
6 & 0 & 0 & 0 & 9 & 0 & 0 & 0 & 9 & 0 & 0 & 0 & 0 & 0 & 0 & 0 & 0 & 0 \\
0 & 0 & 0 & 20 & 0 & 25 & 0 & 0 & 0 & 20 & 0 & 0 & 10 & 0 & 10 & 0 & 5 & 0 \\
0 & 0 & 1 & 0 & 0 & 0 & 1 & 0 & 0 & 0 & 0 & 1 & 0 & 1 & 0 & 1 & 0 & 1 \\
0 & 6 & 0 & 0 & 0 & 0 & 0 & 9 & 0 & 0 & 9 & 0 & 0 & 0 & 0 & 0 & 0 & 0 \\
6 & 0 & 0 & 0 & 9 & 0 & 0 & 0 & 9 & 0 & 0 & 0 & 0 & 0 & 0 & 0 & 0 & 0 \\
0 & 0 & 0 & 16 & 0 & 20 & 0 & 0 & 0 & 16 & 0 & 0 & 8 & 0 & 8 & 0 & 4 & 0 \\
0 & 6 & 0 & 0 & 0 & 0 & 0 & 9 & 0 & 0 & 9 & 0 & 0 & 0 & 0 & 0 & 0 & 0 \\
0 & 0 & 1 & 0 & 0 & 0 & 1 & 0 & 0 & 0 & 0 & 1 & 0 & 1 & 0 & 1 & 0 & 1 \\
0 & 0 & 0 & 8 & 0 & 10 & 0 & 0 & 0 & 8 & 0 & 0 & 4 & 0 & 4 & 0 & 2 & 0 \\
0 & 0 & 1 & 0 & 0 & 0 & 1 & 0 & 0 & 0 & 0 & 1 & 0 & 1 & 0 & 1 & 0 & 1 \\
0 & 0 & 0 & 8 & 0 & 10 & 0 & 0 & 0 & 8 & 0 & 0 & 4 & 0 & 4 & 0 & 2 & 0 \\
0 & 0 & 1 & 0 & 0 & 0 & 1 & 0 & 0 & 0 & 0 & 1 & 0 & 1 & 0 & 1 & 0 & 1 \\
0 & 0 & 0 & 4 & 0 & 5 & 0 & 0 & 0 & 4 & 0 & 0 & 2 & 0 & 2 & 0 & 1 & 0 \\
0 & 0 & 1 & 0 & 0 & 0 & 1 & 0 & 0 & 0 & 0 & 1 & 0 & 1 & 0 & 1 & 0 & 1
\end{bmatrix}$$

Figure 3.4: Non–zero assignments of $F(\omega, t)$ with ε = {0, 0.01}

The respective numbers in the matrices in figure 3.4 is the number of non–zero assignments to the function $F(\omega, t)$ at position i, j. To the left is the case with ε = 0 and to the right, ε = 0.01. Initially, the possible total number of assignments of $\mathrm{F}(\omega, \mathrm{t})$ is $18^2 \cdot 5 \cdot 15^2 = 364500$. ε = 0 and ε = 0.01 reduces this number to 2900 and 488, respectively.

To illustrate the effect the three abovementioned properties has on script effectiveness an illustrative comparison is made to a basically unrefined algorithm which establishes all 18^2 entries of $\boldsymbol{J}^2$ one by one by calculating every five terms in equation 3.3, in which each of these terms is calculated by evaluating the integral expression in equation 3.4 according to equations A.8 and 3.5 by checking Fourier component parity for every "non–zero amplitude"–combination of wavenumbers P and Q. To investigate the reduction in computational expense for the establishment of $\boldsymbol{J}^2$ alone is obviously highly interesting ("local effect") but establishing $\boldsymbol{J}^2$ is only one of several steps within the very MATLAB routine that calculates the EPSD of structural response. The very steps that must be performed for every instant in time and setting for ω (= one "loop iteration") are given below, and the reduction in the elapsed time of performing these four steps when only enhancing step no. 3 ("global effect") is a more correct measure of the enhanced effectiveness of the algorithm.

1. Establish $\widehat{\boldsymbol{H}}_\eta(\omega, t)$.
2. Calculate $S_u(\omega, t)$ and $S_w(\omega, t)$ from the estimated LSF parameters and the chosen method of EPSD modulation (chapters 2.4.2 – 2.4.4).
3. Establish $\boldsymbol{J}^2(\omega, t)$.
4. Calculate $\boldsymbol{S}_{\eta\eta}(\omega, t)$ and $\boldsymbol{S}_{rr}(\omega, t)$ and interpolate all EPSDs (structural and wind) for plotting purposes.

The increase in local and global effectiveness when successively implementing property 1, 2, and 3 is displayed in table 3.2. The loop above is in this case run for 1000 settings for ω and the performance of the implemented algorithm that establishes $\boldsymbol{J}^2$ only, is measured by the *minimum elapsed time* out of the 1000 trials that established $\boldsymbol{J}^2$. Analogue to local performance, global performance is given as the minimum elapsed time for the four steps above to be looped 1000 times, from a total of 30 simulations.

	Local performance (only $\boldsymbol{J}^2$):			Global performance (1 loop iteration):		
Included methods of algorithm optimization:	Minimum calculation time (1000 sims) [μs]:	Incremental increase in speed [%]:	Accumulated reduction factor:	Minimum calculation time (30 sims.) [ms]:	Incremental increase in speed [%]:	Accumulated reduction factor:
Non–symmetric $\boldsymbol{J}^2$	**882**	–	–	**1216**	–	–
Symmetric $\boldsymbol{J}^2$	**537**	64.2	1.64	**730**	66.6	1.67
Properties 1. & 2 with:	**–**	–	–	**–**	–	–
ε = 0.000	**126**	326	7.00	**271**	169	4.49
ε = 0.001	**73**	71.7	12.0	**217**	24.9	5.60
ε = 0.002	**59**	22.9	14.8	**203**	6.90	5.99
ε = 0.005	**45**	32.1	19.5	**188**	7.98	6.47
ε = 0.010	**32**	41.3	27.6	**171**	9.94	7.11

Table 3.2: Effects of algorithm optimization

When comparing the average computational time of executing a single loop iteration by considering the best and worst–case scenario in table 3.2, the establishment of $\boldsymbol{J}^2$ does on average make up roughly 23 % and 89 % of the total loop iteration time, respectively.

Because a relatively large number of settings for ω is required to integrate the response spectrums accurately (see chapter 3.5), the establishment of the aerodynamic stiffness– and damping matrices contributes negligibly to the total computational expense because they are independent of ω and the integrals of the product of the mode shape components (see equations 1.44b and –c) are time–invariant and can thus be calculated prior to the loop iterations. Also, the "administrative" procedure of establishing the very matrices that has the purpose of "setting up", streamline and systematize data for the loop iteration process takes only .15 seconds on average. Therefore, the total running time of the script is very close to proportional to the third column from the right in table 3.2.

As a mere example to illustrate the issue regarding the running time of the MATLAB routine, a case where structural response shall be calculated from a non–stationary wind speed recording is considered. For the purpose being, 1000 settings for ω is assumed to integrate the response spectrum with sufficient accuracy, and 200 discrete settings for time presumably produces a relatively smooth time history curve for structural response. Also, if all four methods of EPSD modulation presented in chapters 2.4.2 – 2.4.4 shall be included for comparison, and if the average loop iteration time is assumed to be 15 % higher than its theoretical minimum limit, the total computational time will be roughly equal to $1.216\text{s} \cdot 200 \cdot 4 \cdot 1.15 = 1119\text{s} \approx 18.6$ min if no symmetry properties are exploited. However, if the measures described by the lowest–most row in table 3.2 is applied, the corresponding computational time will be reduced roughly by a factor 7.1, to 2 min 40 seconds. Such a calculation must surely be performed more than once and a running time of 2 minutes 40 seconds is highly appreciative compared to almost 1/3 of an hour.

Finally, if another structure than the Hardanger Bridge is under investigation in which for instance more of its cross–sectional load coefficients is non–zero, more terms will be present in equation 3.3, consequently reducing the sparsity of $\boldsymbol{J}^2$ accordingly. Also, if some of the included eigenmodes contain more than one displacement component, the maximum number of terms in J_{ij}^2 will no longer be one. However, such can easily be implemented similarly as is done with the Hardanger Bridge and it represents little added complexity to this process, however, the advantage of doing so will be considerable smaller.

3.4 AERODYNAMIC STIFFNESS– AND DAMPING MATRICES

If equations 1.40b, 1.44b and 1.50d are combined, the entry wise contents of $\boldsymbol{\kappa}_{ae}$ can be expressed as,

$$\kappa_{ae_{ij}} \quad = \quad \frac{\rho B^2 L}{2\tilde{M}_i} \int_0^1 \boldsymbol{\varphi}_i^T \hat{\boldsymbol{K}}_{ae} \boldsymbol{\varphi}_j \, d\hat{x} \tag{3.6b}$$

where L_{exp} is set equal to L because wind loading is present along the entire bridge span. Combining equations 1.40b, 1.44c and 1.50e, the entry wise content of $\boldsymbol{\zeta}_{ae}$ will similarly be as follows,

$$\zeta_{ae_{ij}} \quad = \quad \frac{\rho B^2 L}{4\tilde{M}_i} \int_0^1 \boldsymbol{\varphi}_i^T \hat{\boldsymbol{C}}_{ae} \boldsymbol{\varphi}_j \, d\hat{x} \tag{3.6b}$$

In the case of the Hardanger bridge only aerodynamic derivatives P_1^*, H_{1-4}^* and A_{1-4}^* are non–zero, and the fully expanded versions of $\kappa_{ae_{ij}}$ and $\zeta_{ae_{ij}}$ are therefore given by,

$$\begin{aligned}\kappa_{ae_{ij}} \quad = \quad \frac{\rho B^2 L}{2\tilde{M}_i}\int_0^1 [\quad & H_4^* \cdot \varphi_{iz}(\hat{x}) \cdot \varphi_{jz}(\hat{x}) \\ + \quad & BH_3^* \cdot \varphi_{iz}(\hat{x}) \cdot \varphi_{j\theta}(\hat{x}) \\ + \quad & BA_4^* \cdot \varphi_{i\theta}(\hat{x}) \cdot \varphi_{jz}(\hat{x}) \\ + \quad & B^2 A_3^* \cdot \varphi_{i\theta}(\hat{x}) \cdot \varphi_{j\theta}(\hat{x}) \,] \quad d\hat{x}\end{aligned} \tag{3.7a}$$

$$\begin{aligned}\zeta_{ae_{ij}} \quad = \quad \frac{\rho B^2 L}{4\tilde{M}_i}\int_0^1 [\quad & P_1^* \cdot \varphi_{iy}(\hat{x}) \cdot \varphi_{jy}(\hat{x}) \\ + \quad & H_1^* \cdot \varphi_{iz}(\hat{x}) \cdot \varphi_{jz}(\hat{x}) \\ + \quad & BH_2^* \cdot \varphi_{iz}(\hat{x}) \cdot \varphi_{j\theta}(\hat{x}) \\ + \quad & BA_1^* \cdot \varphi_{i\theta}(\hat{x}) \cdot \varphi_{jz}(\hat{x}) \\ + \quad & B^2 A_2^* \cdot \varphi_{i\theta}(\hat{x}) \cdot \varphi_{j\theta}(\hat{x}) \,] \quad d\hat{x}\end{aligned} \tag{3.7b}$$

The most obvious result that arises when $\kappa_{ae_{ij}}$ and $\zeta_{ae_{ij}}$ is being adopted to the Hardanger Bridge is that aerodynamic stiffness only concerns vertical and torsional modes. This very property gives indeed raise to the fact that the eigenfrequencies changes with $\bar{U}$ because the aerodynamic derivatives indeed does so, nevertheless, such behaviour is, as was mentioned in chapter 1.2.4, only considered important when investigating stability limits. The fact that the apparent frequency location of an eigenfrequency is being changed slightly does therefore not have any significant impact on the magnitude of the oscillations of the corresponding mode. Similarly, extreme levels of mean wind speeds that reduces total modal damping in some cases close to zero is beyond the cope of this study, and therefore a detailed investigation into the specific shapes of the non–zero aerodynamic curves is considered unnecessary.

3.5 CONSTRUCTING A NUMERICAL INTEGRATION SCHEME FOR $\boldsymbol{S}_{\eta\eta}(\boldsymbol{t},\boldsymbol{\omega})$

Establishing an effective numerical integration scheme for $\boldsymbol{S}_{\eta\eta}(\omega, t)$ with respect to ω, brings forth a few challenges to which satisfactory solutions must be applied. This concerns mainly how to construct a wise discretization of the frequency axis. In the case of a well–behaved function that undergoes smooth, slow, and predictable changes along the axis in question, an equally spaced mesh of axis settings is obvious not only for simplicity but is also usually sufficient from an accuracy perspective. However in the case of a response spectrum function where the structure in question generally has low damping, quite the opposite curve characteristics prevails. These functions feature narrow and prominent peaks that forms in the vicinity of the structures eigenfrequencies who are also very dominant contributors to the total area under the spectrum curve itself. Between these narrow peaks are generally low magnitude regions that contribute insignificantly to the area under the spectrum curve. Hence, if an equidistant mesh is adopted the value of the constant spacing itself must be determined from what can be considered sufficient from an accuracy perspective at the location of the narrow prominent peaks. Of course, such is extremely ineffective from a global perspective because a highly superfluous number of settings will be allocated to the low magnitude regions in between. Consequently, a discretization with varying spacing is needed, as is schematically illustrated in figure 3.5.

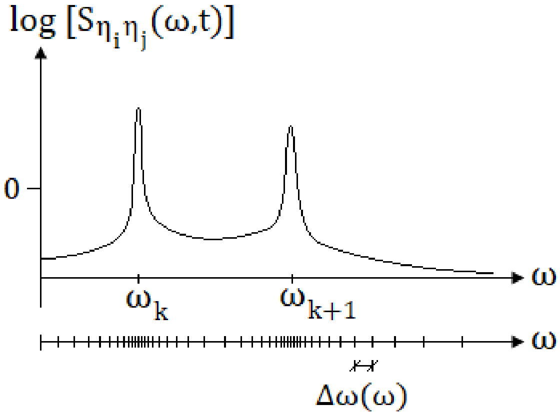

Figure 3.5: Varying axis spacing

For convenience and simplicity the same discretization is of course adopted for all functions $S_{\eta_i\eta_j}$ within $\boldsymbol{S}_{\eta\eta}$ and for all locations across the bridge span, even though $S_{\eta_i\eta_j}$ contains only the sharp peaks associated with modes i and j. However, a problem arises because of a specific feature mentioned in chapter 3.4, namely that aerodynamic stiffness changes the location at where these prominent peaks forms. To try to calculate time varying (mean wind speed dependent) positions of these peaks is deemed unnecessary because as equation 1.51 suggests, the common set of peaks present in $\boldsymbol{S}_{\eta\eta}$ is directly related to the location of local maxima in $\widehat{\boldsymbol{H}}_{\eta}(\omega,t)$, or $\widehat{\boldsymbol{H}}_{\eta}(\omega,\overline{U})$ for this particular purpose. This is because of the linear matrix multiplication between $\widehat{\boldsymbol{H}}_{\eta}^{*}$, $\boldsymbol{S}_{\hat{Q}_v}$ and $\widehat{\boldsymbol{H}}_{\eta}^{T}$. Because $\widehat{\boldsymbol{H}}_{\eta}$ is a complex quantity the desired information can be obtained by visually interpreting a surface plot of the base–10 logarithm of the magnitude of the determinant of $\widehat{\boldsymbol{H}}_{\eta}$ as is shown in figure 3.6. For this exclusive purpose, $\boldsymbol{\zeta}_{ae}$ is omitted from $\widehat{\boldsymbol{H}}_{\eta}$ because the location of the changing prominent peaks caused by $\boldsymbol{\kappa}_{ae}$ is the supreme interest.

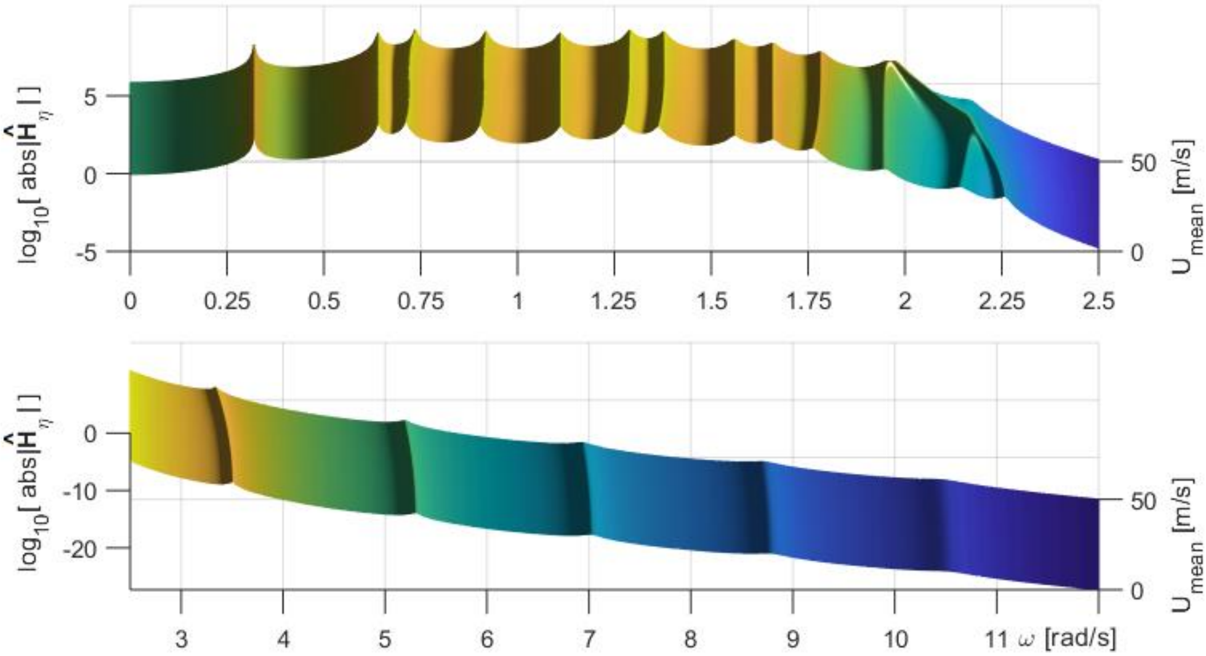

Figure 3.6: Surface plot of $log_{10}[abs|\widehat{\boldsymbol{H}}_{\eta}(\omega,\overline{U})|]$ with $\boldsymbol{\zeta}_{ae}$ = **0**

The surface plot in figure 3.6 clearly illustrates the aforementioned issues of sharp peaks whose location changes with the mean wind speed, and even though this is not the function itself that shall be integrated over the frequency axis, the evolutionary response spectrums will contain peaks at a subset of these exact same locations if they are calculated at an arbitrary position across the bridge span. The magnitude of $\widehat{\boldsymbol{H}}_{\eta}$ itself must therefore not be interpreted as the dynamic amplification factor of the entire MDOF system analogue to the dynamic amplification factor of a SDOF system because the determinant of $\widehat{\boldsymbol{H}}_{\eta}$ is basically a product of the modal dynamic amplification factors, each with its own resonant frequency, eigenfrequency. The fact that the magnitude of $\widehat{\boldsymbol{H}}_{\eta}$ is so small at the region of the torsional modes is simply because the dynamic amplification factor of most of the other modes is very small at the very high end of the frequency domain considered, far away from their respective eigenfrequencies. Consequently, the barely detectable increase in $\widehat{\boldsymbol{H}}_{\eta}$ around the eigenfrequencies of the highest torsional modes does not imply that so is also the case with the response spectrums at the same location. $\widehat{\boldsymbol{H}}_{\eta}$ must therefore only be interpreted in the context of information it is able to provide, namely the very location of these peaks.

To treat the effect of the changing locations of peaks, one may introduce a solution strategy that is not perfect in terms of effectiveness but is at least convenient and simple to implement, namely letting the regions of closely separated frequency settings cover the entire domains that the respective sharp peaks changes within. What can also be seen from figure 3.6 is that the extremities of these very regions seem to be given by $\overline{U}$ = 0 and $\overline{U}$ = 50 m/s because the peaks that change location seem to move in the same direction from $\overline{U}$ = 0 to $\overline{U}$ = 50 m/s. Figure 3.7 illustrates the workings of this proposed method where regions of narrowly spaced settings for ω cover the domain the peaks changes within. The blue and red line in figure 3.7 are simply snapshots of the surface plot in figure 3.6 at $\overline{U}$ = 0 and $\overline{U}$ = 50 m/s, respectively. These somewhat arbitrary aforementioned values for $\overline{U}$ are simply chosen as conservative envelopes of the mean wind speed domain that is covered for the purpose of this thesis.

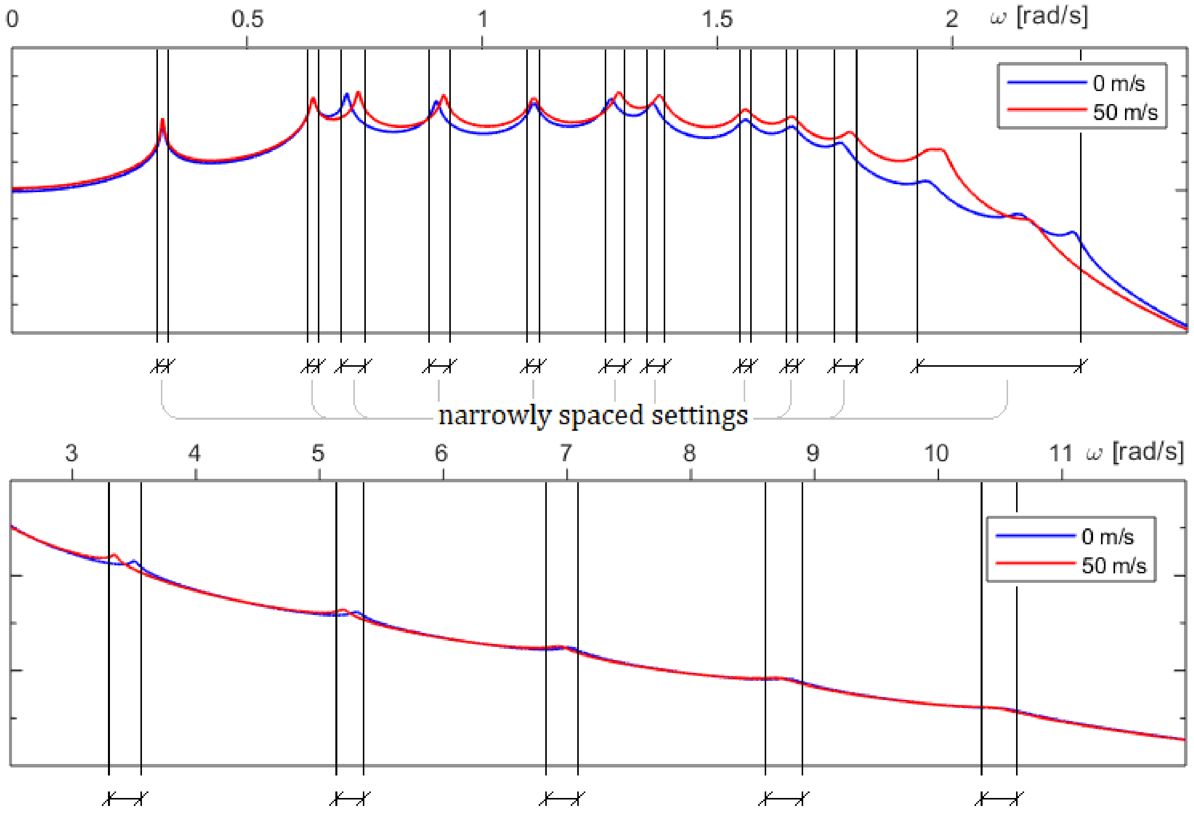

Figure 3.7: Principle of integration scheme

The discretization of the frequency axis itself is done by simply assigning a predetermined number of subdivisions to each of the "sectors" along the frequency axis. The locations of these sectors are determined as is illustrated in figure 3.6 and 3.7, simply by visually considering the domain of change of the peaks themselves. The importance of making sure that the sharp peaks indeed are included within these very regions is fundamental and a corresponding margin of error should therefore be applied.

How one defines the initial number of "elements" within each sector is based on interpretation and is a question to which there is no definite answer. Such should also be determined from considering actual plots of response spectrums because the magnitude and especially the sharpness of the corresponding response spectrum peaks varies from eigenfrequency to eigenfrequency, and a surface plot of $\widehat{\boldsymbol{H}}_\eta$ is actually not a very good tool for providing this very information. Therefore, the density of frequency settings in the different sectors may advantageously be individualized. What information response spectrums also provides is the relative variance contribution from each mode. By knowing the general characteristics of this picture, one may with good reason allocate the most integration accuracy to the most prominent modes, and vice versa, which ever modes these may be for the structure in question. For the Hardanger Bridge, such a variance distribution is shown in chapter 3.6.

On whatever way one defines the different frequency setting sectors, an absolute demand is nevertheless that mesh refinement must be both intuitive and trivial. This can simply be done by introducing a refinement factor, f_r, such that the initial distribution of the number of sector subdivisions can be multiplied with f_r and rounded up to the nearest integer. For this matter, f_r could generally take values of both sides of unity. Hence, the initial level of sector subdivision is not important but rather the frequency setting density ratio between the different sectors in which one should take into account the aforementioned features of the shape of the evolutionary response spectrums. The file "OS2.txt" is attached in appendix B and gives the initial sector subdivisions together with the corresponding frequencies that defines the boarders between the sectors themselves. A cut–off is also applied to the lowest most frequency region in accordance with the properties of the wind field turbulence spectrum presented in chapter 2.3.

3.5.1 Higher order integration elements

When having established a decent discretization of the frequency axis, the area under the response spectrum curves can be determined (estimated) using for instance the *trapezoidal method* in which trapezoids approximates the generally unknown curve shape between the calculated data points. The trapezoidal method has *quadratic convergence*, which means that the error is bounded from above by a factor inversely proportional to N^2 where N is the number of elements within the domain in question. Quadratic convergence is by no means a poor attribute, but it is possible to obtain more accurate result with less computational expense using a higher order method of numerical integration, first and foremost *Simpson's method*. Simpson's method uses instead parabolas to approximate the curve defined by sets of three and three data points, and has quartic convergence, that is the error is bounded by a factor inversely proportional to N^4.

The two methods are illustratively compared by using them to determine the variance of horizontal structural response of the Hardanger Bridge induced by the stationary wind field given by the Kaimal spectrum in appendix C for a mean wind speed of 25 m/s. Table 3.3 shows the estimated variance for different values of the refinement factor, f_r, as given in chapter 3.5 together with the total number of data points on the frequency axis. The lowest and highest frequency is set to be {0,12} rad/s.

	Trapezoidal method			Simpson's method		
f_r:	$\sigma_{r_y}^2$ $[m^2]$:	$log_{10}[E]$:	$n_{\{\omega\}}$:	$\sigma_{r_y}^2$ $[m^2]$:	$log_{10}[E]$:	$n_{\{\omega\}}$:
0.25	0.277 796 851	–0.91	131	0.249 756 947	–1.93	261
0.5	0.256 909 898	–1.39	261	0.247 462 567	–2.61	503
1	0.249 824 400	–1.92	503	0.246 945 433	–3.43	1005
2	0.247 665 174	–2.48	1005	0.246 863 264	–4.43	2009
4	0.247 063 742	–3.07	2009	0.246 854 751	–5.55	4017
8	0.246 906 999	–3.67	4017	0.246 854 098	–6.73	8033
16	0.246 867 323	–4.27	8033	0.246 854 054	–7.95	16065
32	0.246 857 372	–4.87	16065	0.246 854 052	–∞	32129

Table 3.3: Trapezoidal method and Simpson's method

Table 3.3 clearly shows the effectiveness of Simpson's method because it requires only half of the total number of frequency settings to provide an accuracy level within one percent. The error itself is defined on the basis of simply equating the presumed exact value of $\sigma_{r_y}^2$ to its estimated value when using Simpson's method and f_r = 32. The significance threshold, ε, of the inclusion of Fourier components of the mode shapes discussed in chapter 3.3.1 was set to ε = 0.01 when computing table 3.3. If for comparison ε is set to zero, the comparative values of $\sigma_{r_y}^2$ are roughly 0.55 % lower for both the trapezoidal method and Simpson's method, as well for all chosen values of f_r.

Simpson's method is obviously a better choice than the trapezoidal method when integrating the response spectrums but a similar trend does not prevail when applying even higher order integration elements that uses a higher order polynomial to approximate the curve segments. The reason for this is that the length of the integration element of a higher order method quickly becomes larger than the characteristic length of the sharp and prominent peaks in the response spectrums, consequently producing spurious results. Simpson's method seems therefore to be an optimum point when considering several schemes of numerical integration of the specific response spectrums in question.

Finally, to check that the constructed and flexible integration scheme works according to its purpose, convergence can be checked for conservative "envelope" values for the mean wind speed as is done in table 3.4. Considering the mentioned characteristics of the change of the locations of the prominent peaks in the response spectrums in chapter 3.5, convergence is intuitively guaranteed between the envelopes if one experiences proper convergence at the envelopes themselves. This is because the regions of narrowly spaced frequency settings is set to "wrap around" the domain of which each prominent peak in the response spectrum forms as a result of varying $\bar{U}$. Table 3.4 is computed for the bridge midspan and only the eigenmodes that is not zero at this location is included in the corresponding check for convergence. This convergence check procedure can and should also be performed for other locations at the bridge span if structural response at these locations is to be investigated.

	$\bar{U} = 5\ m/s$			$\bar{U} = 50\ m/s$		
f_r:	$\sigma_{r_y}^2$ $[10^{-3}\ m^2]$:	$\sigma_{r_z}^2$ $[10^{-3}\ m^2]$:	$\sigma_{r_\theta}^2$ $[10^{-6}\ rad^2]$:	$\sigma_{r_y}^2$ $[m^2]$:	$\sigma_{r_z}^2$ $[m^2]$:	$\sigma_{r_\theta}^2$ $[10^{-3}\ rad^2]$:
0.25	0.114 479	0.019 600	0.011 258	5.458 733	0.501 500	0.965 018
0.5	0.113 919	0.019 193	0.011 259	5.383 558	0.501 522	0.964 555
1	0.113 830	0.019 216	0.011 259	5.366 588	0.501 525	0.964 626
2	0.113 816	0.019 215	0.011 259	5.363 934	0.501 525	0.964 626
4	0.113 815	0.019 215	0.011 259	5.363 663	0.501 525	0.964 626
8	0.113 815	0.019 215	0.011 259	5.363 643	0.501 525	0.964 626
16	0.113 815	0.019 215	0.011 259	5.363 642	0.501 525	0.964 626
32	0.113 815	0.019 215	0.011 259	5.363 642	0.501 525	0.964 626

Table 3.4: Convergence check for integration scheme (Simpson's method)

3.6 FREQUENCY LIMIT OF ENSURING QUASI–STATIC MEAN WIND RESPONSE

In chapter 2.3 the importance of ensuring not only a *quasi–static* mean response, but also a *quasi–stationary* response was mentioned. In the following a demonstration will be made that determines the location of the frequency region where the mean structural response goes from being as good as quasi–static to no longer being able to be approximated as being so. Together with a time domain simulation algorithm uniquely specialized to the Hardanger Bridge that will be presented in chapter 3.7, it defines an important set of tools that one can use to define an indicative valid domain for the value of the highest included frequency in the mean wind speed. Such will be demonstrated in chapter 4 where time varying structural response from a real–life wind speed recording will be predicted.

First, to determine the upper frequency limit of quasi–static mean response, consider the Hardanger Bridge to be subjected to a deterministic and homogeneous wind loading induced by $\bar{U}$ itself as illustrated in figure 3.8.

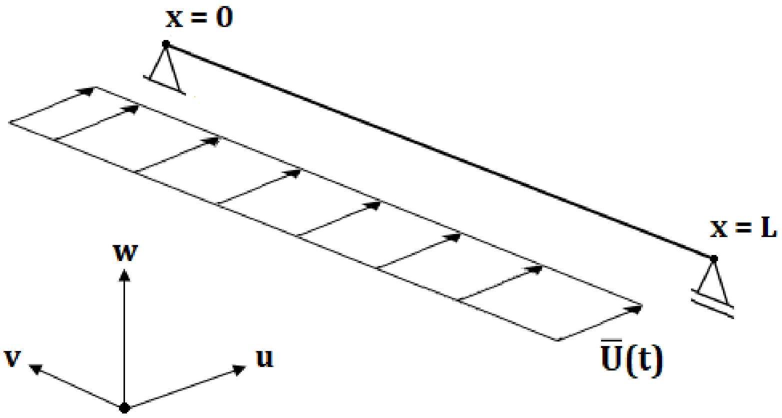

Figure 3.8: Mean wind speed considration

What shall be investigated in particular is the difference between the time varying static response and the steady–state solution ("particular solution") to equation 1.43a when the loading is constituted by $\bar{U}(t)$ only. For this particular purpose, only horizontal motion will be considered because the fundamental mode of the Hardanger Bridge is in horizontal displacement. Hence, if the mean horizontal structural response indeed is quasi–static, such must intuitively also be the case for vertical and torsional motion since the modes constituting such motion have higher eigenfrequencies. Modal damping varies much less than model eigenfrequency for lowest set of modes and makes thus no difference in context of this argumentation. Obviously, homogeneousness implies that only even modes (evenly symmetric wrt. bridge midspan – odd wavenumbers) contribute to the mean response since the odd modes (even wavenumbers) makes the respective modal loads integrate to zero over the bridge span according to equations 1.37a, 1.37c and 1.43e. However, homogeneousness is not a necessary requirement for the validity of only considering horizontal motion because mode 1 will anyway be the most significant contributor to the mean response if mildly non–homogeneous features are present. Nevertheless, in the case of homogeneousness, mode 1, 5 and 9 is the only contributors to the mean horizontal response because mode 2, 8 and 11 integrates to zero.

Aerodynamic stiffness is zero for all horizontal motion and aerodynamic damping is for simplicity excluded because time varying damping cannot be incorporated into the procedure of obtaining the steady state solution of equation 1.43a. Not letting the governing differential equations have constant coefficients will generally violate the fact that their particular solution is harmonic functions. Excluding aerodynamic damping will also be a conservative measure because the aerodynamic derivative P_1^* which is associated with horizontal aerodynamic damping increases system damping with $\bar{U}$ hence increasing the upper frequency limit for quasi–static response, since increased damping reduces modal dynamic amplification. Nevertheless, one might anyway discuss whether it is correct to include aerodynamic damping when considering slow varying deterministic loading since the aerodynamic derivatives that describes this very phenomenon are obtained from wind tunnel testing when considering modal oscillations from turbulent wind. Taking the abovementioned concepts into consideration, the relevant modal versions of equation 1.43a and corresponding mean loads from equation 1.43c is given by,

$$\tilde{M}_i\ddot{\eta}_i + 2\tilde{M}_i\zeta_i\omega_i\dot{\eta}_i + \omega_i^2\tilde{M}_i\eta_i = \bar{\tilde{Q}}_i(t) \ , \quad i = \{1,5,9\} \tag{3.8a}$$

where,

$$\bar{\tilde{Q}}_i(t) \;=\; C_Q \cdot \frac{D}{B} \cdot \bar{C}_D \cdot \int_0^1 \varphi_{iy}(\hat{x})d\hat{x} \cdot [\bar{U}(t)]^2 \;, \qquad C_Q = \frac{1}{2}\rho BL \tag{3.8b}$$

By utilizing the principle of superposition, the steady–state solution of equation 3.8a can be expressed as the sum of the steady–state solutions of the same system subjected to the respective Fourier components of equation 3.8b. Expressing equation 3.8b in terms of a Fourier series expansion of $[\bar{U}(t)]^2$ renders,

$$\bar{\tilde{Q}}_i(t) \;=\; F_{CD,i}\left[\left(\sum_{k=1}^{N} a_k \sin(\omega_k t) + b_k \cos(\omega_k t)\right) + \overline{U^2}\right] \tag{3.9a}$$

where,

$$F_{CD,i} \;=\; C_Q \cdot \frac{D}{B} \cdot \bar{C}_D \cdot \int_0^1 \varphi_{iy}(\hat{x})d\hat{x} \tag{3.9b}$$

$$\overline{U^2} \;=\; \frac{1}{T}\int_0^T [\bar{U}(t)]^2 dt \tag{3.9c}$$

Equation 3.8a takes the following form when considering Fourier component, k, of equation 3.9a,

$$\tilde{M}_i\ddot{\eta}_{ik} + 2\tilde{M}_i\zeta_i\omega_i\dot{\eta}_{ik} + \omega_i^2\tilde{M}_i\eta_{ik} \;=\; F_{CD,i}\left[a_k \sin(\omega_k t) + b_k \cos(\omega_k t) + \overline{U^2}\right] \tag{3.10}$$

Superposition from contributions $a_k \sin(\omega_k t)$ and $b_k \cos(\omega_k t)$ makes up the steady–state solution of equation 3.10,

$$\eta_{ik}(t) \;=\; \frac{F_{CD,i}}{\tilde{K}_i} \cdot \left[A_{ik}\cos(\omega_k t) + B_{ik}\sin(\omega_k t) + \overline{U^2}\right] \tag{3.11a}$$

where,

$$A_{ik} \;=\; \frac{\left[1 - \xi_{ik}^2\right]a_k - [2\xi_{ik}\zeta_i]b_k}{\left[1 - \xi_{ik}^2\right]^2 + [2\xi_{ik}\zeta_i]^2} \tag{3.11b}$$

$$B_{ik} \;=\; \frac{[2\xi_{ik}\zeta_i]a_k + \left[1 - \xi_{ik}^2\right]b_k}{\left[1 - \xi_{ik}^2\right]^2 + [2\xi_{ik}\zeta_i]^2} \tag{3.11c}$$

$$\xi_{ik} \;=\; \frac{\omega_k}{\omega_i} \tag{3.11d}$$

Strømmen (2014, p. 69) provides the derivation of equation 3.11b and the same procedure is used when deriving equation 3.11c. The steady–state response of mode i is simply obtained by summing equation 3.11 over the components $\{k\}$ and the steady state response at relative position $\hat{x}$ at the bridge span is obtained be summing modal contributions $\{i\}$, namely,

$$y(t,\hat{x}) \;=\; \sum_{i=1,5,9}\left[\varphi_{iy}(\hat{x})\cdot\sum_{k=1}^{N}\eta_{ik}(t)\right] \tag{3.12}$$

When producing the Fourier series expansion of $[\bar{U}(t)]^2$ it is important not to include frequencies that extend far beyond the highest included frequency used to extract $\bar{U}(t)$ itself. The reason for this is that if such frequency content reaches within proximity of ω_1, the possibly large dynamic amplification of these Fourier components will give a strong spurious contribution to $y(t,\hat{x})$ hence violating the validity and interpretability of the comparison that this chapter is supposed to present. However, if the highest frequency that was used to extract $\bar{U}(t)$ is also set as being the highest frequency used in the Fourier series expansion of $[\bar{U}(t)]^2$, it will in fact quite well resemble $\bar{U}(t)$ itself. Small deviations in amplitude will be present but the characteristic frequency at which $[\bar{U}(t)]^2$ oscillates is very much preserved, obviously because the highest frequency used in the Fourier series expansion of $[\bar{U}(t)]^2$ is very similar. Frequency preservation is anyway the only important feature because dynamic amplification is what is being investigated, not the numeric value of the amplitude by any means.

Thankfully, the problem of what upper limit of frequency content to include in the Fourier series expansion of $[\bar{U}(t)]^2$ solves itself when using the IFE to extract the mean. However, if one for some reason chooses to use the WMAM or EMD to extract the mean, extraordinary caution must be taken when resembling $[\bar{U}(t)]^2$ in terms of a sum of harmonic components, because the WMAM and EMD produces curves for the mean wind speed that has no kinship to harmonics at all.

The arbitrary generated non–stationary recording in figure 3.9 is used as the basis for comparing static and dynamic mean response of the Hardanger Bridge. As before, the recording viewed in figure 3.9 is only a withdrawn subsection of a longer parent recording from which $\bar{U}(t)$ is extracted.

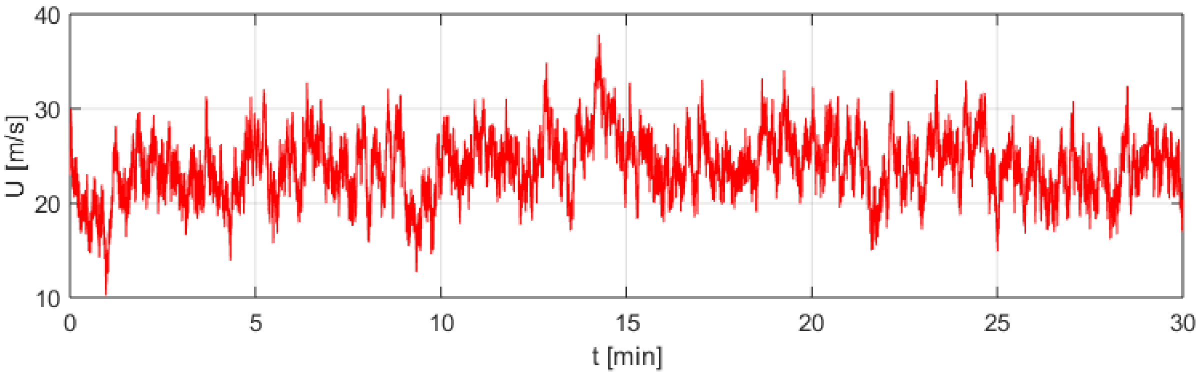

Figure 3.9: Arbitrary generated wind speed recording

As an initial illustration of the comparison between the static and steady–state dynamic response, the mean wind speed is extracted from the recording in figure 3.9 at a maximum included frequency of $\omega_1/10$ and $[\bar{U}(t)]^2$, the Fourier series expansion of $[\bar{U}(t)]^2$, the corresponding static response and steady–state dynamic response is all shown in figure 3.10. Again, the static response and the steady–state dynamic response is of course both defined from the Fourier series expansion of $[\bar{U}(t)]^2$.

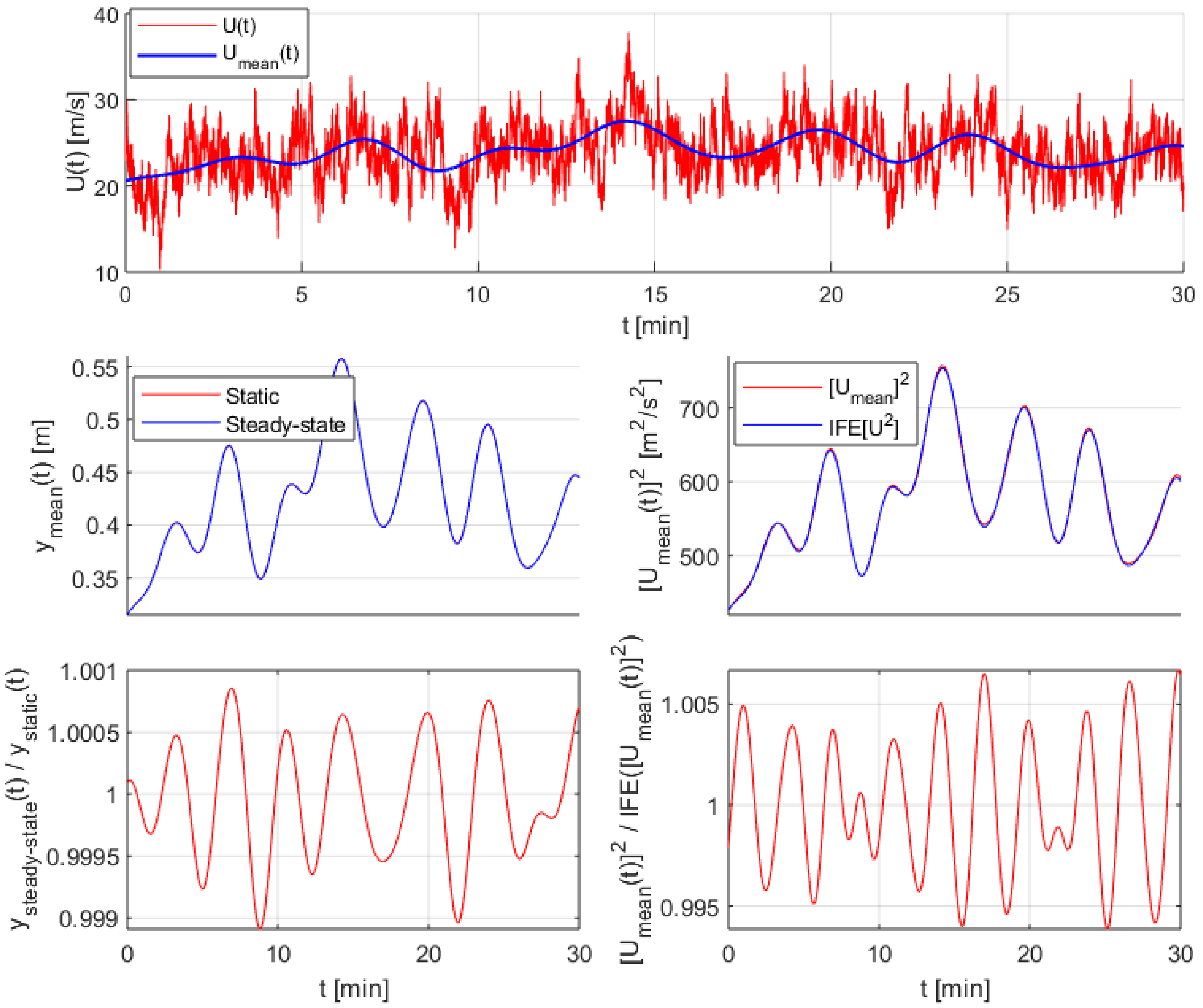

Figure 3.10: Static and steady–state response comparison

Subplot (3,2) in figure 3.10 shows how well the Fourier series expansion of $[\overline{U}(t)]^2$ resembles $[\overline{U}(t)]^2$ itself. The instant ratio of their respective magnitudes is given in subplot (3,5) and they deviate with roughly 0.67 % at the most. This seems also to be the only significant difference between the two since their characteristic frequencies is seemingly identical and the IFE of $[\overline{U}(t)]^2$ shows therefore a more than good enough resemblance to $[\overline{U}(t)]^2$ itself. Subplot (3,1) shows the very comparison between the static and steady–state dynamic response induced by the IFE of $[\overline{U}(t)]^2$. The curves are indistinguishable since the maximum relative deviation between the two is roughly 0.11 %. Obviously, the mean response is as good as quasi–static for $\omega_{max} = \omega_1/10$.

Table 3.5 shows the result of the same procedure shown above but with a larger set of fractions of ω_1 as being the highest included frequency when extracting $\overline{U}(t)$ from the wind speed recording in figure 3.9. For comparison the dynamic amplification factor, $\hat{H}(\omega_{max}/\omega_1)$ for a SDOF system with the same damping as mode 1 is included.

$\frac{\omega_1}{\omega_{max}}$	$log_{10}\left[max\left\|1-\frac{[\bar{U}(t)]^2}{IFE[\bar{U}(t)]^2}\right\|\right]$	$log_{10}\left[max\left\|1-\frac{y_{S.S.}}{y_{static}}\right\|\right]$	$log_{10}\left[\widehat{H}\left(\frac{\omega_1}{\omega_{max}}\right)\right]$
52.385	–2.47	–4.43	–3.44
45.837	–2.67	–4.40	–3.32
40.744	–2.35	–4.24	–3.22
36.669	–2.46	–4.18	–3.13
30.558	–2.44	–4.19	–2.97
26.192	–2.19	–3.83	–2.84
20.372	–2.62	–3.79	–2.62
15.279	–2.11	–3.27	–2.37
12.223	–2.28	–3.03	–2.17
10.186	–2.18	–2.96	–2.01
8.149	–2.03	–2.67	–1.82
6.011	–1.91	–2.27	–1.55
5.023	–1.72	–1.99	–1.38
4.527	–1.91	–2.03	–1.29
4.030	–1.68	–1.83	–1.18
3.526	–1.63	–1.67	–1.06
3.006	–1.35	–1.36	–0.90
2.601	–1.53	–1.41	–0.76
2.209	–1.63	–1.24	–0.59
1.910	–1.31	–0.83	–0.42
1.755	–1.44	–0.92	–0.32
1.503	–1.50	–0.67	–0.10
1.405	–1.35	–0.47	0.01
1.300	–1.40	–0.46	0.16
1.202	–1.50	–0.45	0.35
1.101	–1.24	0.01	0.67
1.051	–1.21	0.15	0.98
1.021	–1.27	0.27	1.35
1.010	–1.25	0.29	1.64
1.002	–1.26	0.33	1.97

Table 3.5: Multimode dynamic amplification of mean horizontal response.

The second column from the right shows the maximum relative difference in magnitude between the static mean response and the steady–state dynamic mean response. How to decide the limiting value of the maximum deviation between the two is simply a matter of definition and interpretation but if a tolerance threshold of 1 % is adopted, the corresponding value of ω_1/ω_{max} seems to be somewhere between 4.5 and 5.0. A tolerance threshold of 0.1 % seems to give $\omega_1/\omega_{max} \approx 11$. It is obvious from table 3.5 that $\widehat{H}$ is a bad tool for assessing the limit value of ω_1/ω_{max} since not only does it overestimate dynamic amplification, but the magnitude of this very overestimation also varies drastically with ω_1/ω_{max}, hence making it unable to provide any useful information.

It must also be emphasized that because the maximum deviation is used as a measure of resemblance, the data in table 3.5 is lightly scattered. To obtain smoother data longer recording can be used, but the general trend is clearly visible by using the 30–minute recording in figure 3.9. Also, the data present in table 3.5 is of course obtained from the specific recording used in this illustration. However, the way the mean wind speed curve follows the local variations in the wind speed recording is dependent on the highest frequency it includes and less on what recording that is in fact used. Hence, another recording with relatively similar characteristics will produce very similar data as displayed in table 3.5, given that the recording is of sufficient length.

3.7 TIME DOMAIN SIMULATIONS

3.7.1 Introduction

So far, the frequency domain buffeting theory has been thoroughly presented and when extended to treat non–stationary wind speed recordings, arising problems has been addressed and to which proposed solutions has been presented. The advantages and convenience with the frequency domain approach is clearly its ability to effectively treat the stochastic features of the dynamic problem at hand, but it has one major disadvantage when it comes to non–stationarity because it completely lacks the ability of treating transient effects. Hence, using the now well–established tool of the non–stationary frequency domain buffeting theory framework without considering transient effects at all would be an almost blindfolded approach when trying to predict the stochastic characteristics of structural response induced by a particular non–stationary wind field. A time domain simulation treats transient effects perfectly fine since structural response is calculated directly via numerical integration of the governing differential equations themselves. However, since structural response is stochastic because the wind field inducing it indeed is so, a single realization of structural response gives really no useful and interpretable piece of information in this context. In order to be able to see a clear picture of the time varying variance of structural response at all, numerous simulations must therefore be carried out in which only the average of all these simulations is able to illustrate the transient effects.

3.7.2 Background for time domain simulation algorithm

Theoretically, the time domain equivalent of the multimode spatial averaging process that is performed in the frequency domain buffeting theory is establishing the modal loads by numerical integration from considering the instant wind velocity at every point across the bridge span, and subsequently solving the system of governing differential equations defined by equation 1.44a, for every time step throughout the considered time window. In practice, it is not necessary to record wind speed data at every point across the bridge span because wind speed recordings at given spatial separations across the bridge span can be generated such that they obey the coherence properties that is characteristic to the process they represent. At how many points across the bridge span such wind speed recordings should be generated depends on the local shape of the wind field and the length of the bridge span. In the case of the Hardanger Bridge, 100 equidistant points should be more than sufficient (Associate Prof. Ole Øiseth, April 27th, 2018) to accurately describe the spatial variations of the wind field.

Strømmen (2010, ch. A.3) derives the process of generating arbitrary realizations of simultaneous recordings processes across the bridge span. The expression for such a stochastic process is given by,

$$x_m(t) \quad = \quad \sum_{n=1}^{m} \sum_{j=1}^{N} \left| \hat{G}_{mn}(\omega_j) \right| \cdot \sqrt{2 S_x(\omega_j) \Delta\omega} \cdot \cos\left(\omega_j t - \varphi_{nj}\right) \qquad (3.13a)$$

where,

$$\widehat{\boldsymbol{S}}_x(\omega,\Delta s) \quad = \quad \widehat{\boldsymbol{G}}_{xx}(\omega,\Delta s)\cdot\widehat{\boldsymbol{G}}_{xx}^{*T}(\omega,\Delta s) \tag{3.13b}$$

$$Re\left[S_{x_m x_n}(\omega,\Delta s)\right] \quad = \quad S_x(\omega)\cdot\hat{C}o_x(\omega,\Delta s) \tag{3.13c}$$

where $\widehat{\boldsymbol{G}}_{xx}$ is the Cholesky decomposition of $\widehat{\boldsymbol{S}}_x$ and φ_{nj} is an arbitrary phase angle that is uniformly distributed on the interval $[0,2\pi]$. Similar to equation 1.28, $\boldsymbol{S}_x(\omega,\Delta s)$ can advantageously be split up into the the auto spectrum and normalized Co–spectrum such that $\widehat{\boldsymbol{G}}_{xx}$ only contains spatial coherence. In the case of non–stationarity all simultaneous realizations $\{x_m(t)\}$ may then together be modulated according to chapters 2.4.3 – 2.4.5 in order to resemble the non–stationary wind field in question.

Simulating the wind field across the bridge span by producing a set of for instance m = 100 equidistant realizations $x_m(t)$ is a quite computational expensive task. To obtain $x_m(t)$, m different time series must be generated and added in accordance with equation 3.13a. Hence, to produce for instance 100 realizations (m = 100) of $x(t)$, 0.5·100·101 = 5,050 individual time series must in total be generated. This procedure must also be performed for every single simulation, and a total of 1,000 simulations or more might be necessary to produce a sufficiently converged curve for the time–varying variance of structural response such that it is accurate enough and indeed interpretable when it comes to providing any desired information at all. Given the general method of simulating structural response induced by a discretely generated wind field presented in chapter 3.7.2, one might start to get an idea of the truly vast number of calculations that must be performed in order to obtain any useful information at all about what transient effects the dynamic structural response might display.

However, this sought information can in fact be obtained via a much more effective and streamlined procedure. This procedure is based on the idea of comparing the frequency domain buffeting response and the simulated time domain buffeting response of a single–degree–of–freedom (SDOF) system. The idea behind this method and its validity is presented in the following. First, consider the Hardanger Bridge to be subjected to a stationary wind field described by the Kaimal spectral formula and the associated parameters given in Appendix C, for $\bar{U}$ = {20, 30, 40} m/s. The corresponding response spectrums for horizontal motion at the bridge midspan is shown in figure 3.11.

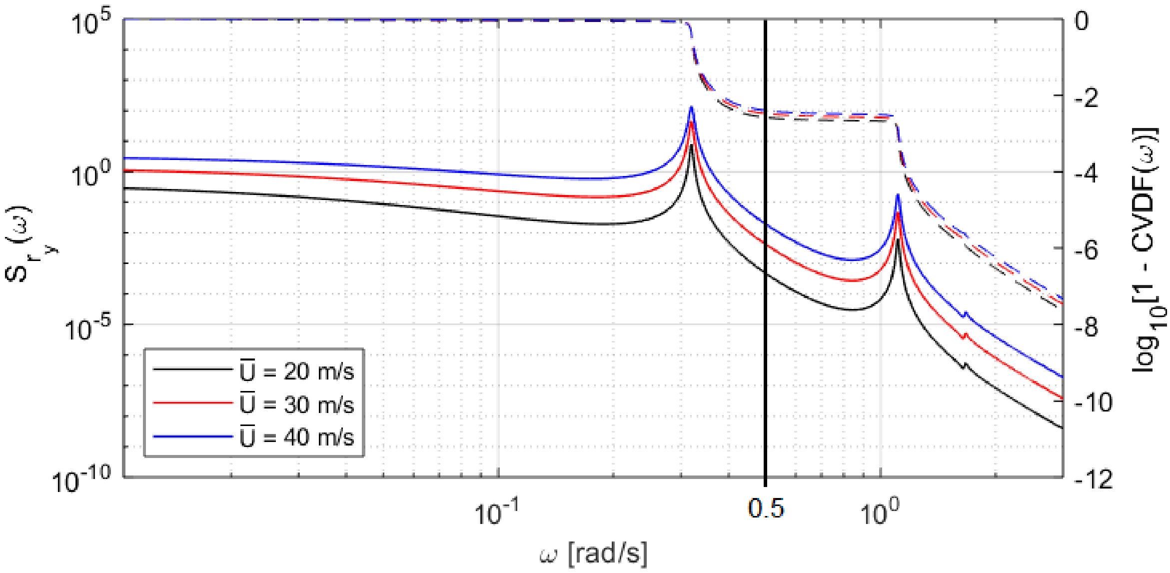

Figure 3.11: Response spectra and cumulative associated variance density functions

The response spectrums in figure 3.11 are calculated via the attached MATLAB script in chapter B.1.3 with a Fourier component threshold ε = 0.010, and by using the frequency axis discretization given by the text file “OS.txt” with a refinement factor f_r = 2. The dashed curves in figure 3.11 are the *cumulative variance density functions*, $CVDF(\omega)$ of the associated spectral curves and gives the relative accumulated variance as a function of ω and is defined by,

$$CVDF(\omega) \quad = \quad \left[\sum_{\tilde{\omega}=\omega_0}^{\tilde{\omega}=\omega} S(\tilde{\omega})\Delta\tilde{\omega}\right] \cdot \left[\sum_{\tilde{\omega}=\omega_0}^{\tilde{\omega}=\omega_n} S(\tilde{\omega})\Delta\tilde{\omega}\right]^{-1} \tag{3.14}$$

where ω_0 and ω_1 denotes the starting– and ending point of the numerical integration of $S_{r_y}(\omega)$, respectively. In this particular case, ω_0 = 0.0105 and ω_n = 11.5 was used.

The cumulative variance density functions in figure 3.11 shows that as good as all of the total variance of the process has been accumulated when integrating $S_{r_y}(\omega)$ just past the eigenfrequency of the first mode. Selecting a frequency limit ω_L = 0.5 rad/s gives $CVDF(\omega_L)$ = {0.9974, 0.9967, 0.9960} for $\overline{U}$ = {20, 30, 40} m/s, respectively. Less than half a percent of the total variance of the process does thus originate from the frequency region past ω = 0.5 rad/s. Consequently, to illustrate transient effects of structural response only the first horizontal mode needs to be considered since this makes up almost all variance of horizontal motion. Also, how rapidly the solution of a homogeneous second order linear differential equation dampens out is proportional to the product of the modal damping ratio and modal eigenfrequency (Strømmen, 2014, p. 66), and this product is clearly smallest for the fundamental mode of the Hardanger Bridge. Consequently, only horizontal motion needs to be considered because transient effects will hence be largest for the very displacement component that houses the fundamental mode, namely horizontal motion. Thus, if transient effects are present at a certain degree for horizontal motion, the prominence of transient effects will always be less for vertical and rotational motion because these displacement components house modes whose product of modal damping ratio and eigenfrequency is larger, hence reducing the time it takes for structural response to settle at a new level of variance.

It should be mentioned that this example only takes into consideration a single specific wind field. Nevertheless, it is probably very unlikely that another spectral function that represents a real wind field displays spectral content which is such that a significantly less fraction of the total structural variance originates from the first mode. To illustrate this fact the integral length scale in the spectral formula used to produce the response spectrum in figure 3.11 for $\overline{U}$ = 30 m/s is multiplied with the factors 2.5 and 0.4, respectively. The resulting response spectrums for the Hardanger Bridge is shown in figure 3.12.

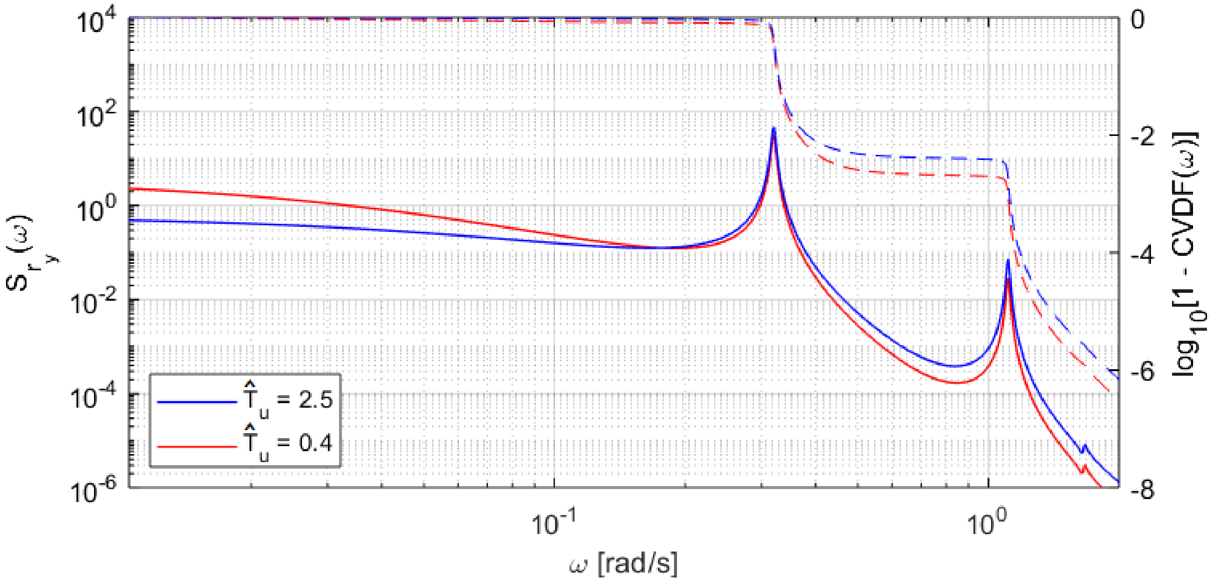

Figure 3.12: Response spectrums from wind spectrums with different time scales ($\bar{U}$ = 30 m/s)

It is obvious to see that changing integral length scales will alter the distribution of the variance in the response spectrum but this has close to zero effect on the variance contribution from the first mode. Namely when scaling the average integral length scale by the factors 2.5 and 0.4, the cumulative variance distribution function takes the respective values 0.9952 and 0.9974 at ω_L = 0.5 rad/s. However as can be seen from figure 3.12, reducing the integral length scale has the effect of moving some of the quasi–static variance contributions in the wind field spectrum over to the frequency regions containing the eigenfrequencies consequently making the variance distribution somewhat more capable of creating resonance. Illustratively, the standard deviation of horizontal structural displacement for $\hat{T}_u$ = 2.5 and $\hat{T}_u$ = 0.4 is 0.664 m and 0.748 m, respectively. Time–varying spectral content might therefore only be important to consider when trying to quantify the magnitude of structural response, but it clearly does not affect the validity of using a SDOF system to investigate transient effects.

Secondly, another simplification that is extremely effective in terms of computational expense is to let the SDOF system be subjected to a wind field that is spatially invariant along the bridge span, consequently needing only a single wind speed recording to define it. Such initially seems very nonchalant since it is far from correct when it comes to predicting the very magnitude of the response of the bridge because of the very fact that the wind speed varies across the bridge is completely ignored. However, the important thing is to keep in mind what piece of information one really wants to acquire. After all, the primary objective of establishing a time domain simulation scheme is nothing but to check that the fluctuations of the time varying variance of structural response calculated by the frequency domain buffeting theory indeed makes sense and thus can seem likely from a structural perspective when considering the eigenfrequency and damping ratio of the fundamental mode. Clearly, the spatial variations in the wind field across the bridge span has of course a large influence on the very magnitude of structural response. However, it has almost no influence on how fast its variance settles from one level to another since the fundamental mode completely dominates the picture of oscillation. Hence, generating a set of simultaneous realizations allocated to the corresponding set of equidistant points across the bridge span with the purpose being of preserving the coherent properties of the wind field such that spatial averaging can be approximated, is of absolutely no benefit when it comes to investigating transient effects of the structure exclusively. Such a mathematical model is simply another way of determining structural response in which its natural and automatic capability of modelling transient effects is simply a neat biproduct that happens to be desirable in this very context.

The logical result of the argumentation presented so far is therefore that the transient effects of the response of the Hardanger Bridge when being subjected to a non–stationary wind field can accurately be investigated by comparing the frequency domain and the simulated time domain buffeting response of a SDOF system that is equated to the fundamental mode of the Hardanger Bridge. This concept of using another path than the most obvious one between the starting point and the specific goal in question is illustrated in figure 3.13 and is nothing new to problem solving in general.

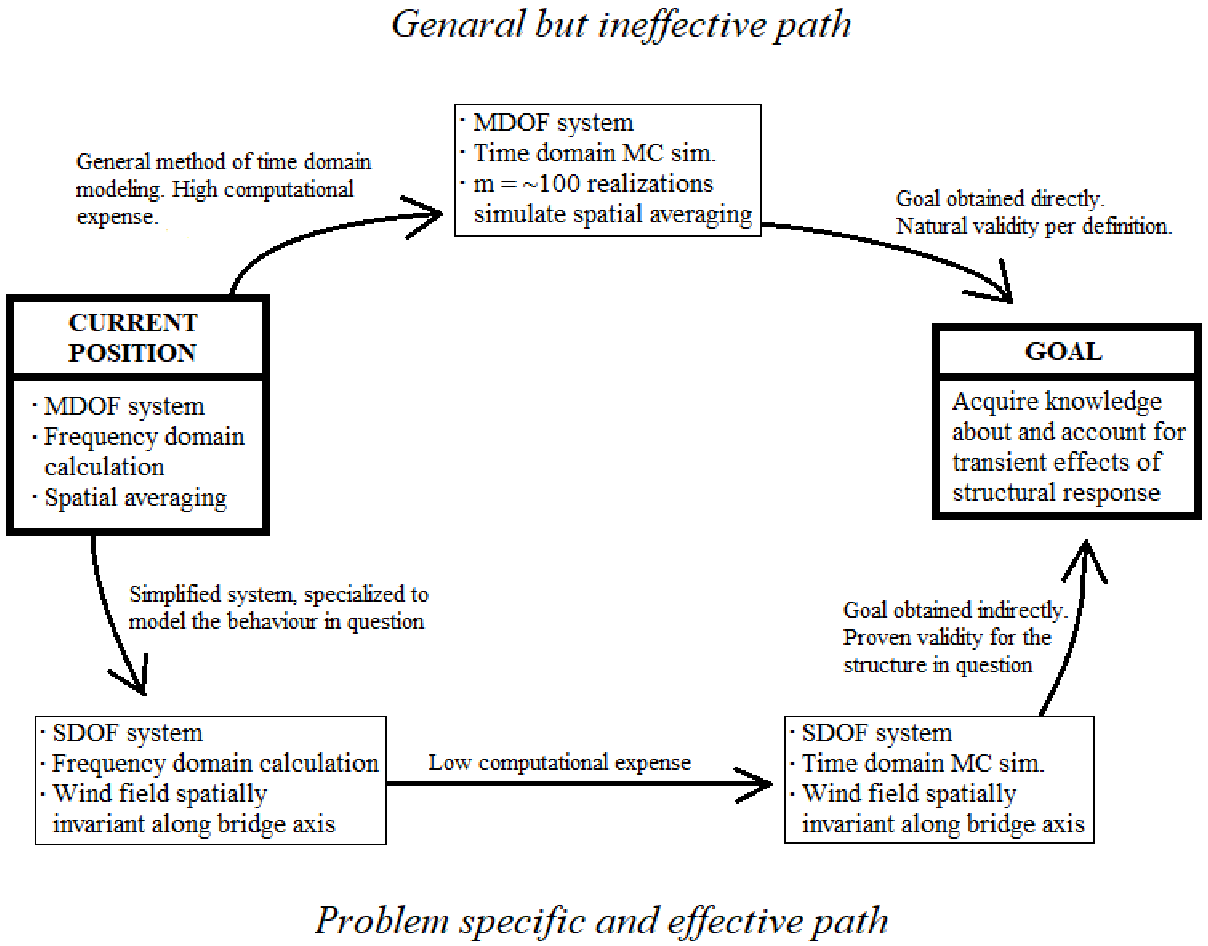

Figure 3.13: Principle of SDOF consideration

3.7.3 Formulation of SDOF time domain simulation algorithm

When carrying out the comparison between the frequency domain– and the simulated time domain buffeting response of the SDOF system, the wind field is for simplicity modelled as being uniformly modulated. The reason for this is to focus only on the issues that matters the most, namely the time varying link via variance of the input and output of the system. As will be shown in chapter 4, the curve of the time varying standard deviation of horizontal structural response will generally have shape–wise similarities to the curves of the time varying horizontal mean (quasi–static) response. This is because the very variable present in the expression for the response spectrum that generally displays the by far largest fluctuations in time is indeed the square of the mean wind speed. The time varying variance and especially the integral time scale in particular produce far smaller variations when it comes to structural response to which they consequently will be relatively modest contributors.

Generating a uniformly modulated signal involves a level of computational expense that is negligibly higher than that of a stationary signal. However, a non–uniformly modulated signal requires the time history of the modulation function to be calculated for every frequency setting used to establish the signal, and computational expense will consequently increase significantly. To use a uniformly modulated signal is therefore somewhat of a virtual optimum point when considering computational expense and accuracy for the purpose in question.

3.7.3.1 Frequency domain buffeting response for SDOF system

Deriving the expression for the response spectrum of the SDOF system starts with considering the modal version of equation 1.44. Again, aerodynamic stiffness is zero for horizontal motion and the governing equation of motion for the SDOF system is thus given by,

$$\tilde{M}_1\ddot{\eta}(t) \;+\; \left[\tilde{C}_1 - \tilde{C}_{1,ae}(t)\right]\dot{\eta}(t) \;+\; \tilde{K}_1\eta(t) \;=\; \tilde{Q}_1(t) \tag{3.15a}$$

where,

$$\tilde{Q}_1 \;=\; \frac{\rho V B}{2}\cdot 2\cdot\frac{D}{B}\cdot\bar{C}_D\cdot L\cdot\int_0^1 \varphi_{1y}(\hat{x})\cdot u(t)\,d\hat{x}$$

$$=\; C_{\tilde{Q}}\cdot u(t)\;,\quad C_Q \;=\; \bar{U}(t)\cdot\rho D\bar{C}_D L\cdot\int_0^1 \varphi_{1y}(\hat{x})\,d\hat{x} \tag{3.15b}$$

The fact that the “virtual” turbulence component $u(t)$ is set as being constant along the bridge span, eliminates the need for spatial averaging to obtain the expression for the modal load $\tilde{Q}_1$. Consequently, the Fourier components of the modal coordinate, η, can be obtained from the Fourier components of $u(t)$ directly,

$$a_\eta(\omega,t) \;=\; \hat{H}_\eta(\omega,t)\cdot\, C_{\hat{Q}}\cdot a_u(\omega,t)\,,\quad C_{\hat{Q}} \;=\; \frac{C_{\tilde{Q}}}{\tilde{K}_1} \tag{3.16a}$$

where,

$$\hat{H}_\eta(\omega,t) \;=\; \frac{1-\xi_1^2-2i\zeta_{tot}}{[1-\xi_1^2]^2+[2\xi_1\zeta_{tot}]^2} \tag{3.16b}$$

$$\xi_1 \;=\; \frac{\omega}{\omega_1} \tag{3.16c}$$

$$\zeta_{tot} \;=\; \zeta_1-\zeta_{1,ae}(t) \tag{3.16d}$$

Only the first term of the fully expanded version of the aerodynamic camping coefficient $\zeta_{ae_{ij}}$ defined by equation 3.7b will be present for the SDOF system defined by mode 1. The aerodynamic derivative

P_1^* who gives it time varying properties is given in Appendix C and when combining it with equations 3.7b and 3.16d, the total time varying SDOF damping ratio is given by,

$$\zeta_{tot}(t) \quad = \quad \zeta_1 \quad + \quad \bar{U}(t) \cdot \frac{\rho D \bar{C}_D L}{2\omega_1 \tilde{M}_1} \cdot \int_0^1 \varphi_{1y}^2(\hat{x}) d\hat{x} \tag{3.17}$$

Further, equations 3.16a and 1.18a are combined to obtain the (evolutionary) power spectral density of the modal coordinate, η, and when formulating $u(t)$ as being uniformly modulated the EPSD of u(t) will obey the definition of equation 2.8,

$$S_\eta(\omega, t) \quad = \quad C_{\hat{Q}}^2 \cdot \sigma_u^2(t) \cdot \left|\hat{H}_\eta(\omega, t)\right|^2 \cdot S_g(\omega) \tag{3.18}$$

Analogue to equations 1.49 and 1.52, the time varying variance of the SDOF response at the bridge midspan is given by,

$$\sigma_{r_y}^2(\hat{x}, t) \quad = \quad \sigma_u^2(t) \cdot \varphi_{1y}^2(\hat{x}) \cdot C_{\hat{Q}}^2 \cdot \int_0^{\omega_L} \left|\hat{H}_\eta(\omega, t)\right|^2 \cdot S_g(\omega)\, d\omega \tag{3.19a}$$

where,

$$\hat{x} \quad = \quad 0.5 \tag{3.19b}$$

$$\omega_L \quad = \quad 0.5 \text{ rad/s} \tag{3.19c}$$

$$\left|\hat{H}_\eta(\omega, t)\right|^2 \quad = \quad \frac{1}{\sqrt{[1 - \xi_1^2]^2 + [2\xi_1 \zeta_{tot}]^2}} \tag{3.19d}$$

A similar numerical integration scheme to what is illustrated in figure 3.5 is used to solve equation 3.19a. The chosen frequency settings are incorporated into the script “SDOFresponse.m” that is attached in Appendix B. The frequency limit ω_L = 0.5 rad/s is based on the mentioned behaviour of the cumulative variance distribution function of the spectrum plots in figure 3.11 and 3.12.

The time varying mean response is as before assumed to be quasi–static given the chosen level of fluctuations in $\sigma_u(t)$ and $[\bar{U}(t)]^2$ (ref. chapters 2.3.3, 2.4.3.1 and 3.6) and is simply obtained by multiplying equation 3.8b with $\varphi_{1y}(\hat{x})$ and dividing by the modal stiffness, namely,

$$\bar{r}_y(t) \quad = \quad \varphi_{1y}(\hat{x}) \cdot \frac{\rho D \bar{C}_D L}{2\tilde{K}_1} \cdot \int_0^1 \varphi_{1y}(\hat{x}) d\hat{x} \cdot [\bar{U}(t)]^2 \tag{3.20}$$

3.7.3.2 Establishment of Monte Carlo simulation algorithm

The algorithm that is given the role to validate the frequency domain response of the SDOF system presented in chapter 3.7.3.1 will be presented in the following. The algorithm itself is relatively straight–

forward since it is really no secret what it fundamentally does. Nevertheless, a single simulation of structural response contains the consecutive steps:

1. Generate an arbitrary stationary wind speed recording, $g(t)$, with unit variance from the same spectrum as $S_g(\omega)$ in equation 3.18.
2. Modulate $g(t)$ according to equation 3.15b to represent the stochastic process $\tilde{Q}_1(t)$.
3. Solve the initial value problem using an appropriate differential equation solver.
4. Estimate time varying variance and add it to the average and collect other relevant data.

A specific set of measures are applied to the individual steps above in order to enhance the performance of the entire algorithm as much as possible. These measures are generally specialized to the characteristics of the Hardanger Bridge in particular and may not be equally valid or convenient when applied to another structure. Nevertheless, the individual measures are presented in the following.

1. Reducing sampling frequency when generating the unit–variance signals

The wind speed recordings from the Hardanger Bridge that will be used in chapter 4 has a sampling frequency of 20 Hz. However, with the highest included frequency in the generated recording, $g(t)$, being 0.5 rad/s which equates to a period of roughly 12.5 seconds, sampling $g(t)$ at 20 Hz would be ineffective in terms of algorithm performance. This is because the inertia of the bridge is so large that its motion will remain almost unaffected by the fact that $\tilde{Q}_1(t)$ has a somewhat discontinuous slope resulting from the discrete sampling process of $g(t)$. One might therefore take advantage of this fact by sampling $g(t)$ at for instance 5 Hz, 4 Hz or 2.5 Hz and interpolate back to 20 Hz after all frequency components have been added, as is illustrated in figure 3.14 with a single harmonic function with period 12.5 s and a sampling frequency of 4 Hz.

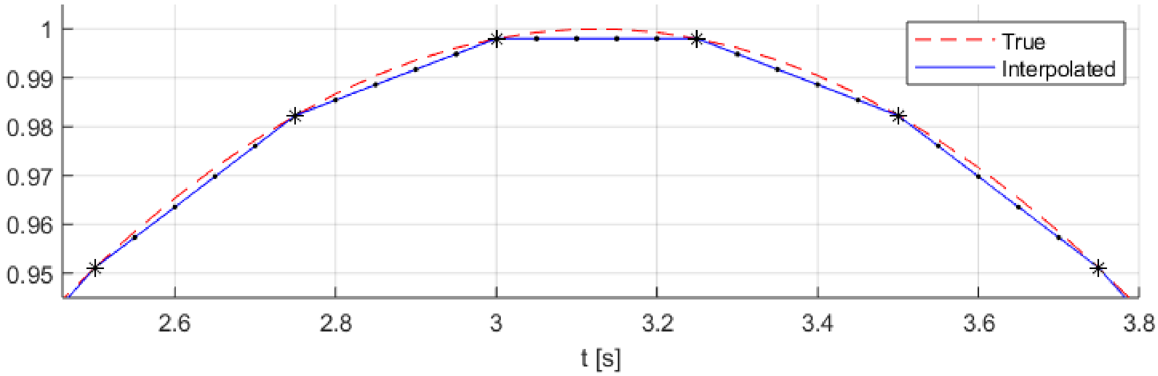

Figure 3.14: Reduced sampling frequency of generated signal

By mere eye–balling, one can see that the relative error associated with the interpolation procedure illustrated in figure 3.14 seems to be within a quarter of a percent which is more than sufficient for the purpose in question.

2. Method for solving the dynamic initial value problem

MATLAB R2018a features many highly effective built–in algorithms for solving initial value problems, for instance the function *ode45*. These built–in functions generally feature adaptive step–size algorithms that is based on the rate of change of the variables and time varying coefficients of the differential equation in question. However, a necessary requirement for these algorithms to work according to their intended purpose is that the coefficients of the differential equation are differentiable mathematical functions. In the case of equation 3.15a, $\tilde{C}_{1,ae}(t)$ and $\tilde{Q}_1(t)$ are discrete vectors and therefore violates this requirement. Consequently, using built–in functions to solve equation 3.15a is not necessarily a good idea based on the format of $\tilde{C}_{1,ae}(t)$ and $\tilde{Q}_1(t)$. The fourth order Runge−Kutta method (RK4) for systems (Kreyszig, 2006, p. 904) is therefore instead adopted. Since equation 3.15a is of second order, it must first be expressed as a system of two mutually dependent first order differential equations,

$$\begin{aligned} \dot{\eta}_1 &= f_1(t) = \eta_2 & & \eta_1(0) = \eta_0 \\ \dot{\eta}_2 &= f_2(t) = \frac{1}{\tilde{M}_1} \cdot \left[\tilde{Q}_1(t) - \tilde{C}_{tot}(t)\eta_2 - \tilde{K}_1\eta_1\right] & , \quad & \eta_2(0) = \dot{\eta}_0 \end{aligned} \tag{3.21}$$

The RK4 method works by obtaining four auxiliary quantities from which a final, weighted slope is determined and then given the role to estimate η_1 and η_2 at the next time step, namely,

$$\boldsymbol{\eta}_{n+1} = \boldsymbol{\eta}_n + \frac{1}{6}[\boldsymbol{k}_1 + 2\boldsymbol{k}_2 + 2\boldsymbol{k}_3 + \boldsymbol{k}_4] \tag{3.22a}$$

where,

$$\begin{aligned} \boldsymbol{k}_1 &= \Delta t \cdot \boldsymbol{f}(t_n, \boldsymbol{y}_n) \\ \boldsymbol{k}_2 &= \Delta t \cdot \boldsymbol{f}(t_n + 0.5\Delta t, \quad \boldsymbol{y}_n + 0.5\boldsymbol{k}_1) \\ \boldsymbol{k}_3 &= \Delta t \cdot \boldsymbol{f}(t_n + 0.5\Delta t, \quad \boldsymbol{y}_n + 0.5\boldsymbol{k}_2) \\ \boldsymbol{k}_4 &= \Delta t \cdot \boldsymbol{f}(t_n + \Delta t, \quad \boldsymbol{y}_n + \boldsymbol{k}_3) \end{aligned} \tag{3.22b}$$

For compatibility purposes only, the computed time history for the modal coordinate η_1 must be multiplied with $\varphi_{1y}(\hat{x})$ to represent horizontal displacement at $\hat{x}$ and such that it indeed can be compared with equation 3.19a.

The RK4 method is of fourth order and has thereby quartic convergence rate. The reason why it is used instead of for instance an explicit or implicit Euler method (first order) is because it is much less prone to amplitudinal drift at a sampling frequency of 20 Hz. After all, almost 100 cycles of the first mode will take place within a one hour time window and amplitudinal drift might therefore be present as a very undesired effect.

3. *Commissioning phase of simulated structural response*

Simply for convenience, the SDOF system is initially set to be at rest, thus equating η_0 and $\dot{\eta}_0$ in equation 3.21 to zero at the point of initialization. However, because of the great inertia of the bridge structure, a significant amount of time must pass before it is no longer visible that the variance of structural response was in fact initialized by these very initial values. If this "commissioning phase" is progressing within the very interval one wants to compare frequency domain and simulated time domain response, the very section affected by this stabilization process is more or less useless when it comes to interpreting the difference between the two methods. Therefore, a "commissioning phase interval" with length T_{CP} prior to what defines $t = 0$ is introduced where the time varying variance of the modal load, $\sigma^2_{\tilde{Q}_1}(t)$, is set to be constant and equal to its value at $t = 0$. The value of T_{CP} is chosen *a posteriori* such that the time varying variance of structural response seems to have stabilized sufficiently at $t = 0$. A post interval elongation of $\sigma^2_{\tilde{Q}_1}(t)$ of length T_A is also chosen but with the purpose being of being able to define the time varying variance of structural response at $t = 0$ and $t = T$, analogue to what is done with the time varying variance and integral time scales of the wind turbulence components. The design of this feature is schematically illustrated in figure 3.15.

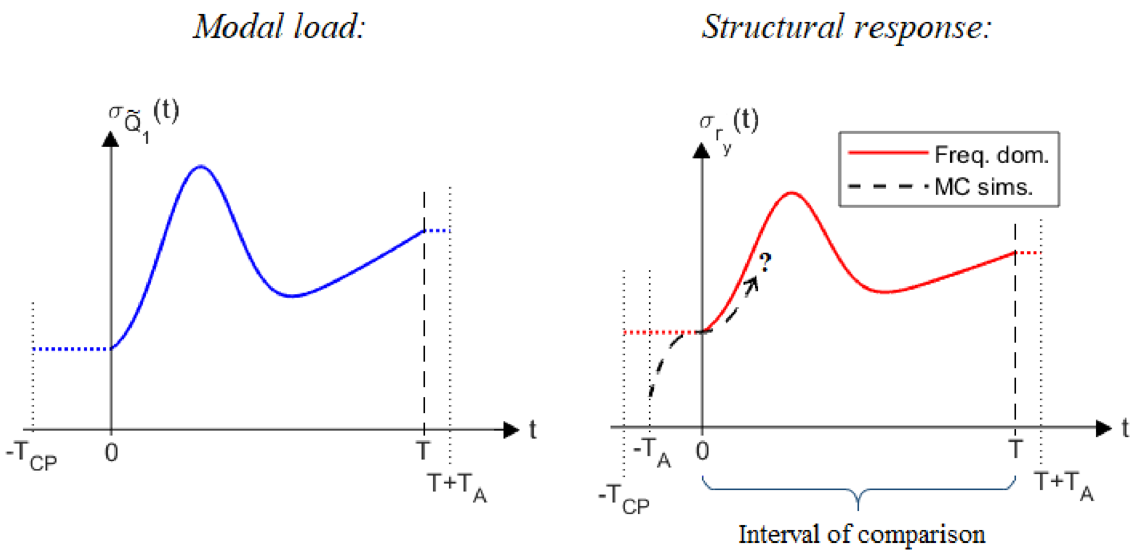

Figure 3.15: Commissioning phase and averaging interval for MC simulations

4. Estimation procedure of time varying variance of simulated structural response:

This procedure is similar as the one used to estimate the time varying variance of the wind turbulence components. However, its effectiveness can be enhanced by a large amount due to the relatively predictable local shape of the time history of the response itself. As a direct result from the fact that almost all variance of structural response originates from frequencies in the close vicinity of the eigenfrequency, ω_1 , the SDOF system will indeed oscillate at a characteristic, “instant” frequency very close to the eigenfrequency itself. Consequently, the time varying variance of structural response can be calculated via a uniform average spanning half a period to either side of $t = t_i$. Since $2\pi/\omega_1 = 19.64$ s ≈ 20 s, the averaging period is set to $T_A = 10$ s, as shown in figure 3.16.

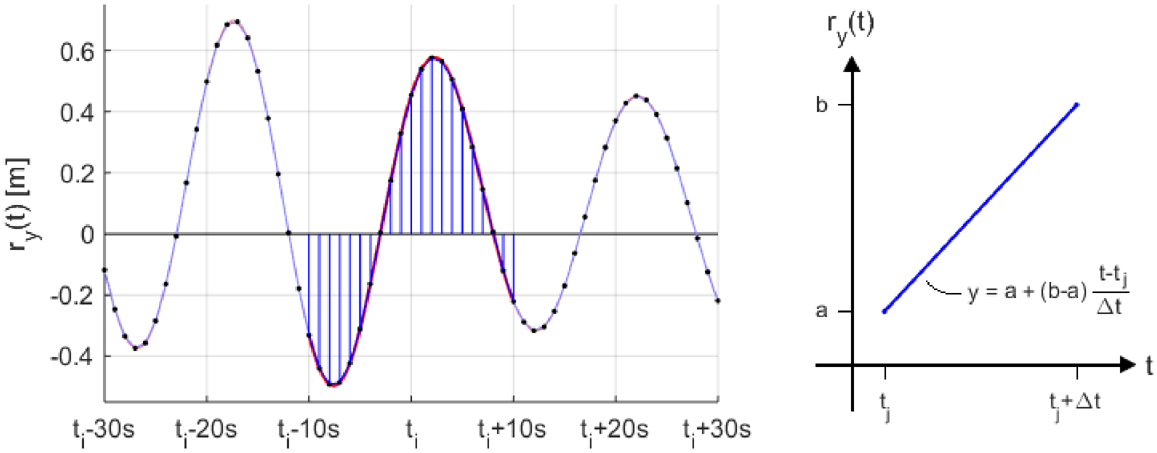

Figure 3.16: Estimation technique of time varying variance

Also due to shape regularity, and as is done in figure 3.16, sampling can be done at 1 Hz and the variance contribution from each of the 20 corresponding “sections” can be calculated from integrating the square of the interpolated linear curves shown to the right in figure 3.16, namely,

$$\int_{t_j}^{t_j+\Delta t} \left[a + (b-a)\cdot\frac{t-t_j}{\Delta t}\right]^2 dt \;=\; \frac{\Delta t}{3}\cdot\left[a^2+ab+b^2\right] \tag{3.23}$$

such that,

$$\sigma_{r_y}^2(t) \;=\; \frac{\Delta t}{6T_A}\cdot\sum_{j=1}^{20}\left[a_j^2+a_jb_j+b_j^2\right] \tag{3.24}$$

3.7.4 Remarks and illustrative examples

Figure 3.17 shows an illustration of a single loop iteration of the now proposed Monte Carlo simulation algorithm. The spectrum formula $S_g = 40.8\cdot[1+50.2\cdot\omega]^{-1.6}$ was used to generate a realization of $g(t)$, and $g(t)$ was subsequently modulated with $\sigma_u = I_u\cdot\bar{U}(t)$ to form $u(t)$ where the mean wind speed is illustrated in the uppermost subplot and defined by $\bar{U}(t) = 15+20\exp\left[\left(\frac{t-30}{12.5}\right)^2\right]$. The resulting modal load $\tilde{Q}_1(t)$ is shown in the middle subplot. The bottom subplot shows the time domain response of the SDOF system induced by $\tilde{Q}_1(t)$ in which $\sigma_{r_y}(t)$ is determined according to equation 3.24. T_{CP} was set equal to 10 min and the time window shown in figure 3.17 does therefore start 10 minutes after the initialization of the time domain response calculation.

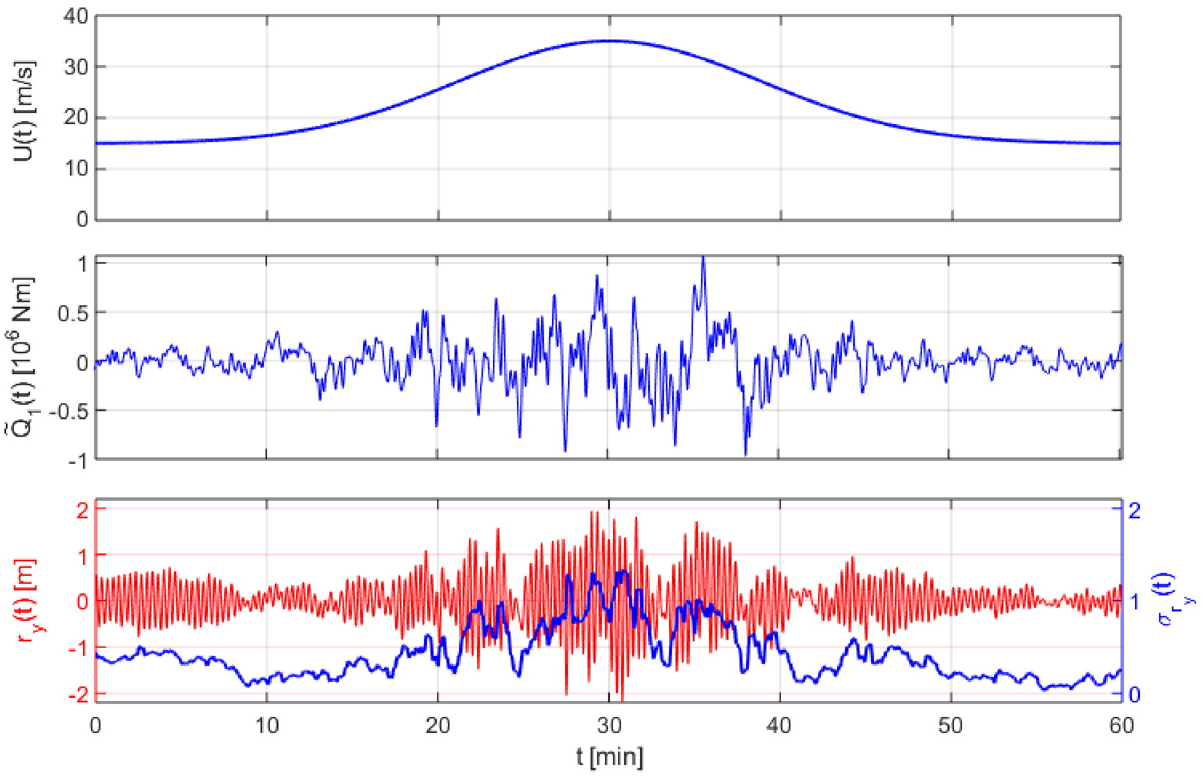

Figure 3.17: Illustrative loop–wise workings of Monte Carlo simulation algorithm

Figure 3.17 clearly illustrates the stochastic behaviour of structural response, resulting from the fact that at which moments the loading and the structural motion are in and out of phase can be considered to be stochastic. From this very reason, structural response exhibits rather characteristic “beats” and it is therefore generally very difficult to determine the shape of the time varying standard deviation of structural response by considering only the time history from a single simulation, because the location of these beats can also be considered to be stochastic. Another consequence of this property is that estimating $\sigma_{r_y}^2(t)$ from a wider time interval than 20 seconds (roughly one period) does not seem to make the averaged time history of $\sigma_{r_y}^2$ converge any faster. Because the location of the characteristic beats will vary randomly from simulation to simulation, selecting a longer averaging period produces only a locally smoother curve for $\sigma_{r_y}(t)$ at that particular simulation, and nothing more. Hence, what is most effective is therefore letting the pure number of simulations itself do the work when it comes to convergence.

To illustrate some transient effects the response of the SDOF system might exhibit, three individual sets of $N = 2500$ simulations of $\tilde{Q}_1(t)$ and the resulting $r_y(t)$ is performed. A comparison between the standard deviations of the frequency domain response and the simulated average time domain response is shown in figure 3.18. In each of the three cases, the virtual storm that induces structural response is the same as the one shown in the uppermost subplot in figure 3.17 but now generalized to $\bar{U}(t) = 15 + 20\exp\left[\left(\frac{t-30}{BW}\right)^2\right]$ where $BW = \{12.5\text{ min}, 5\text{ min}, 2\text{ min}\}$ from top to bottom in figure 4.18, respectively. Turbulence intensity is still constant at $I_u = 0.16$, and the duration of the commissioning phase is still kept at $T_{CP} = 10$ min. The “bandwidth” parameter, BW, determines the sharpness of the mean wind speed time history of the oncoming storm and by assigning it different values, the concept of “build–up time” of the standard deviation of structural response is clearly illustrated.

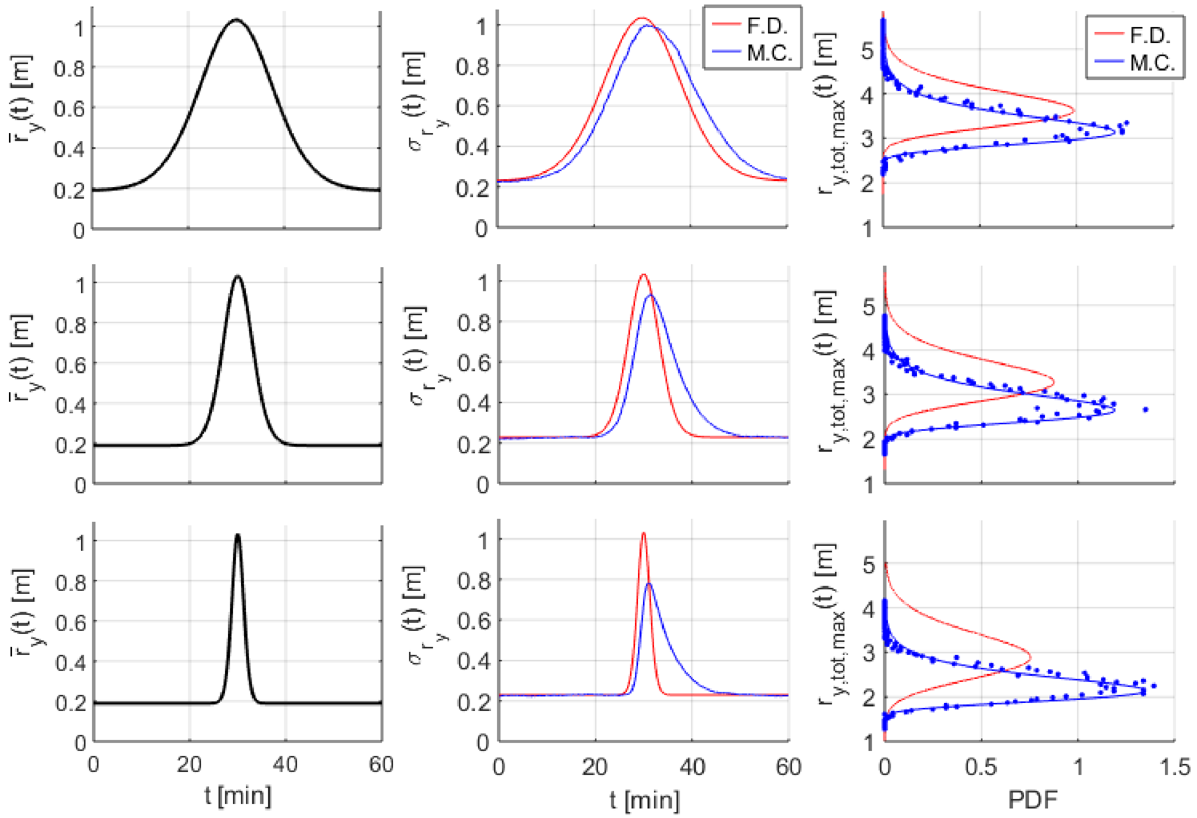

Figure 3.18: Monte Carlo simulation ($N = 2500$) of structural response in time domain.

First and foremost, it is clear that the inertia of the SDOF system has the expected effect of giving the variance of the simulated time domain response limited ability to follow sudden and sharp changes in the variance of the modal loads. If the modal load exhibits gentle variations with time, which is nothing but a decent description of the storm described by $BW = 12.5$ min, the effect is less, and the magnitude of the time varying variance seems to be almost conserved but with a significant time lag being present. In the contrary, $BW = 2$ min seems to be a type of storm whose duration is not long enough and whose variance does not change gently enough in time to allow the variance of structural response to remain in a close to *quasi–stationary state of equilibrium,* as indeed seems to be the case with $BW = 12.5$ min. Hence, if the case with $BW = 2$ min truly represents a real storm, the frequency domain calculation approach cannot accurately describe the time varying structural response since transient effects dominates the input–output relationship. In chapter 4, the frequency domain approach and the now established SDOF time domain simulation approach will be compared when processing real–life wind data.

The rightmost column in figure 3.18 shows the probability distributions of maximum structural response from the considered 60–minute time window. In the case of the frequency domain response, the distribution function (red curve) is calculated directly from equations 2.29 and 2.30. In the case of the time domain simulations, the maximum value of $r_y(t)$ is collected for every single simulation and a discrete density plot of these maximum values numerically estimates their distribution function. The approximated distribution function (blue curve) is determined from a LSF using the Type 1 Gumbel distribution function where the mean value can be calculated in advance such that the variance will be the only degree of freedom.

4 RESULTS

4.1 PRELIMINARIES

Real–life wind speed data recorded at the midspan of the Hardanger Bridge between 17:30 and 23:00 UTC+01:00 on January 29th, 2016 is given the role to illustrate the theory established in chapters 1, 2 and 3 and is shown in figure 4.1. The first and last 20 minutes of this parent recording acts only as a commissioning phase for the IFE–extracted mean wind speed and as a data base when time varying variance and integral time scales are calculated at the extremities of the resulting subset recording. Hence, the very subset recording onto which every time varying variable consequently can be defined starts and ends at 17:50 and 22:40 UTC+01:00, respectively, and is highlighted in deep red colour in figure 4.1. $U(t)$ in figure 4.1 is indeed the instant wind speed perpendicular to the bridge girder in the horizontal plane. The sampling frequency of the recording is 20 Hz.

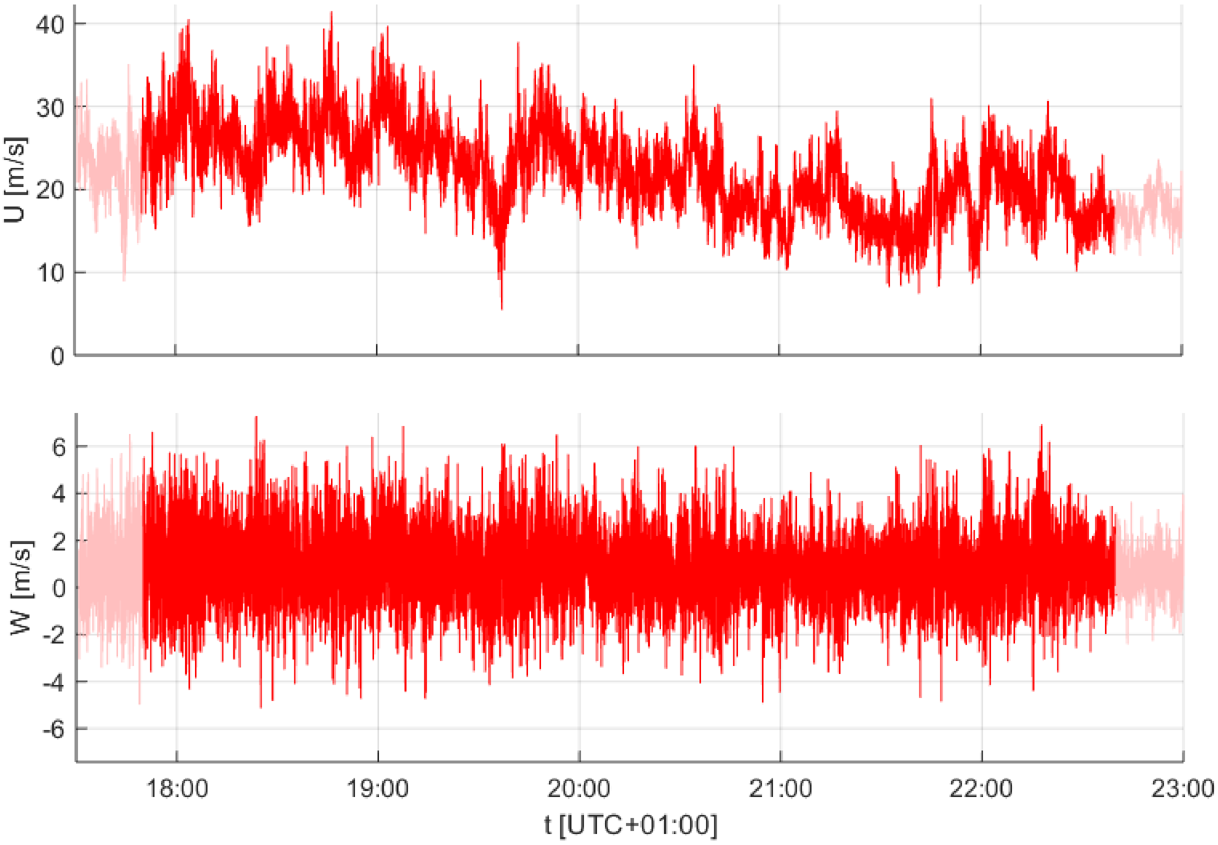

Figure 4.1: Real–life wind speed recording at the Hardanger Bridge

The results presented in this chapter are based on a statistical resemblance of the wind speed recording in figure 4.1 at four different levels, namely by extracting the mean wind speed using four different levels of the highest–most included frequency, ω_{max} in the IFE. For the sake of convenience and compatibility, the characteristic frequency at which the mean wind speed, the time varying variance and the integral time scales fluctuates in time may logically be attempted to be kept as similar as possible which for the calculations in this chapter is done by adopting the following rule,

$$T_A = \frac{\pi}{\omega_{max}} \tag{4.1}$$

such that the averaging time span, $2 \cdot T_A$, equates the period of a harmonic component with frequency ω_{max}. The values of ω_{max} that is chosen in each of the four cases, together with the corresponding values of T_A in accordance with equation 4.1 is given in table 4.1

	Case 1:	**Case 2:**	**Case 3:**	**Case 4:**
ω_1/ω_{max}	100.8	77.6	50.4	30.6
T_A [s]	980	740	490	290

Table 4.1: Considered characteristics of wind speed recording resemblance

For each of the four presented cases in table 4.1, the following arithmetics are performed on the wind speed recording in figure 4.1,

1. Extract the mean wind speeds $\bar{U}(t)$, $\bar{W}(t)$ using the IFE with ω_{max} from table 4.1. Define the turbulence components $u(t)$, $w(t)$ by subtraction. $u(t)$, $w(t)$ should consequently have zero mean.
2. Calculate $\sigma_u^2(t)$, $\sigma_w^2(t)$ using the corresponding value of T_A in table 4.1 and the parabolic weighting function in equation 4.10.
3. Define the normalized turbulence components $g_u(t)$, $g_w(t)$. $g_u(t)$ and $g_w(t)$ should follow a Gaussian distribution with zero mean and unit variance.
4. Calculate integral time scales, $T_u(t)$ and $T_w(t)$ using the integral (area) method illustrated in figure 2.13. ρ_{THR} is set at 0.25.
5. Calculate the time–invariant Fourier frequency spectrums $S_{g,u}(\omega)$ and $S_{g,w}(\omega)$ from $g_u(t)$ and $g_w(t)$. The highest included frequency is set to $\omega = 12$ rad/s.
6. Smooth $S_{g,u}(\omega)$ and $S_{g,w}(\omega)$ using the proposed smoothing algorithm in chapter 2.4.5.1.
7. With the help of the built–in WLSF MATLAB toolbox *cftool*, and the weighting function of equation 2.29, determine the parameters of the spectral formula that is the *presumed* best fit to the smoothed spectral data.

The above steps 1 – 7 establishes all relevant information for the dynamic response calculations in which the following procedures is carried out,

1. For every of the four methods of turbulence component modulation proposed in chapter 2.4, calculate time varying variance of structural response according to equations 1.52 and 1.59, using the proposed solution methods presented in chapters 3.3 and 3.5. The significance level, ε, of mode shape Fourier components is set to $\varepsilon = 0.010$ and the refinement factor, f_r, in the numerical integration scheme is set to $f_r = 2$.
2. Calculate the time varying (quasi-static) mean structural response using to equations 1.60 and 2.2.
3. Calculate the probability density functions of the maximum structural response for the four methods of turbulence components modulation and for the three displacement components using equations 2.30 and 2.31.
4. Compare frequency domain response and simulated time domain response (here: $N = 4000$ sims.) for the equivalent SDOF system to investigate transient effects. Calculate probability density function of maximum response numerically, and by using equations 2.30 and 2.31.

4.2 WIND DATA ANALYSIS AND RESPONSE CALCULATIONS

4.2.1 Case 1

Wind field calculations:

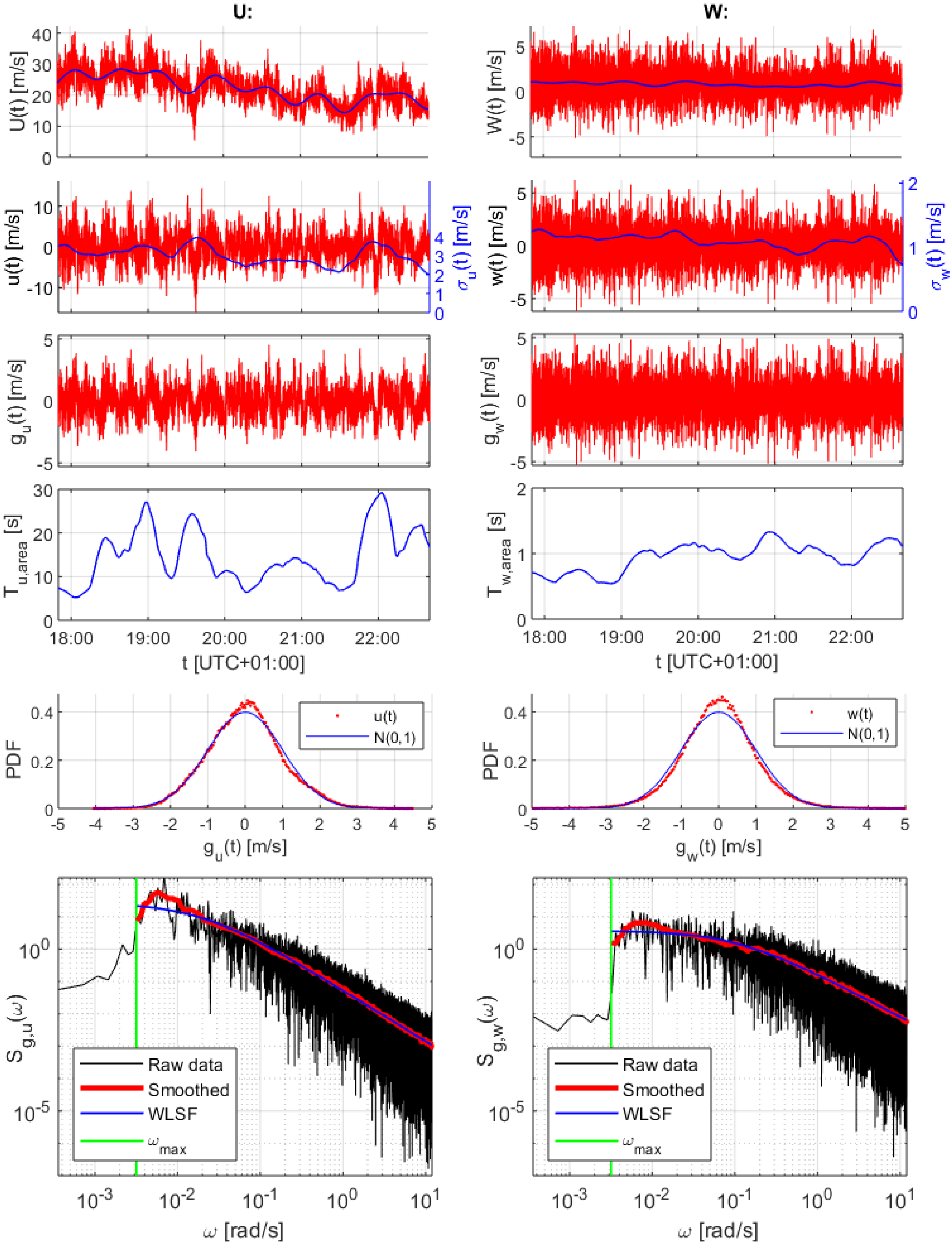

Figure 4.2: Wind speed calculations, case 1.

	U ($n = u$):			**W ($n = w$):**		
	min:	**avg.:**	**max:**	**min:**	**avg.:**	**max:**
Mean wind speed [m/s]	14.38	22.33	28.39	0.53	0.83	1.16
Turbulence, $n(t)$:						
- $E[n(t)]$ [m/s]	-	0.007	-	-	0.001	-
- RMS [m/s]	-	3.036	-	-	1.104	-
- $\sigma_n(t)$ [m/s]	1.983	3.042	3.943	0.721	1.103	1.276
Normalized turbulence, $g_n(t)$:						
- $E[g_n(t)]$ [m/s]	-	0.002	-	-	0.001	-
- RMS [m/s]	-	0.983	-	-	0.995	-
- $\sum_{\omega_{max}}^{12} S_{g,n,raw}(\omega_i)\Delta\omega$	-	0.986	-	-	0.969	-
- $\int_{\omega_{max}}^{12} S_{g,n,WLSF}(\omega)d\omega$	-	0.820	-	-	0.908	-
$T_n(t)$ [s]	5.27	14.62	29.26	0.54	0.95	1.33

Table 4.2: Relevant extracted data from wind field calculations, case 1.

Dynamic response calculations, frequency domain:

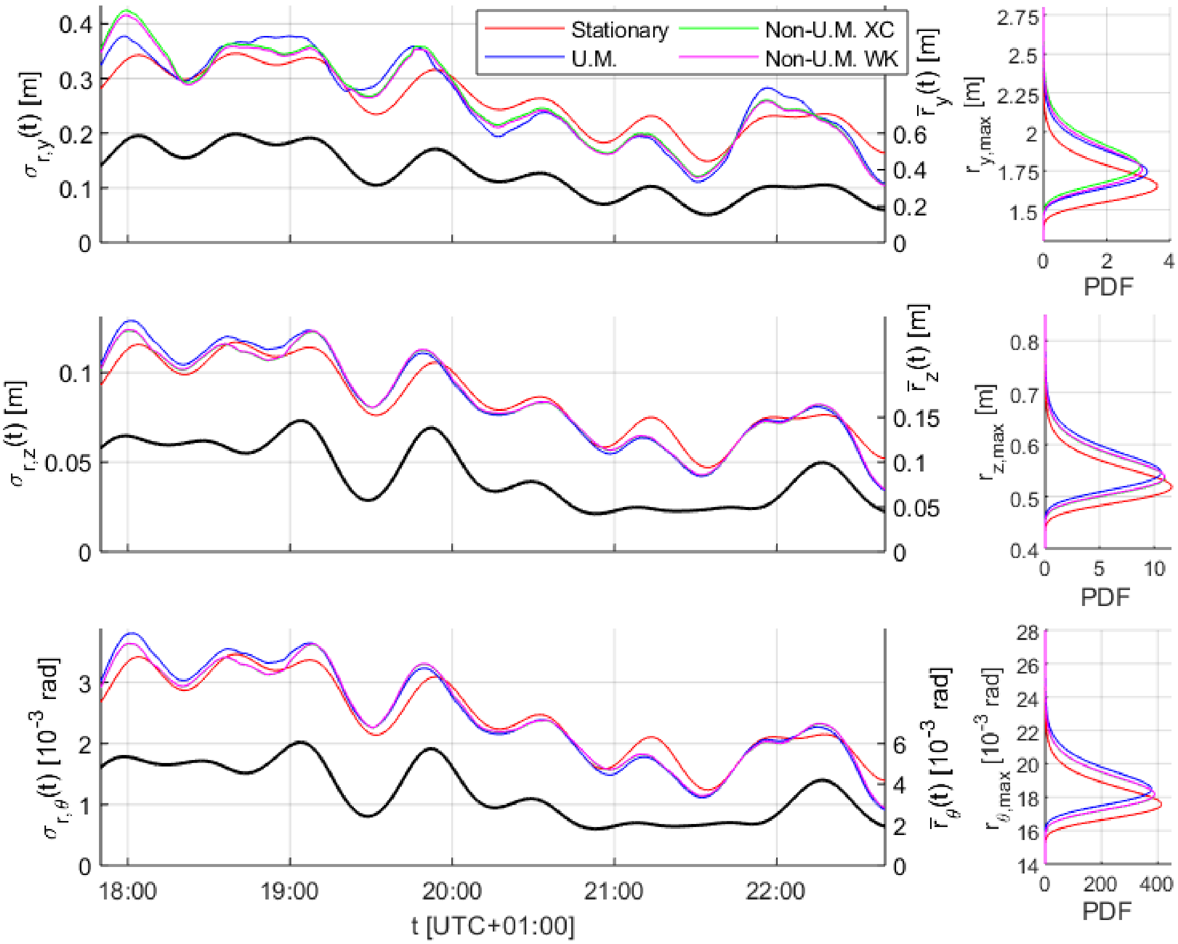

Figure 4.3: Frequency domain structural response, case 1.

Extreme value distribution:

	$r_y(t)$ [m]:		$r_z(t)$ [m]:		$r_\theta(t)$ [10^{-3} rad]:	
Modulation method:	Expected:	CDF = .99	Expected:	CDF = .99	Expected:	CDF = .99
Stationary	1.695	2.048	0.440	0.644	18.0	21.1
Uniform	1.792	2.178	0.544	0.684	18.9	22.4
Non-uniform, XC	1.837	2.265	0.518	0.670	18.6	22.0
Non-uniform, WK	1.813	2.231	0.522	0.672	18.6	22.0

Table 4.3: Expected maximums and extreme levels with 1% probability of exceedance

SDOF system comparison:

Figure 4.4 shows the comparison between the frequency domain response and the simulated time domain response of the simplified, equivalent SDOF system. The bold black line is the time varying mean response. The distribution of maximum response for the frequency domain approach (analytical) and the time domain approach (simulated) is shown to the left in figure 4.4. The bottom plot shows the simulated probability distribution for the moment in time for when the maximum response take place.

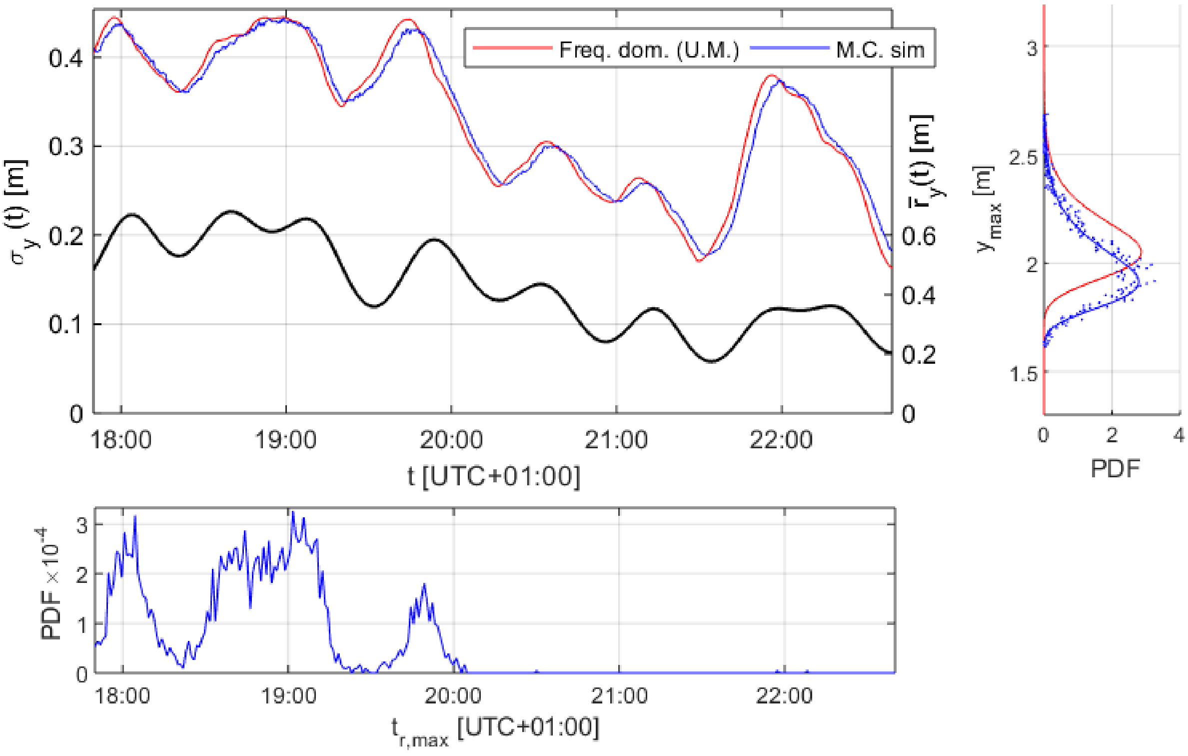

Figure 4.4: SDOF comparison, case 1 ($N = 4000$).

4.2.2 Case 2

Wind field calculations:

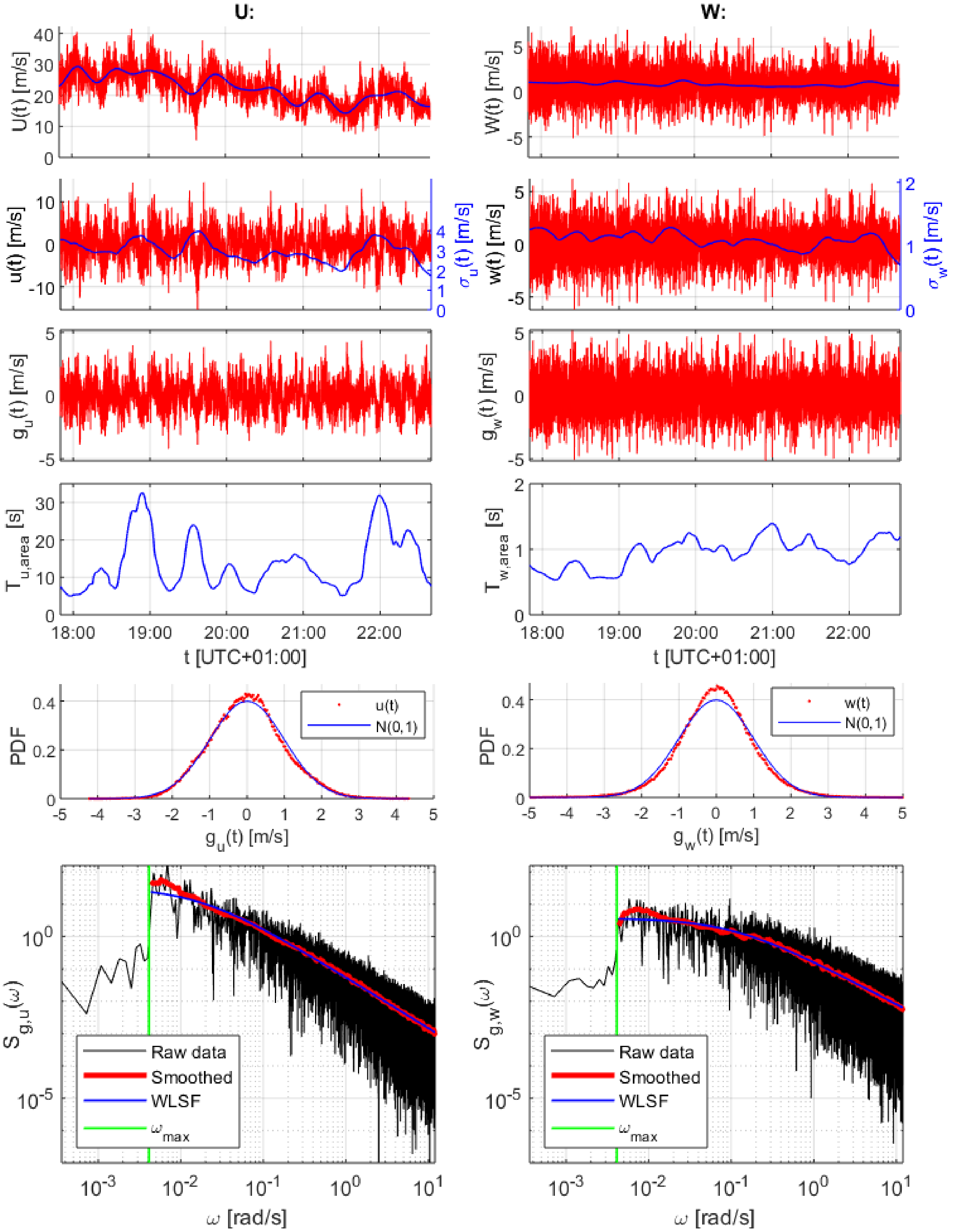

Figure 4.5: Wind speed calculations, case 2.

	U ($n = u$):			**W ($n = w$):**		
	min:	**avg.:**	**max:**	**min:**	**avg.:**	**max:**
Mean wind speed [m/s]	14.28	22.33	29.26	0.55	0.83	1.27
***Turbulence, $n(t)$*:**						
- $E[n(t)]$ [m/s]	-	0.012	-	-	0.002	-
- RMS [m/s]	-	3.006	-	-	1.102	-
- $\sigma_n(t)$ [m/s]	1.703	3.008	3.969	0.705	1.102	1.290
***Normalized turbulence, $g_n(t)$*:**						
- $E[g_n(t)]$ [m/s]	-	0.001	-	-	0.003	-
- RMS [m/s]	-	0.982	-	-	0.991	-
- $\sum_{\omega_{max}}^{12} S_{g,n,raw}(\omega_i)\Delta\omega$	-	0.985	-	-	0.967	-
- $\int_{\omega_{max}}^{12} S_{g,n,WLSF}(\omega)d\omega$	-	0.870	-	-	0.906	-
$T_n(t)$ [s]	4.99	13.75	32.56	0.53	0.94	1.39

Table 4.4: Relevant extracted data from wind field calculations, case 2.

Dynamic response calculations, frequency domain:

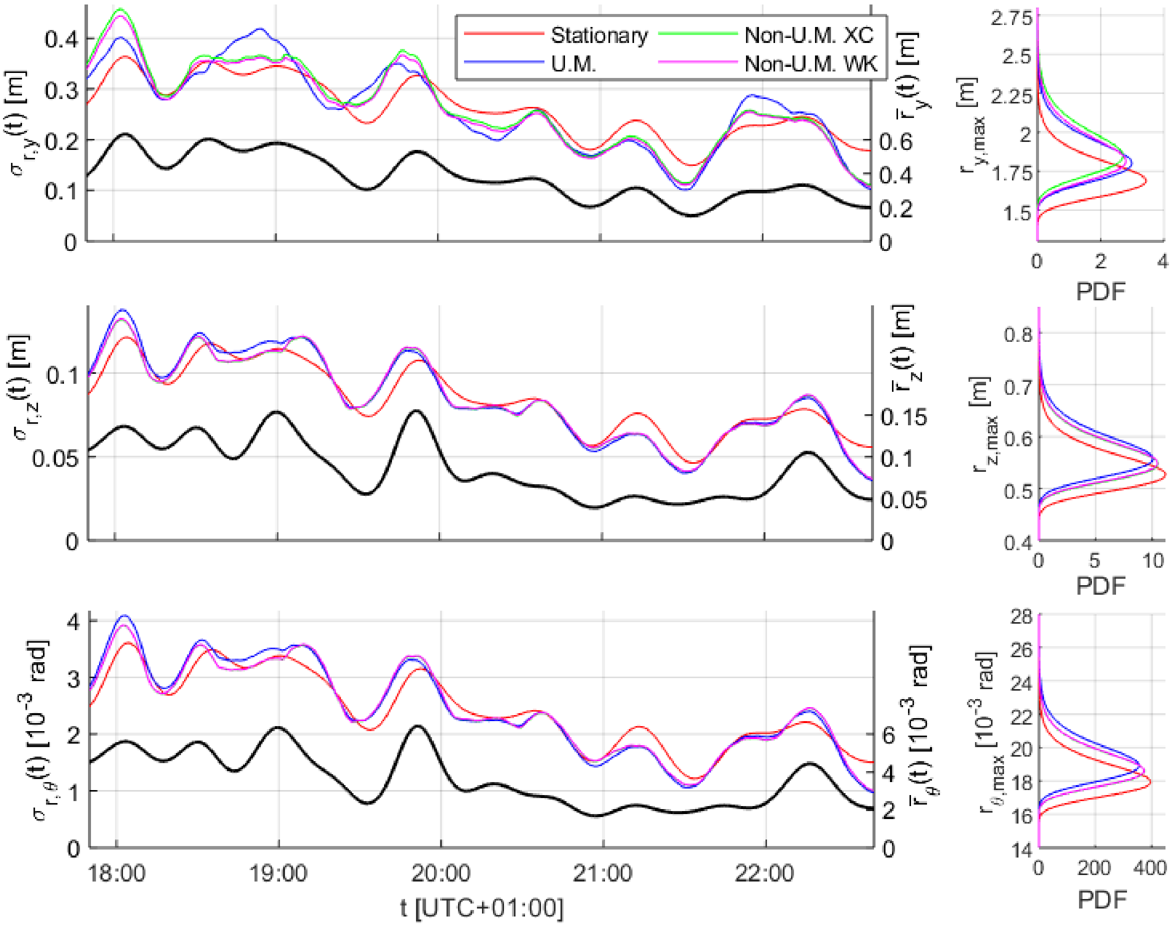

Figure 4.6: Frequency domain structural response, case 2.

Extreme value distribution:

	$r_y(t)$ [m]:		$r_z(t)$ [m]:		$r_\theta(t)$ [10^{-3} rad]:	
Modulation method:	Expected:	CDF = .99	Expected:	CDF = .99	Expected:	CDF = .99
Stationary	1,734	2,105	0,478	0,657	18,4	21,7
Uniform	1,853	2,280	0,567	0,705	19,4	23,2
Non-uniform XC	1,913	2,402	0,547	0,688	19,1	22,6
Non-uniform WK	1,876	2,349	0,550	0,689	19,1	22,6

Table 4.5: Expected maximums and extreme levels with 1% probability of exceedance

SDOF system comparison between frequency domain and simulated time domain response:

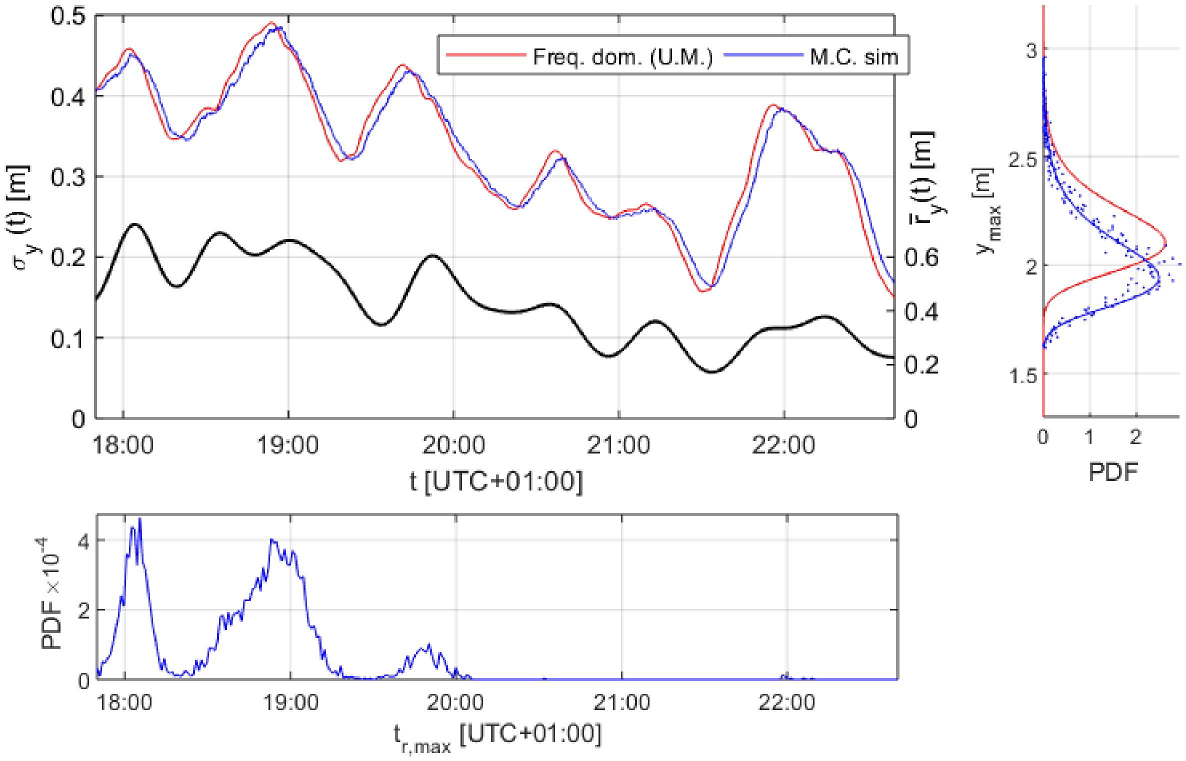

Figure 4.7: SDOF comparison, case 2 ($N = 4000$).

4.2.3 Case 3

Wind field calculations:

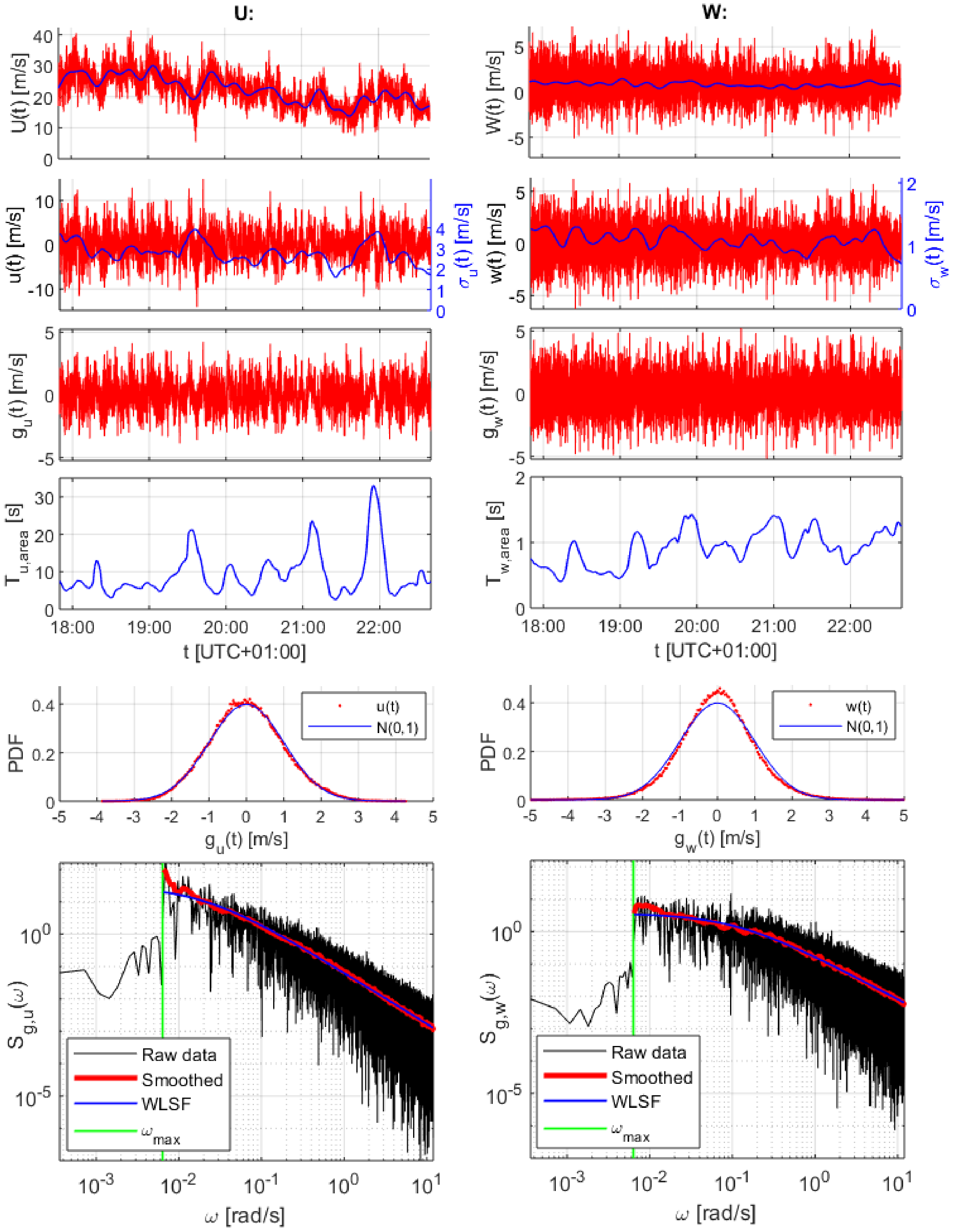

Figure 4.8: Wind speed calculations, case 3.

	U ($n = u$):			**W ($n = w$):**		
	min:	**avg.:**	**max:**	**min:**	**avg.:**	**max:**
Mean wind speed [m/s]	13.81	22.33	30.00	0.32	0.84	1.46
***Turbulence, $n(t)$*:**						
- $E[n(t)]$ [m/s]	-	0.007	-	-	-0.001	-
- RMS [m/s]	-	2.812	-	-	1.095	-
- $\sigma_n(t)$ [m/s]	1.591	2.812	3.937	0.712	1.095	1.326
***Normalized turbulence, $g_n(t)$*:**						
- $E[g_n(t)]$ [m/s]	-	0.002	-	-	-0.001	-
- RMS [m/s]	-	0.981	-	-	0.988	-
- $\sum_{\omega_{max}}^{12} S_{g,n,raw}(\omega_i)\Delta\omega$	-	0.984	-	-	0.965	-
- $\int_{\omega_{max}}^{12} S_{g,n,WLSF}(\omega)d\omega$	-	0.890	-	-	0.905	-
$T_n(t)$ [s]	2.55	9.22	32.99	0.40	0.92	1.43

Table 4.6: Relevant extracted data from wind field calculations, case 3.

Dynamic response calculations, frequency domain:

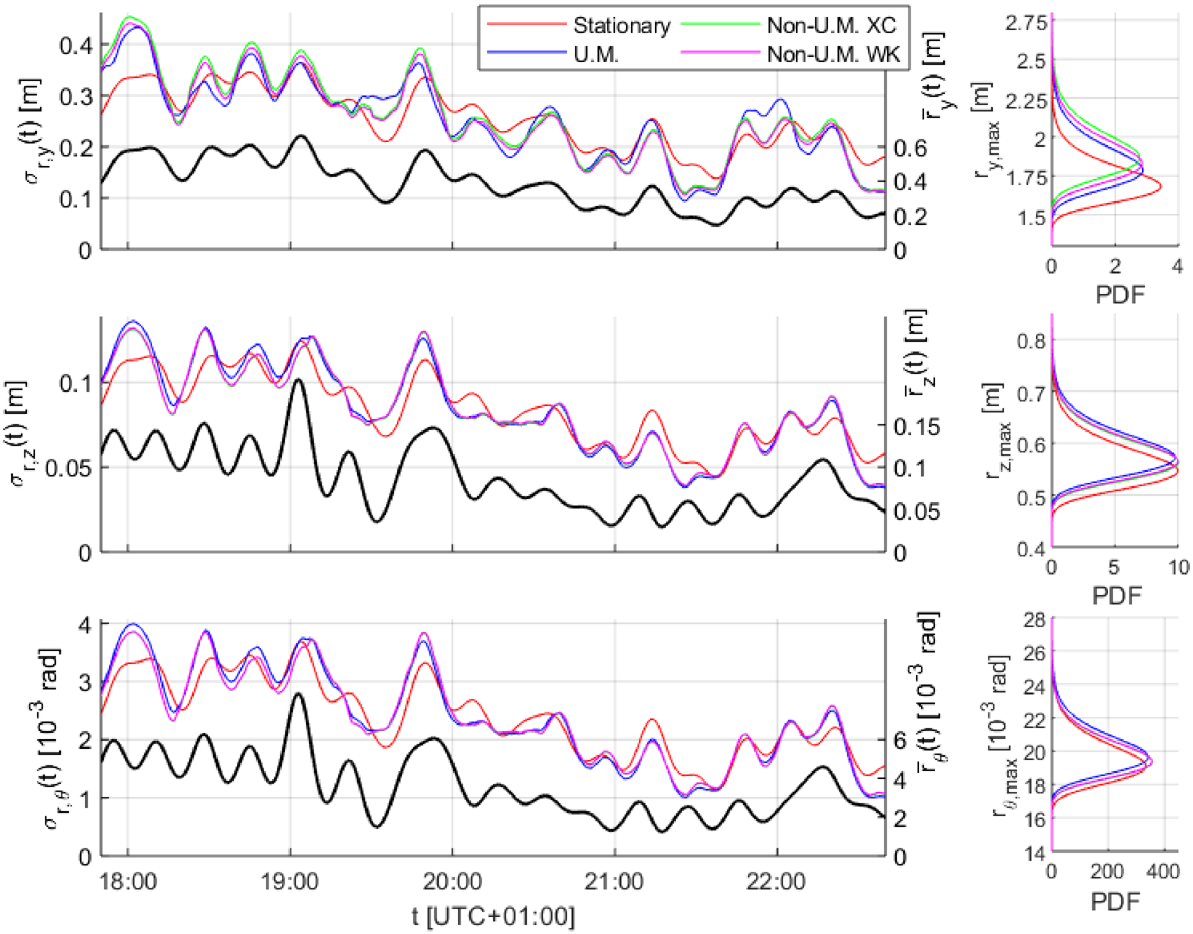

Figure 4.9: Frequency domain structural response, case 3.

Extreme value distribution:

	$r_y(t)$ [m]:		$r_z(t)$ [m]:		$r_\theta(t)$ [10^{-3} rad]:	
Modulation method:	Expected:	CDF = .99	Expected:	CDF = .99	Expected:	CDF = .99
Stationary	1,728	2,100	0,543	0,694	19,6	23,5
Uniform	1,845	2,298	0,587	0,720	20,1	23,9
Non-uniform XC	1,926	2,392	0,575	0,707	19,8	23,5
Non-uniform WK	1,887	2,341	0,577	0,709	19,8	23,5

Table 4.7: Expected maximums and extreme levels with 1% probability of exceedance

SDOF system comparison between frequency domain and simulated time domain response:

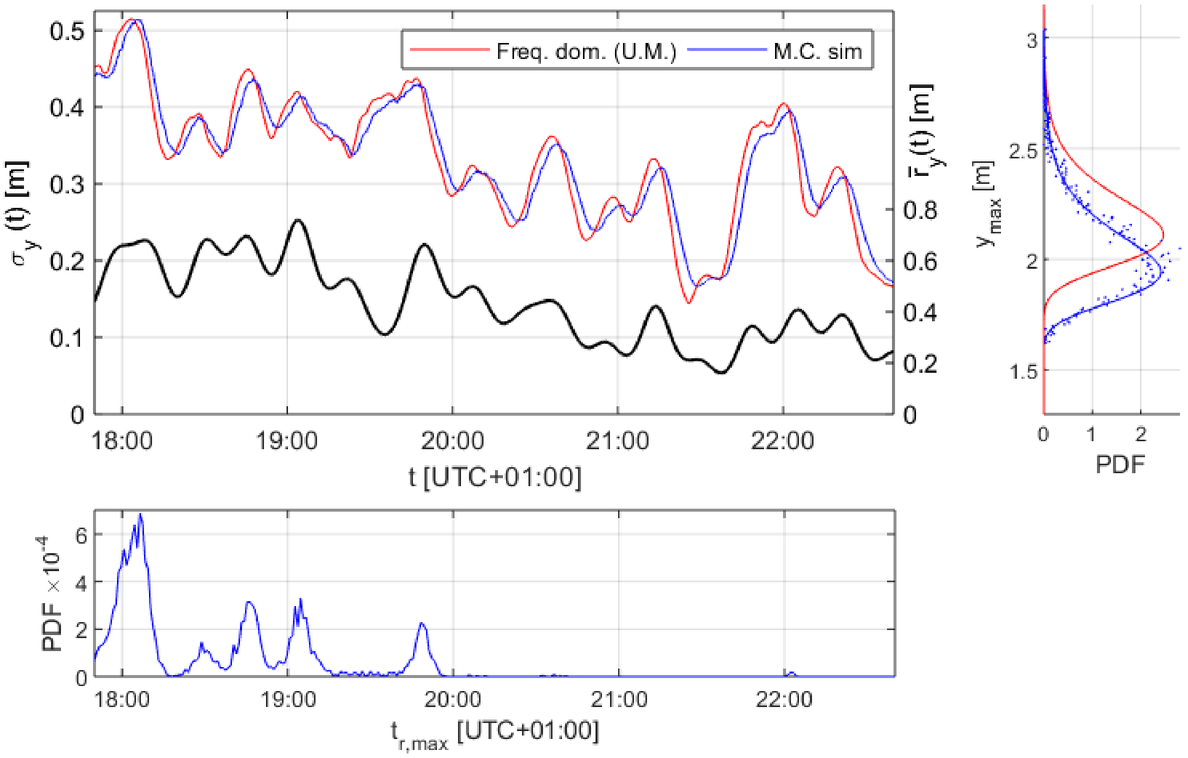

Figure 4.10: SDOF comparison, case 3 ($N = 4000$).

4.2.4 Case 4

Wind field calculations:

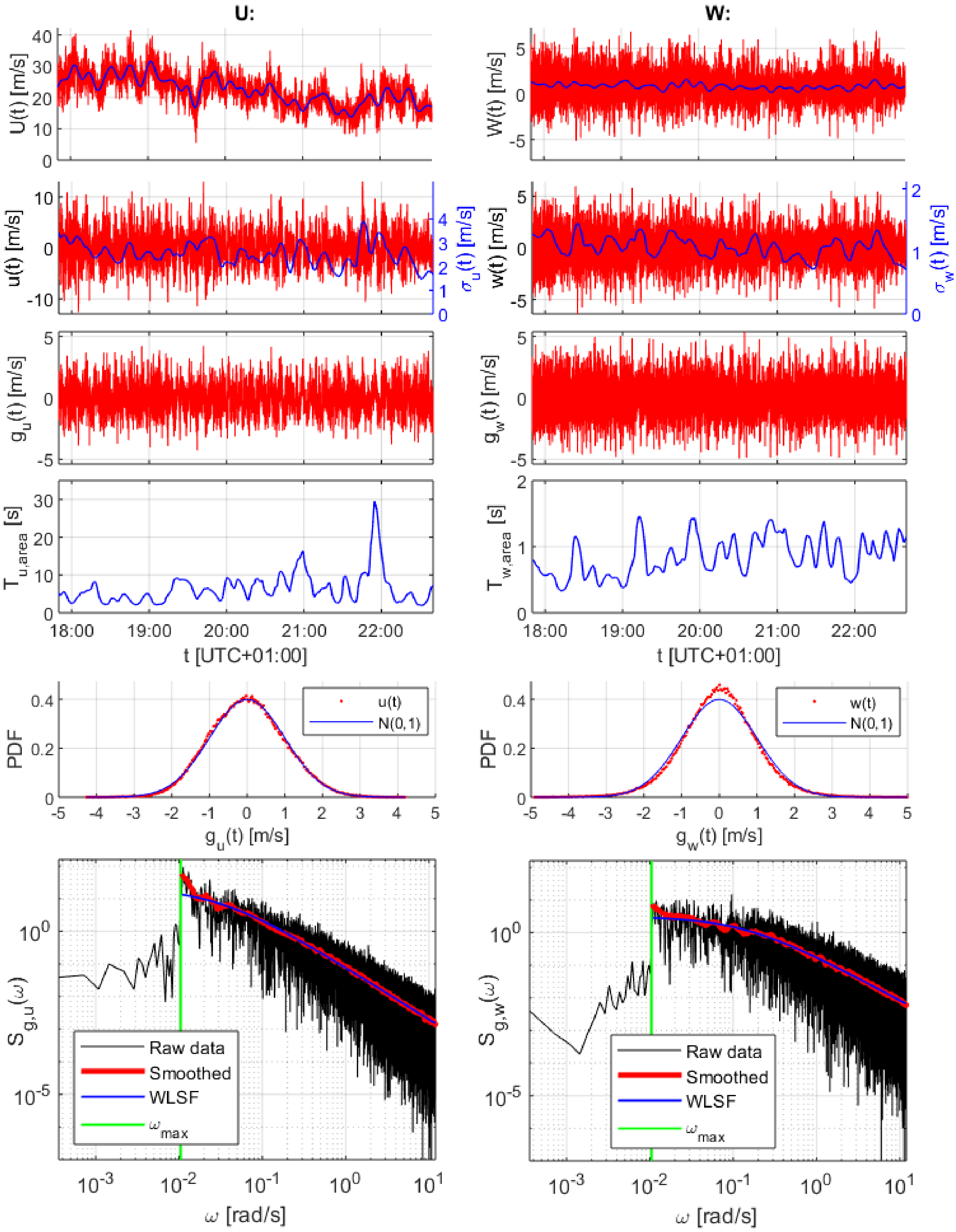

Figure 4.11: Wind speed calculations, case 4.

	U ($n = u$):			W ($n = w$):		
	min:	**avg.:**	**max:**	**min:**	**avg.:**	**max:**
Mean wind speed [m/s]	13.72	22.34	31.56	0.16	0.83	1.59
Turbulence, $n(t)$:						
- $E[n(t)]$ [m/s]	-	0.000	-	-	0.000	-
- RMS [m/s]	-	2.584	-	-	1.082	-
- $\sigma_n(t)$ [m/s]	1.465	2.584	3.901	0.703	1.082	1.444
Normalized turbulence, $g_n(t)$:						
- $E[g_n(t)]$ [m/s]	-	0.001	-	-	-0.001	-
- RMS [m/s]	-	0.977	-	-	0.988	-
- $\sum_{\omega_{max}}^{12} S_{g,n,raw}(\omega_i)\Delta\omega$	-	0.981	-	-	0.964	-
- $\int_{\omega_{max}}^{12} S_{g,n,WLSF}(\omega)d\omega$	-	0.881	-	-	0.903	-
$T_n(t)$ [s]	1.88	6.41	29.59	0.33	0.85	1.46

Table 4.8: Relevant extracted data from wind field calculations, case 4.

Dynamic response calculations, frequency domain:

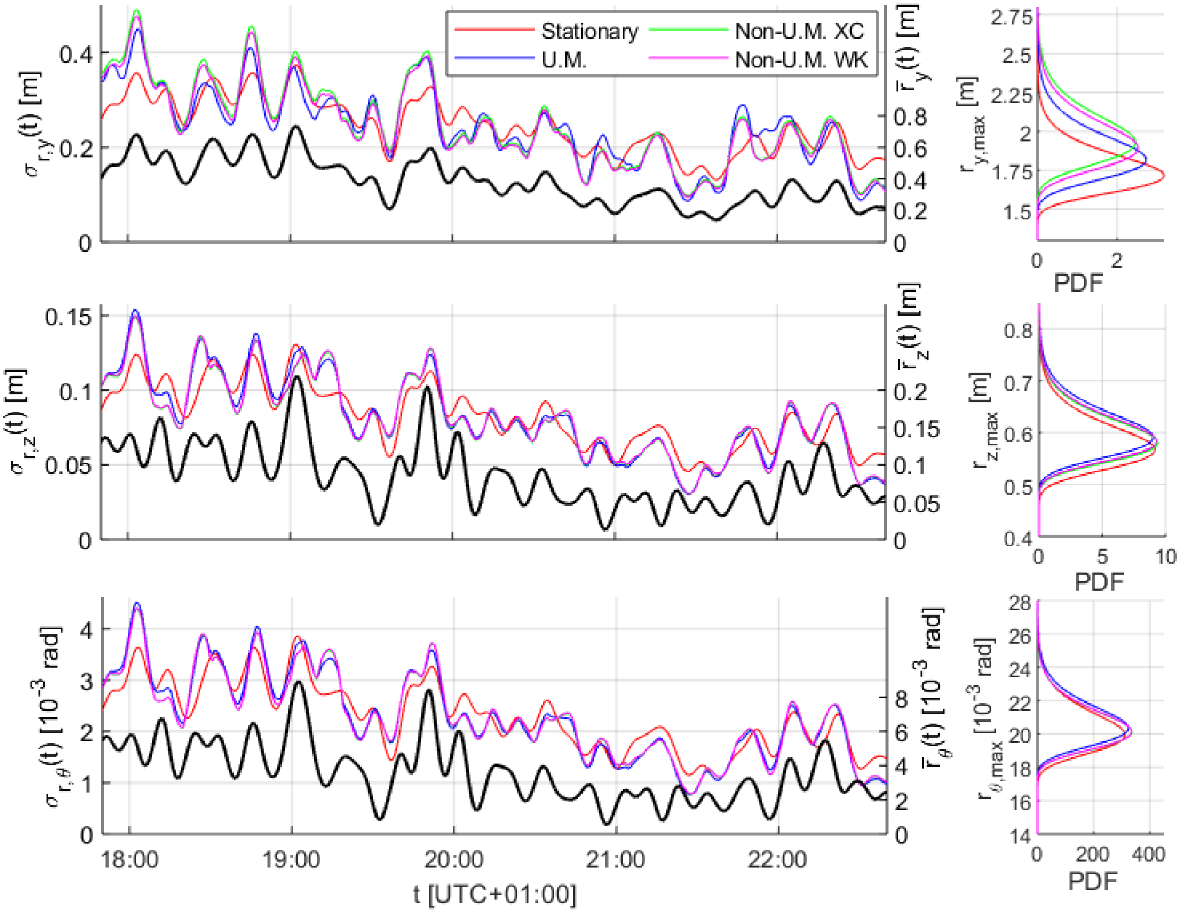

Figure 4.12: Frequency domain structural response, case 4.

Extreme value distributions:

	$r_y(t)$ [m]:		$r_z(t)$ [m]:		$r_\theta(t)$ [10^{-3} rad]:	
Modulation method:	Expected:	CDF = .99	Expected:	CDF = .99	Expected:	CDF = .99
Stationary	1,765	2,166	0,580	0,726	20,5	24,6
Uniform	1,880	2,359	0,609	0,753	20,9	24,9
Non-uniform XC	1,998	2,528	0,597	0,736	20,6	24,4
Non-uniform WK	1,959	2,475	0,600	0,740	20,6	24,5

Table 4.9: Expected maximums and extreme levels with 1% probability of exceedance

SDOF system comparison between frequency domain and simulated time domain response:

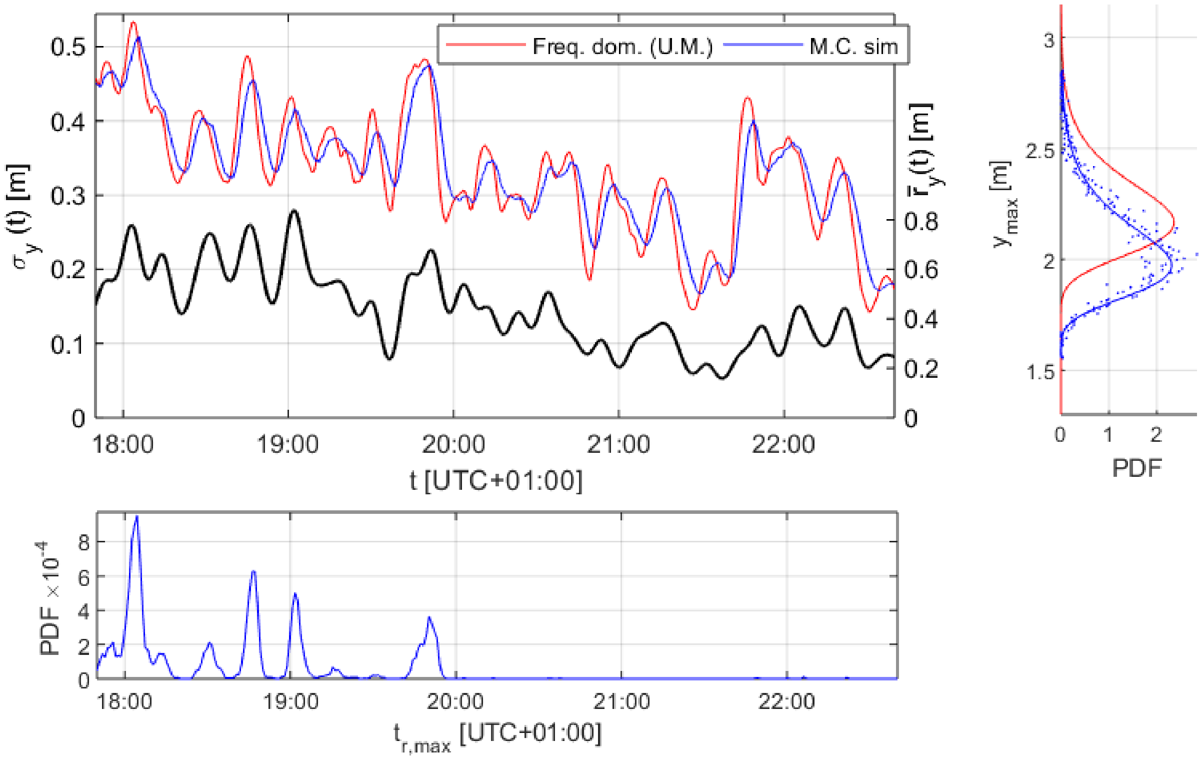

Figure 4.13: SDOF comparison, case 4 (N = 4000).

4.2.5 WLSF spectrum parameters

In the above cases 1 – 4, only the Kaimal spectrum was used to fit the respective spectrum data because it had a far higher capability of doing so when compared to the von Karmán spectrum formulae. The coefficients obtained from the WLSF procedure is shown in table 4.6 in which A_n^* and B_n^* is the coefficients of the Kaimal spectrum given on the format of equation 2.16c, and where β is the slope coefficient from equation 2.29 which simply replaces the exponent 5/3 in the denominator of equation 2.16c. m, n_1 and n_2 is the coefficients from the bandwidth function in equation 2.26.

	$S_{g,u}$:						$S_{g,w}$:					
Case:	A_u^*:	B_u^*:	β:	n_1:	n_2:	m:	A_w^*:	B_w^*:	β:	n_1:	n_2:	m:
1	27.59	51.75	1.58	5	200	1.5	3.703	9.300	1.35	5	200	1.5
2	33.83	57.75	1.58	5	200	1.5	3.715	9.318	1.35	5	200	1.5
3	31.06	49.83	1.58	5	200	1.5	3.649	9.077	1.35	5	200	1.5
4	21.95	33.54	1.60	5	200	1.5	3.158	7.273	1.38	5	200	1.5

Table 4.10: WLSF parameters and Kaimal spectrum coefficients.

4.2.6 Stationary data analysis and response calculation

Wind field calculations:

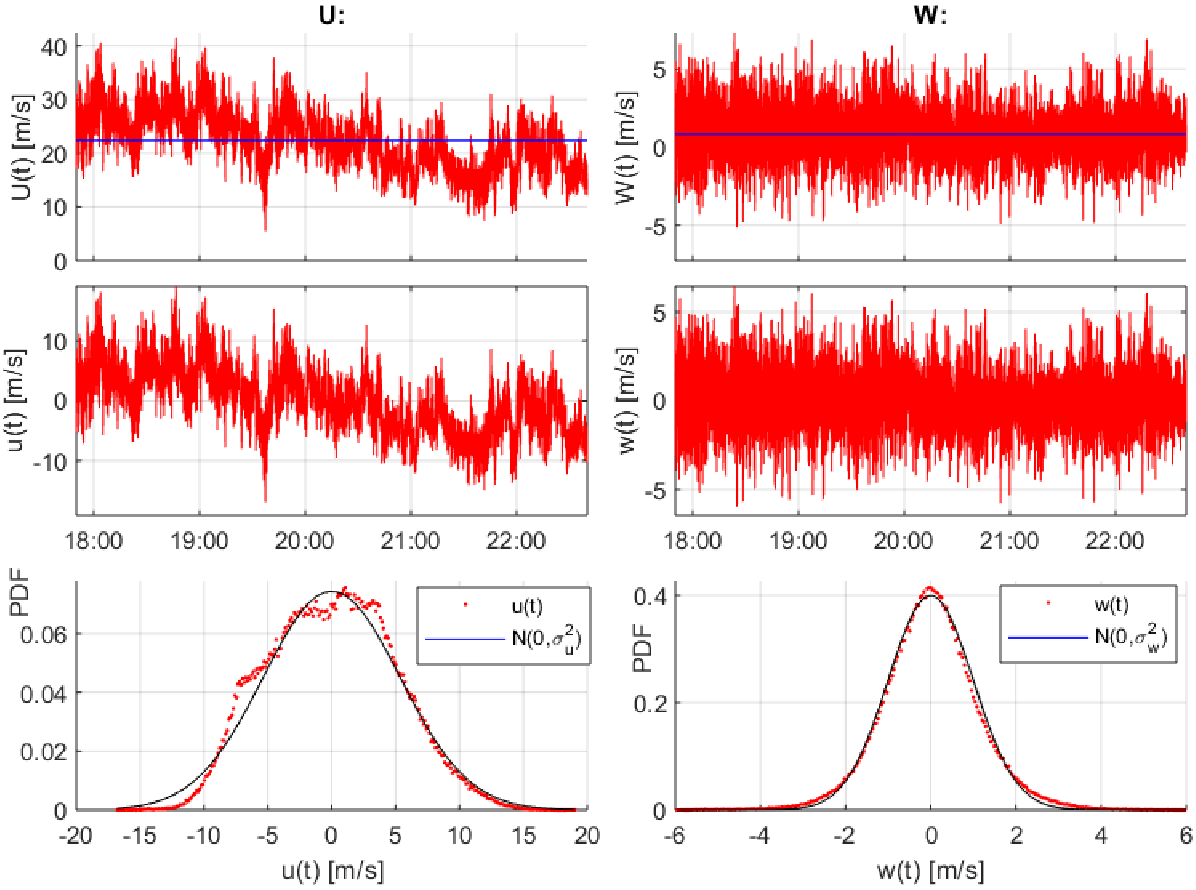

Figure 4.14: Presumed stationary wind speed recordings.

	U:	W:
Mean wind speed [m/s]	22,34	0,83
RMS, turbulence component [m/s]	4,989	1,120

Table 4.11: Relevant extracted data from wind field calculations, stationary consideration.

Spectrum fitting:

In contrast to the spectrum data in cases 1 – 4, Kaimal's spectrum formulae has a very limited ability to fit the calculated spectral data of the turbulence components in figure 4.14. The reason for this is that the rate at which the slope of the smoothed spectrum changes in the log–log domain when moving from low to high frequencies, is to low compared to what the Kaimal spectrum is able to exhibit. This the same reason as to why the von Kármán spectrum is unable to fit the spectrum data in case 1 – 4 well. Nevertheless, this problem is overcome by instead using the following spectrum formula,

$$S_n(\omega) \quad = \quad \frac{A_n^*}{\left[1 + B_n^* \cdot \sqrt{\widehat{\omega}}\right]^{3.2}} \tag{4.2}$$

Table 4.12 gives the results from the identical WLSF procedure as used earlier.

	U ($n = u$):	W ($n = w$):
A_n^*	22180	27.77
B_n^*	13.11	2.67

Table 4.12: Spectrum parameters of enhanced stationary spectrum formula

Figure 4.15 gives the result of the spectrum fitting process.

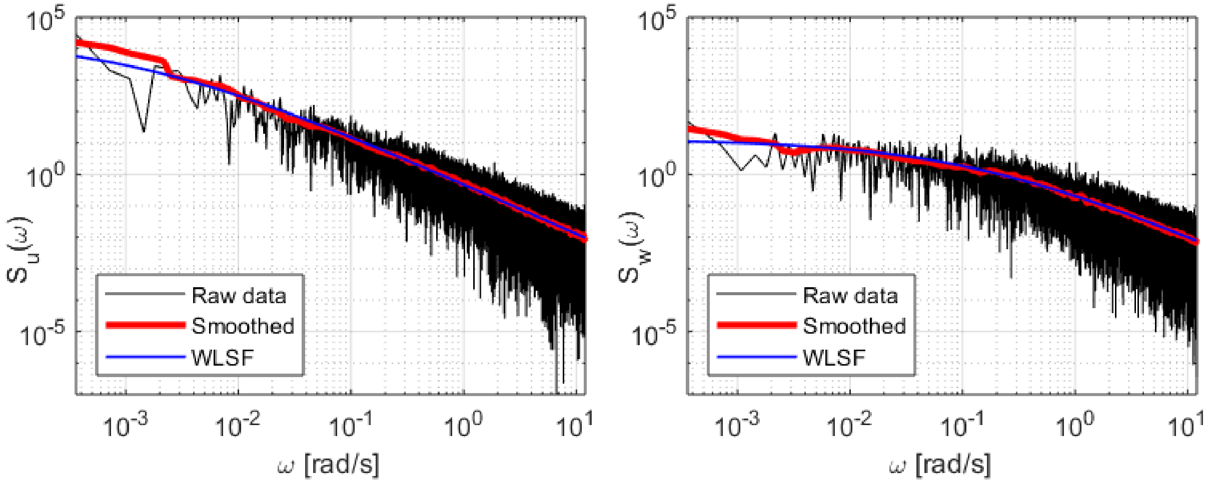

Figure 4.15: WLSF for turbulence component spectrum

Response:

	$r_y(t)$ [m]:	$r_z(t)$ [m]:	$r_\theta(t)$ [10^{-3} rad]:
Mean	0,369	0,0827	3,48
Standard deviation	0,356	0,0899	2,68
$E[r_{max}]$	1,777	0,2794	17,3
CDF = .99	2,141	0,5934	19,8

Table 4.13: Structural response from a stationary consideration

4.2.7 Case comparisons

Distribution of maximum structural response:

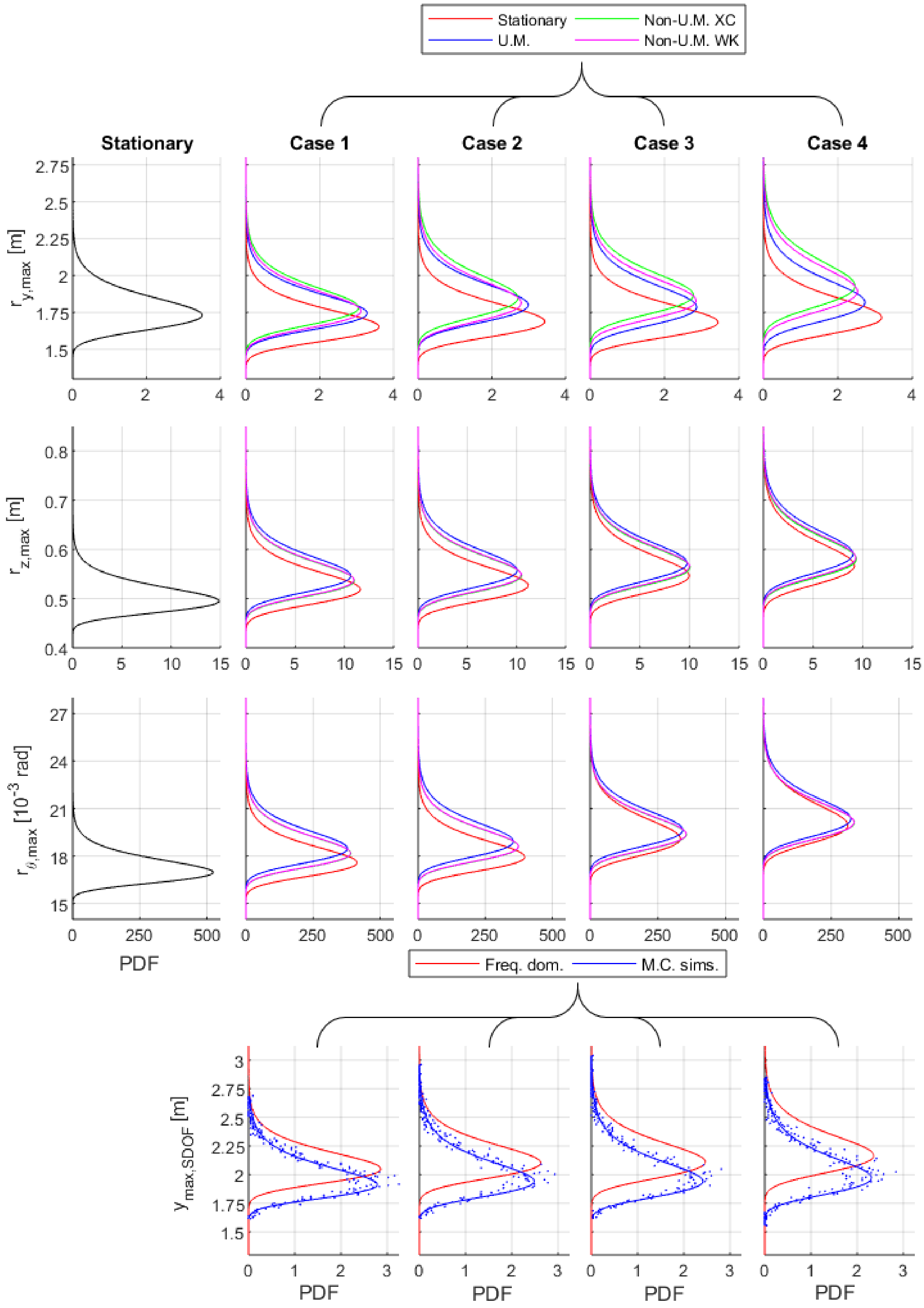

Figure 4.16: Case comparison for maximum response levels.

5 COMMENTS ON THE RESULTS AND DISCUSSIONS

5.1 WIND SPEED RECORDING CALCULATIONS

When studying figures 4.2, 4.5, 4.8, 4.11 and 4.14 together with the associated statistical parameters given in tables 4.2, 4.4, 4.6, 4.8 and 4.11, the following remarks are the most interesting observations:

1. The average value of the mean wind speeds $\bar{U}(t)$ and $\bar{W}(t)$ within the sub–recording in question are almost exactly equal to the average wind speeds within the same time interval (table 4.11), and the average values of the turbulence components is consequently as good as being zero. This indicates that the 20–minute commissioning phase mentioned in chapter 4.1 is of sufficient length and that the curves representing the extracted mean wind speeds $\bar{U}(t)$ and $\bar{W}(t)$ by no means seem to be characterized by the fact that they are indeed periodic on the time interval of the parent recording from which the investigated sub–recording is withdrawn.
2. Similar to above, the average value of the estimated time varying standard deviation is almost exactly equal to the square root of the mean square value (RMS) of the turbulence components. However, when dividing the turbulence components $u(t)$ and $w(t)$ by their estimated time varying standard deviation, the RMS value of the normalized turbulence components $g_u(t)$ and $g_w(t)$ seems to end up slightly below unity. The reason for this small negative deviation from unity is that the time varying standard deviation, $\sigma_n(t)$, which is defined from the time varying variance, $\sigma_n^2(t)$, which indeed varies with time. Consequently, the mean of the square root of the time varying variance is slightly larger than the square root of the mean time varying variance, namely,

$$\sqrt{E[\sigma_n^2(t)]} \quad < \quad E\left[\sqrt{\sigma_n^2(t)}\right] \tag{5.1}$$

   Hence, this non–linear method of normalization (standard deviation is not a linear function of the variance) makes the RMS value of $g_u(t)$ and $g_w(t)$ end up just below unity. The magnitude of this negative deviation from unity progresses from 1.7 % to 2.3 % for $g_u(t)$ and from 0.5 % to 1.2 % for $g_w(t)$ for cases 1 – 4, respectively. This makes sense because the averaging period, T_A, for the calculation of $\sigma_n^2(t)$ is decreases for case 1 through 4, and the magnitude of the fluctuations in $\sigma_n^2(t)$ will consequently be larger, thus amplifying the difference between the right and left–hand side of equation 5.1.

   The abovementioned effect is not spurious or undesirable by any means because the processes $g_u(t)$ and $g_w(t)$ will anyway be modulated “back” with $\sigma_u(t)$ and $\sigma_u(t)$ themselves according to the methods described in chapters 2.4.2 – 2.4.4, thus cancelling the effect described by equation 6.1 when it comes to comparing the RMS value of the generated wind speed recording with the RMS value of the original recording.
3. $g_u(t)$ and $g_w(t)$ seems to be close to normally (Gaussian) distributed. The deviation between the observed data and the zero mean, unit variance, Gaussian probability density curve shown in the figures cannot alone be explained from the variance deviation from unity, but also the fact that they do not perfectly fit such a distribution function in the first place. This effect seems to be smaller when increasing ω_{max}, and the opposite is clearly visible in the case of the stationary consideration in figure 4.14 where the non-stationary features of turbulence component $u(t)$ clearly distorts this image.

4. Another, but much larger deviation is the difference between the area under the fitted spectrum curves and the raw spectrum data. Ideally, they should roughly equate each other but the deviation shown in the tables are not arbitrary or spurious, but indirectly deliberate. The reason for this is simply the importance of applying a curve that fits the smoothed spectrum as well as possible in the very regions this matters the most, namely in the vicinity of the eigenfrequencies. Because of the structural variance distribution properties explained in chapter 3.7.2 through figures 3.11 and 3.12, the variance of horizontal structural response of the Hardanger Bridge in particular is as good as directly dependent on how consistently the applied spectrum curve fits the spectrum data in the relatively narrow region surrounding the lowest eigenfrequency, $\omega_1 = 0.32$ rad/s. Nevertheless, using the initially suggested spectral limit slope $\beta = 5/3$ will in this particular case strongly violate the ability of the applied spectrum curve to fit the high–magnitude spectrum data in the low frequency region. These frequency components will be quasi-static in terms of structural response, but since their magnitudes are very large compared to the ones around ω_1, an attempt to apply a spectrum curve that also fits them relatively well, is desirable. Hence, the value of the area under the fitted spectrum curve generally represents little physical importance because the relation between the variance of the wind field and variance of structural response is close to being non–existing when not taking into account the location of the eigenfrequencies of the structure in question.

5.2 RESPONSE CALCULATIONS

5.2.1 Method of EPSD modulation

When studying the time histories of the standard deviation of structural response in figures 4.3, 4.6, 4.9 and 4.12, some interesting observations immerge. The most obvious one is that the three fundamentally different methods of modulating the turbulence components (chapters 2.4.2 – 2.4.4; stationary, uniformly, and non–uniformly) differ the most for horizontal displacement. This effect seems also to be independent of ω_{max}. The reason for why the modulation methods differ the most for horizontal motion is that $\sigma_n(t)$ and $T_n(t)$ exhibits the largest fluctuations in time for $n = u(t)$, thus creating more violently fluctuating modulation functions for $u(t)$ than for $w(t)$.

When studying the difference between the modulation methods a bit closer, it can be seen that the dynamic response curves originating from the uniformly modulated, and the non–uniformly modulated (both XC and WK) turbulence components clearly stands out when compared to the curve originating from stationary turbulence components. This is nothing but logical, and clearly as expected because when equating the time varying standard deviation to its average value, which indeed is how the stationary turbulence components are “modulated”, the resulting standard deviation of dynamic structural response will clearly tend towards the average over the time window considered. The characteristic frequency at which the curves fluctuate is quite similar, which is simply because the mean wind speeds are present as terms in their mathematical expressions, but the magnitude of the fluctuations are significantly less.

Finally, the XC model and WK model are almost indistinguishable by visually considering the plots in the figures. However, introducing non-uniform modulation functions in one form or the other has the effect of “automatically” or “indirectly” interpreting whether to treat a relatively short fluctuation in the wind speed time history that goes under the radar during the extraction of the mean wind speed, as being a local change in the time varying variance of the signal, or as being a local change in the frequency content. This can be well illustrated by considering the time history for $U(t)$ at the moment in time right before 19:00 UTC+01:00 in case 2 (figure 4.5). At this point, a large peak in the integral time scale occurs almost simultaneously as a local maximum in the time varying variance. Obviously, a uniformly modulated process interprets this only as being an increase in the variance of the signal and a corresponding peak in the variance of structural response is the result (upper–most subplot, figure 4.6). However, since variance is divided by integral time scale in the Kaimal modulation function for $u(t)$ (equation 2.16), the increase in integral time scale compensates for the increase in variance and instead allocates variance contributions from high to low frequency regions in the spectrum.

Features like this are exactly what separates the non-uniformly modulated processes and the uniformly modulated ones. However, this is a feature that is created a posteriori when trying to establish a simple mathematical formula (Kaimal) that is able to take into account spectral content and it operates therefore on an indirect level.

5.2.2 Extreme value distribution

Equation 2.30 suggests that the moments in time for when both the mean structural response and the variance of dynamic structural response is large will by far have the greatest influence on the resulting CDF function for maximum response. This concept is also confirmed by the simulated PDFs for the moment in time for when maximum structural response occurs (figures 4.4, 4.7, 4.10, and 4.13), however with the additional information that it seems to be a relatively rare event that the maximum response originates from elsewhere. Consequently, which method of turbulence component modulation that gives the largest expected value of structural response seems to depend on which method that produces the largest maximum value of the standard deviation of dynamic response.

From the deductive reasoning above, it is clear that the method of stationary turbulence component modulation will produce the lowest maximum value for the expected maximum response as well as the quantile values, because the resulting time varying standard deviation of dynamic response will deviate less from its average value compared to the resulting response from the other methods, hence restricting the possibility for producing high levels of structural response. When comparing the response curves originating from uniform–, and non–uniform modulation, it is somewhat arbitrary what curves produces the largest expected maximum response because it is equally arbitrary what curve that displays the largest maximum value within the considered time window. After all, such has to do with how the time varying variance of the turbulence components, their integral time scale, and indeed how the mean wind speed varies in time, an even though they generally seem to produce local maxima at the same locations, no general rule regarding the magnitude and prominence of the respective local maxima can be established.

Nevertheless, the differences between the PDF curves are relatively small for the uniformly modulated–, and the non–uniformly modulated turbulence components, and the case with stationary turbulence components clearly stands out in comparison, especially when considering horizontal motion. This statement is based on the PDF curves from cases 1 and 2 exclusively because interpreting the relationship between the different PDF curves for cases 3 and 4 cannot be considered equally valid because transient effects is being much more characteristic to the picture of airflow – structure interaction as can be seen in figures 4.10 and 4.13.

In the case of modelling the wind speed recording in figure 4.1 as being stationary, it is fundamentally difficult to compare the resulting PDF to the PDFs in the non-stationary cases because the spectrum fit in figure 4.15 is alone given the task to represent the now presumed stochastic trend that in the non-stationary theory is treated as a deterministic trend. To accurately resemble this trend in terms of a spectral expression is very difficult because of the large magnitude scatter in the low frequency region which is hard to interpret in terms of what process it represents. The average of the scatter may thus deviate vastly from its “true” value because the number of scatter points is very low in the low frequency region.

The maximum value distribution for the SDOF system from the frequency domain approach shows very similar characteristics to the PDF of maximum horizontal response using uniformly modulated turbulence components. The same is logically the case when comparing the time history of the standard deviation of dynamic response and the mean response. This similarity is no surprise at all due to the modal response variance distribution properties illustrated in figures 3.11 and 3.12. The magnitude of the response itself however is slightly larger for the SDOF system because spatial averaging is excluded. This is because the instant wind speed across the bridge span fluctuates in phase hence producing a larger modal load (ref eq. 1.43e). What is interesting is that the time domain simulated expected value of the maximum response of the SDOF seems to stay at almost the same level in cases 1 through 4. The only thing that seems to change is the variance and consequently the high–end quantile values of the maximum response. This has to do with the fact that transient effects become more prominent in cases 1 through 4, which will be covered in chapter 5.2.3. At which specific areas the SDOF system is comparable to the multimode, spatial averaging model of the Hardanger Bridge can be debated, however, it was indeed introduced and formulated because the midspan response of multimode, spatial averaging model was completely dominated by the first mode. Hence, the SDOF system can be considered as being a good candidate at providing information about the behaviour of the maximum response distribution at the bridge midspan when transient effects are included.

Finally, the equivalent SDOF system that was adopted with the exclusive purpose being investigating the nature of transient effects suggests that the analytical probability distribution obtained from the time varying variables of structural response seems to slightly overestimate the real (simulated) probability distribution of maximum horizontal response (see figure 4.16). This can be considered valid since the SDOF system very well resembles the behaviour of horizontal motion of the Hardanger Bridge, when not considering the magnitude of the response itself. Obviously, it would have been somewhat surprising if the analytical PDF distribution in equation 2.30 and 2.31 estimated the simulated PDF spon–on, especially when considering the fact that according to Strømmen (2010, p. 29), a necessary requirement in the derivation of equation 2.30 is that the process is “fairly broad banded”, which certainly is not the case for structural response. Nevertheless, the deviation between the two is not vast and the analytical distribution is not a bad measure.

5.2.3 Time domain simulations – transient effects

The response of the SDOF system in cases 1 and 2 indicates that transient effects play a relatively small role when predicting the time varying standard deviation of structural response in these particular cases. The simulated curve for the time varying standard deviation seems to resemble its frequency domain collague very well in terms of shape with an almost perfect conservation of magnitude, and where only a short and enevitable time–lag is present. However, when decreasing the extraction frequency ratio ω_1/ω_{max} to 50.4 and 30.6 as is done in cases 3 and 4, such is no longer the case. As can be seen in figures 4.10 and 4.13, the simulated time domain standard deviation of dynamic response is characterized by not being given a sufficient amount of “build–up” time to settle at its “steady–state” level suggested by the frequency domain method. The latter response solution will simply fluctuate too rapidly in time for this to be possible.

The frequency limit at which transient effects starts to become a significant feature of structural response seems therefore to be somewhere in the vicinity of $\omega_{lim,trans} = \omega_1/50$. Of course, this depends on what level of accuracy one defines to be sufficient in order to characterize transient effects as not being a significant feature of structural response, but the difference between cases 1 and 2, and 3 and 4 is clear in terms of the presence of transient effects. If one extracts the mean wind speed in which the highest included frequency component has a frequency above $\omega_{lim,trans}$, the frequency domain buffeting response framework will not be able to predict time varying variance (standard deviation) of the dynamic response because of its missing ability to model transient effects, and a full–scale time domain simulation algorithm according to equation 3.13 must be applied.

5.2.4 Defining the characteristics of the wind speed recording

Regardless whether a time domain simulation scheme or the frequency domain approach established in this thesis is adopted, the stochastic and deterministic features of the wind speed recording in question must anyway be clearly defined. This procedure is indeed based on interpretation because there exists no general rule that gives the proper separation point between the deterministic time varying mean wind speed and the remaining stochastic turbulence components. When choosing this separation point by assigning ω_{max} and T_A numerical values, the infinitely large family that the wind speed recording in question now per definition is a member of, defines the basis from which we can determine expected values and probability distributions of structural response parameters. To briefly illustrate what impact such a choice has on the typical characteristics of the resulting defining family of recordings, three arbitrary realizations are generated from the subrecording of $U(t)$ in figure 4.1. ω_{max} and T_A is selected in accordance with chapters 4.2.4 (case 4), 4.2.1 (case 1), and 4.2.6 (stationary), and with applying a non-uniform modulation according to the XC–model to $u(t)$. First, the most "accurate" method of resemblance covered in this thesis is shown in figure 5.1, namely by assigning ω_{max} and T_A the same values as was done in case 4.

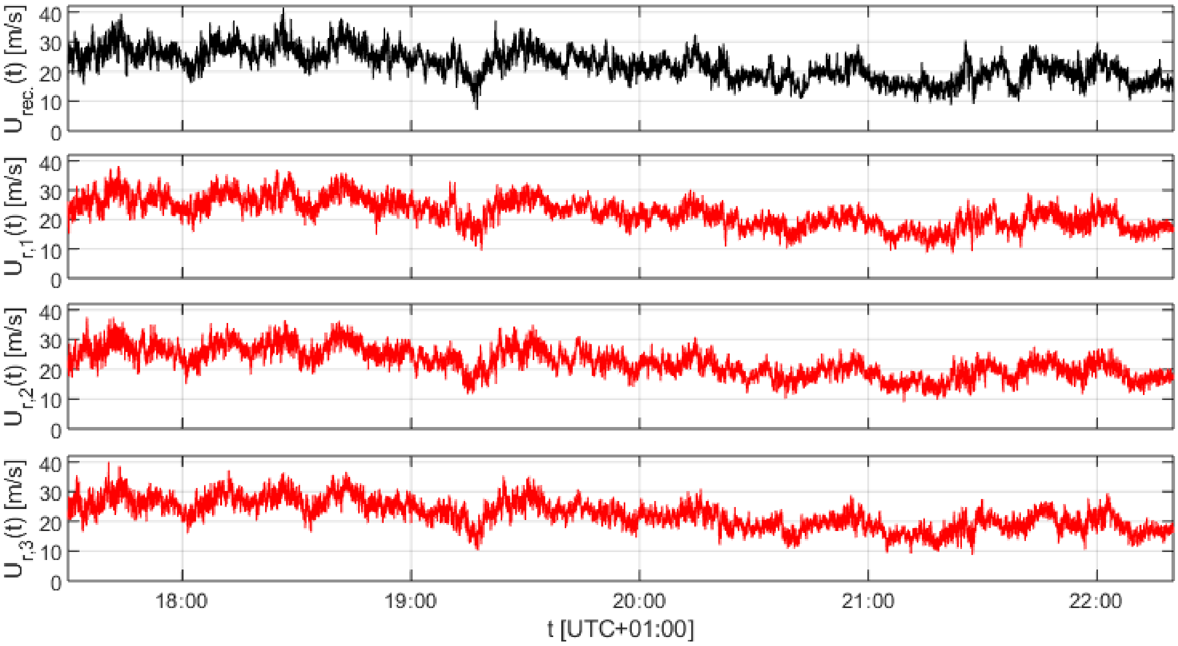

Figure 5.1: Arbitrary realizations of wind speed recording according to case 4.

Secondly, three arbitrary realizations of $U(t)$ in figure 4.1 according to the chosen definitions in case 1 are shown in figure 5.2.

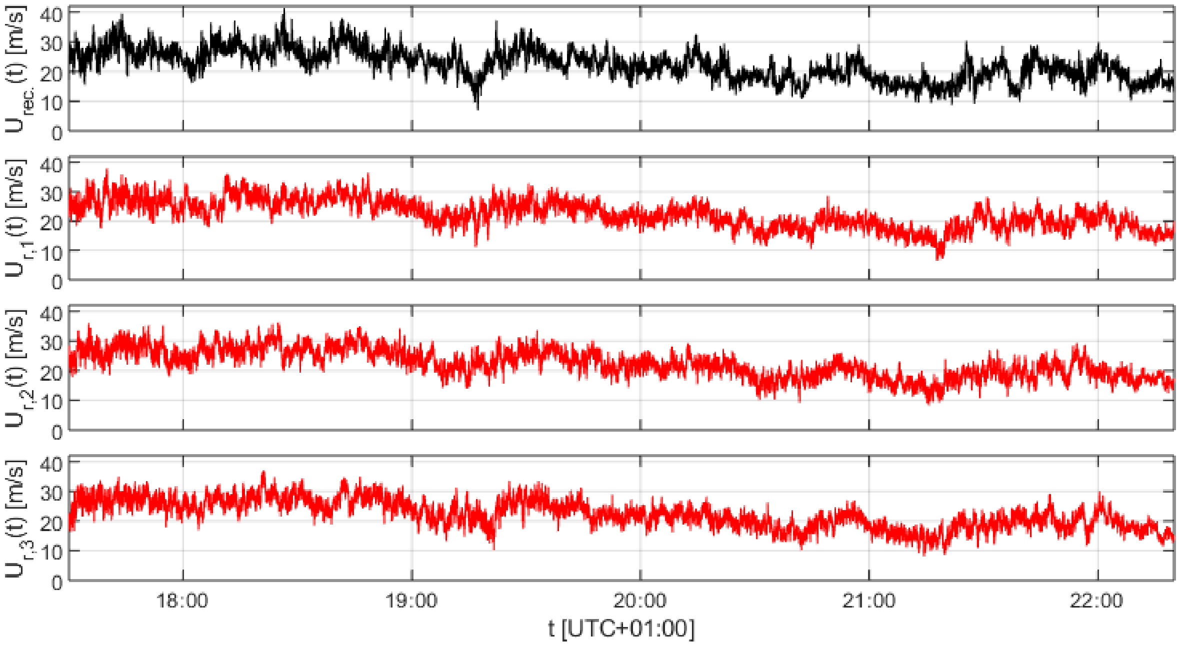

Figure 5.2: Arbitrary realizations of wind speed recording according to case 1.

Finally, the same procedure is repeated when modelling $U(t)$ as being stationary and is shown in figure 5.3.

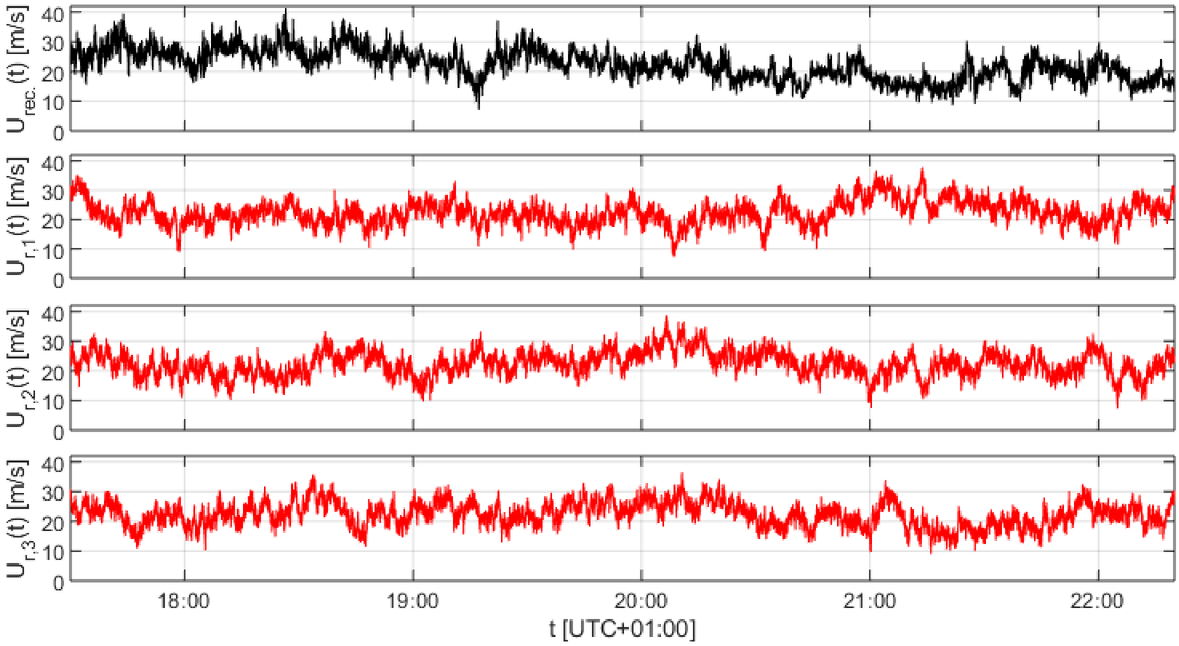

Figure 5.3: Arbitrary realizations of wind speed recording when assuming stationarity.

Clearly, the levels at which the realizations in figures 5.1 – 5.3 resemble the process they indeed are defined to represent is strongly dependent on ω_{max} and T_A in which increasing ω_{max} and reducing T_A increases the level of resemblance. The realizations in figure 5.1 are defined to produce the closest resemblance to the original recording, which is clearly visible where only small local deviations are visible from this presented perspective. However as shown in chapter 4.2.4 (figure 4.13), transient effects prevail at this level of resemblance and the proposed non–stationary frequency domain buffeting theory framework is therefore unable to accurately describe the airflow–structure interaction.

The realizations in figure 5.2 which are defined from the characteristics defined in chapter 4.2.1 originates from a process whose statistical characteristics varies slowly enough in time such that transient effects do not prevail (see figure 4.4). However, this process does not locally resemble the original wind speed recording as good as the ones in figure 5.1 but only over a wider time window. The response calculation in chapter 4.2.1 can therefore be interpreted as introducing an evolutionary wind field that exhibit similar shape at a wider time perspective such that the frequency domain method can predict the resulting response with good accuracy.

The same story goes for the presumed stationary consideration, but this method effectively characterizes the wind speed recording in question in a very general sense without preserving local shape at all. This idea may seem convenient at first because characterizing the storm in question as simply one of many sounds effective and neat, but accuracy is generally very difficult to guarantee because of the reasons mentioned about its raw spectral data characteristics in chapter 5.2.2 (see figure 4.15). Adopting a stationary statistical formulation onto an obviously non–stationary wind speed recording as the one in figure 4.1 is therefore not a particularly good idea because it seems to be nothing but safe to extract a deterministic trend at at least the level used in case 1, and not doing so might therefore be a bit naive.

The concepts above clearly illustrate the fact that it is initially not clear and intuitive where one should draw the line between what should be considered to be stochastic and what should not. There are also many equally valid separations from a structural point of view, each resulting in its own and unique time history for the variance of dynamic response. Hence, one might question whether the local values of the calculated time history of the variance of dynamic response does make any sense at all because it is dependent on user specified information and can therefore never be estimated from a single wind speed recording exclusively. Hence, it should there for not be interpreted as anything more than a tool that is needed to calculate the probability distribution of the maximum structural response resulting from a particular storm that is being modelled.

6 CONCLUSIONS

The investigation into the associated issues of non–stationary winds and the accordingly adapted frequency domain buffeting theory framework reveals several interesting observations.

First, the most appropriate method to extract a time varying, deterministic trend from the presumed non-stationary wind speed recording in question is found to be an incomplete Fourier series expansion (IFE). The IFE abled deductive reasoning to establish the general fact that in order for the extracted mean wind speed to produce a quasi–static mean structural response, which indeed is a necessary requirement for the separation between mean–, and stochastic dynamic structural response to be valid, the highest possible included frequency component in the IFE was roughly 1/5th the frequency of the lowest structural mode that is evenly symmetric with respect to the midspan.

Second, it is found that the proposed frequency domain buffeting response approach is only able to determine the expected time varying variance of dynamic structural response with decent accuracy when the highest included frequency component in the IFE extraction of the mean wind speed is below roughly 1/50th of the frequency of the fundamental mode of the Hardanger Bridge. Extracting the mean wind speed at frequencies above this limit is found to violate the validity of the obtained frequency domain solution because transient effects becomes a predominant part of the airflow–structure interaction picture. If such from some reason nevertheless is considered desirable, time domain simulations should instead be used to calculate the expected dynamic structural response.

Third, the time varying variance of structural response in particular is found to not be a physical property that makes any sense to a local observer because the local shape of its time history is strongly dependent on how one chooses to resemble the statistical properties of the wind speed recording from which one wants to estimate the expected structural response. However, what is probably the most interesting observation from this thesis is that the probability distributions of maximum structural response do not seem to be strongly dependent on what maximum frequency is used to extract the mean wind speed, or equally, which averaging period, T_A, is used to calculate the time varying variance of the wind field turbulence components. This is of high convenience because it solves part of the problem of what highest frequency one should include in the mean wind speed, given that such eliminates transient effects in the first place. This means that the great inertia of the Hardanger Bridge gives raise to the fact that if ones supreme goal is to mathematically predict the distribution of maximum structural response from a particular wind field, it is not necessary to define the time varying statistical properties of the wind field with an excessive level of accuracy. The most important action is to withdraw a suitable, time varying trend, exhibiting gentle changes in time.

Fourth, whether one chooses to modulate the turbulence components uniformly or non–uniformly seems to be of relatively minor importance in terms of maximum response distribution.

7 FURTHER WORK

The part of the airflow–structure interaction that has only been briefly investigated in this thesis are transient effects of structural response. As demonstrated, this effect is a very important one to consider when performing a non–stationary assessment of the airflow–structure interaction. Therefore, the most important suggestion for further work is to establish a full MDOF, spatial averaging model that is able to provide exactly the same statistical information as the proposed non–stationary frequency domain framework, but instead obtained from time domain simulations. Such an approach will be able to investigate every feature of transient effects of the response of any system, regardless of its modal properties. Such an approach will also be able to validate the analytical probability distribution functions for maximum structural response to a greater degree than what the simplified SDOF system is able to provide information about.

Also, one must not forget that this thesis isolates non–stationary effects, and in real life complex terrain will generally always challenge the assumption of wind field homogeneousness, and for a mild storm, vortex shedding might also represent a significant part of the total wind loading process.

BIBLIOGRAPHY

[1] Chen, X. (2015) *Analysis of Multimode Coupled Buffeting Response of Long-Span Bridges to Nonstationary Winds with Force Parameters from Stationary Wind*. J. Struct. Eng., 2015, 141(4): 04014131

[2] Hass, J.; Weir, M. D.; Thomas, G. B. jr. (2009*) Calculus Part 1*. Harlow: Pearson Education Limited

[3] Hu, L.; Xu, Y.; Huang, W. (2013) *Typhoon-induced non-stationary buffeting response of long bridges in complex terrain*. Engineering Structures 57 (2013) 406–415

[4] Huang, N.; Shen, Z.; Long, S.; Wu, M. C.; Shih, H.; Zheng, Q.; Yen, N.; Tung, C.; Liu, H. (1998) *The empirical mode decomposition and the Hilbert spectrum for nonlinear and non-stationary time series analysis*. Proc. R. Soc. Lond. A (1998) 454, 903-995

[5] Kaimal, J. C.; Wyngaard, J. C.; Izumi, Y.; Coté, O. R. (1972) *Spectral characteristics of surface-layer turbulence*. Quart. J. R. Met. Soc. Vol. 98, pp. 563-589

[6] Kreyszig, E. (2006) *Advanced Engineering Mathematics*, 9th edition. John Wiley & Sons, Inc.

[7] Ma, X.; Xu, F.; Wang, X. (2016) *Estimation of Evolutionary Power Spectral Density of Typhoon Wind Speed*, The 2016 World Congress on Advances in Civil, Environmental, and Materials Research (ACEM16)

[8] Priestley, M. B. (1965) *Evolutionary Spectra and Non-Stationary Processes*. Journal of the Royal Statistical Society. Series B (Methodological), Vol. 27, No. 2(1965), pp. 204-237

[9] Rottmann, K. (2010) *Matematisk Formalsamling*. 11th Edition. Oslo: Spektrum Forlag

[10] Strømmen, E. (2006) *Theory of Bridge Aerodynamics*. 1st Edition. Springer-Verlag Berlin Heidelberg, New York

[11] Strømmen, E. (2010) *Theory of Bridge Aerodynamics*. 2nd Edition. Springer-Verlag Berlin Heidelberg, New York

[12] Strømmen, E. (2014) *Structural Dynamics*. 1st Edition. Springer International Publishing, Switzerland

[13] Tao, T; Wang, H.; Wu, T. (2016) *Comparative Study of the Wind Characteristics of a Strong Wind Event Based on Stationary and Nonstationary Models*. J. Struct. Eng., 2017, 143(5): 04016230

[14] von Kármán, T. (1948) *Progress in the statistical theory of turbulence*. California Institute of Techonolgy, Pasedena

[15] Wang, H.; Wu T.; Tao, T.; Li, A.; Kareem, A. (2016). *Measurements and analysis of non-stationary wind characteristics at Suton Bridge in Typhoon Damrey*. J. Wind Eng .Ind. Aerodyn. 151 (2016) 100–106

[16] Wang, L.; Kareem, A. (2005) *Modeling of Non-Stationary Winds in Gust-Fronts*. 9th ASCE Specialty Conference on Probabilistic Mechanics and Structural Reliability

[17] Wikipedia. Hardanger Bridge. *https://en.wikipedia.org/wiki/Hardanger_Bridge#/media/File:Hardangerbrua_(15028061131).png*, May 16th, 2018.

[18] Xu, Y. L., et al. (2000). *Field measurement results of Tsing Ma suspension bridge during Typhoon Victor*. Struct. Eng. Mech., 10(6), 545–559.

[19] Xu, Y. L.; Chen, J. (2004) *Characterizing Nonstationary Wind Speed Using Empirical Mode Decomposition*. J. Struct. Eng., 2004, 130(6): 912-920

APPENDIX A – ADDITIONAL CALCULATIONS

A.1 INCLUSION OF MEAN VERTICAL WIND SPEED

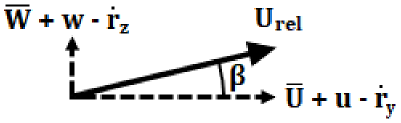

Figure A.0.1: Non–stationary colleague of figure 1.5

The wind angle β simply gets another term added to it, namely,

$$\beta \;=\; \arctan\left(\frac{\bar{W} + w - \dot{r}_z}{\bar{U} + u - \dot{r}_y}\right) \;\approx\; \frac{\bar{W} + w - \dot{r}_z}{\bar{U}} \tag{A.1}$$

The expression for the fluctuating part of the angle of incidence, α_f, undergoes an analogue change,

$$\alpha_f \;=\; r_\theta + \beta \;=\; r_\theta + \frac{\bar{W}}{\bar{U}} + \frac{w}{\bar{U}} - \frac{\dot{r}_z}{\bar{U}} \tag{A.2}$$

$\bar{W}$ will logically be much smaller than the fluctuations from which it is supposed to represent a withdrawn trend, hence nothing happens to the expression of U_{rel} to which $\bar{W}$ would have given only a negligible contribution,

$$U_{rel}^2 \;=\; (\bar{U} + u - \dot{r}_y)^2 \;+\; (\bar{W} + w - \dot{r}_z)^2 \;\approx\; \bar{U}^2 + 2\bar{U}u - 2\bar{U}\dot{r}_y \tag{A.3}$$

If the linearization of the load coefficients as shown in equation 1.30a is substituted back into equation 1.29 and equation 1.29 subsequently is multiplied with the coordinate transformation matrix in equation 1.32a, the following emerges,

$$\begin{Bmatrix} q_y \\ q_z \\ q_\theta \end{Bmatrix} \;=\; \frac{1}{2}\rho B U_{rel}^2 \cdot \begin{bmatrix} a_r\left(\bar{C}_D + \alpha_f C_D'\right) - \beta\left(\bar{C}_L + \alpha_f C_L'\right) \\ a_r\beta\left(\bar{C}_D + \alpha_f C_D'\right) + \left(\bar{C}_L + \alpha_f C_L'\right) \\ B\left(\bar{C}_M + \alpha_f C_M'\right) \end{bmatrix}, \qquad a_r \;=\; \frac{D}{B} \tag{A.4}$$

Because linearity is a requirement when establishing the expression for the buffeting loads, β and α_f cannot exist as factors of a product since this would violate linearity. However, because their magnitude in most practical purposes is quite modest, terms containing them as mutual factors can be neglected as is the case with the rightmost term for q_y in equation A.4.

If equation A.2 and A.3 is inserted into equation A.4 the final, but for now somewhat cluttered expression for the buffeting loads is obtained. As before, linearity must be maintained, hence terms that is nonlinear in either u, v, $\dot{r}_y$, $\dot{r}_z$ or r_θ must be omitted, however their magnitude in most practical cases gives their absence a negligible global implication. For the record, this calculation will be shown for each entry of $\boldsymbol{q}$, starting with q_y,

$$\begin{aligned}\frac{2}{\beta B}q_y &= U_{rel}^2\cdot\left[a_r\bar{C}_D + a_r C_D' r_\theta + \frac{a_r C_D'}{\bar{U}}(\bar{W}+w-\dot{r}_z) - \frac{\bar{C}_L}{\bar{U}}(\bar{W}+w-\dot{r}_z)\right]\\ &= \bar{U}^2 a_r\bar{C}_D + \bar{U}\bar{W}[a_r C_D' - \bar{C}_L] + \bar{U}[a_r C_D' - \bar{C}_L]w + \bar{U}[2a_r\bar{C}_D]u + \bar{U}[-2a_r\bar{C}_D]\dot{r}_y \\ &\quad + \bar{U}[a_r C_D' + \bar{C}_L]\dot{r}_z + \bar{U}^2[a_r C_D']r_\theta\end{aligned} \tag{A.5a}$$

q_z,

$$\begin{aligned}\frac{2}{\beta B}q_z &= U_{rel}^2\cdot\left[\frac{a_r\bar{C}_D}{\bar{U}}(\bar{W}+w-\dot{r}_z) + \bar{C}_L + C_L' r_\theta - \frac{C_L'}{\bar{U}}(\bar{W}+w-\dot{r}_z)\right]\\ &= \bar{U}^2\bar{C}_L + \bar{U}\bar{W}[a_r + C_L'] + \bar{U}[a_r + C_L']w + \bar{U}[2\bar{C}_L]u + \bar{U}[-2\bar{C}_L]\dot{r}_y \\ &\quad + \bar{U}[-a_r\bar{C}_D - C_L']\dot{r}_z + \bar{U}^2[C_L']r_\theta\end{aligned} \tag{A.5b}$$

q_θ,

$$\begin{aligned}\frac{2}{\beta B}q_\theta &= U_{rel}^2\cdot\left[B\bar{C}_M + BC_M' r_\theta + \frac{BC_M'}{\bar{U}}(\bar{W}+w-\dot{r}_z)\right]\\ &= \bar{U}^2 B\bar{C}_M + \bar{U}\bar{W}[BC_M'] + \bar{U}[BC_M']w + \bar{U}[2B\bar{C}_M]u + \bar{U}[-2B\bar{C}_M]\dot{r}_y \\ &\quad + \bar{U}[-BC_M']\dot{r}_z + \bar{U}^2[BC_M']r_\theta\end{aligned} \tag{A.5c}$$

If equations A.5a–c are organized onto matrix form the exact the same result as shown in equation 1.37 emerges, apart from equation 1.37c which takes the form of equation 2.2.

A.2 ANALYTICAL CALCULATION OF EQUATION 3.4

The analytical calculation of equation 3.4 starts by exploiting a neat symmetry property with respect to the line $\hat{x}_1 = \hat{x}_2$. This symmetry property is illustrated by introducing the virtual coordinate system shown in figure A.2.

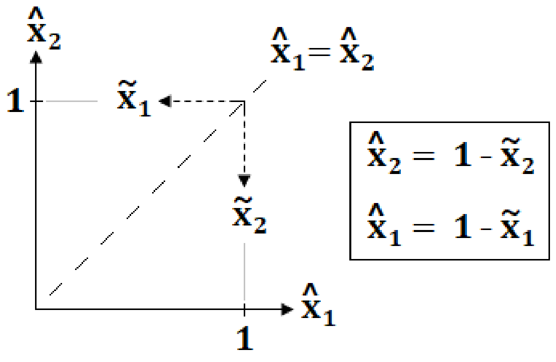

Figure A.0.2: Virtual coordinate system

The exponential function in equation 3.4 is obviously symmetric about $\hat{x}_1 = \hat{x}_2$ and needs no further investigation. However, the harmonic part of the integrand, $f_h(\hat{x}_1, \hat{x}_2)$, will undergo the following transformation when the coordinate substitution in figure A.2 is applied:

$$\begin{aligned}
f_h(\hat{x}_1, \hat{x}_2) &= sin(p(1 - \tilde{x}_1))\, sin(q(1 - \tilde{x}_2)) \\
&= [sin(p)\, cos(-p\,\tilde{x}_1) - cos(p)\, sin(-p\tilde{x}_1)] \\
&\quad \cdot [sin(q)\, cos(-q\,\tilde{x}_2) - cos(q)\, sin(-q\tilde{x}_2)] \quad \text{(Rottmann, 2010, s. 87)} \\
&= cos(p)\, cos(q) \cdot sin(p\tilde{x}_1)\, sin(q\tilde{x}_2) \\
&= \gamma \cdot f_h(\tilde{x}_1, \tilde{x}_2)\,, \qquad \gamma = \begin{cases} 1, & P, Q \text{ both even or both odd} \\ -1, & P, Q \text{ even, odd or odd, even} \end{cases}
\end{aligned} \tag{A.6}$$

Together with the fact that the normalized Co–spectrum is symmetric with respect to $\hat{x}_1 = \hat{x}_2$, the following must be true,

$$\int_0^1 \int_0^{\hat{x}_1} f(\omega, t)\, d\hat{x}_2 d\hat{x}_1 \quad = \quad \gamma \cdot \int_0^1 \int_{\hat{x}_1}^1 f(\omega, t)\, d\hat{x}_2 d\hat{x}_1 \tag{A.7}$$

Which subsequently implies that,

$$F(\omega, t) \;=\; 2\int_0^1 \int_0^{\hat{x}_1} sin(p\hat{x}_1) \cdot sin(q\hat{x}_2) \cdot e^{C(\hat{x}_1 - \hat{x}_2)} d\hat{x}_2 d\hat{x}_1, \qquad \gamma = 1 \tag{A.8a}$$

$$F(\omega, t) \;=\; 0, \qquad \gamma = -1 \tag{A.8b}$$

The procedure of obtaining the analytical solution to equation A.8a requires two distinct cases to be taken into consideration, in which the first demands $p^2 \neq q^2$. Because p and q are already known to be positive according to the definition of the mode shapes in “A.txt” in Appendix C, $p \neq q$ will be sufficient. This first case is initialized by expressing equation A.8a as,

$$F(\omega, t) \;=\; 2\int_0^1 sin(p\hat{x}_1)\, e^{D\hat{x}_1} \left[\int_o^{\hat{x}_1} sin(q\hat{x}_2) e^{-C\hat{x}_2}\, d\hat{x}_2 \right] d\hat{x}_1 \tag{A.9}$$

Rottmann (2010, p. 144, eq. 132) provides the necessary information to evaluate the integral inside the bracket parenthesis in equation A.9, and after a few steps of rearrangement, equation A.8 can be expressed as,

$$F(\omega, t) \;=\; -\frac{2}{q^2 + C^2} [C I_1 + q I_2 - q I_3] \tag{A.10a}$$

where,

$$\begin{Bmatrix} I_1 \\ I_2 \\ I_3 \end{Bmatrix} = \int_0^1 \begin{Bmatrix} sin(p\hat{x}_1)\, sin(q\hat{x}_1) \\ sin(p\hat{x}_1)\cos(q\hat{x}_1) \\ sin(q\hat{x}_1)e^{C\hat{x}_1} \end{Bmatrix} d\hat{x}_1 \tag{A.10b}$$

Hass, Weir and Thomas (2009, p. T–3, eqs. 62a and b) provides the solution to I_1 and I_2, respectively,

$$I_1 = \frac{1}{2}\left[\frac{sin(p-q)\hat{x}_1}{p-q} - \frac{sin(p+q)\hat{x}_1}{p+q}\right]_0^1 = 0 \tag{A.11a}$$

$$\begin{aligned} I_2 &= -\frac{1}{2}\left[\frac{cos(p-q)\hat{x}_1}{p-q} + \frac{cos(p+q)\hat{x}_1}{p+q}\right]_0^1 \\ &= \frac{1}{2}\left[\frac{1-cos(p-q)}{p-q} + \frac{1-cos(p+q)}{p+q}\right] \end{aligned} \tag{A.11b}$$

Rottmann (2010, p. 144, eq. 132) does also provide the solution to I_3, namely,

$$I_3 = \frac{p}{p^2+C^2}\left[1-e^C\, cos\, p\right] \tag{A.11c}$$

The final expression for the solution to equation A.8a when $p \neq q$ is given by,

$$F(\omega,t) = \frac{2q}{q^2+C^2}\left[\frac{cos(p-q)-1}{2(p-q)} + \frac{cos(p+q)-1}{2(p+q)} - \frac{p(1-e^C\, cos\, p)}{p^2+C^2}\right] \tag{A.12}$$

The case $p = q$ involves an identical solution strategy as shown above. However, when setting $q = p$, equation A.10a and A.10b takes the following form:

$$F(\omega,t) = -\frac{2}{p^2+C^2}\left[CI_1 + pI_2 - pI_3\right] \tag{A.13a}$$

where,

$$\begin{Bmatrix} I_1 \\ I_2 \\ I_3 \end{Bmatrix} = \int_0^1 \begin{Bmatrix} \sin^2(p\hat{x}_1) \\ sin(p\hat{x}_1)\cos(p\hat{x}_1) \\ sin(p\hat{x}_1)e^{C\hat{x}_1} \end{Bmatrix} d\hat{x}_1 \tag{A.13b}$$

Obviously, $I_1 = 1/2$. $I_2 = 0$ because $sin(p\hat{x}_1)\cos(p\hat{x}_1)$ also will have period 1 and zero mean when this is the case with $sin(p\hat{x}_1)$ and $\cos(p\hat{x}_1)$. I_3 is identical as in the case $p \neq q$, and given by equation A.10c, except that q is now substituted with p. Thus, when $p = q$, equation A.8a will take the form,

$$F(\omega,V) \;=\; \frac{2}{p^2 + C^2}\left[\frac{p^2(1 - e^C \, cos\, p)}{p^2 + C^2} - \frac{C}{2}\right] \tag{A.14}$$

APPENDIX B – MATLAB SCRIPTS

The MATLAB scripts given in this chapter is produced with the exclusive purpose being of providing the necessary computing power to solve the very problems associated with this very thesis. The majority of the result presented in this thesis are obtained via cross runs of several of the scripts below, where output data of one script serves as being input data to another. Hence, no effort is done to provide general information of how to use them. They must therefore be used with the greatest of care.

B.1 SCRIPTS

B.1.1 Wind speed recording calculations

```
%
clear
plotmode = 1;
includespectrum = 0;
meanmethod = 1; % For extractions of mean. -1: Stationary, 0: Do not extract, 1: Fourier, 2:
EMD, 3: MAM
guwtype = 1; % Calculate spectrum of 1: gu(t) and gw(t) 2: u(t) and w(t)
istart = 24001; % Extraction index extremeties for recordings. Only plot for this interval!
iend = 372001;
nuaxinit = 300; % number of compartments in PDF for turbulence components
avgspant = 450; % [s]
rhoTHR = 0.25; % for T char
nL = 201; % number of turbulence length scale claculations
ncolL = 0; % collect rho function at ncolL number of places.
omegamaxUM = 0.32/100;
%
imunit = sqrt(-1);
% time-series, U, W:
tic
dt = 0.05; % SAMPLING FREQUENCY
U = load('UHardanger29012016.txt')';
W = load('WHardanger29012016.txt')';
T = 0:dt:((length(U)-1)*dt); % Corresponing time values of sample series
nU = length(U);
nW = length(W);
if nW ~= nU
    disp(' vectors U ans W are not the same length!')
    return
end
TU = (nU-1)*dt; % Sample duration
T = 0:dt:TU; % Corresponing time values of sample series
TUSE = (dt*round(iend-istart)); % Sub recording duration
Tplot = 0:dt:TUSE; % T hub for chosen sub recording
nTUSE = length(Tplot); % elementlength of the chosen sub recording vector
disp(['Load:      ' num2str(round(toc,3,'significant')) ' s'])
% Extracting time-varying mean:
tic
Uavg = (0.5*(U(1)+U(nU)) + sum(U(2:nU-1)))*dt/TU;
Wavg = (0.5*(W(1)+W(nU)) + sum(W(2:nU-1)))*dt/TU;
domega = 2*pi/TU;
omegasettings = domega:domega:omegamaxUM;
NOset = length(omegasettings);
omegamaxUM = omegasettings(NOset);
Umean = zeros(2,nU);
if meanmethod == -1
    Uavg = (0.5*(U(istart)+U(iend)) + sum(U(istart+1:iend-1)))*dt/TUSE;
    Wavg = (0.5*(W(istart)+W(iend)) + sum(W(istart+1:iend-1)))*dt/TUSE;
    Umean = [Uavg;Wavg]*ones(1,nU);
elseif meanmethod == 1
    for wn = 1:NOset
        omega = omegasettings(wn);
        ak = U.*cos(omega*T);
        ak = (dt/TU)*(ak(1)+ak(end)+2*sum(ak(2:end-1)));
        bk = U.*sin(omega*T);
```

```
        bk = (dt/TU)*(bk(1)+bk(end)+2*sum(bk(2:end-1)));
        Umean(1,:) = Umean(1,:) + ak*cos(omega*T) + bk*sin(omega*T);
    end
    Umean(1,:) = Umean(1,:) + Uavg;
    for wn = 1:NOset
        omega = omegasettings(wn);
        ak = W.*cos(omega*T);
        ak = (dt/TU)*(ak(1)+ak(end)+2*sum(ak(2:end-1)));
        bk = W.*sin(omega*T);
        bk = (dt/TU)*(bk(1)+bk(end)+2*sum(bk(2:end-1)));
        Umean(2,:) = Umean(2,:) + ak*cos(omega*T) + bk*sin(omega*T);
    end
    Umean(2,:) = Umean(2,:) + Wavg;
elseif meanmethod == 2
    [imf,residual] = emd(U);
    imfcomps = [10];
    Umean(1,:) = residual';
    for i = imfcomps
        Umean(1,:) = Umean(1,:) + (imf(:,i))';
    end
    [imf,residual] = emd(W);
    imfcomps = [10];
    Umean(2,:) = residual';
    for i = imfcomps
        Umean(2,:) = Umean(2,:) + (imf(:,i))';
    end
elseif meanmethod == 3
    TUavgP = 720;
    ispanmean = round(TUavgP/dt);
    weightsmeanON = 1;
    WUM = 1-(((-ispanmean+0.5):(ispanmean-0.49))/ispanmean).^2;
    WUM = WUM/sum(WUM);
    if weightsmeanON == 0
        Umean(1,ispanmean+1) = dt*sum(0.5*(U(1:2*ispanmean)+U(2:2*ispanmean+1)));
        Umean(2,ispanmean+1) = dt*sum(0.5*(W(1:2*ispanmean)+W(2:2*ispanmean+1)));
        for i = ispanmean+2:(nU-ispanmean)
            Umean(1,i) = Umean(1,i-1) - 0.5*dt*((U(i-ispanmean-1)+U(i-ispanmean))-
(U(i+ispanmean-1)+U(i+ispanmean)));
            Umean(2,i) = Umean(2,i-1) - 0.5*dt*((W(i-ispanmean-1)+W(i-ispanmean))-
(W(i+ispanmean-1)+W(i+ispanmean)));
        end
        Umean = Umean/(2*TUavgP);
    elseif weightsmeanON == 1
        MMU = 0.5*(U(1:2*ispanmean)+U(2:2*ispanmean+1));
        MMW = 0.5*(W(1:2*ispanmean)+W(2:2*ispanmean+1));
        Umean(1,ispanmean+1) = sum(MMU.*WUM);
        Umean(2,ispanmean+1) = sum(MMW.*WUM);
        for i = ispanmean+2:(nU-ispanmean)
            MMU = [MMU(2:end) 0.5*(U(i+ispanmean-1)+U(i+ispanmean))];
            MMW = [MMW(2:end) 0.5*(W(i+ispanmean-1)+W(i+ispanmean))];
            Umean(1,i) = sum(MMU.*WUM);
            Umean(2,i) = sum(MMW.*WUM);
        end
    end
end
Umeanavg = (Umean(1,istart)+Umean(1,iend)+2*sum(Umean(1,istart+1:iend-1)))*0.5/(nTUSE-1);
Wmeanavg = (Umean(2,istart)+Umean(2,iend)+2*sum(Umean(2,istart+1:iend-1)))*0.5/(nTUSE-1);
uwmat = [U - Umean(1,:);W - Umean(2,:)];
disp(['Mean:     ' num2str(round(toc,3,'significant')) ' s'])
% Time-varying variance:
tic
ispan = round(avgspant/dt);
weightsON = 1; % 1: Vektet tids-offset, 0: ikke vektet.
varuw = zeros(2,nTUSE); % [var(u);var(w)]
varcomps = zeros(2,2*ispan);
if weightsON == 1
    b = ispan/1.96; % 95 % conf. interval
    weights = zeros(1,2*ispan);
    for i = -ispan:(ispan-1)
        weights(i+ispan+1) = 1-((i+0.5)/ispan)^2;
    end
    weights = weights/sum(weights); % normalized, sum = 1
end
for v = 1:2
    for i = (istart-ispan):(istart+ispan-1)
        a = uwmat(v,i);
        b = uwmat(v,i+1);
```

```
        varcomps(v,i+1-(istart-ispan)) = ((a^2)+(a*b)+(b^2))/3;
    end
    if weightsON == 1
        varuw(v,1) = sum(varcomps(v,:).*weights);
    else
        varuw(v,1) = sum(varcomps(v,:));
    end
    if weightsON == 1
        for i = istart+1:iend
            a = uwmat(v,i+ispan-1);
            b = uwmat(v,i+ispan);
            vari = ((a^2)+(a*b)+(b^2))/3;
            varcomps(v,:) = [varcomps(v,2:2*ispan) vari];
            varuw(v,i-istart+1) = sum(varcomps(v,:).*weights);
        end
    else
        for i = istart+1:iend
            a = uwmat(v,i+ispan-1);
            b = uwmat(v,i+ispan);
            vari = ((a^2)+(a*b)+(b^2))/3;
            varcomps(v,:) = [varcomps(v,2:2*ispan) vari];
            varuw(v,i-ispan) = sum(varcomps(v,:));
        end
        varuw(v,:) = varuw(v,:)/(2*ispan);
    end
end
uwvarcontrol = [0;0]; % calculated variance from time series of u(t)
uwavgcontrol = [0;0]; %                                         w(t)
for v = 1:2
    for i = 2:nTUSE
        a = uwmat(v,i-2+istart);
        b = uwmat(v,i-1+istart);
        uwvarcontrol(v) = uwvarcontrol(v) + ((a^2)+(a*b)+(b^2))/3;
        uwavgcontrol(v) = uwavgcontrol(v) + (a+b)/2;
    end
    uwvarcontrol(v) = uwvarcontrol(v)/(nTUSE-1);
    uwavgcontrol(v) = uwavgcontrol(v)/(nTUSE-1);
end
if guwtype == 1
    guw = [uwmat(1,istart:iend)./sqrt(varuw(1,:));uwmat(2,istart:iend)./sqrt(varuw(2,:))]; %
g: zero mean, unit variance;
elseif guwtype == 2
    guw = [uwmat(1,istart:iend);uwmat(2,istart:iend)]; % g: zero mean
end
if guwtype == 1
    guwvarcontrol = [0;0]; % calculated variance from time series of gu(t)
    guwavgcontrol = [0;0]; %                                         gw(t)
    for v = 1:2
        for i = 2:nTUSE
            a = guw(v,i-1);
            b = guw(v,i);
            guwvarcontrol(v) = guwvarcontrol(v) + ((a^2)+(a*b)+(b^2))/3;
            guwavgcontrol(v) = guwavgcontrol(v) + (a+b)/2;
        end
        guwvarcontrol(v) = guwvarcontrol(v)/(nTUSE-1);
        guwavgcontrol(v) = guwavgcontrol(v)/(nTUSE-1);
    end
end
varuwavg = (varuw(:,1)+varuw(:,nTUSE)+2*sum(varuw(:,2:nTUSE-1),2))*0.5/(nTUSE-1);
% propability density, guw(1:2,:):
dgax = (max(guw,[],2)-min(guw,[],2))/nuaxinit;
gax(1,1:nuaxinit) = (min(guw(1,:))+(dgax(1)/2)):dgax(1):(max(guw(1,:))-(dgax(1)/2.5)); %
midpoint values
gax(2,1:nuaxinit) = (min(guw(2,:))+(dgax(2)/2)):dgax(2):(max(guw(2,:))-(dgax(2)/2.5)); %
midpoint values
ngax = size(gax,2);
probdensguw = zeros(2,ngax);
for v = 1:2
    for i = 1:(iend-istart)
        y = 0.5*(guw(v,i)+guw(v,i+1));
        j = sum((min(abs((y-gax(v,:))))==abs((y-gax(v,:)))).*(1:ngax));
        probdensguw(v,j) = probdensguw(v,j) + 1;
    end
end
scaleg = sum(probdensguw,2).*dgax;
probdensguw(1,:) = probdensguw(1,:)/scaleg(1);
probdensguw(2,:) = probdensguw(2,:)/scaleg(2);
```

```
pdfgauss1 = zeros(2,nuaxinit);
pdfgauss2 = zeros(2,nuaxinit);
sumvar1 = [0;0];
sumvar2 = [0;0];
avg1 = [0;0];
avg2 = [0;0];
for v = 1:2
    for i = 1:(iend-istart)
        a = guw(v,i);
        b = guw(v,i+1);
        sumvar1(v) = sumvar1(v) + ((a^2)+(a*b)+(b^2))/3;
    end
    if guwtype == 1
        avg1(v) = guwavgcontrol(v);
    else
        avg1(v) = uwavgcontrol(v);
    end
    sumvar1(v) = sumvar1(v)/(iend-istart) - (avg1(v)^2);
    %
    sumvar2cands = 0.2*sumvar1(v):0.001:3*sumvar1(v);
    avg2(v) = sum(gax(v,:).*probdensguw(v,:))*dgax(v);
    for i = 1:size(sumvar2cands,2)
        sigmasq = sumvar2cands(i);
        SSD = sum((1/sqrt(2*pi*sigmasq)*exp(-0.5/sigmasq*(gax(v,:)-avg2(v)).^2) -
probdensguw(v,:)).^2);
        if i == 1
            SSDmin = SSD;
            sigmasqmin = sigmasq;
        else
            if SSD < SSDmin
                SSDmin = SSD;
                sigmasqmin = sigmasq;
            end
        end
    end
    sumvar2(v) = sigmasqmin;
    %
    pdfgauss1(v,:) = 1/sqrt(2*pi*sumvar1(v))*exp(-0.5/sumvar1(v)*(gax(v,:)-avg1(v)).^2);
    pdfgauss2(v,:) = 1/sqrt(2*pi*sumvar2(v))*exp(-0.5/sumvar2(v)*(gax(v,:)-avg2(v)).^2);
end
disp(['Variance: ' num2str(round(toc,3,'significant')) ' s'])
% Characteristic time, Tchar:
if meanmethod ~= 0
    tic
    iL = round((istart:(iend-istart)/(nL-1):(iend+0.01))); % indices in u for calculation L(t)
    TL = (iL-istart)*dt; % corresponding time values of timeseries of L(t)
    nTL = length(TL);
    itmattau = zeros(3,nTL,2); % % [index for cov = rhoTHR;int(rho(tau),0,tau_0)], layers: u;w
    icolL = round(1:((nTL-1)/(ncolL-1)):(nTL+0.01)); % indices in u at which rho function is
to be calculated
    rhotaucollect = zeros(1,1,2);
    Tchar = zeros(2,nTL,2); % rows: methods, cols: time, layers: u;w
    Tcharavg = zeros(2,2); % rows: u;w, cols: methods 1 and 2
    if weightsON == 0
        weights = ones(1,2*ispan)/(2*ispan);
    end
    for v = 1:2
        Icomps = zeros(1,2*ispan);
        for i = 1:nTL
            iu = iL(i); % index in u
            ut = uwmat(v,iu-ispan:iu+ispan); % indices in u for u(t)
            tau = -dt;
            ispantau = 0;
            itau = 0;
            variu = varuw(v,iu-istart+1); % calculated variance at t = T(iu);
            rhoutau = 1; % rho(tau) function
            rhou = 1;
            while (rhou>=rhoTHR) && (iu+ispan+ispantau<nU)
                itau = itau + 1;
                tau = tau + dt;
                ispantau = round(tau/dt); % shift in index in u
                utau = uwmat(v,iu-ispan+ispantau:iu+ispan+ispantau); % indices for u(t+tau)
                for j = 1:(2*ispan)
                    a = ut(j);
                    b = ut(j+1);
                    c = utau(j);
                    d = utau(j+1);
```

```
                    Icomps(j) = ((a*d)+(b*c))/2 + (b-a)*(d-c)/3;
                end
                rhou = (sum(Icomps.*weights))/variu; % should be exactly 1 for first iteration
(tau = 0)!
                rhoutau(itau) = rhou;
            end
            I = - rhoTHR*tau;
            for j = 2:itau
                I = I + 0.5*(rhoutau(j-1)+rhoutau(j))*dt; % trapezoidal integration method
            end
            itmattau(1:2,i,v) = [itau;I];
            if rhou > rhoTHR
                itmattau(3,i,v) = 1; % index out of bound before rho could reach rhoTHR!
OTHERWISE: 0
            end
            [ismemb,icol] = ismember(i,icolL);
            if ismemb == 1
                rhotaucollect(icol,1:itau,v) = rhoutau;
            end
        end
        Tchar(1,1:nTL,v) = dt*itmattau(1,:,v); % time until correlation coefficient <= rhoTHR
        Tchar(2,1:nTL,v) = itmattau(2,:,v); % integral method
    end
    TcharIP(1:2,1:nTUSE,1) = [Tchar(:,1,1),zeros(2,nTUSE-1,1)]; % rows: M1;M2, layers: u;w
    TcharIP(1:2,1:nTUSE,2) = [Tchar(:,1,2),zeros(2,nTUSE-1,1)];
    for i = 2:nL % interpolation onto the sizes of uwmat and varuw
        di = 1/(iL(i)-iL(i-1));
        ipf = di:di:1;
        j0 = iL(i-1) + 2 - istart;
        j1 = iL(i) + 1 - istart;
        for v = 1:2
            TcharIP(:,j0:j1,v) = TcharIP(:,j0-1,v) + (Tchar(:,i,v)-Tchar(:,i-1,v))*ipf;
        end
    end
    for v = 1:2
        for meth = 1:2
            Tcharavg(v,meth) = (Tchar(meth,1,v)+Tchar(meth,nTL,v)+2*sum(Tchar(meth,2:nTL-
1,v)))/(2*(nTL-1));
        end
    end
    disp(['T char:   ' num2str(round(toc,3,'significant')) ' s'])
end
% Calculate spectrum of g(t)
if includespectrum == 1
    tic
    domegaSg = 2*pi/TUSE; % 2*pi/T
    omegamaxSg = 12;
    omegasettingsSg = domegaSg:domegaSg:omegamaxSg;
    NOsetSg = length(omegasettingsSg);
    LSFimin = min(setdiff((omegasettingsSg>=omegamaxUM).*(1:NOsetSg),0));
    omegasettingsSgLSF = omegasettingsSg(LSFimin:NOsetSg);
    Sguw = zeros(2,NOsetSg);
    for v = 1:2
        for wn = 1:NOsetSg
            omega = omegasettingsSg(wn);
            ak = exp(-imunit*omega*Tplot).*guw(v,:);
            ak = 0.5*dt*(ak(1)+ak(end)+2*sum(ak(2:end-1)));
            Sguw(v,wn) = (ak*ak')/(TUSE*pi);
        end
    end
    SguLSF = Sguw(1,LSFimin:NOsetSg);
    SgwLSF = Sguw(2,LSFimin:NOsetSg);
    NOsetSgLSF = NOsetSg - LSFimin + 1;
    disp(['Spectrum: ' num2str(round(toc,3,'significant')) ' s'])
end
%
```

B.1.2 Spectrum smoothing algorithm

```
%
CO = 0; % cut-off
v = 1;
Sg = Sguw(v,1+CO:end);
omegasettingsSg = omegasettingsSg(1+CO:end);
NOsetSg = NOsetSg - CO;
nn1 = 5;
```

```
nexp = 1.5;
nn2 = 200;
nx = zeros(1,NOsetSg-nn2);
nx(nn1+1:NOsetSg-nn2) = nn1 + (nn2-nn1)*((log(omegasettingsSg(nn1+1:NOsetSg-nn2))-
log(omegasettingsSg(nn1+1)))/(log(omegasettingsSg(NOsetSg-nn2))-
log(omegasettingsSg(nn1+1)))).^nexp;
nx = floor(nx);
omegasettingsSgsmoothed = omegasettingsSg(1:NOsetSg-nn2);
Sgsmoothed = zeros(1,NOsetSg-nn2);
comissioningavg = 2*(1:nn1) - 1;
comissioningavg(1) = 2;
for i = 1:nn1
    Sgsmoothed(i) = sum(Sg(1:comissioningavg(i)))/comissioningavg(i);
end
for i = (nn1+1):(NOsetSg-nn2)
    nxi = nx(i);
    Sgsmoothed(i) = sum(Sg(i-nxi:i+nxi))/(2*nxi+1);
end
weightsomegaSg = (1./Sgsmoothed).^2;
if v == 1
    ysmoothed1 = 22180*(1+27.77*omegasettingsSgsmoothed.^0.5).^-3.2;
elseif v == 2
    ysmoothed1 = 13.11*(1+2.669*omegasettingsSgsmoothed.^0.5).^-3.2;
end
ysmoothed1 = SgP(rowSP,(3*(v-1))+1)*(1+SgP(rowSP,(3*(v-
1))+2)*omegasettingsSgsmoothed.^1).^SgP(rowSP,(3*(v-1))+3);
%
```

B.1.3 Frequency domain response calculations

```
%
% SCRIPT SETTINGS:
colors = 'rbgm';
calctype = 1;
Tcharmethod = 2; % 1: Duration method, 2: Integral method
modulationtypes = [1 2 3 4]; % Non-stationary modulation methods
spectrumtype = 1; % 1: Kaimal, 2: von Kármán, 3: avgerage Kaimal, von K
xresponse = 0.5; % relative length coordinate for response output!
refinementfactor = 2; % relative bridge span coordinate for response calc.
Etype = 2; % Elementtype for numerical integration
rfT = 1; % number og time data points (also for calctype = 2 !)
nipomegainit = 1; % interpolation refinement at omega_1
nipEPSDt = 1; % interpolation factor t axis (# sub points)
eliminationfactor = 0.010; % significant subcomponent amplitude threshold
%
if calctype == 1
    % WLSF spectrum coefficients:
    SP = load('SPECTRUMPARAMS.txt');
    SgKu = [SP(rowSP,1),SP(rowSP,2),SP(rowSP,3)]; % A B n
    SgKw = [SP(rowSP,4),SP(rowSP,5),SP(rowSP,6)]; % A B n
    SgvKu = [6.148 75.52 -0.833]; % A B n
    SgvKw = [0.3757 14.09 3.775 -1.833]; % A B C n
elseif calctype == 2 % for surface plot of |H(omega,V)|^2.
    V1 = 0.01;
    V2 = 50;
    Vsettings = V1:(V2-V1)/(rfT-1):V2;
    omegasettingsH = 0.000:0.001:12.00;
    NOsetH = length(omegasettingsH);
    Hplot = zeros(rfT,NOsetH);
end
    % Mathematical constants:
imagunit = sqrt(-1);
    % geometrical characteristics:
L = 1310; % [m]
B = 18.3; % [m]
D = 3.25; % [m]
ar = D/B; % "Aspect Ratio"
    % Wind field parameters:
rho = 1.25; % [kg/m^3]
Cux = 1.4*L;
Cwx = 1.0*L;
    % Load coefficients:
CD = 0.7;
dCL0 = 5;
```

```
AndCL = 3.2*B;
bndCL = 0.5;
dCM0 = 1.5;
AndCM = 2.4*B;
bndCM = 0.5;
    % Mode characteristics:
modechar = load('MC.txt'); % modal mass (m tilde), frequency, damping
modeshapes = load('A.txt'); % modal fourier component matrix
Nmod = size(modechar,1); % Number of MODes
kmax = size(modeshapes,2); % Highest wavenumber of all mode components
modmass = modechar(:,1); % MODal MASS, m_tilde
eigenfreq = modechar(:,2); % modal EIGENFREQuencies
moddamping = modechar(:,3); % MODal damping ratio
for i1 = 0:(Nmod-1) % Calculation modal masses M tilde
    i = (i1*4)+1;
    modmass(i1+1) = modmass(i1+1)*sum(sum((modeshapes(i:(i+3),:)).^2));
end
modmass = modmass*0.5*L;
modstiffn = (eigenfreq.^2).*modmass;
if calctype == 1
    % Discretization of omega axis
    omegamaxUM = 2*pi/TUSE;
    elements(1,1:3) = [1  1  2]; % trapezoidal method
    elements(2,1:4) = [1  4  1  6]; % simpson's method
    elements(3,1:6) = [7 32 12 32 7 90]; % Boole's rule
    elementnN = [2;3;5];
    NelN = elementnN(Etype);
    elemchoice = elements(Etype,1:NelN);
    intscheme = load('OS2.txt');
    intscheme(:,2) = ceil(refinementfactor*intscheme(:,2));
    i = max(1,min(setdiff(((omegamaxUM<=intscheme(:,1)).*(1:size(intscheme,1))'),0)) - 1);
    intscheme(i,1) = omegamaxUM;
    intscheme = intscheme(i:end,:);
    omegasettings = intscheme(1,1);
    Nsections = size(intscheme,1) - 1;
    NOsetR = 1; % Number of Omega SETtings
    omegaweights = zeros(1,1+(NelN-1)*intscheme(1,2)); % corresponding weighting values for
num. int.
    for i = 1:Nsections
        startsection = intscheme(i,1);
        endsection = intscheme(i+1,1);
        sectionlength = endsection - startsection;
        Nsel = intscheme(i,2); % Number of Section ELements
        elemscaling = sectionlength/(Nsel*elements(Etype,NelN+1));
        sectionweights = elemchoice;
        Nsn = NelN; % Number of Section Nodes
        for el = 2:Nsel
            sectionweights = [sectionweights,zeros(1,NelN-1)];
            sectionweights(Nsn:Nsn+NelN-1) = sectionweights(Nsn:Nsn+NelN-1) + elemchoice;
            Nsn = Nsn + NelN - 1;
        end
        sectionweights = sectionweights*elemscaling;
        if i ~= 1
            omegaweights = [omegaweights,zeros(1,Nsn-1)];
        end
        omegaweights(NOsetR:NOsetR+Nsn-1) = omegaweights(NOsetR:NOsetR+Nsn-1) +
sectionweights;
        NOsetR = NOsetR + Nsn - 1;
        deltaomegaset = sectionlength/(Nsn-1);
        omegasection = (startsection+deltaomegaset):deltaomegaset:endsection;
        omegasettings = [omegasettings omegasection];
    end
end
    % Modeshapes:
mstmp = modeshapes;
modeshapes = zeros((Nmod*3),kmax);
for i = 1:Nmod % Eliminates cable displacement mode components
    i1 = (3*i) - 2;
    i2 = (4*i) - 3;
    modeshapes(i1:(i1+2),:) = [mstmp(i2,:);mstmp(i2+2,:);mstmp(i2+3,:)];
end
for i = 1:Nmod*3
    Amax = eliminationfactor*max(abs(modeshapes(i,:)));
    for j = 1:kmax
        if abs(modeshapes(i,j)) <= Amax
            modeshapes(i,j) = 0;
        end
```

```
    end
end
zerocol = 1;
while zerocol == 1
    if sum(modeshapes(:,kmax)) == 0
        kmax = kmax - 1;
    else
        zerocol = 0;
    end
end
modeshapes = modeshapes(:,1:kmax);
for i = 1:(Nmod*3) % Control of consistent mode component parity
    wavenumbersi = 0.5*setdiff((modeshapes(i,1:kmax)~=0).*(1:kmax),0);
    parity = sum(wavenumbersi==round(wavenumbersi));
    if (parity ~= 0) && (parity ~= length(wavenumbersi))
        disp([' OBS! Mode ' num2str(ceil(i/3)) ', component ' num2str(i-floor(i/3))])
        disp('       consists of terms with different parity!')
        return
    end
end
modeparM = zeros(3,Nmod); % "MODE PARity Matrix"
for i1 = 1:Nmod % Production of "modeparmat"!
    for i2 = 1:3
        i = (3*(i1-1)) + i2;
        j = 1;
        while (j <= kmax)
            if modeshapes(i,j) == 0
                j = j + 1;
            else
                if floor(j/2) == (j/2) % j even
                    modeparM(i2,i1) = 2;
                else % j odd
                    modeparM(i2,i1) = 1;
                end
                break
            end
        end
    end
end
PHIrx = zeros(3,Nmod);
for j = 1:Nmod % Production of modal matrix evaluated at "xevaluation"
    for i = 1:3
        if modeparM(i,j) ~= 0
            row = ((j-1)*3) + i;
            f = 0;
            for k = 1:kmax
                f = f + (modeshapes(row,k))*sin(k*pi*xresponse);
            end
            PHIrx(i,j) = f;
        end
    end
end
indexMJ = [1 1;2 2;2 3;3 2;3 3];
numnzeJ = 0; % NUMber of Non Zero Entries in J
snzeJ = []; % "Specified Non Zero Components of (phi,i)'*Sqq*(pji,j)"
for i = 1:Nmod % Collecting nonzero terms of Jij (upper part + diagonal)
    for j = i:Nmod
        nzt = 0; % "index for possible nonzero term"
        for k = 1:5
            parcheck = (modeparM(indexMJ(k,1),i))*(modeparM(indexMJ(k,2),j));
            if (parcheck == 1) || (parcheck == 4) % equal parity and non-zero
                nzt = k; % add term number for further investigation
                break % only one is possible for every pair {i,j}
            end
        end
        if nzt ~= 0 % term with equal parity at position i,j
            numnzeJ = numnzeJ + 1;
            snzeJ(numnzeJ,1:3) = [i j nzt];
        end
    end
end
if calctype == 1
    % Mean response prerequisites:
    indexmatRM = (modeparM'==1);
    ImatRM = zeros(Nmod,3);
    infomatRM = [];
    pseudosumcomps = sum(indexmatRM.*[ones(Nmod,1),2*ones(Nmod,1),3*ones(Nmod,1)],2);
```

```
    for i = 1:Nmod
        if pseudosumcomps(i) ~= 0
            infomatRM = [infomatRM;pseudosumcomps(i)];
        end
    end
    infomatRM = [setdiff(sum(indexmatRM,2).*(1:Nmod)',0),infomatRM];
    for i = 1:size(infomatRM,1)
        rowMS = (3*(infomatRM(i,1)-1))+infomatRM(i,2);
        I = 0;
        for j = 1:2:kmax % odd modes only (even integrates to zero)
            I = I + (2/(j*pi))*modeshapes(rowMS,j);
        end
        ImatRM(infomatRM(i,1),infomatRM(i,2)) = I;
    end
    qmeancoeff = [[ar*CD;0;0],[0;ar+dCL0;B*dCM0]];
end
disp('   Prelim. calcs. done!')
    % Aerodynamic derivatives, aerodynamic stiffness and damping:
adcKae = load('adcoeffKae.txt');
adcKae = diag([1 B B (B^2)])*adcKae;
adcCae = load('adcoeffCae.txt');
adcCae(1,3) = -2*CD*ar; % "CD" needs no scaling since an = bn = 0
adcCae = diag([1 1 B B (B^2)])*adcCae;
%
CCae = 0.25*rho*(B^2);
CKae = 0.5*rho*(B^2);
indexMAE = [1 1;2 2;2 3;3 2;3 3];
termCae = []; % NUMber of non zero TERMS at CAE,ij
resptermsCae = []; % respective non zero TERMS at CAE,ij
respICae = []; % Respective Non Zero Integrals at CAE,ij
numenCae = 0; % NUMber of non zero ENtries in CAE
termKae = []; % NUMber of non zero TERMS at KAE,ij
resptermsKae = []; % respective non zero TERMS at KAE,ij
respIKae = []; % Respective Non Zero Integrals at KAE,ij
numenKae = 0; % NUMber of non zero ENtries in KAE
% Collection, systematization, and descr. of nonzero terms in Cae and Kae
for i = 1:Nmod
    Mi = modmass(i);
    factorCae = CCae/(Mi*eigenfreq(i));
    factorKae = CKae/Mi;
    for j = 1:Nmod
        nt = 0; % Non zero Terms at cae,ij
        rrI = 0; % respective Row Integral at cae,ij
        rrt = 0; % respective Row Term at cae,ij\
        for k = 1:5
            parcheck = (modeparM(indexMAE(k,1),i))*(modeparM(indexMAE(k,2),j));
            if (parcheck == 1) || (parcheck == 4) % True: Possibly terms with equal
wavenumber!
                nt = 1;
                rrt = k;
                break
            end
        end
        if nt == 1 % True: Possibly nonzero term. Further investigation needed
            rowik = ((i-1)*3) + indexMAE(rrt,1);
            rowjl = ((j-1)*3) + indexMAE(rrt,2);
            I = 0;
            for i1 = 1:kmax
                ampik = modeshapes(rowik,i1);
                if ampik ~= 0
                    for j1 = 1:kmax
                        ampjl = modeshapes(rowjl,j1);
                        if (ampjl ~= 0) && (i1 == j1)
                            I = I + ampik*ampjl;
                        end
                    end
                end
            end
            I = 0.5*L*I;
            if I ~= 0 % Term is non-zero by integral test!
                numenCae = numenCae + 1;
                termCae(numenCae,1:3) = [i j rrt];
                respICae(numenCae,1) = I*factorCae;
                if rrt >= 2 % not also a non-zero term in Kae!
                    numenKae = numenKae + 1;
                    termKae(numenKae,1:3) = [i j (rrt-1)];
                    respIKae(numenKae,1) = I*factorKae;
```

```
                end
            end
        end
    end
end
if (calctype==1) && (ismember(4,modulationtypes)==1)
    % Averages, WK model:
    npavg = 500;
    avgirr = [1,round(nTUSE/(npavg-1):nTUSE/(npavg-1):nTUSE)];
    if (spectrumtype == 1) || (spectrumtype == 3) % Kaimal
        Ekaimalu =
sum(((TcharIP(Tcharmethod,avgirr,1)).*((1+SgKu(2)*(omegasettings')*TcharIP(Tcharmethod,avgirr,
1)/Tcharavg(1,Tcharmethod)).^SgKu(3))),2)/npavg;
        Ekaimalw =
sum(((TcharIP(Tcharmethod,avgirr,2)).*((1+SgKw(2)*(omegasettings')*TcharIP(Tcharmethod,avgirr,
2)/Tcharavg(2,Tcharmethod)).^SgKw(3))),2)/npavg;
    end
    if (spectrumtype == 2) || (spectrumtype == 3) % von Kármán
        Evonkarmanu =
sum(((TcharIP(Tcharmethod,avgirr,1)).*((1+SgvKu(2)*((omegasettings')*TcharIP(Tcharmethod,avgir
r,1)/Tcharavg(1,Tcharmethod)).^2).^SgvKu(3))),2)/npavg;
        Evonkarmanw =
sum(((TcharIP(Tcharmethod,avgirr,1)).*(1+SgvKw(2)*((omegasettings')*TcharIP(Tcharmethod,avgirr
,1)/Tcharavg(1,Tcharmethod)).^2).*((1+SgvKw(3)*((omegasettings')*TcharIP(Tcharmethod,avgirr,1)
/Tcharavg(1,Tcharmethod)).^2).^SgvKw(4))),2)/npavg;
    end
end
%
CSetaRM = rho*B*L/2;
kappaae = zeros(Nmod);
zetaae = zeros(Nmod);
Hsub = zeros(Nmod);
omegamat1 = diag(1./eigenfreq);
omegamat2 = omegamat1.^2;
moddampM = diag(moddamping).*omegamat1;
IDmat = eye(Nmod);
KiKj = (diag(1./modstiffn)*ones(Nmod)).*(ones(Nmod)*diag(1./modstiffn));
%
if calctype == 1
    irr = [1,round(nTUSE/(rfT-1):nTUSE/(rfT-1):nTUSE)];
    TR = Tplot(irr);
    UWmeanR = Umean(:,istart-1+irr);
    Rmean = zeros(3,rfT);
    varTmat = zeros(3,rfT,max(modulationtypes));
    varTmatdr = varTmat;
    CovmatR = zeros(3,NOsetR);
    CovmatdR = CovmatR;
    %
    ipft = (1/nipEPSDt):(1/nipEPSDt):1;
    IPtEPSDplot = zeros(1,(rfT-1)*nipEPSDt+1);
    IPomegaEPSDplot = omegasettings(1);
    IPFmatomega = zeros(2,NOsetR);
    kIPomega = nipomegainit*IPomegaEPSDplot/(omegasettings(2)-omegasettings(1));
    for wn = 2:NOsetR
        omega = omegasettings(wn-0);
        domegawn = omegasettings(wn) - omegasettings(wn-1);
        nipfomega = ceil(domegawn*kIPomega/omega);
        IPFmatomega(wn) = nipfomega;
        ipfomega = (1/nipfomega):(1/nipfomega):1.00001;
        IPomegaEPSDplot = [IPomegaEPSDplot,omegasettings(wn-1) + (omegasettings(wn)-
omegasettings(wn-1))*ipfomega];
    end
    nIPomegaEPSDplot = length(IPomegaEPSDplot);
    for ti = 2:rfT
        i1 = nipEPSDt*ti - (2*nipEPSDt) + 2;
        i2 = i1 + nipEPSDt - 1;
        IPtEPSDplot(i1:i2) = TR(ti-1) + (TR(ti)-TR(ti-1))*ipft;
    end
    %
    uEPSD = zeros((rfT-1)*nipEPSDt+1,nIPomegaEPSDplot,4); % x:omega, y:t, stacks: methods of
moduation
    wEPSD = uEPSD; % verical turbulence component
    RyEPSD = uEPSD; % horizontal response
    RzEPSD = uEPSD; % vertical response
    RthetaEPSD = uEPSD; % torsional response
end
%
```

```
if calctype == 1
    Test = rfT*NOsetR/971;
    disp(['Estimated computational time:  ' num2str(Test) ' seconds'])
    disp(['Estimated completion at:       ' num2str(datestr(datenum(clock + [0 0 0 0 0 
Test]))))])
elseif calctype == 2
    Test = rfT*NOsetH/67276;
    disp(['Estimated computational time:  ' num2str(Test) ' seconds'])
    disp(['Estimated completion at:       ' num2str(datestr(datenum(clock + [0 0 0 0 0 
Test]))))])
end
tic
return
WNtime = zeros(4,NOsetR);
for ti = 1:rfT
    if calctype == 1
        V = UWmeanR(1,ti); % Mean wind speed, U
        W = UWmeanR(2,ti); % Mean wind speed, W
        varu = varuw(1,irr(ti)); % variance, u
        varw = varuw(2,irr(ti)); % variance, w
        TCu = TcharIP(Tcharmethod,irr(ti),1); % Time scale
        TCw = TcharIP(Tcharmethod,irr(ti),2); % Time scale
        TCurel = TCu/Tcharavg(1,Tcharmethod); % Relative time scale
        TCwrel = TCw/Tcharavg(2,Tcharmethod); % Relative time scale
    elseif calctype == 2
        V = Vsettings(ti);
    end
    Vreli = (V/B)./eigenfreq;
    CSeta = ((rho*V*B*L/2)^2);
    % Establishment of "zetaae"
    Vih = Vreli(termCae(1,1));
    Vihmat = [(Vih^3);(Vih^2);Vih;1];
    coeffzeta = adcCae*Vihmat; % columnvector
    iprev = termCae(1,1);
    for row = 1:numenCae
        i = termCae(row,1);
        if i ~= iprev % True: Arriving new row in "zetaae"! Refresh coefficients!
            Vih = Vreli(i);
            Vihmat = [(Vih^3);(Vih^2);Vih;1];
            coeffzeta = adcCae*Vihmat;
            iprev = i;
        end
        zetaae(i,termCae(row,2)) = respICae(row)*coeffzeta(termCae(row,3));
    end
    % Establishment of "kappaae"
    Vih = Vreli(termKae(1,1));
    Vihmat = [(Vih^3);(Vih^2);Vih;1];
    coeffkappa = adcKae*Vihmat;
    iprev = termKae(1,1);
    for row = 1:numenKae % Production of "kappaae"
        i = termKae(row,1);
        if i ~= iprev % True: Arriving new row in "kappaae"! Refresh coefficients!
            Vih = Vreli(i);
            Vihmat = [(Vih^3);(Vih^2);Vih;1];
            coeffkappa = adcKae*Vihmat; % columnvector
            iprev = i;
        end
        kappaae(i,termKae(row,2)) = respIKae(row)*coeffkappa(termKae(row,3));
    end
    if calctype == 1
        for modform = modulationtypes
            for wn = 1:NOsetR
                WNT1 = toc;
                omega = omegasettings(wn);
                omegasq = omega^2;
                omegarel = omega/V;
                % Establishment of dynamic amplification matrix, H:
                for i = 1:Nmod
                    Hsub(i,i) = omegamat2(i,i)*omegasq;
                end
                H = inv(IDmat - kappaae - Hsub + 2*imagunit*omega*(moddampM - zetaae));
                WNtime(1,wn) = toc - WNT1;
                WNT2 = toc;
                % Production of the joint acceptance function matrix
                if modform == 1 % stationary turbulence components
                    if (spectrumtype == 1) || (spectrumtype == 3) % Kaimal
                        Su1 = uwvarcontrol(1)*SgKu(1)*(1+SgKu(2)*omega)^SgKu(3);
```

```
                        Sw1 = uwvarcontrol(2)*SgKw(1)*(1+SgKw(2)*omega)^SgKw(3);
                    end
                    if (spectrumtype == 2) || (spectrumtype == 3) % von Kármán
                        Su2 = uwvarcontrol(1)*SgvKu(1)*(1+SgvKu(2)*omegasq)^SgvKu(3);
                        Sw2 =
uwvarcontrol(2)*SgvKw(1)*(1+SgvKw(2)*omegasq)*((1+SgvKw(3)*omegasq)^SgvKw(4));
                    end
                elseif modform == 2 % uniformly modulated turbulence components
                    if (spectrumtype == 1) || (spectrumtype == 3) % Kaimal
                        Su1 = varu*SgKu(1)*(1+SgKu(2)*omega)^SgKu(3);
                        Sw1 = varw*SgKw(1)*(1+SgKw(2)*omega)^SgKw(3);
                    end
                    if (spectrumtype == 2) || (spectrumtype == 3) % von Kármán
                        Su2 = varu*SgvKu(1)*(1+SgvKu(2)*omegasq)^SgvKu(3);
                        Sw2 =
varw*SgvKw(1)*(1+SgvKw(2)*omegasq)*((1+SgvKw(3)*omegasq)^SgvKw(4));
                    end
                elseif modform == 3 % non-uniformly modulated, XC model
                    if (spectrumtype == 1) || (spectrumtype == 3) % Kaimal
                        Su1 = varu*SgKu(1)*TCurel*((1+SgKu(2)*TCurel*omega)^SgKu(3));
                        Sw1 = varw*SgKw(1)*TCwrel*((1+SgKw(2)*TCwrel*omega)^SgKw(3));
                    end
                    if (spectrumtype == 2) || (spectrumtype == 3) % von Kármán
                        Su2 = varu*SgvKu(1)*TCurel*(1+SgvKu(2)*((TCurel*omega)^2))^SgvKu(3);
                        Sw2 =
varw*SgvKw(1)*TCwrel*(1+SgvKw(2)*((TCwrel*omega)^2))*((1+SgvKw(3)*((TCwrel*omega)^2))^SgvKw(4)
);
                    end
                elseif modform == 4 % non-uniformly modulated, WK model
                    if (spectrumtype == 1) || (spectrumtype == 3) % Kaimal
                        Su1 =
varu*TCu*((1+SgKu(2)*TCurel*omega)^SgKu(3))/Ekaimalu(wn)*SgKu(1)*((1+SgKu(2)*omega)^SgKu(3));
                        Sw1 =
varw*TCw*((1+SgKw(2)*TCwrel*omega)^SgKw(3))/Ekaimalw(wn)*SgKw(1)*((1+SgKw(2)*omega)^SgKw(3));
                    end
                    if (spectrumtype == 2) || (spectrumtype == 3) % von Kármán
                        Su2 =
varu*TCu*((1+SgvKu(2)*(TCurel*omega)^2)^SgvKu(3))/Evonkarmanu(wn)*SgvKu(1)*((1+SgvKu(2)*omegas
q)^SgvKu(3));
                        Sw2 =
varw*TCw*(1+SgvKw(2)*(TCwrel*omega)^2)*((1+SgvKw(3)*(TCwrel*omega)^2)^SgvKw(4))/Evonkarmanw(wn
)*SgvKw(1)*(1+SgvKw(2)*omegasq)*((1+SgvKw(3)*omegasq)^SgvKw(4));
                    end
                end
                % Use the average of Kaimal and von Karman spectral values!
                if spectrumtype == 1
                    Su = Su1;
                    Sw = Sw1;
                elseif spectrumtype == 2
                    Su = Su2;
                    Sw = Sw2;
                elseif spectrumtype == 3 % Average
                    Su = 0.5*(Su1+Su2);
                    Sw = 0.5*(Sw1+Sw2);
                end
                WNtime(2,wn) = toc - WNT2;
                WNT3 = toc;
                dCL = dCL0/((1+(AndCL*omegarel))^bndCL);
                dCM = dCM0/((1+(AndCM*omegarel))^bndCM);
                CoeffJij = zeros(5,1);
                CoeffJij(1,1) = Su*4*ar*(CD^2);
                CoeffJij(2,1) = Sw*(dCL+(ar*CD))^2;
                CoeffJij(3,1) = Sw*B*dCM*(dCL+(ar*CD));
                CoeffJij(4,1) = CoeffJij(3,1);
                CoeffJij(5,1) = Sw*(B*dCM)^2;
                CCo = -omegarel*[Cux;Cwx;Cwx;Cwx;Cwx];
                J = zeros(Nmod);
                for row = 1:numnzeJ
                    i = snzeJ(row,1);
                    j = snzeJ(row,2);
                    term = snzeJ(row,3); % rowvector
                    Coeff = CoeffJij(term); % columnvector
                    rowik = ((i-1)*3) + indexMJ(term,1);
                    rowjl = ((j-1)*3) + indexMJ(term,2);
                    c = CCo(term);
                    csq = c^2;
                    epc = exp(c);
```

```
                    I = 0;
                    for i1 = 1:kmax % a
                        Aik = modeshapes(rowik,i1);
                        if Aik ~= 0
                            a = pi*i1;
                            asq = a^2;
                            f1 = 1/(asq+csq);
                            f2 = 1-epc*cos(a);
                            for j1 = 1:kmax % b
                                Ajl = modeshapes(rowjl,j1);
                                if Ajl ~= 0
                                    b = pi*j1;
                                    if i1 == j1
                                        I = I + 2*Aik*Ajl*f1*(asq*f1*f2-c/2);
                                    else
                                        aplusb = (a+b);
                                        aminusb = (a-b);
                                        I = I + Aik*Ajl*(((cos(aminusb)-
1)/aminusb+(cos(aplusb)-1)/aplusb)/2+a*f1*f2)*2*b/((b^2)+csq);
                                    end
                                end
                            end
                        end
                    end
                    term = I;
                    J(i,j) = term*Coeff;
                    if i ~= j
                        J(j,i) = term*Coeff;
                    end
                end
                WNtime(3,wn) = toc - WNT3;
                WNT4 = toc;
                J = J.*KiKj;
                SRR = CSeta*PHIrx*real(transpose(H')*J*transpose(H))*transpose(PHIrx);
                SdRR = SRR*omegasq;
                Sry = SRR(1,1);
                Srz = SRR(2,2);
                Srtheta = SRR(3,3);
                Sdry = SdRR(1,1);
                Sdrz = SdRR(2,2);
                Sdrtheta = SdRR(3,3);
                CovmatR(1:3,wn) = [Sry;Srz;Srtheta];
                CovmatdR(1:3,wn) = [Sdry;Sdrz;Sdrtheta];
                % Interpolation of all EPSDs
                tiIP = nipEPSDt*ti - nipEPSDt + 1;
                if wn == 1
                    Suprev = Su;
                    Swprev = Sw;
                    Sryprev = Sry;
                    Srzprev = Srz;
                    Srthetaprev = Srtheta;
                    uEPSD(tiIP,1,modform) = Su;
                    wEPSD(tiIP,1,modform) = Sw;
                    RyEPSD(tiIP,1,modform) = Sry;
                    RzEPSD(tiIP,1,modform) = Srz;
                    RthetaEPSD(tiIP,1,modform) = Srtheta;
                    i2 = 1;
                else
                    nipfomega = IPFmatomega(wn);
                    ipfomega = (1/nipfomega):(1/nipfomega):1.00001;
                    i1 = i2 + 1;
                    i2 = i1 + nipfomega - 1;
                    uEPSD(tiIP,i1:i2,modform) = Suprev + (Su-Suprev)*ipfomega;
                    wEPSD(tiIP,i1:i2,modform) = Swprev + (Sw-Swprev)*ipfomega;
                    RyEPSD(tiIP,i1:i2,modform) = Sryprev + (Sry-Sryprev)*ipfomega;
                    RzEPSD(tiIP,i1:i2,modform) = Srzprev + (Srz-Srzprev)*ipfomega;
                    RthetaEPSD(tiIP,i1:i2,modform) = Srthetaprev + (Srtheta-
Srthetaprev)*ipfomega;
                    Suprev = Su;
                    Swprev = Sw;
                    Sryprev = Sry;
                    Srzprev = Srz;
                    Srthetaprev = Srtheta;
                end
                WNtime(4,wn) = toc - WNT4;
            end
            if ti >= 2
```

```
                i1 = nipEPSDt*ti - (2*nipEPSDt) + 2;
                i2 = i1 + nipEPSDt - 1;
                uEPSD(i1:i2-1,:,modform) = uEPSD(i1-1,:,modform) + ((ipft(1:end-
1))')*(uEPSD(i2,:,modform)-uEPSD(i1-1,:,modform));
                wEPSD(i1:i2-1,:,modform) = wEPSD(i1-1,:,modform) + ((ipft(1:end-
1))')*(wEPSD(i2,:,modform)-wEPSD(i1-1,:,modform));
                RyEPSD(i1:i2-1,:,modform) = RyEPSD(i1-1,:,modform) + ((ipft(1:end-
1))')*(RyEPSD(i2,:,modform)-RyEPSD(i1-1,:,modform));
                RzEPSD(i1:i2-1,:,modform) = RzEPSD(i1-1,:,modform) + ((ipft(1:end-
1))')*(RzEPSD(i2,:,modform)-RzEPSD(i1-1,:,modform));
                RthetaEPSD(i1:i2-1,:,modform) = RthetaEPSD(i1-1,:,modform) + ((ipft(1:end-
1))')*(RthetaEPSD(i2,:,modform)-RthetaEPSD(i1-1,:,modform));
            end
            varTmat(:,ti,modform) = CovmatR*(omegaweights');
            varTmatdr(:,ti,modform) = CovmatdR*(omegaweights');
        end
    elseif calctype == 2
        for wn = 1:NOsetH
            omega = omegasettingsH(wn);
            omegasq = omega^2;
            omegarel = omega/V;
            % Establishment of dynamic amplification matrix, H:
            for i = 1:Nmod
                Hsub(i,i) = omegamat2(i,i)*omegasq;
            end
            Hplot(ti,wn) = (abs(1/det(IDmat - kappaae - Hsub + 2*imagunit*omega*(moddampM -
zetaae))));
        end
    end
    if calctype == 1
        Rmean(:,ti) = CSetaRM*PHIrx*inv(IDmat-
kappaae)*inv(diag(modstiffn))*ImatRM*((V^2)*qmeancoeff(:,1)+(V*W)*qmeancoeff(:,2));
    end
end
grosstime = toc;
% CDF and pdf of maximum reponse:
drymax = 0.001;
drzmax = 0.0002;
drthetamax = (10^-3)*0.01;
RYmax = 1.3:drymax:2.8;
RZmax = 0.4:drzmax:0.85;
RTHETAmax = 0.014:drthetamax:0.028;
CDFRy = zeros(4,length(RYmax));
CDFRz = zeros(4,length(RZmax));
CDFRtheta = zeros(4,length(RTHETAmax));
pdfRy = 0;
pdfRz = 0;
pdfRtheta = 0;
for j = modulationtypes
    if rfT == 1
        for i = 1:length(RYmax)
            CDFRy(j,i) = exp(-
TUSE*(1/(2*pi))*(sqrt(varTmatdr(1,:,j))./sqrt(varTmat(1,:,j))).*exp(-0.5*((RYmax(i)-
Rmean(1,:)).^2)./varTmat(1,:,j)));
        end
        for i = 1:length(RZmax)
            CDFRz(j,i) = exp(-
TUSE*(1/(2*pi))*(sqrt(varTmatdr(2,:,j))./sqrt(varTmat(2,:,j))).*exp(-0.5*((RZmax(i)-
Rmean(2,:)).^2)./varTmat(2,:,j)));
        end
        for i = 1:length(RTHETAmax)
            CDFRtheta(j,i) = exp(-
TUSE*(1/(2*pi))*(sqrt(varTmatdr(3,:,j))./sqrt(varTmat(3,:,j))).*exp(-0.5*((RTHETAmax(i)-
Rmean(3,:)).^2)./varTmat(3,:,j)));
        end
    else
        for i = 1:length(RYmax)
            amat =  (1/(2*pi))*(sqrt(varTmatdr(1,:,j))./sqrt(varTmat(1,:,j))).*exp(-
0.5*((RYmax(i)-Rmean(1,:)).^2)./varTmat(1,:,j));
            CDFRy(j,i) = exp(-0.5*(amat(1) + amat(end) + 2*sum(amat(2:end-1)))*TUSE/(rfT-1));
        end
        for i = 1:length(RZmax)
            amat =  (1/(2*pi))*(sqrt(varTmatdr(2,:,j))./sqrt(varTmat(2,:,j))).*exp(-
0.5*((RZmax(i)-Rmean(2,:)).^2)./varTmat(2,:,j));
            CDFRz(j,i) = exp(-0.5*(amat(1) + amat(end) + 2*sum(amat(2:end-1)))*TUSE/(rfT-1));
        end
        for i = 1:length(RTHETAmax)
```

```
            amat =  (1/(2*pi))*(sqrt(varTmatdr(3,:,j))./sqrt(varTmat(3,:,j))).*exp(-
0.5*((RTHETAmax(i)-Rmean(3,:)).^2)./varTmat(3,:,j));
            CDFRtheta(j,i) = exp(-0.5*(amat(1) + amat(end) + 2*sum(amat(2:end-1)))*TUSE/(rfT-
1));
        end
    end
    for i = 2:(length(RYmax)-1)
        pdfRy(j,i-1) = 0.5*(CDFRy(j,i+1)-CDFRy(j,i-1))/drymax;
    end
    for i = 2:(length(RZmax)-1)
        pdfRz(j,i-1) = 0.5*(CDFRz(j,i+1)-CDFRz(j,i-1))/drzmax;
    end
    for i = 2:(length(RTHETAmax)-1)
        pdfRtheta(j,i-1) = 0.5*(CDFRtheta(j,i+1)-CDFRtheta(j,i-1))/drthetamax;
    end
end
% Quantiles and expected values:
q = 0.99;
Ey = zeros(4,1);
Ez = Ey;
Etheta = Ey;
Qy = Ey;
Qz = Ey;
Qtheta = Ey;
for i = modulationtypes
    Ey(i) = sum(pdfRy(i,:).*RYmax(2:end-1)*drymax);
    Ez(i) = sum(pdfRz(i,:).*RZmax(2:end-1)*drzmax);
    Etheta(i) = sum(pdfRtheta(i,:).*RTHETAmax(2:end-1)*drthetamax);
    Qy(i) = RYmax(setdiff((abs(CDFRy(i,:)-q)==min(abs(CDFRy(i,:)-q))).*(1:length(RYmax)),0));
    Qz(i) = RZmax(setdiff((abs(CDFRz(i,:)-q)==min(abs(CDFRz(i,:)-q))).*(1:length(RZmax)),0));
    Qtheta(i) = RTHETAmax(setdiff((abs(CDFRtheta(i,:)-q)==min(abs(CDFRtheta(i,:)-
q))).*(1:length(RTHETAmax)),0));
end
%
```

B.1.4 Quasi-static mean response control

```
%
% Fourier series expansion of U^2 and UW:
Usq(1,1:nU) = (Umean(1,:)).^2;
Usq(2,1:nU) = Umean(1,:).*Umean(2,:);
omegamaxUMR = omegamaxUM;
omegasettingsUMR = domega:domega:omegamaxUMR;
NOsetUMR = length(omegasettingsUMR);
compmatUMR = zeros(NOsetUMR,4);
Usqavg(1:2,1) = [Usq(1,1)+Usq(1,nU)+2*sum(Usq(1,2:end-
1));Usq(2,1)+Usq(2,nU)+2*sum(Usq(2,2:end-1))]*0.5/(nU-1);
UmeanFSE = zeros(2,nU) + [Usqavg(1,1);Usqavg(2,1)].*ones(2,nU); % Umean Fourier Series
Expansion
for wn = 1:NOsetUMR
    omega = omegasettingsUMR(wn);
    for v = 1:2
        ak = 0;
        bk = 0;
        for j = 2:nU
            t0 = T(j-1);
            t1 = T(j);
            s = (Usq(v,j)-Usq(v,j-1))/dt;
            p = Usq(v,j-1) - s*t0;
            ak = ak + p/omega*sin(omega*t1)+s/(omega^2)*(omega*t1*sin(omega*t1)+cos(omega*t1))
- (p/omega*sin(omega*t0)+s/(omega^2)*(omega*t0*sin(omega*t0)+cos(omega*t0)));
            bk = bk + s/(omega^2)*(sin(omega*t1)-omega*t1*cos(omega*t1))-p/omega*cos(omega*t1)
- (s/(omega^2)*(sin(omega*t0)-omega*t0*cos(omega*t0))-p/omega*cos(omega*t0));
        end
        ak = ak*2/TU;
        bk = bk*2/TU;
        compmatUMR(wn,(v-1)*2+[1,2]) = [ak,bk];
        UmeanFSE(v,:) = UmeanFSE(v,:) + ak*cos(omega*T) + bk*sin(omega*T);
    end
end
% Quasistatic mean:
rfT = 1500;
irr = [1,round(nTUSE/(rfT-1):nTUSE/(rfT-1):nTUSE)];
TR = T(istart-1+irr);
TRplot = TR-TR(1);
UsqR = UmeanFSE(:,istart-1+irr); % [U^2;UW]
```

```
RmeanQS = zeros(3,rfT);
CSetaRM = rho*B*L/2;
IDmat = eye(Nmod);
for ti = 1:rfT
    RmeanQS(:,ti) =
CSetaRM*PHIrx*IDmat*inv(diag(modstiffn))*ImatRM*((UsqR(1,ti))*qmeancoeff(:,1)+(UsqR(2,ti))*qme
ancoeff(:,2));
end
% Steady-state mean:
Cdmat = CSetaRM*[ar*0.7;ar+dCL0;B*dCM0];
rows = [1 4 5 6 9 10 13 15 17]; % non-zero contributing modes
cols = [1 3 1 3 1  3  3  3  3]; % start column in compmatUMR
comp = [1 2 1 2 1  2  3  3  3]; % component
nzcM = length(rows);
etaR = zeros(Nmod,rfT);
for i = 1:nzcM
    row = rows(i);
    A = Cdmat(comp(i))*ImatRM(row,comp(i));
    K = modstiffn(row);
    etaR(row,:) = Usqavg((comp(i)==1)+2*(comp(i)>=2))*ones(1,rfT);
    zeta = moddamping(row);
    omeganat = eigenfreq(row);
    col = cols(i);
    for k = 1:NOsetUMR
        omega = omegasettingsUMR(k);
        xi = omega/omeganat;
        Hsq = 1/(((1-(xi^2))^2)+((2*xi*zeta)^2));
        aki = compmatUMR(k,col);
        bki = compmatUMR(k,col+1);
        alphaki = aki*(1-(xi^2))-bki*2*zeta*xi;
        betaki = aki*2*zeta*xi+bki*(1-(xi^2));
        for ti = 1:rfT
            t = TR(ti);
            etaR(row,ti) = etaR(row,ti) + Hsq*(alphaki*cos(omega*t)+betaki*sin(omega*t));
        end
    end
    etaR(row,:) = etaR(row,:)*A/K;
end
RmeanSS = PHIrx*etaR;
%
```

B.1.5 Monte Carlo simulation of time domain SDOF system response

```
%
inputmethod = 2; % 1: U(t) and var(t) from UEMDWD. 2: U(t) function and turbulence intensity
constant
Tscalemethod = 2; % 1: Duration, 2: Integral. (only for inputmethod = 1 and modulationmethod =
2!)
%
ASg = 40.8;
BSg = 50.2;
nSg = -1.6;
%
ipfF = 3; % interpolatoin factor for F
Ta = -1200; % "initial stabilazatoin set-off [s]
Tavgspan = 10; % averaging span for response variance calculation [s]
varavgres = 1; % time resolution of response variance averaging [s]
rft = 500; % # time points for freq. dom. variance calc.
MCsimpoints = 4000;
domega = 2*pi/1500;
omegamin = omegamaxUM;
omegamax = 0.5;
omegasettingsMC =
unique([omegamin:domega:0.31,0.31:(domega/2):0.317,0.317:(domega/4):0.319,0.319:(domega/8):0.3
21,0.321:(domega/4):0.323,0.323:(domega/2):0.33,0.33:domega:omegamax]);
domegamatMC = omegasettingsMC(2:end) - omegasettingsMC(1:end-1);
omegasettingsMC = 0.5*(omegasettingsMC(1:end-1)+omegasettingsMC(2:end)); % midpoint rule
NOsetMC = length(omegasettingsMC);
% U(t) function (inputmethod == 2):
BW = [12.5 5 2];
if inputmethod == 2
    TUSE = 3600;
    Tplot = 0:dt:TUSE;
    nTUSE = length(Tplot);
    U2 = 15 + 20*exp(-((Tplot-1800)/(60*BW(ijk))).^2);
    Iu = 0.16;
```

```
end
%  Frequency domain response:
PHIrx = 1.0365; % mode shape value at midspan
omega1 = 0.32;
I1 = 0.64450921;
I2 = 0.50073574;
irr = round(1:(nTUSE-1)/(rft-1):(nTUSE+1.1));
TplotSDOF = (irr-1)*dt;
if inputmethod == 1
    zeta = 0.005 + rho*CD*D*L*I2*Umean(1,istart-1+irr)/(2*omega1*modmass(1));
elseif inputmethod == 2
    zeta = 0.005 + rho*CD*D*L*I2*U2(irr)/(2*omega1*modmass(1));
end
mM = modmass(1);
mK = mM*(omega1^2);
ryvarT = zeros(1,rft); % structural displacement
dryvarT = ryvarT; % structural velocity
for i = 1:rft
    if inputmethod == 1
        V = Umean(1,istart-1+irr(i));
        varu = varuw(1,irr(i));
    elseif inputmethod == 2
        V = U2(irr(i));
        varu = (V*Iu)^2;
    end
    CT = (PHIrx^2)*((rho*V*D*L*CD*I1/mK)^2)*varu;
    int1 = 0;
    int2 = 0;
    for wn = 1:NOsetMC
        omega = omegasettingsMC(wn);
        ksi = (omega/omega1);
        Hsq = 1/(((1-(ksi^2))^2)+((2*zeta(i)*ksi)^2));
        Sg = ASg*((1+BSg*omega)^nSg);
        int1 = int1 + Hsq*Sg*domegamatMC(wn);
        int2 = int2 + (omega^2)*Hsq*Sg*domegamatMC(wn);
    end
    ryvarT(i) = CT*int1;
    dryvarT(i) = CT*int2;
end
if inputmethod == 1
    rymeanT = (0.5*PHIrx*I1*rho*D*CD*L/mK)*(Umean(1,istart:iend).^2);
elseif inputmethod == 2
    rymeanT = (0.5*PHIrx*I1*rho*D*CD*L/mK)*(U2.^2);
end
% MC simulation:
ispanavg = Tavgspan/varavgres;
avgspanratio = varavgres/dt;
kCD = PHIrx*rho*D*CD*L*I1;
TF1 = unique([Ta:dt*ipfF:0,Tplot(1:ipfF:end),TUSE:dt*ipfF:TUSE+Tavgspan]); % Time values for
F1
nTF1 = length(TF1);
TF = Ta:dt:(TUSE+Tavgspan);
if inputmethod == 1
    Uhist = [ones(1,round(-
Ta/dt))*Umean(1,istart),Umean(1,istart:iend),ones(1,round(Tavgspan/dt))*Umean(1,iend)];
elseif inputmethod == 2
    Uhist = [ones(1,round(-Ta/dt))*U2(1),U2,ones(1,round(Tavgspan/dt))*U2(end)];
end
mC = 2*0.005*mM*omega1 + rho*CD*D*L*I2*Uhist;
nTF = nTUSE + round(-Ta/dt) + round(Tavgspan/dt);
TFvaravg = 0:varavgres:TUSE; % center time values for resposne variance calc.
ipf = (1/ipfF):(1/ipfF):1.001;
istartavg = -(Ta/dt) + 1;
iendavg = istartavg + nTUSE - 1;
varR = zeros(1,(nTUSE-1)/avgspanratio+1);
MCvarR = varR;
maxrespvect = zeros(1,MCsimpoints);
tic
Test = MCsimpoints*(TUSE-Ta)/6000*0.38;
disp(['Estimated computational time:  ' num2str(Test) ' seconds'])
disp(['Initialized at:                ' num2str(datestr(datenum(clock)))])
disp(['Estimated completion at:       ' num2str(datestr(datenum(clock + [0 0 0 0 0 Test]))))])
for i = 1:MCsimpoints
    % Generate unit variance signal
    F1 = zeros(1,nTF1);
    for wn = 1:NOsetMC
        omega = omegasettingsMC(wn);
```

```
        domega = domegamatMC(wn);
        pha = 2*pi*rand;
        c = sqrt(2*domega*ASg*((1+BSg*omega)^nSg));
        F1 = F1 + c*sin(omega*TF1-pha);
    end
    % Interpolate onto dt
    F = [F1(1),zeros(1,round((TUSE+Tavgspan-Ta)/dt))];
    j1 = 1;
    for j = 2:nTF1
        j1 = j1 + ipfF;
        F(j1-ipfF+1:j1) = F1(j-1) + ipf*(F1(j)-F1(j-1));
    end
    % Scale wrt. V and variance
    if inputmethod == 1
        F = kCD*F.*Uhist.*[ones(1,round(-
Ta/dt))*sqrt(varuw(1,1)),sqrt(varuw(1,1:nTUSE)),ones(1,round(Tavgspan/dt))*sqrt(varuw(1,nTUSE)
)];
    elseif inputmethod == 2
        F = kCD*Iu*F.*(Uhist.^2);
    end
    R = [0.0,zeros(1,(TUSE+Tavgspan-Ta)/dt);zeros(1,1+(TUSE+Tavgspan-Ta)/dt)]; % Response from
F
    % Calculate response
    for j = 2:nTF
        u11 = R(1,j-1);
        u12 = R(2,j-1);
        k1 = dt*[u12;(F(j-1)-mC(j-1)*u12-mK*u11)/mM];
        u21 = u11 + 0.5*k1(1);
        u22 = u12 + 0.5*k1(2);
        F2 = 0.5*(F(j-1)+F(j));
        mC2 = 0.5*(mC(j-1)+mC(j));
        k2 = dt*[u22;(F2-mC2*u22-mK*u21)/mM];
        u31 = u11 + 0.5*k2(1);
        u32 = u12 + 0.5*k2(2);
        k3 = dt*[u32;(F2-mC2*u32-mK*u31)/mM];
        u41 = u11 + k3(1);
        u42 = u12 + k3(2);
        k4 = dt*[u42;(F(j)-mC(j)*u42-mK*u41)/mM];
        R(:,j) = R(:,j-1) + (k1+(2*k2)+(2*k3)+k4)/6;
    end
    % find maximum response:
    [maxR,locmaxR] = max(R(1,istartavg:iendavg)+rymeanT);
    maxrespvect(i) = maxR;
    maxrespvectT(i) = (locmaxR-1)*dt;
    % estimate variance:
    varcomps = zeros(1,2*ispanavg);
    j1 = 0;
    for j = (istartavg-Tavgspan/dt):avgspanratio:(istartavg+(Tavgspan-varavgres)/dt)
        a = R(1,j);
        b = R(1,j+avgspanratio);
        j1 = j1 + 1;
        varcomps(j1) = ((a^2)+(a*b)+(b^2))/3;
    end
    varR(1) = sum(varcomps);
    j1 = 1;
    for j = (istartavg+avgspanratio):avgspanratio:iendavg
        j1 = j1 + 1;
        a = R(1,j);
        b = R(1,j+avgspanratio);
        vari = ((a^2)+(a*b)+(b^2))/3;
        varcomps(:) = [varcomps(2:2*ispanavg) vari];
        varR(j1) = sum(varcomps);
    end
    varR = varR/(2*ispanavg);
    MCvarR = MCvarR + varR;
end
MCvarR = MCvarR/MCsimpoints(end);
%
% pdf for maximums from frequency domain parameters:
a = round(0.8*min(maxrespvect),3); % smallest possible value for Rmax
dRmax = 0.0005;
Rmaxkappa = a:dRmax:1.2*round(max(maxrespvect),3);
n = length(Rmaxkappa);
CDFR = zeros(1,n);
rymeanTkappa = rymeanT(irr);
for i = 1:n
```

```
   amat =  (1/(2*pi))*(sqrt(dryvarT)./sqrt(ryvarT)).*exp(-0.5*((Rmaxkappa(i)-
rymeanTkappa).^2)./ryvarT);
   CDFR(i) = exp(-0.5*(amat(1) + amat(end) + 2*sum(amat(2:end-1)))*TUSE/(rft-1));
end
varRmaxFD = 0; % "Frequency Domain"
avgRmaxFD = 0;
pdfR = zeros(1,n-2);
for i = 2:n-1
    pdfR(i-1) = 0.5*(CDFR(i+1)-CDFR(i-1))/dRmax;
    avgRmaxFD = avgRmaxFD + 0.5*(CDFR(i+1)-CDFR(i-1))*Rmaxkappa(i);
end
for i = 2:n-1
    varRmaxFD = varRmaxFD + 0.5*(CDFR(i+1)-CDFR(i-1))*(Rmaxkappa(i)^2);
end
varRmaxFD = varRmaxFD - (avgRmaxFD^2);
% pdf for r max for Monte Carlo simulation:
nuaxinit = round(MCsimpoints/20); % number of compartments
dgax = (max(maxrespvect)-min(maxrespvect))/nuaxinit;
gax = 0;
gax(1,1:nuaxinit) = (min(maxrespvect)+(dgax/2)):dgax:(max(maxrespvect)-(dgax/2.5)); % midpoint
values
ngax = size(gax,2);
probdensRmax = zeros(1,ngax);
for i = 1:MCsimpoints
    y = maxrespvect(i);
    j = min(setdiff((abs(gax'-y)==min(abs(gax'-y))).*((1:ngax)'),0));
    probdensRmax(j) = probdensRmax(j) + 1;
end
scaleg = sum(probdensRmax).*dgax;
probdensRmax = probdensRmax/scaleg;
Rmaxavg = sum(maxrespvect)/MCsimpoints;
% estimate variance of Rmax from a LSF procedure with fixed average
varstart = 0.001;
varend = 1.000;
vardiscr = varstart:(varend-varstart)/9999:varend;
for i = 1:length(vardiscr)
    vari = vardiscr(i);
    my = Rmaxavg-0.5772*vari;
    z = (gax-my)/vari;
    lsf = sum(((1/vari)*exp(-(z+exp(-z)))-probdensRmax).^2);
    if i == 1
        Rmaxvar = vari;
        lsfmin = lsf;
    else
        if lsf < lsfmin
            Rmaxvar = vari;
            lsfmin = lsf;
        end
    end
end
my = Rmaxavg-0.5772*Rmaxvar;
PDFextR = min(gax):0.001:max(gax);
z = (PDFextR-my)/Rmaxvar;
PDFest = (1/Rmaxvar)*exp(-(z+exp(-z)));
% pdf for location of r max for Monte Carlo simulation:
nuaxinitLOC = 300; % number of compartments
dgaxLOC = TUSE/(nuaxinitLOC-1);
gaxLOC = 0;
gaxLOC(1,1:nuaxinitLOC) = 0:dgaxLOC:TUSE; % midpoint values
ngaxLOC = size(gaxLOC,2);
probdensLOCRmax = zeros(1,ngaxLOC);
for i = 1:MCsimpoints
    y = maxrespvectT(i);
    j = min(setdiff((abs(gaxLOC'-y)==min(abs(gaxLOC'-y))).*((1:ngaxLOC)'),0));
    probdensLOCRmax(j) = probdensLOCRmax(j) + 1;
end
scalegLOC = sum(probdensLOCRmax).*dgaxLOC;
probdensLOCRmax = probdensLOCRmax/scalegLOC;
%
QV = [];
i = 0;
for quant = [0.900 0.990 0.999]
    i = i + 1;
    QV(i) = Rmaxavg - Rmaxvar*0.5772 - Rmaxvar*log(-log(quant));
end
%
disp(['Calculation complete at:      ' num2str(datestr(clock))])
```

```
disp(['Elapsed computational time:     ' num2str(toc) ' seconds'])
%
```

B.2 INPUTFILES

“A.txt”:

```
1       0       0.0383  0      -0.0021  0       0.0004  0      -0.0001  0       0       0       0       0       0       0
0.8955  0      -0.0287  0       0.0048  0      -0.0016  0       0.0006  0      -0.0003  0       0.0001  0       0       0
0       0       0       0       0       0       0       0       0       0       0       0       0       0       0       0
0       0       0       0       0       0       0       0       0       0       0       0       0       0       0       0
0       1       0       0.0402  0      -0.004   0       0.0008  0      -0.0002  0       0.0001  0       0       0       0
0       0.4818  0      -0.0555  0       0.0128  0      -0.005   0       0.002   0      -0.001   0       0.0005  0      -0.0003
0       0       0       0       0       0       0       0       0       0       0       0       0       0       0       0
0       0       0       0       0       0       0       0       0       0       0       0       0       0       0       0
0       0       0       0       0       0       0       0       0       0       0       0       0       0       0       0
0       0       0       0       0       0       0       0       0       0       0       0       0       0       0       0
0       1       0      -0.0058  0      -0.0009  0      -0.0002  0      -0.0001  0       0       0       0       0       0
0       0       0       0       0       0       0       0       0       0       0       0       0       0       0       0
0       0       0       0       0       0       0       0       0       0       0       0       0       0       0       0
0       0       0       0       0       0       0       0       0       0       0       0       0       0       0       0
-0.801  0       1       0       0.0521  0       0.0141  0       0.0054  0       0.0025  0       0.0013  0       0.0007  0
0       0       0       0       0       0       0       0       0       0       0       0       0       0       0       0
0.1416  0       1       0       0.0198  0      -0.0026  0       0.0006  0      -0.0002  0       0       0       0       0
0.4937  0       0.2171  0      -0.0444  0       0.0118  0      -0.0048  0       0.0021  0      -0.0011  0       0.0005  0
0       0       0       0       0       0       0       0       0       0       0       0       0       0       0       0
0       0       0       0       0       0       0       0       0       0       0       0       0       0       0       0
0       0       0       0       0       0       0       0       0       0       0       0       0       0       0       0
0       0       0       0       0       0       0       0       0       0       0       0       0       0       0       0
1       0       0.8131  0      -0.2185  0      -0.0439  0      -0.0157  0      -0.007   0      -0.0036  0      -0.002   0
0       0       0       0       0       0       0       0       0       0       0       0       0       0       0       0
0       0       0       0       0       0       0       0       0       0       0       0       0       0       0       0
0       0       0       0       0       0       0       0       0       0       0       0       0       0       0       0
0       0.0058  0       1       0      -0.0004  0      -0.0001  0       0       0       0       0       0       0       0
0       0       0       0       0       0       0       0       0       0       0       0       0       0       0       0
0      -0.1817  0      -0.2059  0       0.006   0      -0.0012  0       0.0003  0      -0.0001  0       0       0       0
0       1       0       0.1406  0      -0.0206  0       0.0073  0      -0.0028  0       0.0014  0      -0.0007  0       0.0004
0       0       0       0       0       0       0       0       0       0       0       0       0       0       0       0
0       0       0       0       0       0       0       0       0       0       0       0       0       0       0       0
-0.2884 0       0.1161  0       0.011   0      -0.0015  0       0.0003  0      -0.0001  0       0       0       0       0
0.8232  0       1       0      -0.0239  0       0.0073  0      -0.0024  0       0.0012  0      -0.0005  0       0.0003  0
0       0       0       0       0       0       0       0       0       0       0       0       0       0       0       0
0       0       0       0       0       0       0       0       0       0       0       0       0       0       0       0
0       0       0       0       0       0       0       0       0       0       0       0       0       0       0       0
0       0       0       0       0       0       0       0       0       0       0       0       0       0       0       0
0.1572  0       0.0742  0       1       0      -0.0194  0      -0.0057  0      -0.0024  0      -0.0012  0      -0.0006  0
0       0       0       0       0       0       0       0       0       0       0       0       0       0       0       0
0      -0.1016  0       1       0       0.212   0      -0.0035  0       0.0009  0      -0.0003  0       0.0001  0       0
0       0.386   0       0.5646  0      -0.0712  0       0.0225  0      -0.0091  0       0.0041  0      -0.0021  0       0.0011
0       0       0       0       0       0       0       0       0       0       0       0       0       0       0       0
0       0       0       0       0       0       0       0       0       0       0       0       0       0       0       0
0       0       0       0       0       0       0       0       0       0       0       0       0       0       0       0
0       0       0       0       0       0       0       0       0       0       0       0       0       0       0       0
0       0.0009  0       0.0004  0       1       0       0       0       0       0       0       0       0       0       0
0       0       0       0       0       0       0       0       0       0       0       0       0       0       0       0
0       0       0       0       0       0       0       0       0       0       0       0       0       0       0       0
0       0       0       0       0       0       0       0       0       0       0       0       0       0       0       0
0       0       0       0       0       0       0       0       0       0       0       0       0       0       0       0
1       0      -0.0297  0      -0.0056  0      -0.002   0      -0.0009  0      -0.0005  0      -0.0003  0       0.0002  0
0       0       0       0       0       0       0       0       0       0       0       0       0       0       0       0
0       0       0       0       0       0       0       0       0       0       0       0       0       0       0       0
0       0       0       0       0       0       0       0       0       0       0       0       0       0       0       0
0       1       0       0       0       0       0       0       0       0       0       0       0       0       0       0
0       0       0       0       0       0       0       0       0       0       0       0       0       0       0       0
0       0       0       0       0       0       0       0       0       0       0       0       0       0       0       0
0       0       0       0       0       0       0       0       0       0       0       0       0       0       0       0
0.0297  0       1       0     -0.003    0       0.0009  0      -0.0004  0      -0.0002  0      -0.0001  0       0       0
0       0       0       0       0       0       0       0       0       0       0       0       0       0       0       0
0       0       0       0       0       0       0       0       0       0       0       0       0       0       0       0
0       0       0       0       0       0       0       0       0       0       0       0       0       0       0       0
0       0       0       1       0       0       0       0       0       0       0       0       0       0       0       0
0       0       0       0       0       0       0       0       0       0       0       0       0       0       0       0
0       0       0       0       0       0       0       0       0       0       0       0       0       0       0       0
0       0       0       0       0       0       0       0       0       0       0       0       0       0       0       0
0.0057  0       0.0028  0       1       0      -0.0008  0      -0.0003  0      -0.0001  0       0       0       0       0
0       0       0       0       0       0       0       0       0       0       0       0       0       0       0       0
0       0       0       0       0       0       0       0       0       0       0       0       0       0       0       0
0       0       0       0       0       0       0       0       0       0       0       0       0       0       0       0
0       0       0       0       0       1       0       0       0       0       0       0       0       0       0       0
```

“adcoeffCae.txt”:

```
 0           0           0           0
 0.0025     -0.0670     -3.5945      0.4179
-0.0620     -0.5221      0.2902     -0.0299
-0.0322      0.1028     -0.7196     -0.0614
-0.0174     -0.1663      0.0899      0.0009
```

“adcoeffKae.txt”:

```
-0.3174      1.6264     -2.6660      -0.3497
-0.7465      5.7567     -1.7383      -0.2249
 0.0025     -0.1056      0.0216       0.0365
 0.1984      0.6324      0.0948      -0.0512
```

“MC.txt”:

```
12199   0.32    0.005
10090   0.64    0.0052
12937   0.71    0.005
12937   0.9     0.0051
10284   1.11    0.0062
12937   1.27    0.0058
12937   1.36    0.006
59547   1.56    0.0079
73761   1.66    0.0084
12937   1.76    0.0077
10885   1.95    0.01
12937   2.14    0.01
427243  2.25    0.005
427243  3.49    0.0052
427243  5.28    0.0063
427243  7.00    0.0083
427243  8.76    0.0112
427243  10.50   0.015
```

“OS2.txt”:

```
0.0050  3
0.0384  6
0.30   6
0.34   5
0.625  5
0.655  3
0.695  4
0.725  4
0.88  6
0.92  4
1.10  6
1.12  3
1.27  6
1.29  3
1.35  6
1.375 4
1.55  6
1.57  3
1.65  6
1.67  3
1.75  4
1.77  4
1.92  4
1.96  6
2.13  20
2.26  10
3.40  15
3.58  15
5.20  15
5.33  15
6.92  15
7.08  16
8.69  10
8.85  8
10.30 8
10.60 8
12    0
```

APPENDIX C – INPUT VALUES OF THE HARDANGER BRIDGE

Geometridata	Vinddata	
B 18.3 m	ρ	1.25 kg/m^3
H 3.25 m	I_u	0.16
L 1310 m	I_w	0.08
L_{exp} L	${}^xL_u=100*(z_f/10)^{0.3}=$	162 m
	${}^xL_w={}^xL_u/12=$	13.5 m
	A_u	1.08
	A_w	1.5
	C_{ux}	1.4
	C_{wx}	1
	$\dfrac{\omega S_n(\omega)}{\sigma_n^2}=\dfrac{A_n\hat{\omega}_n}{\left(1+1.5A_n\hat{\omega}_n\right)^{5/3}}$ hvor:	
	$\begin{cases}\hat{\omega}_n=\omega\cdot{}^{xf}L_n/V\\ n=\text{u eller w}\end{cases}$	
	$\hat{C}oh_{nn}(\omega,\Delta x)\approx\exp\left(-C_{nx}\cdot\omega\cdot\Delta x/V\right)$ hvor:	
	$n=u$ eller w	

Lastkoeffisientdata				Svingeformdata		
	C_{n_0}:	a_n:	b_n:	Svingeform nr. $i=1-18$		
$\bar{C}_D$:	0.7	0	0	$\tilde{m}_i$:	ω_i:	ζ_i:
C'_D:	0	0	0	12199	0.32	0.005
$\bar{C}_L$:	0	0	0	10090	0.64	0.0052
C'_L:	5	3.2	0.5	12937	0.71	0.005
$\bar{C}_M$:	0	0	0	12937	0.9	0.0051
C'_M:	1.5	2.4	0.5	10284	1.11	0.0062
				12937	1.27	0.0058
				12937	1.36	0.006
				59547	1.56	0.0079
				73761	1.66	0.0084
$C_n(\omega)=\dfrac{C_{n_0}}{\left(1+a_n\hat{\omega}\right)^{b_n}}$				12937	1.76	0.0077
				10885	1.95	0.01
				12937	2.14	0.01
hvor: $C_n=$ $\bar{C}_D$, C'_D, $\bar{C}_L$, C'_L,				427243	2.25	0.005
$\bar{C}_M$ eller C'_M				427243	3.49	0.0052
				427243	5.28	0.0063
og: $\hat{\omega}=\omega B/V$				427243	7.00	0.0083
				427243	8.76	0.0112
				427243	10.50	0.015
				$\tilde{m}_i$, $i=1-12$ har enhet kg/m		
				$\tilde{m}_i$, $i=13-18$ har enhet kgm^2/m		

Aerodynamisk deriverte

$$AD_i = p_1\hat{V}_i^3 + p_2\hat{V}_i^2 + p_3\hat{V}_i + p_4$$

hvor:

AD_i er aerodynamisk deriverte $\begin{bmatrix} P_j^* \\ H_j^* \\ A_j^* \end{bmatrix}$,

$j = 1 - 6$,

som er assosiert med svingeform nr. i

og hvor: $\hat{V}_i = V/B\omega_i$

	p_1:	p_2:	p_3:	p_4:
P_1^*:	0	0	$-2\bar{C}_D\,D/B$	0
P_2^*:	0	0	0	0
P_3^*:	0	0	0	0
P_4^*:	0	0	0	0
P_5^*:	0	0	0	0
P_6^*:	0	0	0	0
H_1^*:	0.0025	–0.0670	–3.5945	0.4179
H_2^*:	–0.0620	–0.5221	0.2902	–0.0299
H_3^*:	–0.7465	5.7567	–1.7383	–0.2249
H_4^*:	–0.3174	1.6264	–2.6660	–0.3497
H_5^*:	0	0	0	0
H_6^*:	0	0	0	0
A_1^*:	–0.0322	0.1028	–0.7196	–0.0614
A_2^*:	–0.0174	–0.1663	0.0899	0.0009
A_3^*:	0.1984	0.6324	0.0948	–0.0512
A_4^*:	0.0025	–0.1056	0.0216	0.0365
A_5^*:	0	0	0	0
A_6^*:	0	0	0	0

Svingeformene:

$$\phi_{i_j}(\hat{x}) = \sum_{k=1}^{16} a_{i_{jk}} \cdot \sin(k\pi\hat{x})$$

hvor: $\hat{x} = x/L$ og

$a_{i_{jk}}$ er gitt i $\mathbf{A}$–matrisen i neste kolonne, og hvor:

$$\begin{cases} i = \text{svingeform nr. 1-18} \\ j = \text{retn./komp.} \begin{cases} \text{yg: y-retn. girder} \\ \text{yc: y-retn. cable} \\ \text{z: z-retn. girder} \\ \theta\text{: girder torsjon} \end{cases} \\ k = \text{Fourierkomponent nr. 1-16} \end{cases}$$

$$\mathbf{A} = \begin{array}{c} \text{Svinge} \\ \text{form} \\ \text{nr.i} \end{array} \left\{ \begin{bmatrix} \begin{pmatrix} i=1 \\ k=1 \end{pmatrix} & & \cdots & & \begin{pmatrix} i=1 \\ k=16 \end{pmatrix} \\ \vdots & & \vdots & & \vdots \\ a_{i_{yg_1}} & & a_{i_{yg_k}} & & a_{i_{yg16}} \\ a_{i_{yc_1}} & \cdots & a_{i_{yc_k}} & \cdots & a_{i_{yc61}} \\ a_{i_{z_1}} & & a_{i_{z_k}} & & a_{i_{z16}} \\ a_{i_{\theta_1}} & & a_{i_{\theta_k}} & & a_{i_{\theta16}} \\ \vdots & & \vdots & & \vdots \\ \begin{pmatrix} i=18 \\ k=1 \end{pmatrix} & & \cdots & & \begin{pmatrix} i=18 \\ k=16 \end{pmatrix} \end{bmatrix} \right. \begin{array}{l} \\ \\ \leftarrow \text{Brobj. i y-retn.} \\ \leftarrow \text{Kabel i y-retn.} \\ \leftarrow \text{Brobj. i z-retn.} \\ \leftarrow \text{Torsj. av brobj.} \\ \\ \\ \end{array}$$